CRANFIELD UNIVERSITY

CHEE KEONG TAN

AN INVESTIGATION ON THE DIAGNOSTIC AND PROGNOSTIC CAPABILITIES OF ACOUSTIC EMISSION (AE) ON A SPUR GEARBOX

SCHOOL OF INDUSTRIAL AND MAUNFACTURING SCIENCE

AND

SCHOOL OF ENGINEERING

PhD THESIS

CRANFIELD UNIVERSITY

SCHOOL OF INDUSTRIAL AND MAUNFACTURING SCIENCE AND SCHOOL OF ENGINEERING

PhD Thesis

Academic Year 2005-2006

CHEE KEONG TAN

AN INVESTIGATION ON THE DIAGNOSTIC AND PROGNOSTIC CAPABILITIES OF ACOUSTIC EMISSION (AE) ON A SPUR GEARBOX

Supervisors: **Prof. Phil Irving**

Dr. David Mba

AUGUST 2005

ABSTRACT

The aim of this research project is to explore a new technique, Acoustic Emission (AE), on both the diagnostic and prognostic capabilities in monitoring gear teeth degradation (pitting), and compare with the more widely used techniques such as vibration monitoring and Spectrometric Oil Analysis (SOA). Furthermore, by employing the experimental results and past literature, a model in predicting the amount of gear surface pitting wear using AE activity level was proposed. The successful formulation of this proposed model may be able to predict the remaining life of the gear after pitting has been detected, thereby allowing timely replacement to be carried out without the risk of catastrophic failure.

A series of experimental tests which include seeded defect simulations, study on the effect of operating parameters over AE (under isothermal conditions), AE source determination tests and accelerated gear fatigue tests have been performed to investigate the diagnostics and prognostics capabilities of AE via a back-to-back gearbox set up. The experimental results achieved have highlighted some significant findings: (a) The variation in rotating speeds, change the AE levels in a much significant amount as compared to the same variation in applied load. (b) The prime source of AE was postulated to be asperity contact under rolling and sliding of the meshing gear teeth surfaces. (c) AE technique has a far better degradation (pitting) monitoring capability compared to vibration and SOA techniques.

These findings have made a vast contribution in condition monitoring of gearbox using AE technique and the proposed model has also offered opportunity to make AE a potentially viable and effective tool in diagnosis and prognosis of gearbox or even other rotating machinery defects.

ACKNOWLEDGEMENTS

First and foremost, I would like to thank the Ministry of Defence, Singapore, Defence Science Technology Agency (DSTA) and Cranfield University for sponsoring and financing my PhD study.

I would like to express my sincere gratitude and appreciation to my research supervisors, Dr. David Mba (SoE) and Prof. Phil Irving (SIMS) for their guidance and advice during my study in Cranfield University. I would also like to express my appreciation to the SoE design office and those technicians who in one way or another assisted me in the experimental work. Without their helpful and continuous effort, it would not be possible to complete the PhD work within such a short time frame.

My sincere appreciation to all my mates in Damage Tolerance Group for their friendship and helping hands, especially PJ, Abilio, Jian Hong, Mimmo, Ben and Matt. And also special thanks to my personal friends; Martusia and Anucha, in Cranfield University who always encourage me, have faith in me and cooked for me.

Finally, my everlasting gratitude and appreciation to my parents and family members for their support, encouragement and inspiration.

LIST OF FIGURES

LIST OF TABLES

1 INTRODUCTION

1.1 Background

In the aviation industry, particularly for the helicopter platform, it is important to detect damage in the rotating components before catastrophic failure occurs, especially the gearboxes. It was reported by Vinall [1] that 22% of the fatal accidents between 1964 and 1979 in the UK were caused by the malfunction or failure of the gearbox systems. In the USA, a similar percentage (20.1%) of fatal helicopter accidents was attributed to the failure of the gearboxes between 1956 and 1986 [2]. This indeed is an alarming figure. Furthermore, the maintenance of helicopter gearbox contributed to 30% of the total helicopter maintenance costs [3]. Hence, a failure in the gearbox will lead to long downtime and stoppage of operation, which translates to high maintenance and usage costs. In addition, the gearbox is the most critical and complicated component on the helicopter platform, catastrophic failure of which will lead to loss of life and assets. Hence, it is reasonable to make gearbox the subject of study in this research project. Among the major sub-components of the gearbox, gear failure had contributed 16% of the helicopter fatalities and subsequently fatal helicopter accidents [2]. National Aeronautics and Space Administration (NASA) has realised this fact and focussed their researches in detection of gear failure, especially in the surface distress failure modes, such as pitting and scuffing [4].

Traditionally, gearboxes and other critical rotating components in the helicopter platform were maintained based on preventive maintenance philosophy due to flight safety requirements. This type of maintenance policy entailed scheduled checks, and removal and repair of the unserviceable item before failure occurs. This approach had resulted in high maintenance costs and under utilisation of component life. The implementation of Helicopter Health and Usage Monitoring Systems (HHUMS) has facilitated the transition of preventive maintenance philosophy to condition based maintenance philosophy [5, 6].

Condition based maintenance will result in the reduction of maintenance costs which was evident in Byington's report [5]. Although the usage of HHUMS could reduce maintenance costs, the principle of ensuring flight safety must still be enforced. This enforcement entails accurate detection and timely diagnosis of potential faults via the usage of current technologies.

The current techniques employed in HHUMS are either onboard the helicopter or off-line. These techniques include wear debris and vibration monitoring [5, 6, 7, 8, 9, 10, 11]. The wear debris monitoring technique usually captures wear debris information from the used oil, the oil filter and the magnetic chip detector using various analysis methods such as Spectrometric Oil Analysis (SOA) and Ferrography Analysis (FA). These analysis methods were among the first condition monitoring techniques used in the aviation industry, especially the helicopter platform, to monitor rotating components such as engine, transmission, drive trains and rotor systems. With the development and viability of vibration analysis techniques for fault diagnosis and monitoring, it became the only condition monitoring technique onboard of all helicopters equipped with HHUMS. This technique achieved the monitoring tasks through the measured vibration level in the gearbox using accelerometers mounted at various critical locations onboard the aircraft. The recorded vibration data was further processed into different types of vibration parameters which will change when gearbox or gear damage develops.

1.2 Helicopter Health and Usage Monitoring Systems (HHUMS)

HHUMS are defined as the application of a set of equipment, techniques and procedures by which selected incipient failure or degradation of components can be determined. In general, HHUMS comprise three major elements:

a) Health: Monitoring component condition through vibration analysis techniques.

b) Usage: Monitoring components usage via recording of the flight regimes flown.

c) Others: Monitoring other aspects of the rotational components such as Rotor-Track and Balance (RTB), and recording critical flight data for investigation purposes such Cockpit Voice Flight Data Recorder (CVFDR) and Flight Data Recorder (FDR).

In order to support these three elements of HHUMS, several monitoring devices such as accelerometers, optical sensors, tachometer blade trackers, magnetic chip detectors and counters have to be installed onboard the helicopter to capture the respective monitoring data. A typical HHUMS configuration of the AH-64A aircraft is depicted in figure 1.1. The recorded data, in this case the vibration signatures of the monitored component could be downloaded to the computers for further analysis via cartridges, tapes or PCMCIA cards. The aircraft maintainer analysing the data could follow up with any necessary maintenance actions if the component condition was found to be unsatisfactory.

Figure 1.1 Typical HHMUS configurations for AH-64A.

The benefits of HHUMS have been well established and recognised [5, 9, 10, 12, 13]. These benefits are listed as follows:

(a) Reduction in life cycle and maintenance costs
(b) Early warning of incipient component failure
(c) Improved safety
(d) Greater aircraft availability
(e) Lower insurance cost

All the abovementioned benefits can only be realised, provided that HHUMS accurately detect the fault present in the component. Pusey et al [5] highlighted a report by Chamberlain that 64% (1980-1990) and 79% (1992-1993) of the mechanical faults that attributed to helicopter mishaps could be prevented by the implementation of HHUMS. Subsequently, both the US Army and Stewart Hughes Limited have reported that HHUMS have successfully detected approximately between 60% and 70% of the fault arisings respectively [4, 14, 15]. Although the performance of HHUMS is progressing, there are still some shortcomings especially in the fields of health monitoring and usage utilisation.

The following are the drawbacks or shortcomings in current HHUMS, some of which are key focus of this research project.

(a) The usage of vibration monitoring and SOA techniques do not give an early detection of defects. Irving et al [6] have pointed out that the failure mechanisms of gear and bearings within a gearbox usually have no more than 10% to 20% or even as small as 1% of total life remaining when cracks or pits developed in excess of 1 to 2 mm. This inability to detect gearbox faults earlier has been demonstrated for both the vibration and SOA techniques. Thus, new technique needs to be explored so that timely fault detection can be achieved. As Acoustic Emission (AE) is generated from microscopic processes within materials.

researchers believed that AE will be able to detect the defect well in advance of the two current established techniques.

(b) The prognostic capability; the ability to reliably and accurately predict the remaining useful life of an operating component, of current HHUMS is not fully realised. Currently, there is no working HHUMS that has prognosis capability. Prognostic capability not only would provide the prediction of the time to failure but it would also give the operators an opportunity to modify their operations to extend the component's life and adjust the maintenance schedule to reduce downtime and maintenance costs [16]. Prognosis of the helicopter component could be done in two ways: (a) the usage of health monitoring data is unable to provide damage progression information below the detectability threshold. Hence, prognosis could only be done through the extrapolation of past trends (b) the other way of performing prognosis is to use usage monitoring techniques. In helicopter gearboxes, the key input for determining the service life will be the service torque. Reviewing the service torque spectrums would allow stresses acting on the sub-components such as gear tooth root, between gear surfaces and bearings, to be determined. With the known material and fatigue properties of the bearings and gears, prognosis could be performed through either the safe life or damage tolerance approaches [4, 17].

(c) Not all of the mechanical damage can be detected using current HHUMS, for instance, corrosion, damage in splines and epicyclics. In addition, due to the nature of the defect and characteristics of each individual condition monitoring technique, some failures could be detected by only one monitoring technique but not others. In general, the vibration monitoring technique is good in detecting fracture modes of failure where minimal wear debris is released into the system. On the other hand, wear debris and SOA monitoring techniques are able to pick up defects such as pitting, spalling and scuffing where wear debris is removed from the damaged surfaces [9]. These observations have been highlighted as important lessons learnt in both the Canadian Forces and the US Army [4, 18].

Hence, the possible solution to this problem may require fusion of various condition monitoring techniques to provide a better fault diagnosis and detection capability. The industry, operators and academics have attempted to perform the integration of these condition monitoring techniques to increase the probability and accuracy of fault detection [8, 19-22]. They have concluded that combination of various condition monitoring techniques are highly complementary which reinforce indications seen in each technique, and have unique strength in highlighting specific wear conditions.

In view of the shortcomings of the current HHUMS monitoring techniques, it was proposed that an alternative monitoring technique, AE, to be explored and compared to the current HHUMS monitoring techniques. Close examination of the AE technique in the areas of defect detection and prognosis potential would be carried out.

1.3 Project objectives

The objectives of the project are as follows:

(a) Assess the defect detection capability of the AE technique through seeded defect tests.
(b) Establish a relationship between AE and gear operating parameters such as load, speed and oil film thickness.
(c) Identify the possible sources of AE excitation during meshing of gear teeth.
(d) Compare and quantify the effectiveness of AE in relation to SOA and vibration techniques in detecting and monitoring the natural progression of pitting wear on a gear set.
(e) Establish the relationship between gear operational life and AE, vibration and SOA.
(f) Establish the relationship between AE r.m.s. and the damage status of gear tooth surfaces.

1.4 Gearboxes

1.4.1 Helicopter gearboxes

The gearboxes or transmissions are deemed as the most critical and complicated rotating component of a helicopter platform. The gearboxes serve the platform with two functions. The primary function is to deliver shaft power to the rotor to provide lift and to transmit the thrust to the hull. The secondary function includes driving the tail rotor systems and vital services such as hydraulic systems, generators and cooling systems in the helicopter. In general, the six types of gearboxes which are commonly used in the single and multi-rotors helicopters are listed as follows:

- Main Gearbox (MGB) or main transmission
- Intermediate Gearbox (IGB) or 45 degrees gearbox
- Tail Gearbox (TGB) or 90 degrees gearbox
- Noise Gearbox (NGB)
- Combiner Gearbox (C-box)
- Accessary Gearbox (AGB)

Among these gearboxes, the MGB is considered as the most complex and heavily maintained rotating component in the helicopter. Typically, the MGB consists of the following major sub-components:

- Gears, includes planetary, spur and helical gears to transmit power
- Bearings to support rotating components such as gears and shafts
- Input and output shafts to convert power from the engine(s) to thrust and lift via the gearbox
- Pumps to circulate the lubricating oil for the bearings and gears

- Filters to capture wear debris from the gearbox and improve the cleanliness of the lubricating oil
- Chip detector or magnetic plug to capture metallic debris from the gearbox and provide warning on the degradation status of the gearbox
- Clutch systems to enable the engine to disengage from the gearbox
- Cooling systems to remove heat from the lubricating oil and lower the temperature of the gearbox
- Sensing and indicating systems to provide information and warning on the operating conditions of various systems in the gearbox

Figure 1.2 shows a conventional single rotor helicopter which has a main transmission, 45 degree gearbox and 90 degree gearbox and their respective locations in the helicopter. For further appreciation of the various sub-components and their layouts in the gearbox, a simple MGB from the OH-58 is presented in Figure 1.3.

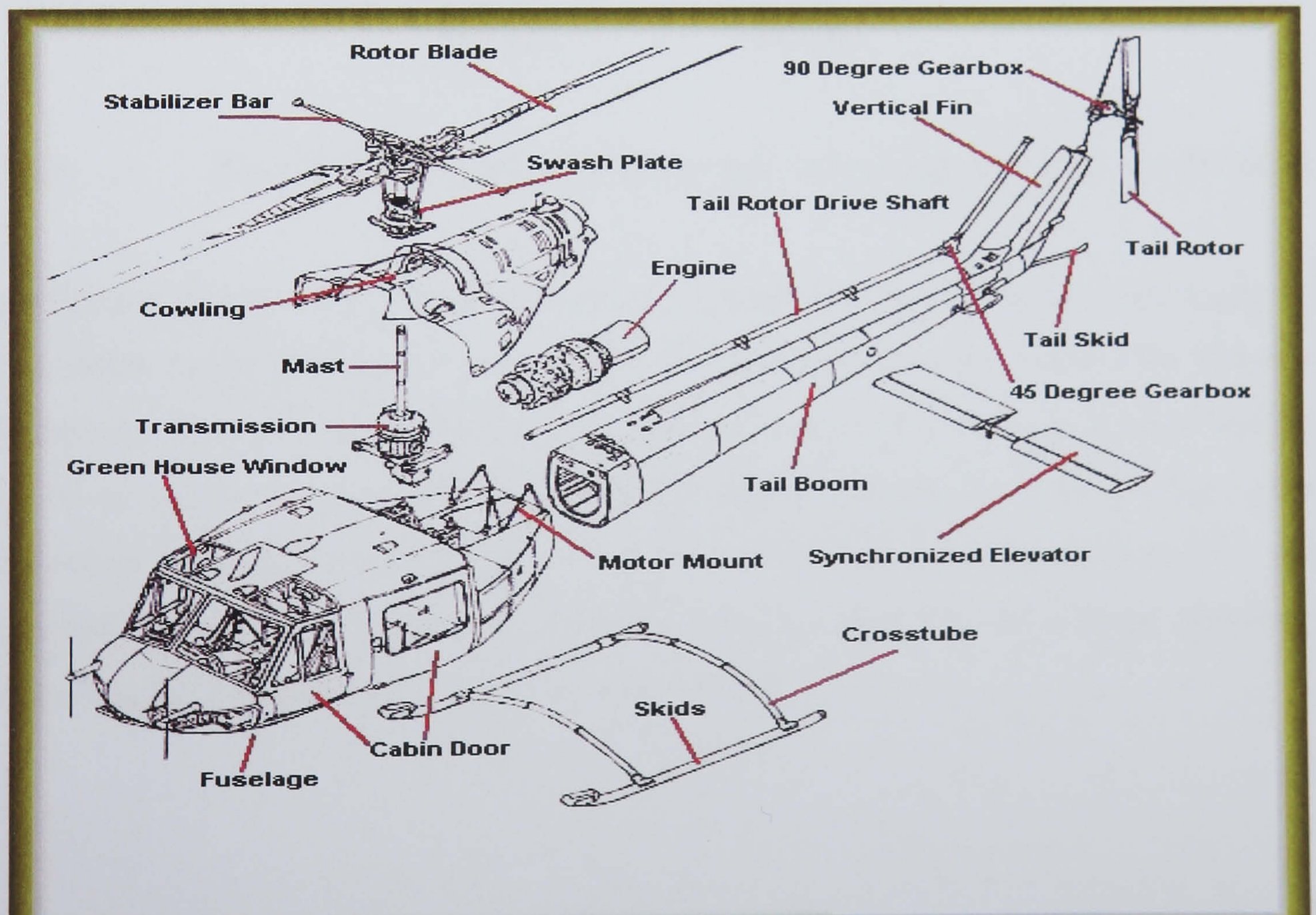

Figure 1.2 Illustration and location of the various types of gearboxes of the UH1C helicopter.

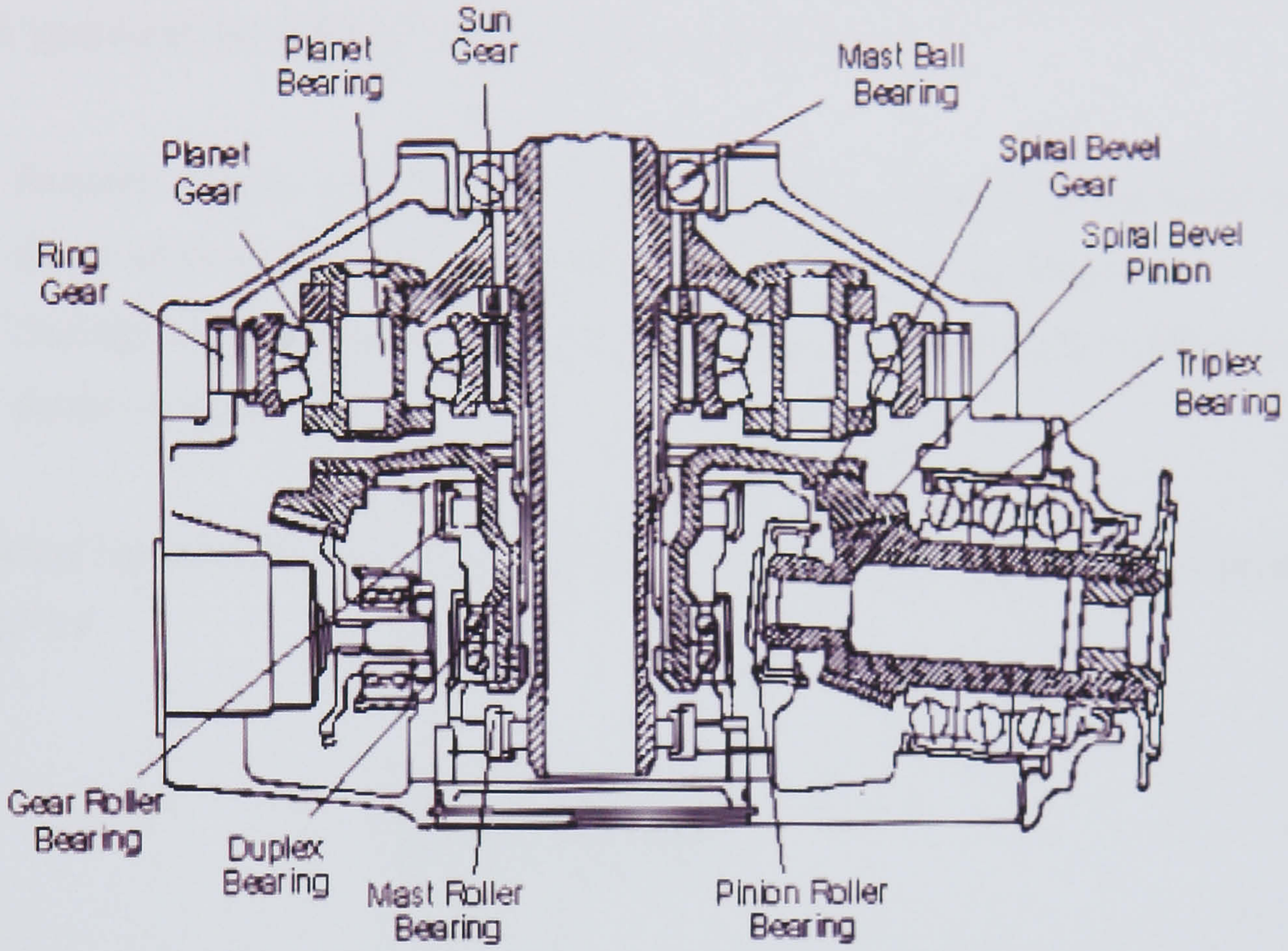

Figure 1.3 Illustration of the gearbox layout and sub-components of an OH-58 MGB.

A helicopter gearbox design is usually based on single load path of failure, i.e. single sub-component failure will lead to catastrophic failure of the gearbox. Hence, the failure of the gearbox will not only lead to loss of assets but also the loss of lives. Typical gearbox defects or failure usually arises from defective sub-components such as bearings, gears, lubricating systems and shafts [13, 15]. Based on the helicopter accident analysis data provided by UK CAA [23, table 5], defective or failed gears were the highest contributor to gearbox failures that lead to the loss of helicopters.

1.4.2 Gear failure modes

In general, a gear may fail in various modes through different damage processes. In general, gear tooth failure falls into the following two forms:

- Fracture of gear tooth which usually happens at the root of the tooth where a whole section of the tooth breaks away- tooth root bending fatigue
- Damage or destruction of the working surfaces of the gear tooth- surface wear and contact fatigue

A graphical representation of various forms of the two major failure modes was depicted in figure 1.4.

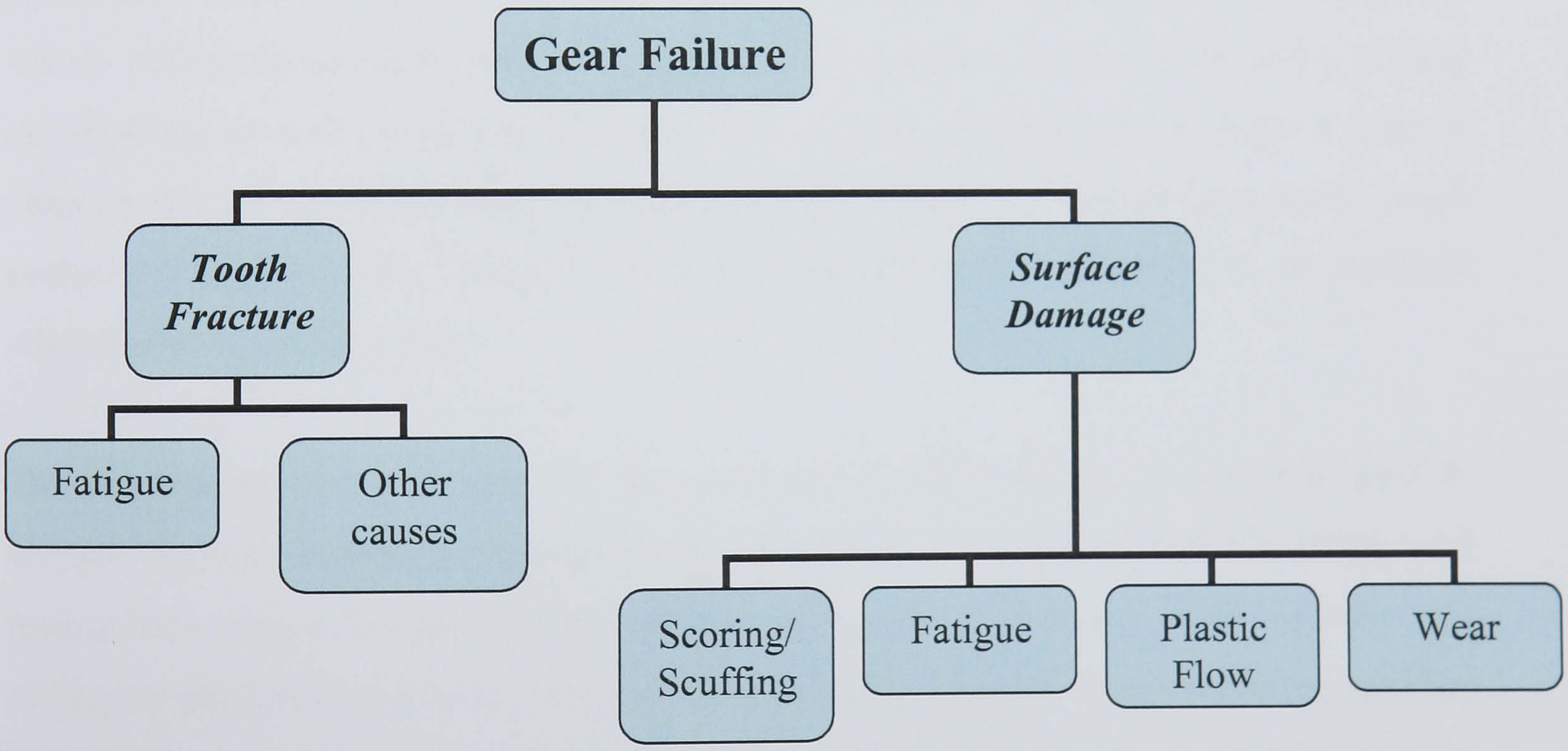

Figure 1.4 Classification of the various gear failure modes summarised from [24].

In general, tooth bending fatigue failure usually starts from small stress raisers such as an inclusion or cavity at or near the root of the tooth. The crack propagates from the initial defect site progressively until partial tooth failure or loss of the whole tooth occurs. Other causes of tooth fracture can be attributed to overload or impact. However, if the gear

teeth are supported by a very thin rim and web, the bending stress over the rim and web become very significant. The initial crack will propagate from the root section through the web and rim of the gear. This type of failure frequently causes catastrophic damage to the gearbox.

Surface damage of the gear tooth usually occurs on the working tooth surfaces and is classified into wear, plastic flow, scoring/scuffing and pitting. Since pitting is the main interest in this research, the former three types of surface damage will only be briefly summarised in this section and their detailed descriptions can be found in [24]. Wear usually occurs when there is inadequate lubricant film between the two meshing surfaces to prevent metal-to-metal contact. Other factors that may lead to wear of the gear tooth are abrasive particles in the lubricant and presence of corrosion within the gearbox. Plastic flow usually occurs under a combination of extreme load and sliding speed conditions. These conditions cause the gear tooth surface material to flow plastically which, with progression in time, leads to catastrophic failure. Cold and hot flows, ridging and rippling are some examples of plastic flow in gears. Scuffing or scoring is a thermal phenomenon which occurs when the lubricating film breaks down to allow metal to metal contact of the gear teeth. This gives a local welding followed by tearing of the surfaces when the welds are sheared.

The last category of gear tooth surface damage is pitting. Pitting can present itself in various degrees of severity; micro-pitting and spalling. Although both micro-pitting and pitting show similar features microscopically, micro-pitting is usually differentiated from pitting by shallower pits in the affected zone [25, 26]. In most of the literature, spalling and pitting are used interchangeably but with different degrees of severity assigned to them. Ding and Rieger [27] defined pitting as the formation of shallow craters of depth less than 10 μm which originate from surface defects; while spalling is formed by deeper cavities of typical depth between 20 and 100 μm that are developed from sub-surface defects. Ding and Rieger went further to attempt to differentiate the formation of spalling from pitting; the detailed investigation is described in [27].

Pitting occurs when two meshing gear teeth come into contact under load. This contact can be either along a line, point or small circular/elliptical areas. Due to the small contact area, high shear stresses can build up at or near the surface. Usually the maximum shear stress occurs at some distance below the surface. Pitting in gear teeth usually develops in three areas; (a) along the pitch-line where pure rolling stress is experienced, (b) addendum and (c) dedendum where both rolling and sliding stress are present. When the velocities of the two contacting curved surfaces are the same, pure rolling conditions prevail. The stress distribution resulting from this condition usually established at the pitch-line as shown in figure 1.5. The maximum shear stress occurs at some distance underneath the surface just at the front of the contact point. Cracking will start at this point where the maximum shear stress is located and propagate parallel to the surface. The continuing rolling action and the hydrodynamic pressures from the lubricant will force the crack to deviate upwards to the surface and material is removed to form pit. The formation of the rolling contact fatigue pits does not come with surface plastic deformation.

When there is a velocity difference between two contacting curved surfaces, such as the gear teeth, a sliding/rolling condition prevails. With the introduction of a sliding element, there are some modifications to the stress distribution of the contacting surface. These modifications are shown in figure 1.5. The effect of the sliding element is to move the maximum shear stress nearer to the surface with a higher shear stress level compared to the pure rolling condition. Gear teeth contact each other with a complex combination of sliding and rolling that vary along the gear tooth involute profile. At the addendum, positive sliding occurs where both rolling and sliding are in the same direction. At the dedendum where rolling and sliding are in the different directions, a negative sliding condition prevails. Figure 1.6 illustrates the direction of sliding and rolling along the meshing gear teeth involute profile. It is most likely that contact fatigue and pitting will be initiated from the dedendum [28, 29]. In contrast to rolling contact fatigue, the sliding-rolling contact fatigue present in the dedendum causes plastic deformation on the gear tooth surfaces. Under real situations, pitting usually occurs first at (a) the dedendum of the smaller gear (usually the pinion) since it undergoes more stress cycles (provided the

two meshing gears are of the same material and hardness) (b) the lowest point of single tooth contact where it takes the full load together with the high sliding speed.

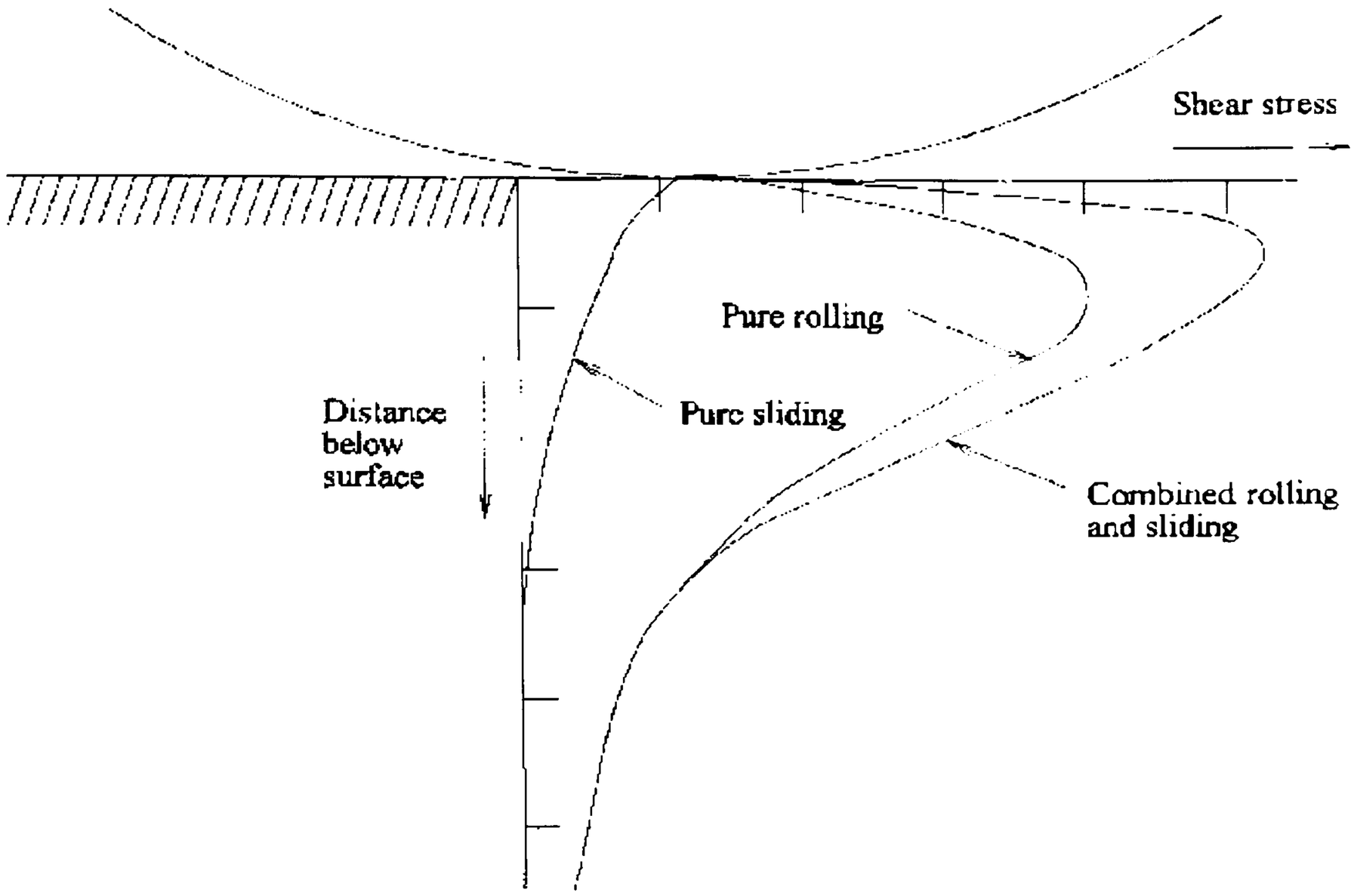

Figure 1.5 Stress distributions at and near two contacting surfaces under pure rolling conditions and sliding-rolling conditions [28].

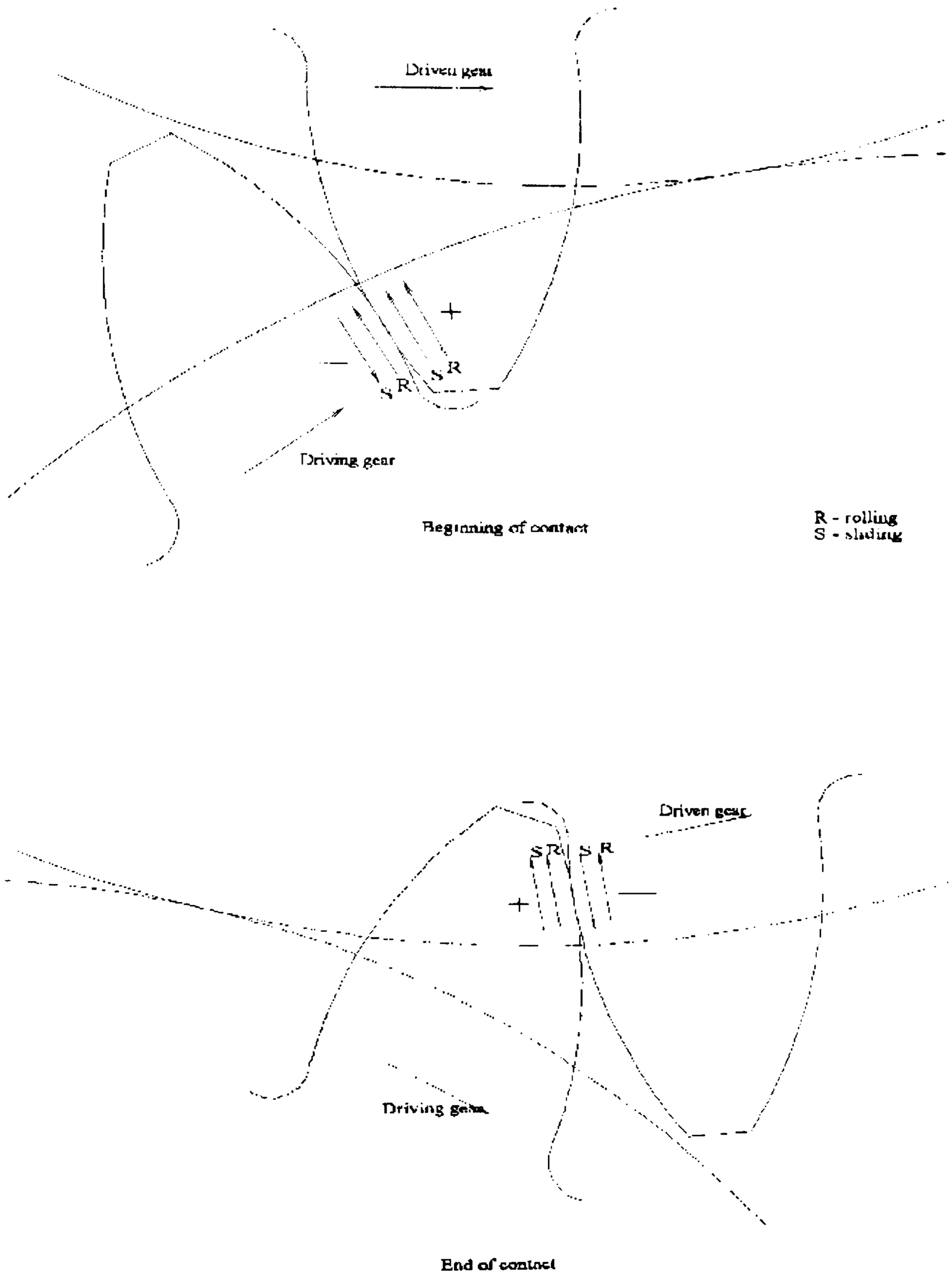

Figure 1.6 Combination of sliding and rolling in gear teeth [28].

1.4.3 Elastohydrodynamic Lubrication (EHL)

In critical and highly stressed rotating machine elements such as bearings and gears, Elastohydrodynamic Lubrication (EHL) is the dominant mode of lubrication for meshing surfaces. Indeed, it was the gear lubrication problem that led to the studies and development of knowledge of EHL. The operating experiences accumulated in gearbox operation suggested that severe metal-to-metal contact was not actually happening even in highly loaded gears if appropriate lubrication was provided. This observation pointed toward the fact that the meshing gear teeth surfaces were separated by the protective oil film between them. Dowson has provided a comprehensive and detailed review of the history, development and future of EHL throughout the 20th century [30, 31].

In the early 20th century, calculated value for the minimum oil film thickness for the lubrication of gear teeth was based on hydrodynamic lubrication theory. However, the predicted film thickness based on this analysis methodology was much smaller than the surface roughness of the gear tooth surfaces. This revealed the inadequacy of hydrodynamic lubrication theory to explain gear lubrication. In the mid 20th century, researchers realised that additional factors, such as lubricant viscosity and local elastic deformation, have to be included into the analysis. This major conceptual breakthrough resulted in the derivation of various empirical dimensionless minimum oil film thickness equations detailed in [30, 31]. In all these equations, it was clearly evident that the minimum oil film thickness was strongly influenced by the speed of rotation and material parameters. Furthermore, since the range of material parameters is very small in practice, at any rate for metallic contacts [32]; the speed parameter became the most dominant factor in determining the oil film thickness. Although an increase in the load parameter has negligible effect on the minimum oil film thickness, it actually increases the size of the effective loading carrying region, and thus the load bearing capacity. The minimum oil film thickness behaviours observed thus far were applicable to both line and point contacts, as the nominal point contact oil film thickness was modified and estimated from the line contact ones.

The typical features of an EHL line contact in terms of pressure distribution are shown in figure 1.7. For the requirement of continuity mass flow of the lubricating film within the two meshing surfaces, the product of the density and film thickness of the lubricant has to be constant. Hence, an almost constant film thickness occupies most of the central region of the Hertzian contact zones. At the exit end, the film pressure will have to return to ambient condition when the fluid film exits the meshing surfaces. As this pressure quickly reduces to atmospheric pressure, a restriction or choke point will occur (see figure 1.7). In order to maintain the continuity of mass flow of the film, the mass flow at the entraining end has to increase. Coupling this phenomenon and the geometrical form, a secondary pressure peak arises at the exit end. This feature characterises EHL. The magnitude of the secondary pressure peak always far exceeds the maximum Hertzian pressure. It is also at this exit end where the minimum film thickness is located. This minimum film thickness is usually 80% of the central film thickness.

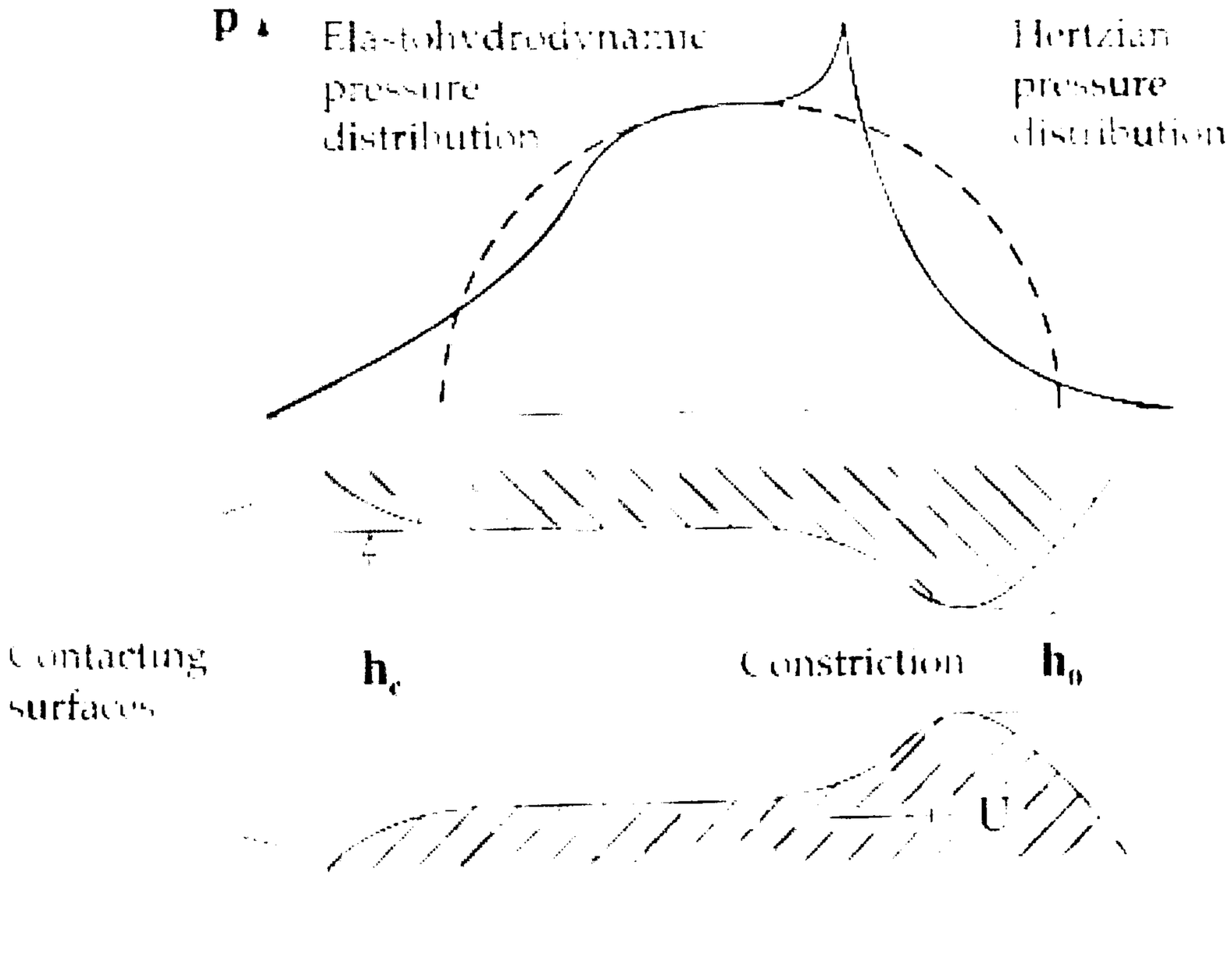

Figure 1.7 Pressure distributions in an EHL line contact and the constriction at the exit end [33].

Dowson and Higginson [32] provide detailed graphical plots to illustrate the changes in the secondary pressure peak with changing load and speed. For compressible lubricant, an increase in load has very little effect on the magnitude of the secondary pressure peak as compared to a change in the material and speed parameters. Between the material and speed parameters, the speed parameter turns out to be the more dominant factor in determining the secondary pressure peak behaviour. When the speed parameter increases, not only does the amplitude of the secondary pressure peak increase but the secondary pressure peak also moves towards the inlet or entraining end. If the speed is high enough, the secondary pressure peak can occur at the inlet end. With the inclusion of lubricant compressibility, this behaviour remains largely the same in general. However, additional factors such as lubricant compressibility and magnitude of the pressure must be considered in determining the film thickness and the pressure distribution.

It is important to recognise that the analysis of EHL detailed above was done without the consideration of surface roughness. For very highly stressed machine elements, such as gears and bearings, surface roughness is of the order of the film thickness. In such cases, asperity contacts between the meshing surfaces are unavoidable, although the lubricant film actually separates the two meshing surfaces. In determining the pitting life of such machine elements, the degree of asperity contact taking place in the lubricated zone becomes a major consideration.

1.4.4 Gear life

Currently, there is no official standard from the International Standards Organisation (ISO) and British Standards (BS) to determine the predicted remaining life of gears under defective conditions such as scoring, pitting and tooth bending fatigue. However, the ISO, BS and American Gear Manufacturing Association (AMGA) do provide methods and standards for users to calculate the limiting stresses distribution between defect occurrence and remaining life. In the context of this thesis, only those standards involving pitting will be mentioned. The following standards provide various

methodologies for gear designers to determine the permissible contact stress in a pair of involute spur gears.

- BS436: Part 3: 1986:- Method for calculation of contact and root bending stress limitations for metallic involute gears [34]
- ISO 6336-02:- Calculation of surface durability (pitting) [35]
- ANSI/AGMA 2101-C95:- Fundamental rating factors and calculation methods for involute spur and helical gear teeth [36]

Common to these three standards are the approaches that the maximum surface contact stress should be limited to a value less than the surface endurance limit of the gear material. As long as this requirement is met, no pitting should occur during the gear operational life. Although does not necessarily hold true for practical world, it provides sufficient awareness to the designer as well as the user that pitting can occur beyond the design life eventually. In general, the ISO and BS standards present this limit in terms of contact stress whereas AGMA expresses the pitting resistance in terms of power and torque. For illustration purposes, only the BS contact stress calculation will be briefly mentioned in this section. The details of the other methodologies can be found elsewhere [53, 36].

The British Gear Association (BGA) has developed a complex program to calculate the load capacity of gear in term of contact stress based on BS436 part 3 [34]. This program will be employed for this investigation to ascertain whether pitting will occur for the accelerated gear fatigue tests. The permissible and actual contact stresses can be calculated based on equations (1) and (2) of BS436 part 3 respectively. In these equations, effects such as material and processing, tooth profile, contact ratio, lubricant etc present themselves as correction factors in determining the contact stresses. The effect and computation of each correction factor is illustrated in [34]. Similar approach is employed in ISO 6336-02 and ANSI/AGMA 2101-C95, differing only in the details of the correction factors.

National Aeronautics and Space Administration (NASA) Lewis Research Centre adopted a different approach in predicting gear tooth life from the standards mentioned above. In the mid-1970s, Coy et al [37, 38] developed and formulated a model for surface fatigue life of low-contact ratio spur gears. This surface fatigue life model was based on the Lunberg-Palmgren theory that is commonly applied to bearing life prediction. In addition to Lunberg-Palmgren theory, Weibull analysis was also employed to allow this model to predict the expected fatigue life (with 90% probability of survival) of a single gear tooth, gear and gear set. Furthermore, Coy and co-workers derived an expression to determine the dynamic capacities of gear tooth, gear and gear set. This dynamic capacity is defined as the transmitted tangential load that gives a 90% probability of survival of the gear set for one million pinion revolutions. In the late 1970s, Townsend et al [39] conducted life tests for three different loads on three groups of AISI 9310 steel spur gears. The objectives of these tests were to experimentally determine the load-life relations of the tested gears and to improve on the life prediction model detailed in [37, 38]. The gear surface fatigue life was found to be inversely proportional to the applied load to the power 4.3 at L_{10} life as compared to 1.5 and in between 8.5 to 9.5 used in [37] and [36] respectively. Furthermore, the Weibull slope was observed to increase with load varying linearly with contact stress. The average value for the Weibull slope was 2.5, which was 0.5 lower than [37]. For the subsequent 10 years, as different gear materials, methods of manufacturing and lubricants evolved, Coy and co-workers [40] updated the surface fatigue life prediction model for spur gears and relate this model to the experimental results from the various NASA tests. Since this update, this surface life prediction model has been used widely by NASA researchers and documented as in the NASA reference publication for gearing [41].

2 LITERATURE REVIEW

2.1 *Acoustic Emission (AE)*

AE, typically between 25 kHz and 1 MHz, is defined as transient elastic waves generated due to the rapid release of energy from localised sources in a material. There are a large variety of source mechanisms which give rise to these AE activities. Among these AE source mechanisms are crack initiation and propagation, plastic deformation, friction (asperity contacts), fluid cavitations and turbulence.

There are three types of AE waveforms:

(a) Burst type waveform which characterised by short rise time and an exponential decay (See figure 2.1(a)).

(b) Continuous type waveform (See figure 2.1 (b)).

(c) Mixed type waveform in which a burst type waveform is superimposed on a background of continuous type waveform as shown in figure 2.1 (c).

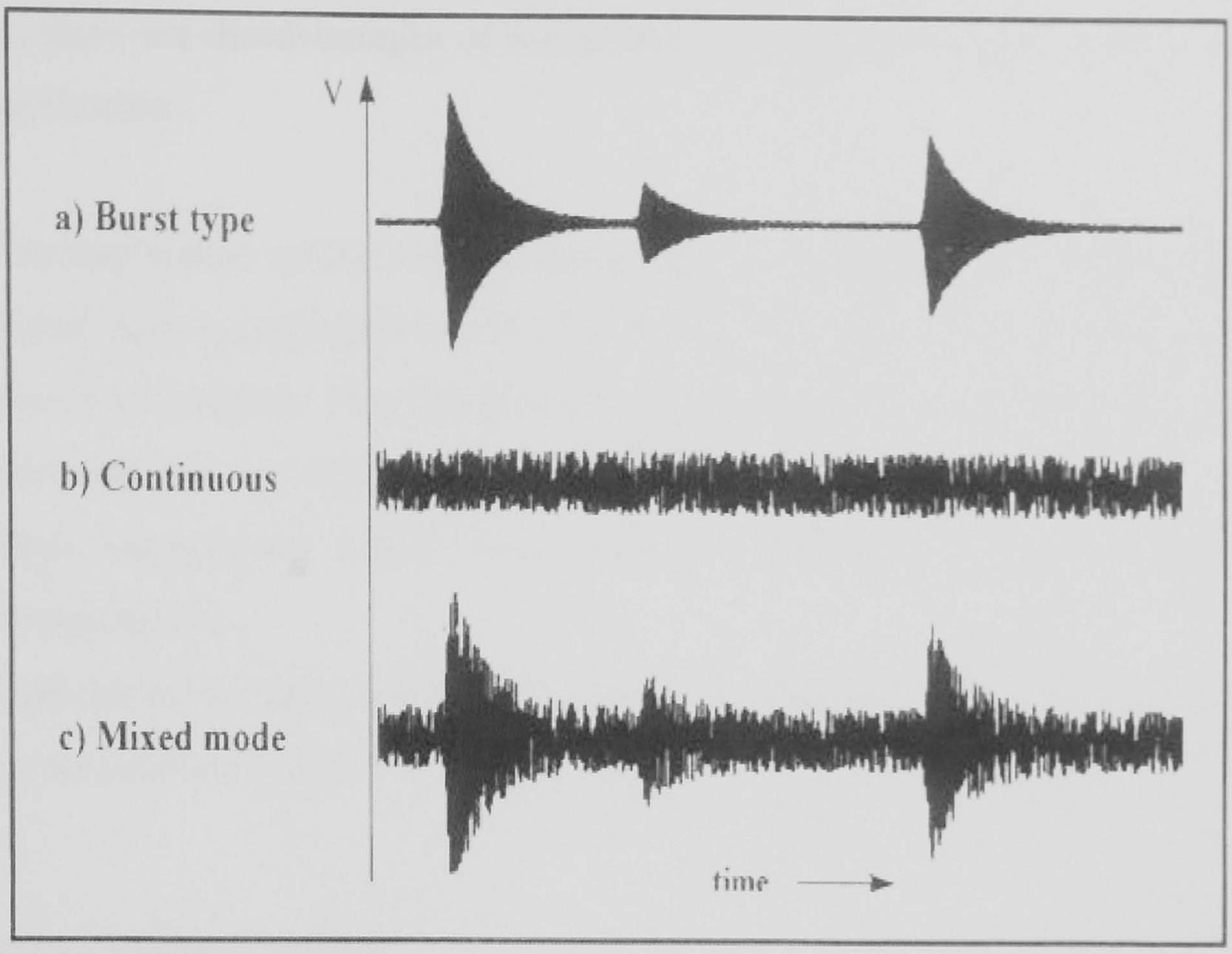

Figure 2.1 Illustration of different types of AE waveforms [42].

AE was originally developed as a method of Non-Destructive Testing (NDT) where it was readily applied on structural components. In the late 1960's [42], this technique was further explored in the field of condition monitoring of rotating machinery. The advantages of this technique that motivates its application and development are:

- As AE is non-directional, one AE sensor is sufficient to collect the monitoring data compared to other condition monitoring techniques such as vibration monitoring which requires three accelerometers for the principle axes or an expensive tri-axial accelerometer.
- As AE only detects high frequency elastic waves, it is thus insensitive to structural resonances and typical mechanical background noises (Typically less than 20 kHz).
- Since AE is produced at microscopic level of the material, it is highly sensitive and offers opportunities for identifying defects at an earlier stage.

However, there are disadvantages of this technique that need to be carefully considered during application.

- The application of the AE technique may be hindered by the attenuation of the signal during propagation and as such the AE sensor has to be as close to its source as possible. This limitation may pose a practical constraint when applying this technique to certain rotating machinery.
- High background noises may lead to difficulties in data collection and interpretation.
- Difficulties in determining the AE source mechanisms when more than one co-exists simultaneously.

2.1.1 Brief history of AE

Dated back in 6500 BC, AE activity was used by potters as an assessment tool to evaluate the quality of their products. AE could provide an accurate indication on whether the ceramics pots were defective or failed structurally. The earliest application of AE was in metal working, termed as "tin cry". The first documentation of this observation was made in the eighth century by Jabir ibn Hayyan. Subsequent observations and experimental work on AE have been detailed in many standard texts, for instance [43].

These earlier observations and experimental work were not further investigated until 1945 to 1950, when Josef Kaiser performed his investigations on the AE phenomenon. The most significant discovery in the AE field was the irreversible AE phenomenon that now bears his name, the 'Kaiser effect'. The 'Kaiser effect' is defined by Holroyd [42] as *'Material does not start to re-emit AE activity until the applied stress exceeds that which it has previously experienced'*. In Kaiser's Doctorate thesis, he also suggested a distinction between burst and continuous type AE waveforms. He further concluded that AE was emitted from (a) frictional rubbing of grains against each other in polycrystalline materials and (b) inter-granular fracture. The contribution of Kaiser's work in AE

investigation and development were presented in the papers by Drouillard [43], Henning [44] and Tensi [45].

The first extensive research into AE phenomena following Kaiser's discoveries was performed by Schofield [43] in United States of American (USA). His research programme was directed towards the application of AE to the field of material engineering. Schofield's work in AE has indeed spurred many researchers towards employing AE as a technique to study the behaviour and problems of engineering materials. The application of AE technique in predicting and locating failure has further expanded in the Aerospace and Nuclear industries [43].

In view of the great potential of AE, working groups in various continents, such as USA, Europe and Japan, were formed to unite and organise the AE communities. The results of the working groups were significant and marked development of AE in these respective areas were achieved: (a) research into the AE phenomenon, (b) application in material research, (c) application in the field of non-destructive testing (NDT), and (d) application in the field of condition monitoring for both structural and rotating components.

The advancement made in the acquisition and instrumentation systems has seen the AE technique popularly employed in diverse applications in industry. Firstly, in the field of NDT, AE is used as an inspection tool to detect and locate defects in pressure vessels, nuclear reactors and piping [46, 47]. Secondly, AE has been widely applied to process monitoring which includes [42, 47]; machining processes (tool wear and breakage), fabrication processes (welding and bond curing) and forming processes (punching, extrusion, and peening). The last most important application is the condition monitoring on large structures such as bridges, aircraft [46, 47] and buildings, to ensure structural integrity. In recent times, although still in its infancy, the application of AE technique is gaining ground as a condition monitoring tool on rotating machinery. A chronology of some of the earlier work is detailed in Holroyd [42]. There are vast opportunities for development of the AE technique on various forms of rotating machinery, including engines, bearings, pumps and gearboxes.

2.1.2 Application of AE to gear fault detection

The research into the application of AE to gear fault detection and monitoring involves studies of AE behaviour and response to typical gear failures, namely surface damage and tooth fracture through either natural or seeded defects or both. Detailed descriptions and discussions of these investigations are presented in this section.

Miyachika et al [48] presented a study on AE in a bending fatigue test of spur gear teeth. Three different gears with common module, pressure angle and number of teeth were used. Two of the gears were case hardened to different case depths. These gears were made from SC415 steel with a face width of 10 mm. The remaining gear (face width of 8 mm) was made from S45C steel without any case hardening. An AE sensor was fixed on the gear via a holder to keep the sensor in place. AE measurements such as raw signals and their frequency spectra, cumulative event count, event count rate and peak amplitude were recorded during the fatigue process under different tooth load conditions. In addition, crack length measurements were made. However, the type and characteristics of the sensor, the sampling rate employed and the loading frequency were not presented in this paper.

During the fatigue test, it was observed that there was marked increased in AE cumulative event count and event count rate just before crack initiation for both case hardened gears. For the normalized gear, such observation was not noted. Miyachika attributed this observation to the noise level ratio of the hardened gears. It was also found that as the tooth load decreased, the number of cycles until the marked cumulative event count occurred increased. Miyachika drew the conclusion that the prediction of crack initiation using AE technique is possible for case hardened gear but difficult for normalised gears.

Miyachika et al [49] extended their investigations into the recently developed super-carburised gear material. The investigation was performed under the same test set and procedures as detailed above, with additional analysis techniques; AE cumulative energy count and wavelet transforms of AE signals. From the results, Miyachika drew the same conclusion as for the hardened gear; the prediction of crack initiation by means of AE method is possible for the various carburised gears tested.

Singh et al [50] explored the AE technique an alternative to the more widely used vibration and debris monitoring methods for detection of gear tooth crack growth. They employed a single tooth bending machine with the load on the tooth varied sinusoidally at 40Hz frequency. An AE sensor and accelerometer were mounted on a spur gear near to the loading tooth. The test terminated when the loaded tooth broke-off. Raw AE waveforms and fatigue cycles were recorded during the test. There was no information given on the type of gear, sensors, the applied load and the sampling rate used. The test revealed that AE detected the first sign of failure when the gear reached 90% of its final life. As the crack progressed, AE amplitude increased. During the final stage of gear tooth fracture, a significantly high amplitude AE burst was detected. On the other hand, the vibration level did not change significantly in the initial stage of crack initiation and propagation until the final stage of failure. Hence, Singh concluded that the AE method offered an advantage over vibration monitoring techniques.

In order to study the practical aspects of sensor placement in a real life gearbox situation, Singh et al [50] performed an assessment of the transmissibility of an AE signal within a gearbox. The tests were performed with different torque levels using Nielsen source technique, i.e. lead pencil breaks to simulate AE activity in the gearbox. Firstly, various individual interfaces with varying torques were studied and quantified. Following that, Singh evaluated the total loss of strength of the AE signal across multiple interfaces and compared with the sum of losses obtained from individual interfaces. Several AE transmission paths were examined. From the results obtained, Singh et al concluded that the attenuation across the gearbox was an accumulation of losses across each individual

interface within the transmission path and the optimum path of propagation will be the one with the smallest cumulative loss.

Wheitner et al [51] performed a series of gear tooth bending fatigue tests to verify the effectiveness of AE and system stiffness measurements for monitoring crack initiation and propagation. The tests were carried out using standard Society of Automotive Engineers (SAE) gear geometry, testing procedures and fatigue test fixtures. The AE sensor had a resonant frequency of 300 kHz and was attached to the gear at the root of the tooth via super glue. The tooth stiffness measurements were done through an accelerometer mounted to the base of the fixture. The test gears were of various materials, surface finishes and surface treatments as detailed in [51]. All the testing was performed by applying sinusoidal load of 10 Hz and load ratio of 0.1. A run-out life of 10^6 cycles was employed for all the test cases. Wheitner et al noticed non-zero AE counts before the initiation point of the gear tooth root fatigue crack which was attributed to the background noise of the test machine. In general, AE activity increased with crack propagation and very rapidly at the failure point. All the test gears exhibited similar trends in stiffness measurements. At high load and low fatigue lives, crack propagation life contributed a significant proportion of the gear total life as compared to crack initiation life. Wheitner went further to conclude that both the AE and system stiffness measurements were effective in monitoring the cracking processes of the gear tooth. However, in most cases, AE activity was detected before the first change in stiffness compliance was registered.

Siores et al [52] explored several AE analysis techniques to correlate possible failure modes of a gearbox during its useful life. The gearbox employed for the failure interrogation included 2 gear sets (input and output), a DC shunt motor and a variable speed controller to alter the motor speed for the tests. The AE sensor employed was mounted on the gearbox casing and had a resonant frequency of 175 kHz. Prior to the start of the test, the gearbox was allowed to wear-in at 1200 rpm for four one-hour intervals at full load condition. Common gear failures such as excessive backlash, shaft misalignment, tooth breakage, scuffing and worn teeth were seeded on the test gears and

gearbox according to the procedures detailed in [52]. All the seeded defect conditions were tested at 300 and 600 rpm with AE r.m.s, standard deviation and duration of AE signal being measured at a sampling frequency of 158 Hz. Siores concluded that the monitored AE parameters exhibited identifying qualities for the respective failure modes.

The literature review [48 to 52] has indicated that the AE technique is able to detect bending fatigue failure and the fault detection was well advance than the vibration monitoring technique. This conclusion is encouraging and motivating for AE technique to be the new condition monitoring tool. However, to ensure that this technique is robust, the defect detection capability on the other modes of gear failure; surface damage and surface fatigue, has to be explored.

Singh et al [53] performed two experiments to study the feasibility of applying AE to detect gear pitting. Both simulated and natural pits were used to evaluate this detection technique. The first experiment employed an UH1H generator drive offset quill which consisted of the driver, driven and idler gears. In this experiment, the idler gear contained a simulated pit of same width and depth of 1.25 mm. This pit was simulated by removing a thin strip of material from the pitch-line on one of the teeth of the idler gear by an Electrical Discharge Machining (EDM) process. An AE sensor with a resonant frequency of 280 KHz and an accelerometer were mounted on the gearbox housing near the output shaft bearing. A tachometer was used as a trigger to ensure each cycle of the measurements started with the same idler tooth in contact. The test gearbox was first run with no pit on the idler gear and then replaced by the idler gear with simulated pits. AE and vibration data were recorded during the run. This procedure was repeated for several combinations of load and speed. From the test results, Singh concluded that both detection techniques were able to pick up the simulated defect but the AE technique exhibited much greater signal to noise ratio (SNR). He also suggested that neither detection techniques was able to detect the simulated pit at extremely high speeds or unloaded conditions as the noise level increases whilst the amplitude of the defect signal arising from contact of the pitted region decreases.

Singh [53] performed a second experiment using a back-to-back gearbox to study the detectability of natural pits. Similar acquisition systems to the first experiment were employed with both the AE sensor and accelerometer mounted on the housing of the test gearbox. The input speed to the gearbox was 1775 rpm with an unknown torque loading. During the early stage of the test, there were no defects on the mating gear tooth surfaces and the signals (both AE and vibration) showed no significant peaks above the operational noise level. After 30 minutes of operation, pits started to develop on the pinion teeth and periodically occurring peaks were observed from the AE signals. A further 15 minutes run saw pitting on multiple teeth and the detected AE signals revealed more frequently occurring peaks above noise level. There was no visible peak noted for the accelerometer signal. During the test, the AE sensor was also placed on the slave gearbox housing and bearing location between the two gearboxes to assess the detectability of the natural pits from these locations. Singh concluded that the AE sensor should be as close to the monitored part as possible in order to maximise the detection capability of pits using the AE technique.

Raad et al [54] illustrated the application of the AE monitoring technique for gear fault detection using an industrial gear rig. No information on the gear test rig, applied torque and speed were given in this paper. The experiment was performed above the rated load of the gears for two weeks until near breakage of two teeth. Various types of AE sensor (resonant and wide band) and accelerometers were mounted on the bearing. Signals were recorded at regular intervals and visual inspection of gears was performed at the end of each day. The recorded AE and vibration data were analysed using four different methodologies: visual comparison, Kurtosis, spectral density and envelope analysis. The visual comparison revealed that AE bursts appeared coincidentally with spalling. However, these AE bursts disappeared after the defect was established. There was no clear indication from vibration signatures. The Kurtosis values for all teeth revealed the spalling defects as there was an increase in amplitude after 3000 cycles. However, this method was unable to localise the spalling defect to individual tooth. The first sign of spalling observed from the vibration technique was at 5000 cycles. Using the spectral density analysis method, the increase in energy before and after the spall detection was

common to both AE and vibration signals. In the final analysis of the AE and vibration signals, the spectrum of the squared envelope was used. Vibration technique was able to pick up the defect by displaying peaks at twice the shaft frequency. However, these peaks were not present in the AE spectrum until the logarithm of the squared envelope was employed. The observed peaks occurred at the same frequency for both AE and vibration techniques. Raad concluded that this first evaluation of AE as a condition monitoring tool was promising.

Sentoku [55] presented an investigation on tooth surface failure caused by repeated gear revolution with AE measurements. A power circulating type gear testing machine was employed. The testing machine consisted of a pair of test and power return spur gears with a forced lubrication system that supplied oil directly to the engaged teeth surfaces from the side of the gear pairs. It is important to note that the oil temperature was maintained constantly at 40±2 ^{0}C. This eliminated the effect of oil film thickness on AE activity. An ultra-compact AE sensor of resonant frequency 350 kHz was mounted on the gear wheel using screws. The AE signal was transmitted from the sensor to the data acquisition card via a mercury slip ring. A strain gauge was also adhered to the tooth root to correlate the extracted AE parameters with tooth root strains. During the tests, the roughness of the gear tooth surfaces and pitting size were measured at regular intervals.

The first test was performed under an applied stress of 960 MPa and pinion speed of 992 rpm using hardened gears. From the results obtained, Sentoku observed no change in AE amplitude except the unevenness of AE wave lines were smaller with increasing number of cycles. At this stage of test, no surface damage was noted. Subsequently, Sentoku performed a second test using heat treated ground gears. During the early stage of the test, both AE amplitude and the pitting area ratio remained unchanged. However, when pitting on the three monitored gear teeth began, AE wave lines started to change. Subsequently, AE amplitudes increased with both the pitting area ratio and the numbers of cycles. Sentoku explained that the increase in AE amplitude was caused by friction due to increasing pitting. Similar observations were noted for AE energy. Hence, with the

results obtained from the test, he drew the conclusion that the AE technique is able to detect gear tooth pitting.

Badi et al [56] performed an investigation on usage of AE and vibration monitoring techniques for condition monitoring of a typical drive-line. Their test rig comprised a drive and simple spur gearbox, loaded by a pneumatically operated brake disk. The rotating components were connected by flexible couplings and supported by bearing blocks. The rig was instrumented with both accelerometers and AE sensors at several locations along the drive line. However, Bali only reported the results from the sensor which gave the optimum location for fault detection. Seeded defects such as "blip" and "shaved" gear faults were introduced on the test gears to simulate scuffing and pitting defects on gear teeth. There was no further information on the testing procedures used in this experiment. Analysis techniques such as Crest Factor and Kurtosis were employed to compare the faulted gears and reference gear (with no seeded defect) for both AE and vibration techniques. For the "blip" gear fault, both monitoring techniques were able to identify the defect through the analysis techniques employed. As for the "shaved" gear fault, only the AE technique was able to detect the defect. Badi concluded that the analysis techniques used were ideally suited for identifying faults of an impulsive nature. However, for a more comprehensive methodology, other analysis techniques should be explored.

Tandon and Mata [57] performed seeded defect tests on spur gears using IAE gear lubricant testing machine to assess the fault detection capability of the AE technique and make comparison with the more widely used vibration technique. Both hardened and ground spur gears were employed for the tests. The test gears were lubricated by a jet of oil. Load was applied to the testing machine through an arm where weights could be added. The AE sensor and accelerometer employed had resonant frequencies of 375 and 39 kHz respectively. Both the AE and vibration signals were measured close to the bearings of the test gearbox. All the tests were carried out at a single speed (1000 rpm) and varying load conditions (0 to 10 kg). AE and vibration measurements were first taken for gears that have no seeded defect, which were treated as reference signals.

Subsequently, a simulated pit of constant depth (500 μm) and variable diameter (from 250 to 2200 μm in incremental order) was introduced on a gear tooth pitch-line by spark erosion. From the tests, Tandon and Mata made the following observations: (a) there was some increase in AE with increase in load. (b) AE parameters increased as the defect size (diameter of pit) increased. (c) AE (ring-down) counts showed slightly better results than other AE parameters measure. (d) The AE technique detected the seeded defect at smaller size (500 μm) than the vibration technique (1000 μm). (e) In general, the distribution of AE events, counts and peak amplitude became broader due to the presence of a defect.

Al-Balushi and Samanta [58] introduced an energy-based feature extracted from AE signatures for monitoring and diagnosing gear faults. This feature, termed energy index (EI), was defined as the square of the ratio of the r.m.s value for a segment of the signal to the overall r.m.s value of the entire signal. Various different forms of EI were derived and compared with existing statistical methods for early fault detection was reference to experimental work on a back-to-back spur gearbox. Three miniature ultra-sound transducers were implanted onto the rolling element bearing adjacent to the gear wheel for collection of AE data. A triggering system was used to ensure that all the acquired data had identical starting locations on the gear. The tests were performed using brand new gears and terminated after 40 hours when the gear failed. AE signals were acquired for 1 rev of the test gear at hourly intervals. However, information such as the characteristics of the sensors, the applied load and the reason of the varying rotational speeds were not mentioned. Al-Balushi and Samanta illustrated that the proposed EI and the various derived forms were able to locate the broken and pitting teeth more effectively than the traditional Kurtosis and Crest Factor methods. By employing the proposed analysis technique, the defective tooth was picked up in a helicopter gearbox via analysis of the gearbox vibration data.

While exploring the applicability of the AE technique to gear health diagnosis, Toutountzakis et al [59] made some interesting observations of AE activity due to misalignment and natural pitting. The test was performed on a back-to-back spur gearbox

with the AE sensors placed on the pinion and bearing casing of the pinion shaft. The AE sensors used had a relatively flat response in the region between 150 and 750 kHz. A silver contact air-cooled slip ring was employed to transmit the AE signal for further processing. AE parameters such as r.m.s and energy values were recorded during the tests. Prior to the test proper, AE measurements for defect free gears were firstly recorded. As the rotational speed increased, measured AE parameters increased for both AE sensor locations. Furthermore, Toutountzakis et al observed that change in speed resulted in changing AE parameters. During one of the tests, they noted increasing AE r.m.s (at the pinion location) for 6 hours before the test was paused for inspection. The results of the inspection revealed signs of pitting and scuffing which indicated a misalignment in the gearbox. The gearbox was reassembled and the test continued. An interesting observation was made: "A reduction in AE parameters was noted initially, but these values gradually increased to values which did not depart from the initial gradient of the increasing trend." Toutountzakis et al concluded that there is potential application of the AE technique for gear health diagnosis.

The observations and results of the papers discussed above [53 to 59] can be summarised as follows for both the seeded and natural gear surface defects, i.e. pitting:

(a) The AE technique can detect pitting in advance of the vibration condition monitoring technique.

(b) It is possible to detect a gear tooth surface defect with the AE sensor mounted on the bearing or gearbox casing. However, the defect detection capability will be further improved if the AE sensor is placed as close to the source as possible since attenuation can pose a problem to the effectiveness of AE detecting the defect.

(c) In general, AE activity such as r.m.s increases with increasing pitting, defect size and numbers of cycles.

(d) There is a change in AE activity level when there is a change in rotational speed or applied load.

Hence, through the various seeded and natural defects tests, researchers have been able to demonstrate the ability of AE technique to detect the two most common but critical types of gear damage; tooth fracture and surface damage. In order to ensure this technique is robust and applicable for operational gearboxes, investigation into the fundamental relationships between AE measurements, gearbox operating parameters and contacting gear teeth surfaces must be considered.

2.1.3 Relationship between AE, contacting surfaces and wear

The work reviewed in the previous section revealed insufficient research into the source mechanism of AE during gear mesh, and the effect of gearbox operating parameters on AE activity. For this technique to be robust enough for real world applications, these fundamentals should be investigated and understood. With this consideration in mind, a brief review is presented in this section.

Boness et al [60] noted that AE source mechanisms during wear included asperity contact, micro-crack initiation and growth, plastic deformation and flow which are the basic wear mechanisms. Furthermore, Boness et al stated that the rubbing together of surfaces was a continuous process and, as such, the AE signature will be predominantly continuous with superimposed AE burst attributed by the rapid high-amplitude events. Such an event can be contributed by a single asperity fracture. Boness at al [60] measured AE for dry and lubricated contacts under pure sliding conditions. Tests with a full elastohydrodynamic film between highly polished surfaces did not generate any AE activity above the electronic noise of the acquisition system, inferring that asperity contact was the prime source for AE. Boness also observed the irreversibility of the AE signal; when a sliding contact was terminated and restarted, the AE r.m.s value returned to its previous running value. This observation was also noted by Toutountzakis et al [59]. Based on the observations that integrated AE r.m.s signal varied directly with wear volume, Boness proposed an empirical relationship to correlate them [60, 61]. In a separate report on the same study, Boness et al [61] varied the ratio of film thickness to

the composite roughness of the surfaces, λ, to observe the relationship between film thickness, wear and AE activity. It was observed that increasing the λ values resulted in a decrease of AE r.m.s. This observation suggested that, as film thickness increases, less asperity contacts were encountered between the meshing surfaces, thus decreasing the AE r.m.s activity levels. Furthermore, no wear was observed for λ values greater than 0.93, however, AE r.m.s was detected up to a λ value of 1.26. These observations confirm the sensitivity of AE measurements for detecting asperity contact.

Sarychev et al [62] investigated AE in friction contact and the effect of surface roughness, sliding speed and applied load on AE activity. AE and friction can be related through the elastic interaction between micro-asperities of the contacting surfaces, and the formation and destruction of friction bonds due to the friction contact. The results from Sarychev's work revealed that AE activity increased with sliding speed in a greater magnitude compared to increase by increasing applied load. In relating AE to sliding friction and wear, Jiaa and Dornfeld [63] showed that under steady state, the AE r.m.s signal increases with increasing applied load and sliding speed. In addition, AE activity is also affected by the friction coefficient. By combining the work of Dornfeld and Diei, Jiaa et al proposed a power function relation between AE r.m.s and the rate of frictional energy dissipation [63]. The observations made by Sarychev and Jiaa were further strengthened by Mechefske and Sun [64]; (a) more AE activity during poor lubrication between the sliding surfaces, this infers that asperity contact is the prime source of AE, and (b) greater sliding speed produced higher AE r.m.s level since AE signal intensity is proportional to strain rate.

During spur gear experiments, Smith [65] noted transient shock pulses during gear mesh at the gear mesh frequency. It was concluded that these shocks were attributed to asperity contact and were termed 'Smith shocks'. Whilst a single asperity model was presented as the probable cause of the shocks, the likelihood of such a scenario in practice is low, since multiple contacts will be present. However, it was shown that based on an asperity width of 5 μm and sliding and rolling velocities in the order of 500 mm/s, the rise time for such a transient event was 10 μs. It must be noted that the sensors employed by Smith

had a natural frequency of 50 kHz, outside the range of AE. But with rise times of the order detailed, or less than 10 μs, higher frequencies will be excited, particularly within the AE range.

Clearly, based on the various researchers' work in relating AE to contact surfaces and wear, the following conclusions can be made:

- The prime source of AE activity is asperity contact
- AE activity increases with increased wear
- AE activity increases with increasing sliding speed and applied load
- AE activity is sensitive to friction
- AE signature from contacting surfaces consists of continuous type waveform with a burst type waveform superimposed
- AE activity level resumes its previous level when the contacting surfaces producing the AE activity were terminated and restarted under identical operating conditions

2.2 Vibration technique for gear diagnostics

The application of the vibration technique to defect diagnostics and condition monitoring to mechanical equipment and rotating machinery has a long history. However, in the past quarter of a century, due to the development of Helicopter Health and Usage Monitoring Systems (HHUMS), much research has been devoted to the application of vibration techniques for helicopter drive-train and gearbox components. In this section, a review of the various vibration analysis techniques and their capabilities in damage detection will be detailed.

2.2.1 Development of vibration diagnostics on helicopter gearboxes

The objective of the various vibration analysis techniques is to ensure that changes in the vibration signals collected via the accelerometers mounted on the gearbox housing are able to provide information about the condition or health and the gearbox. The difficulty in achieving this objective is the ability of the various techniques in differentiating a damaged component in the gearbox from the changes caused by varying operating conditions. Initially, the research interest in gearbox damage detection lay in the area of analysis of vibration signals using available signal processing tools. In the mid 1970s, statistical characteristics of the signals in the time domain were the focus of study [66]. Statistical damage detection methods are the traditional techniques, which are based on the statistical measurement of the energy of the vibration signals. Stewart's investigation into changes of gearbox vibration signals due to gear damage and McFadden's basic mathematical model of gearbox vibration signals formed the foundation of this technique. This technique correlates features extracted from the vibration signals to particular types of gearbox damage. Stewart, Martin and NASA derived various statistical indicators [66] from these features root mean squared (r.m.s), Crest factor, Kurtosis, FM4. The listing, theory and characteristic of these indicators are presented in [66 to 68]. Since the introduction of the Fast Fourier Transform (FFT), the vibration signals in the time domain can be transformed into the frequency domain. In the frequency domain, a whole range of characteristic components such as harmonics of tooth mesh frequency and sidebands can be observed from a gearbox spectrum. The characteristic components have been classified and correlated to various gearbox damages [68]. Analysis methods such as base-band spectra, narrow-band, demodulated spectra and Cepstrum have been employed in the diagnostics of gearbox defects.

In the late 1980s, because the statistical damage detection methods were unable to capture transient phenomena produced by local gear defects, researchers began to investigate time-frequency analysis methods. In general, gearbox vibration signatures consist of three major components: (a) a sinusoidal component due to time varying load, (b) a broad-band impulsive component due to impact and (c) random noise. In an

undamaged gearbox, the sinusoidal components dominate and are most visible in the time domain. As damage propagates through the gearbox, both the broad-band and random noises (most visible in the time domain) dominate the sinusoidal components which exhibit both modulation and amplitude reduction. Hence, the application of joint time-frequency analysis methods will provide all the important information on gearbox diagnostics in both domains which the statistical methods failed to do. Some examples of the time-frequency analysis methods are Wigner-Ville Distribution (WVD), spectrogram and Power Spectrum Density (PSD) [66, 68, 69]. Wavelet analysis in general can be classified under the umbrella of a time-frequency analysis method. The wavelet analysis method allows frequency content of the signal and time domain information to be analysed simultaneously without the interference of cross-terms that are usually present in the WVD and spectrogram analysis methods. The two widely used wavelet analysis are the continuous wavelet transform (CWT) and the discrete wavelet transform (DWT).

With the increased interest in time-frequency analysis methods, model based gearbox detection techniques also began to appear. The research into the model based damage detection methods primarily focused in the application of neural networks and time-series analysis. The model based techniques offered a very different approach compared to the above mentioned methods. The fundamental idea of these techniques is to train to a system to recognise healthy gearbox signals, deviations from these signals and determine the type of damage in the gearbox. Neural networks are defined as a massively parallel distributed process that is able to obtain knowledge through learning processes, retain the knowledge and apply it as required. In general, a neural network damage detection system does not process the vibration signal by itself. The network utilises the results from other damage detection techniques and learns the behaviour of each technique in both the healthy and damaged condition. This thus allows the network to take advantage of the strengths of each of the techniques. There are two standard neural network architectures commonly employed in the field of gearbox diagnostics; self organising map (SOM), feed-forward back-propagation network and a hybrid of both networks [66, 69].

Time-series analysis diagnostic technique differs from the neural network damage detection technique through the form of which the data is input. Time-series analysis processes the vibration signal directly. There are two primarily time-series analysis techniques that have been applied to gearbox diagnostic; autoregressive modelling (AR) and autoregressive moving average modelling (ARMA) [66]. Although these techniques received little attention in the gearbox diagnostic world, the ability to detect defects and compensate for changes in gearbox operating load has indeed raise interest in the research world.

The emerging technologies of gearbox damage detection can be divided into two areas. The first is vibration technique based adaptive signal processing, which combine both model based and joint time-frequency signal processing techniques for damage detection. The second is a system which combines output from various types of sensors, such as accelerometers, acoustic emission sensors and oil debris sensors. This technique can be realised through the usage of data fusion where output for the multiple diagnostic algorithms is processed. This multi-dimensional damage detection analysis technique may potentially offers more accurate diagnosis and lower false alarm rate.

2.2.2 Effect of surface damage on gear tooth stiffness and vibration characteristic

Drosjack and Houser [70] proposed a model to predict the vibration of a gear system when a single pit occurs at the pitch-line of a single gear tooth. The model was developed based on the assumption that pitting is represented as the combination of a change in stiffness due to modification of the Hertzian contact zone and an impulsive reaction at the mesh caused by velocity difference before and after loss of contact between the gear pair. The modelling procedures were proven to able to predict changes in the vibration of the gear system and correlated well with the experimental results of the simulated pitch-line defect tests. Yesilyurt et al [71] stated that tooth damage will cause a reduction in gear tooth stiffness, and that the extent of this reduction can be used to assess the severity of

the tooth damage. A model was developed and vibration analysis technique was employed for damage detection and assessment since accurate measurement of tooth stiffness is extremely difficult. In order to asses the effectiveness of this model, experimental work was performed through test gears of different face width simulating different gear tooth stiffness. The experimental results revealed that tooth surface wear caused near linear reduction of gear tooth stiffness with time. Hence, Yesilyurt et al concluded that gear tooth surface damage altered the gear vibration characteristic through reduction in tooth stiffness and deviation of tooth involute profile with the latter contributing the more significant effect. In the same field of investigation, Choy et al [72] proposed a model to simulate and analyse the effect of gear surface damage on the vibration of a gearbox system. This model employed the concept that gear surface damage alters the gear mesh stiffness through changes in its phase and magnitude. In addition, a frictional effect was introduced into the model since gear tooth surface roughness changes with the severity of the damage such as pitting. Finally, experimental results from a gear fatigue test rig were used to evaluate the proposed model.

In summary, the presence of gear tooth surface damage will change the stiffness and vibration characteristic of the gear through (a) modification of the Hertzian contact zone, (b) impulsive reaction between the pair and (c) alteration of the gear tooth involute profile.

2.3 Spectrometric Oil Analysis (SOA)

SOA has been routinely used for or elemental analysis of wear metals, contaminants and additives in lubricating oil of rotating machinery for more than 50 years [73]. The principles of spectroscopy can be dated back 400 years to Newton. He observed that sunlight is divided into spectral colours when passed through a glass prism. This discovery is still the operational basis of all modern spectrometers. Since Newton's discovery, continuous research has resulted in the first spectrographic instrument in the 19th century. Between 1826 and 1860, researchers, such as Talbot, Herschel, Bunsen and

Kirchhoff, discovered and recommended the usage of spectroscopy methods to determine the presence of specific elements in a sample. The historical developments of the spectrometers and spectroscopic methods are detailed in [73]. The application of the SOA technique in condition monitoring of helicopter rotating components, such as engines and gearboxes, can be dated back 30 to 40 years [74]. The US Army has since employed the SOA technique under the Army Oil Analysis Program (AOAP) to monitor the condition of aircraft and helicopter components. The AOAP later developed into Joint Oil Analysis Program (JOAP) which is used by all three services of the USA.

The advantage of using SOA is that it can detect both magnetic and non-magnetic particles and their respective concentrations so that diagnostic action can be carried out. At some instance, it would be possible to identify the source of degradation when uncommon elements such as silver are present. This may lead to identification of trouble area of a particular part of the monitored component [75]. Another benefit of the SOA technique is the ability to identify defects where chemical reactions were involved such as corrosion and oxidation. However, SOA technique does have its limitations as it detects only small particles. It could not possibly detect catastrophic failure and failures that entailed release of large particles that SOA technique could not detect [75].

The basic idea of spectrometry is to excite the wear particles in the oil sample through heat or radiation; and the wavelengths emitted or absorbed by the various wear elements within the oil sample can be identified and quantified. Some common elements which are present in a gearbox that the SOA technique can detect are; Iron, Copper, Magnesium, Silicon, Silver and Carbon. The various types of spectrometers [73, 76, 77 Chapter 15] using different SOA techniques are listed below and are typically capable of detecting wear particles of less than 10 μm [74]. The advantages, disadvantages and the capabilities of the SOA technique and spectrometers are also entailed in [73, 76, 77 Chapter 15 and 78].

(a) Atomic Emission Spectrometer (AES)

(b) Atomic Absorption Spectrometer (AAS)

(c) Inductive Coupled Plasma (ICP) Spectrometer

(d) X-Ray Fluorescence (XRF) Spectrometer

(e) Rotating Disc Electrode (RDE) Spectrometer

2.3.1 Normalising SOA data

The concentration of elements measured using SOA is usually in term of part-per-million (ppm). Equations 2.1 and 2.2 provide the definition of ppm in 10^6 g or 10^6 ml of sample; depending on whether the oil sample is measured in term of mass or volume respectively.

$$ppm = (mass\ of\ element\ in\ sample(g)/mass\ of\ sample(g)) \times 10^6 \quad (2.1)$$

$$ppm = (mass\ of\ element\ in\ sample(g)/volume\ of\ sample(ml)) \times 10^6 \quad (2.2)$$

The rate of wear of a particular element can be measured in terms of the gradient of the absolute elemental concentration against time. This slope can indicate a potential fault or abnormal wear condition if it becomes steeper. For preventive maintenance, this slope is usually used as a limit (rate-of-change limit) to trigger necessary maintenance action [79]. For components where the nature and history of previous wear/defect and wear behaviours were known, it is standard practice to set a threshold limit based on either percentage or statistically derived absolute change from a normal baseline. When this threshold is exceeded, a warning or alarm would alert the operator that the condition of the component warrants investigation. However, it is important to note that this threshold limit is only applicable to a given component in a given application or on a group of similar components [79].

According to the JOAP manual [75], for accurate trending of the SOA indicators. the effect of the time that has elapsed since the last sampling and the periodic fluid change, loss or addition must be taken into consideration.

During normal operation, lubricant is lost through many means such as leakage, vaporisation, misting, combustion and maintenance actions. The lost lubricant takes with it part of the wear debris information needed for trending. Any new volume of lubricant will dilute the concentration of the wear debris in the system. Normalisation of the SOA data to compensate for fluid loss and dilution can be achieved by employing the method proposed by Fitch [80]. Also, small variations between the sampling intervals can result in inaccurate trending. Since wear debris is produced in a continuous manner and the sampling intervals will not always be exactly the same, standardisation of the SOA data to a standard sampling interval becomes important if the wear debris generation rates are to be fairly compared. This fair comparison would assist in determining the severity of the component's wear condition. By combining the two factors discussed above, Davis [79] proposed the following equation to normalise the SOA data.

$$X_{normalised} = \frac{X * t_1}{(1-(\frac{v}{V})) * t_0} \tag{2.3}$$

Where X = measured concentration of the element of interest

$X_{normalised}$ = normalised elemental concentration of the interest element

t_1 = actual elapsed time between samples

t_0 = nominal elapsed time between samples

V = total system oil volume

v = volume of oil added since last sampling

3 EXPERIMENTAL METHODS

3.1 Experimental Gearbox

The gearbox employed for the experimental programme was a back-to-back type consisting of a pair of slave gears and test gear, connected by two parallel shafts. A metal coupling was used to connect the slave and test gearboxes on the motor input side. On the power return shaft side, two loading plates were employed. Torque was applied by rotating the loading plates against each other, thus twisting the shafts via the torque loading bolt [81] (see figure 3.1). An electric motor was used to run the gearbox. Once the gearbox has run up to operating speed, the driving motor compensates for the power losses in the system only, while the test gears can be operated under very high load. This type of gearbox is employed typically for gear fatigue tests. The gearbox employed for the experimental work was designed and fabricated at Cranfield University. The design details of this gearbox and its sub-components were presented in [81].

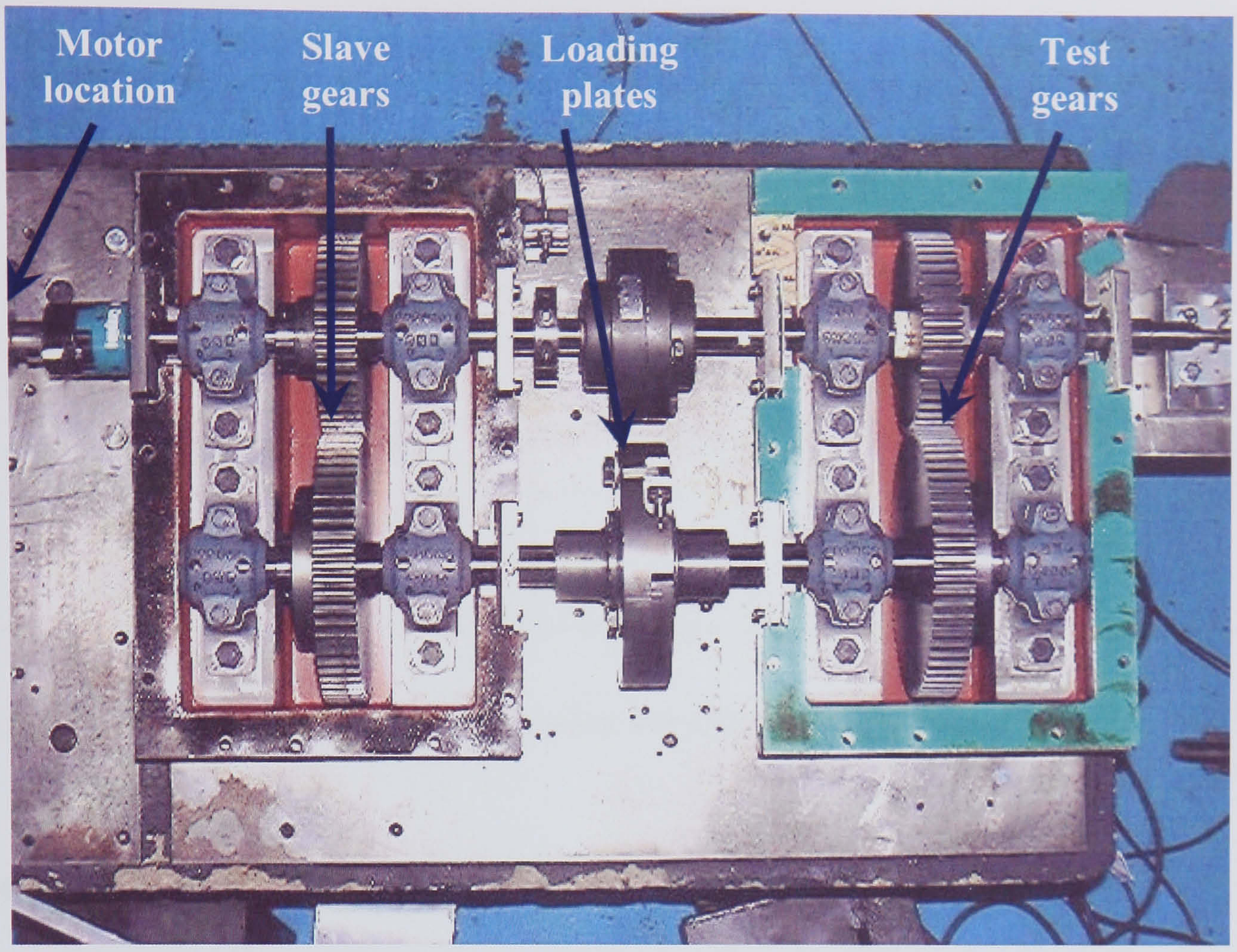

Figure 3.1 Back-to-back gearbox

3.1.1 Gears

The spur gears used for the experiment were manufactured by the HPC Gears Limited, and were made from 045M15 steel without any heat or surface treatment. The pinion (or driver gear) and wheel (or driven gear) had 49 and 65 teeth respectively. The contact ratio and centre distance between the pinion and wheel were 1.77 and 171 mm respectively. The pinions came in two face widths; 15 and 30 mm, where the smaller face width pinion was employed for the accelerated gear fatigue tests. The rest of the tests were performed using 30 mm face width pinion. Table 3.1 provides the detailed specifications of the gears.

	Pinion	Wheel
Number of teeth	49	65
Pressure angle	20°	20°
Pitch circle diameter	147 mm	195 mm
Face width	15 and 30 mm	30 mm
Module	3 mm	3 mm
Hardness (measured)	137 Hv30	137 Hv30
Surface roughness in radial direction (measured)	1.3723 μm	1.3723 μm

Table 3.1 Specifications of spur gears used for the experimental work.

3.1.2 Electrical Motors

Three single speed Alternating Current (AC) electrical motors were used to power the back-to-back gearbox. The rated power and operating speed of the motors are specified in table 3.2. The operating speeds of the gearbox were measured at the input shaft using a tachometer with 1 rpm accuracy.

Electrical Motor	Rated running speed	Rated power
A	2820 rpm	2.2 kW
B	1425 rpm	0.55 kW
C	690 rpm	1.1 kW

Table 3.2 Running speed and power rating of the electrical motors.

3.1.3 Lubrication

For the accelerated gear fatigue test, mineral oil (TMC 20W-50) was used as the lubricant for the test gears in an attempt to accelerate the pitting wear on the gear teeth surfaces. For other tests, multi-grade Extra-Pressure (EP 80W-90) oil with additives was used to keep natural pitting and wear to a minimum level. The properties of the two lubricants are listed in table 3.3.

The back-to-back gearbox employed splash lubrication. This method allows the rotation of the gears to splash the oil around the gearbox and thus lubricate the gears. Drago [24] provided a general guideline that this method of lubrication is only suitable for pitch-line velocities of less than 25.4 m/s. The maximum pitch-line speed employed for this project was computed to be 21.7 m/s. Hence, it was deemed that splash lubrication is sufficient and appropriate for this experimental purpose.

Lubricant properties	**Castrol EP 80W-90**	**TMC 20W-50**
Kinematics viscosity (mm^2/s)		
@ 40°C	132.0	136.0
@ 100°C	13.9	17.0
Viscosity index (VI)	101	136
Density @ 15°C (g/cm^3)	0.893	0.888

Table 3.3 Properties of the lubricants.

3.1.4 Loading plates

The loading plates were located between the wheels of the slave and test gearboxes (see figure 3.1). The loading plates consisted of two half coupling flanges with one of the flanges having a threaded hole. Torque could be applied to the system by tightening or loosening a bolt into or out of the threaded hole. This simple mechanism allowed the pair

of coupling flanges to be rotated relative to each other and so lock torque applied to the system. Using a strain gauge rosette connected in Wheatstone half-bridge configuration, Vayionas [81] has determined that the maximum applied torque in this system is 267 Nm. A verification torque measurement was performed prior to the start of the experimental work. Using the same principle but employing fibre optic rather than strain gauge for torque measurement, the maximum applicable torque was determined to be 257 Nm which deviated approximately 3.7% from the previous measurements. The details and results of the applied torque calibration are presented in Appendix A.

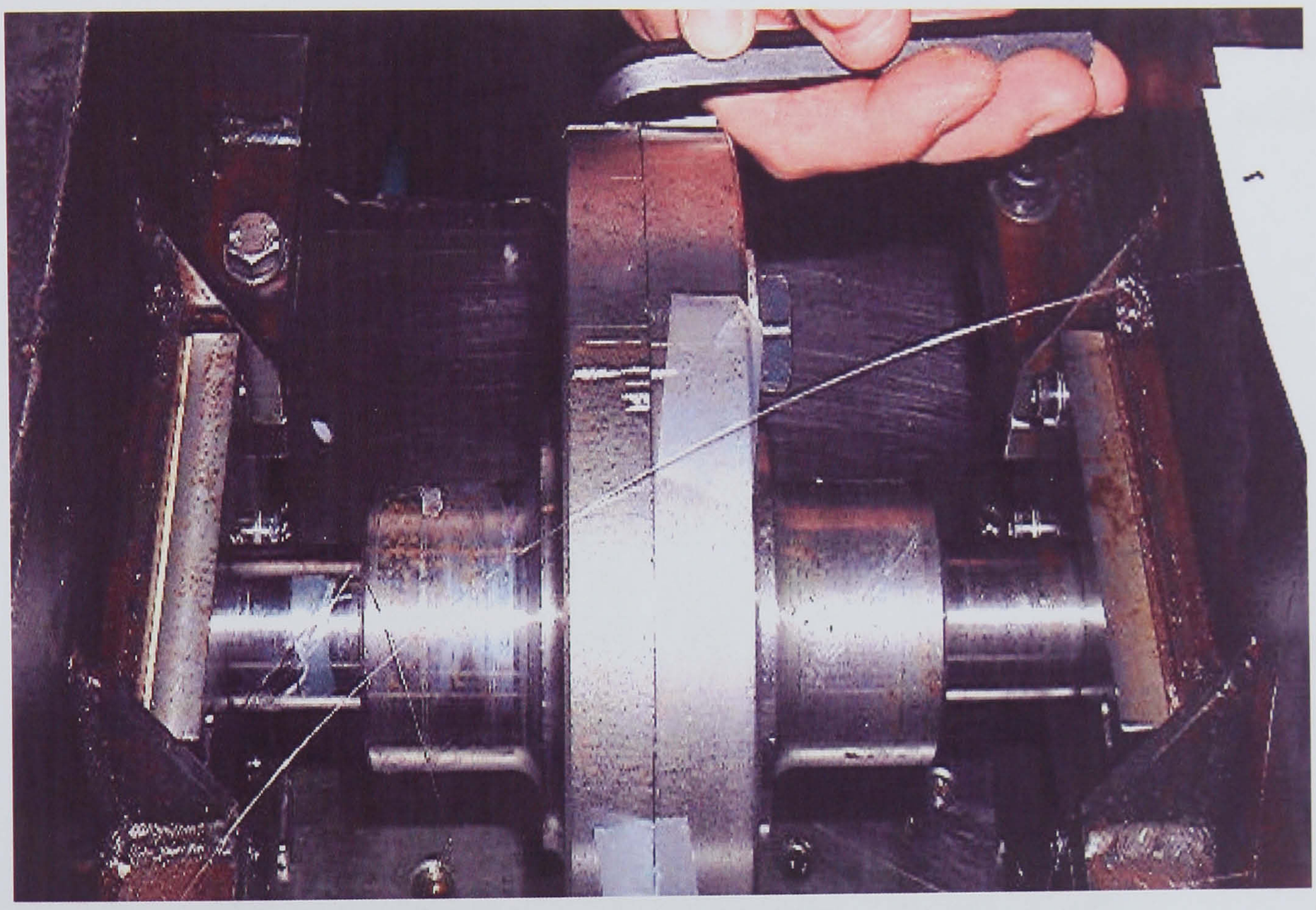

Figure 3.2 Applied torque measurement and calibration through fibre optics.

3.2 *Instrumentation*

3.2.1 AE Sensors

Two AE sensors from Physical Acoustic Corporation (PAC) were employed for this experimental work. For the seeded defect tests, a miniature sensor (Nano 30) was used. The operating frequency of this sensor is between 125 and 750 kHz. For all other tests, a wideband type sensor (WD) with operating frequency between 100 to 1000 kHz was employed. During tests, the AE sensors were mounted on both the pinion and the pinion input shaft bearing housing. The sensors were held in place with strong adhesive superglue (see figure 3.3).

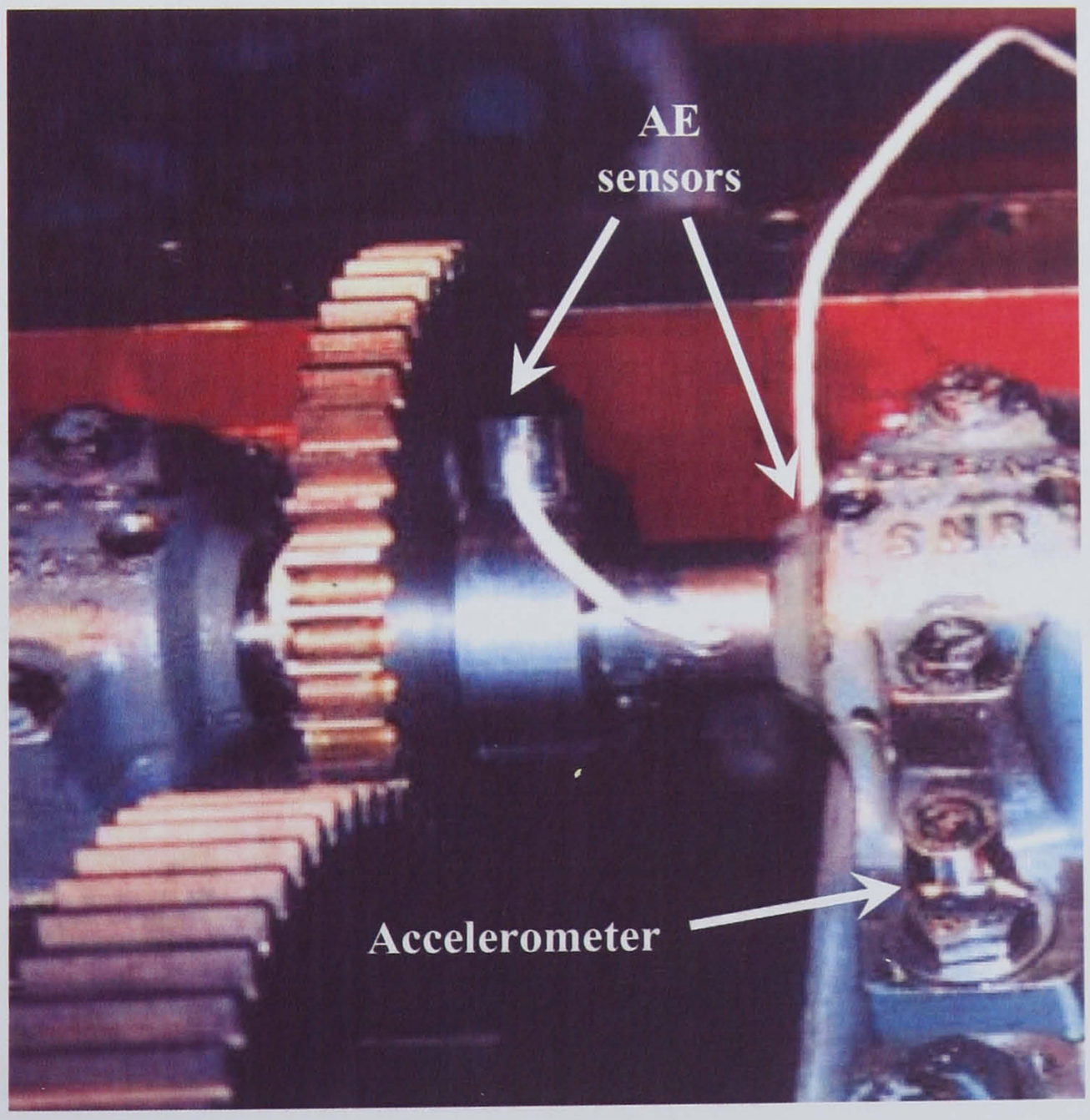

Figure 3.3 Locations of the AE sensors and accelerometer.

3.2.2 Slip ring

A PH-12 silver contacts slip ring (12 channels) made by IDM Electronics Ltd was used to transmit the AE signals from the AE sensor mounted on the pinion to the data acquisition board. The slip ring was connected in line with the input shaft of the gearboxes at the end of the test gearbox, figure 3.4. Compressed air was supplied to reduce the slip ring contact temperature in operation and to keep the contacts clean. The air supply flow rate employed was 1400 kg/mm^2 as specified by the manufacturer.

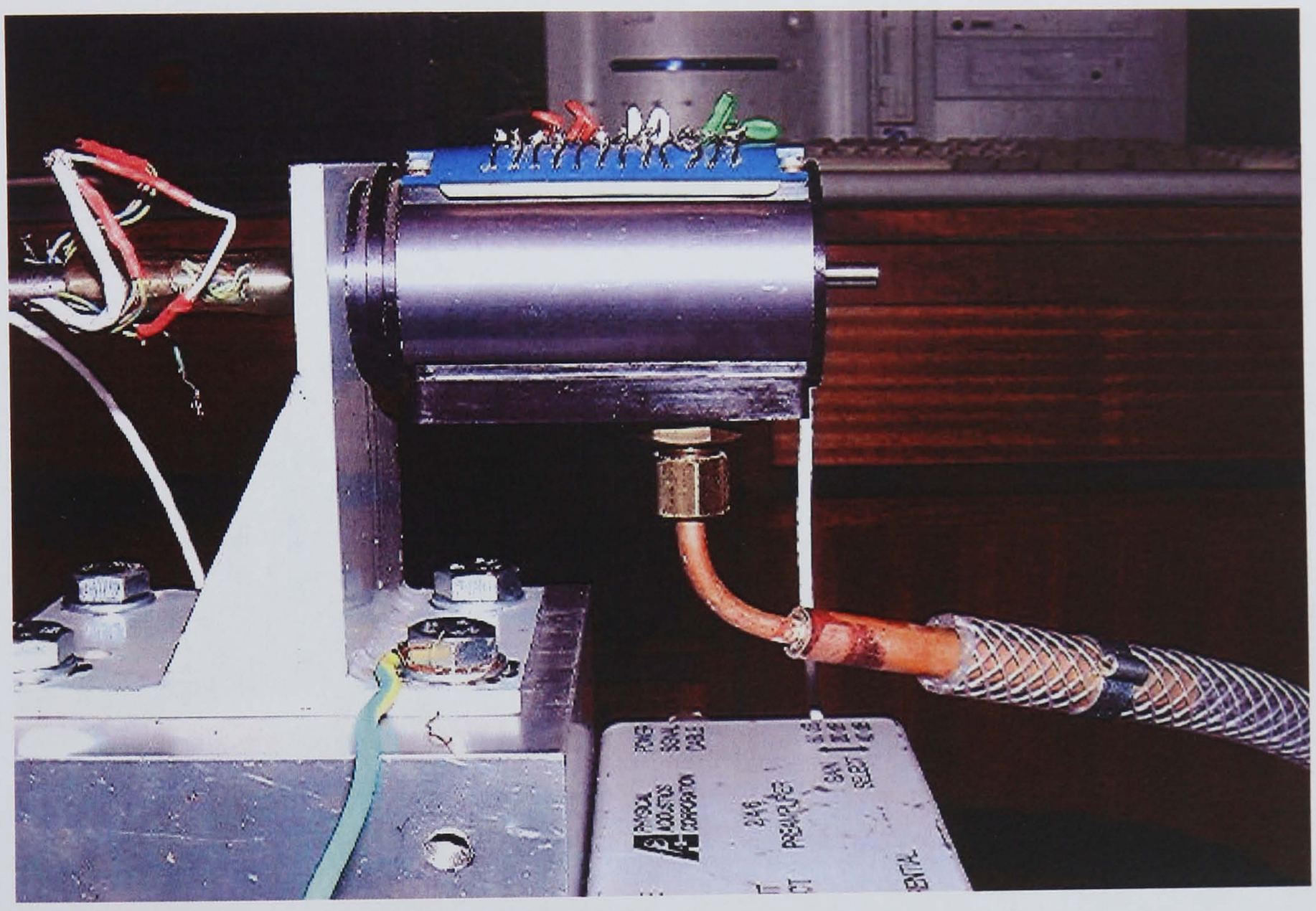

Figure 3.4 Slip ring, slip ring mounting and attached compressed air tube

3.2.3 Pre-amplifier

The PAC preamplifier has three gain settings (20/40/60 dB), plug in filter and both single-ended and differential sensor inputs. The AE signal output from the pre-amplifier was connected via BNC or coaxial cable directly to the data acquisition card.

3.2.4 Trigger sensor

The trigger sensor consisted of a light source and receiver, and a metallic disc with 2 mm diameter hole. The trigger sensor was attached between the end of the input pinion shaft and the slip ring (see figure 3.5). Once every revolution, when the light receiver detected the light from the light source through the hole, a pulse signal was generated and the trigger activated. The trigger sensor was important during the seeded defect study and accelerated gear fatigue tests. During the seeded defect study, this trigger mechanism acquired AE data only from the portion of the pinion gear tooth where the defect was located. The trigger mechanism was set such that the defective gear tooth was at the mid point of the acquisition window. In the accelerated gear fatigue tests, the trigger sensor was connected to a cycle counter so that the gear fatigue life in number of cycles could be monitored.

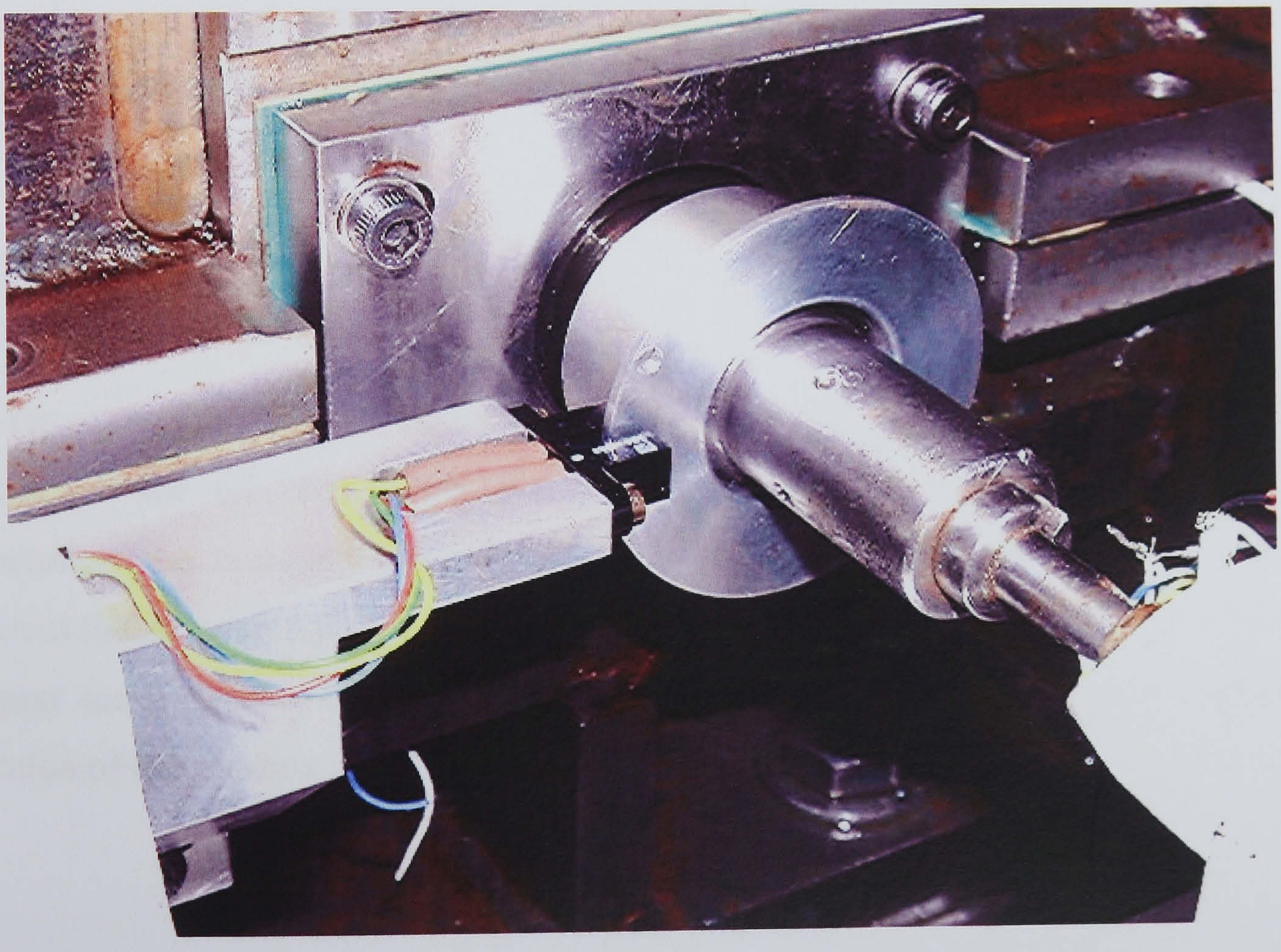

Figure 3.5 Trigger sensor consisted of optical light source and receiver.

3.2.5 Accelerometer

The accelerometer used for vibration measurement in this experimental work was a single crystal piezoelectric transducer with operating frequency between 10 and 8000 Hz (ISOBASE Model 236 from Endevco Dynamic Instrument Division). The accelerometer was mounted on the pinion shaft bearing housing to record the vibration measurements of the gear system, see figure 3.3.

3.2.6 Charge amplifier

The charge amplifier employed was a single channel PE amplifier (Endevco Dynamic Instrument Division, Model 2721B). The accelerometer was connected to charge amplifier, and the signal output from the charge amplifier was fed to a commercial data acquisition card. Under the various test conditions, a 1 and 0.1 V peak from the charge amplifier were calibrated to 1 g using the calibration table provided by Endevco.

3.2.7 Thermocouples

A K-type (Chromel-Alumel) thermocouple, rated from -200^{0}C to 1370^{0}C, was employed to measure the oil temperature for computation of film thickness. The oil sump temperature was measured through an opening on top of the gearbox casing using the specified thermocouple probe. The location for acquiring oil temperatures was adjacent to the gear mesh position as this was the closest point that can be accessed during the operation of the gearbox.

3.2.8 Data acquisition cards

For the capturing of raw AE waveforms, a MISTRAS AE DSP-32/16 data acquisition card (two channels) produced by PAC was employed. The AE DSP card has a maximum sampling rate of 10 MHz with 16-bit precision. Continuous AE parameters such as Average Signal Level (ASL), r.m.s and absolute energy were recorded via another data acquisition card, PCI-2. This data acquisition card can provide up to 10 MHz of sampling rate and incorporated 16-bit precision. Prior to the Analogue to Digital Converter (ADC), the card employed anti-aliasing filters that can be controlled directly by software. In addition, vibration waveforms from the gearbox were recorded using a 8-channel National Instruction (NI) data acquisition card, NI 6023E with 12-bit precision and a maximum sampling rate of 200 kHz.

3.2.9 Software

The software, MI-TRA, was used for the data acquisition of raw AE waveforms via the AE DSP-32/16 data acquisition card. However, the computation of continuous AE level was performed by another software package, AEWIN. AE Energy and r.m.s values were calculated in real time by the software package. The software employed a hardware accelerator so that calculations can be performed in real time. The hardware accelerator takes each value from the ADC and squares it. The results are added into an accumulator for a programmable time interval, based on the user set time constant. At the start of the time interval the accumulator is cleared and at the end of the time interval the accumulator value is stored. The r.m.s is then calculated by taking the square root of the sum of the accumulated squared ADC readings. The energy value computed was directly related to what the sensor experienced and is measured in Atto-Joules. For the vibration measurements, a programmable software; LabView, controlled and managed all the vibration data acquisitions. Finally, for the analysis of all the experimental results, MatLab was utilised.

3.3 Experimental procedures

3.3.1 Seeded defect tests

The seeded defect tests were used to evaluate the capability of the AE technique to detect defects. Firstly, an attenuation test was conducted to understand the characteristics of the test gearbox and the transmission path of the possible defect to the sensors. Secondly, simulated defects of various sizes were employed to assess the damage detection capability of the AE technique.

3.3.1.1 Attenuation Test

Prior to the start of the simulated defect test, an attenuation test on the gearbox's components was undertaken. A 0.5 mm diameter and 3 mm length 2H lead pencil was broken at different positions in order to establish the attenuation of the AE signal. This technique is known as the Hsu-Nielsen source test [82]. The test device (see figure 3.6) is an aid to simulate an AE event using the fracture of a brittle graphite lead in a suitable fitting. This generates an intense AE signal, similar to a natural AE source that the sensor detects as a strong burst. The primary purpose of this test is to ensure the transmissibility of the AE signatures from the source to the AE sensor. In addition, the Hsu-Nielsen source test could also verify that the AE sensor was in good contact with the part being monitored and the AE acquisition systems were functioning properly.

Figure 3.7 presents a schematic diagram for the attenuation test displaying the different simulation positions and different interfaces the AE signatures would have to propagate across. Table 3.1 and figure 3.8 show the relative attenuation values. The reference signal employed for the attenuation calculations was the AE response from a lead break next to the AE sensor on the pinion gear. Five pencil breaks were performed from each position and averaged.

The greatest attenuation of simulated AE signatures was observed on the bearing. This was expected due to the number of interfaces the AE signal would need to propagate across. The position of the balls in the loaded zone affects attenuation of the AE signal. If a ball is in the loaded zone while the AE waves were travelling through, better transmissibility can be expected. Relatively high attenuation was also observed for lead breaks on the wheel. This was expected since the wheel is furthest away from the sensor; however, the attenuation values of lead breaks on the pinion and shaft were similar. It was expected that the attenuation would be greater on the shaft due to the interface between the shaft and the pinion but this was not the case. This is attributed to experimental errors and the close proximity at both locations.

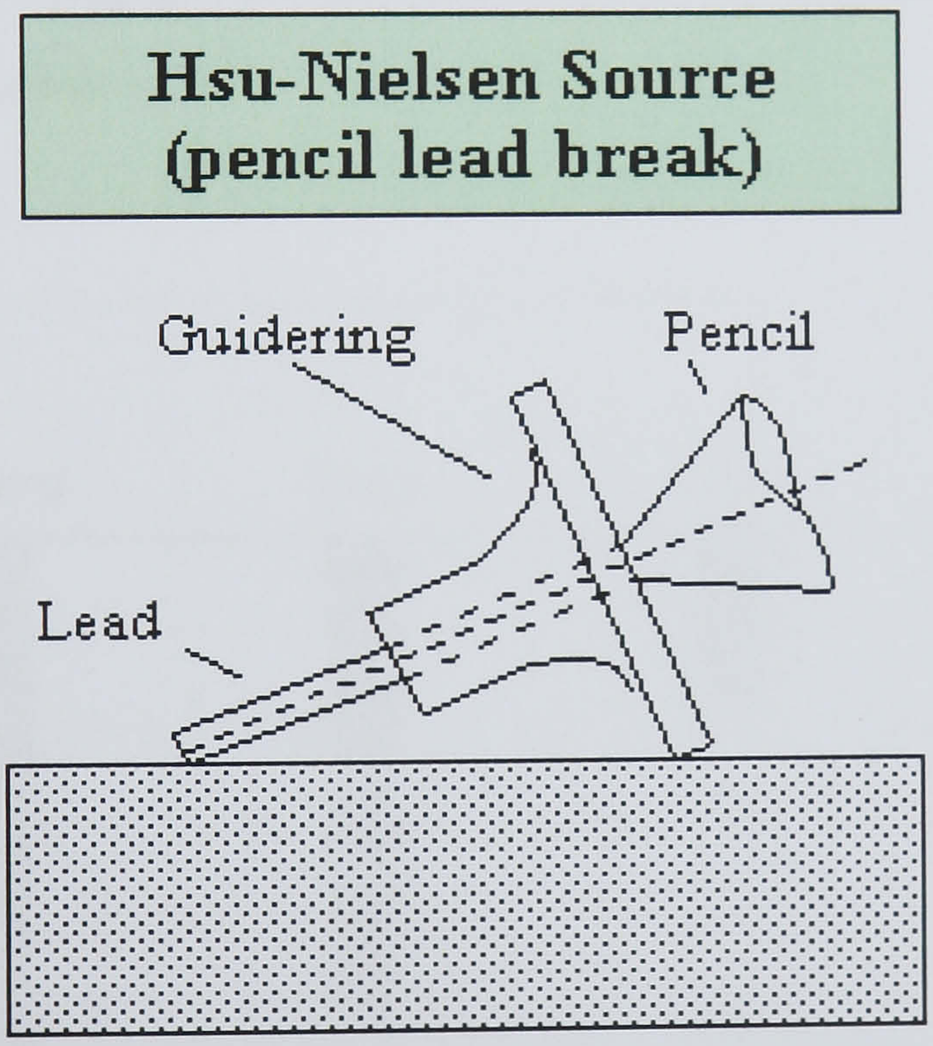

Figure 3.6 Hsu-Nelson source test [82].

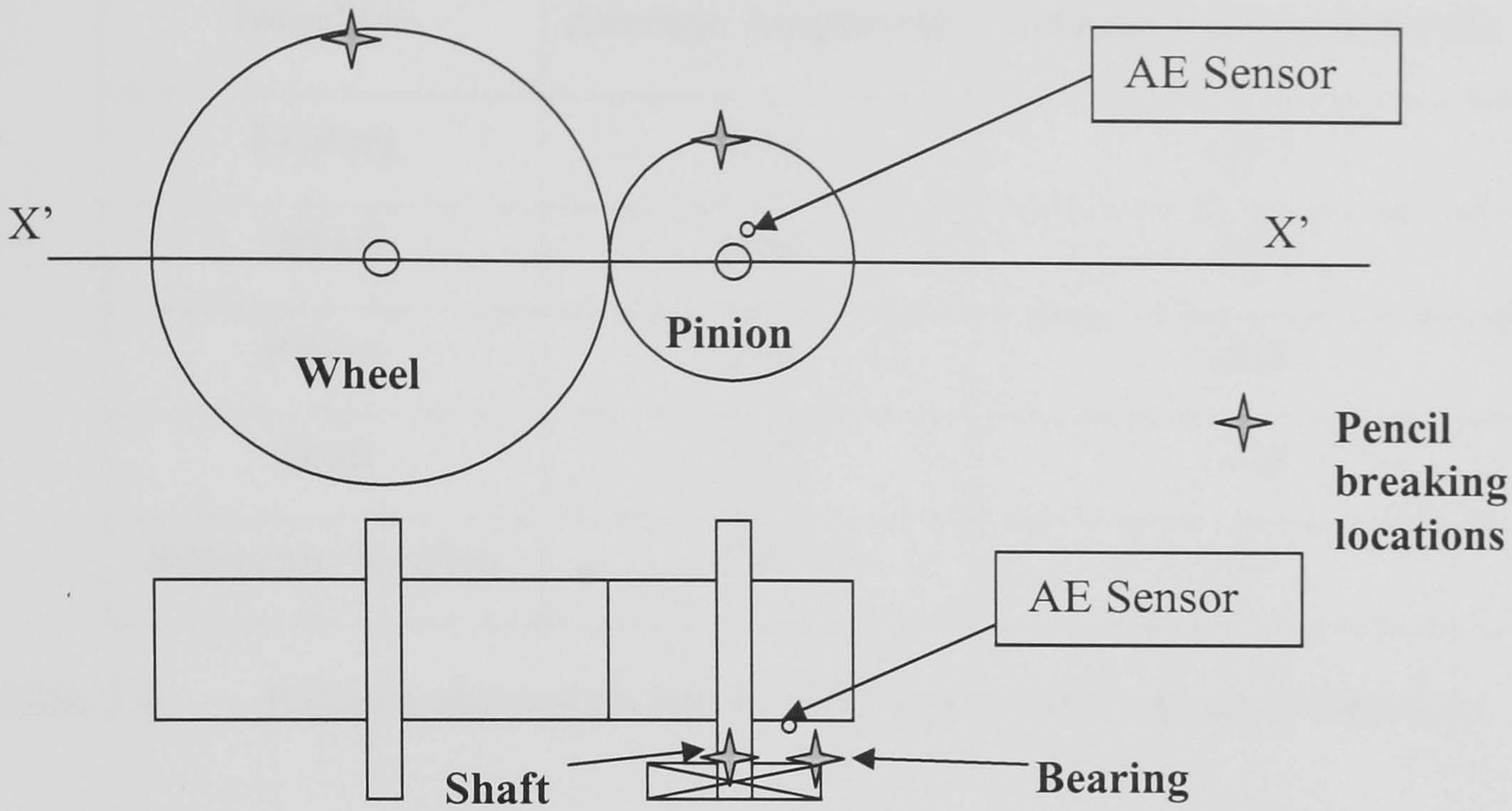

Figure 3.7 Schematic diagram for the attenuation test displaying different interfaces and its locations.

Figure 3.8 Relative attenuation values for sensor on the pinion.

Interface	Average Amplitude	Relative Attenuation (dB)
Bearing	0.10	-34.1
Wheel	0.26	-25.8
Pinion	1.83	-8.9
Shaft	2.12	-7.6
Reference Position	5.07	0

Table 3.4 Relative attenuation values with respect to the reference position.

3.3.1.2 Simulated defect tests

The gearbox was run-in for more than 15 hours before the actual test was carried out. This was to ensure running in of the gear teeth surfaces. The test started with a defect free condition so that the operational background noise characteristics were observed. The gearbox was then run for 30 minutes prior to acquiring AE data for the no load condition. The gearbox was then shut down to adjust to the next torque level (55 Nm). After another 30 minutes of continuous running, the AE signal for this load condition was acquired. This procedure was repeated for the load condition of 110 Nm.

For the simulated defect condition, a pitch-line defect of 1 mm in diameter (see figure 3.9) was introduced and AE data was collected by repeating the loading procedures detailed in the former paragraph. Lastly, the test was repeated for a large addendum defect (extended from the pitch-line towards the tooth tip) measuring 12 mm (across face width) by 3 mm (see figure 3.10). The simulated defects were introduced on the flank of a tooth using an engraving machine.

All the simulated defect tests were performed under single speed condition; 745 rpm and a sampling rate of 10 MHz. Based on the sampling rate of 10 MHz, the acquisition time

available for recording was 0.0256 seconds which represented 0.31 revolutions (16 teeth) of the pinion at 745 rpm. For all the test conditions, a total of 50 data sets, each equivalent to a time frame encompassing sixteen teeth, were acquired and averaged in each region. The averaging could be accomplished due to the trigger mechanism employed ensuring that the acquisition system always started at the same position.

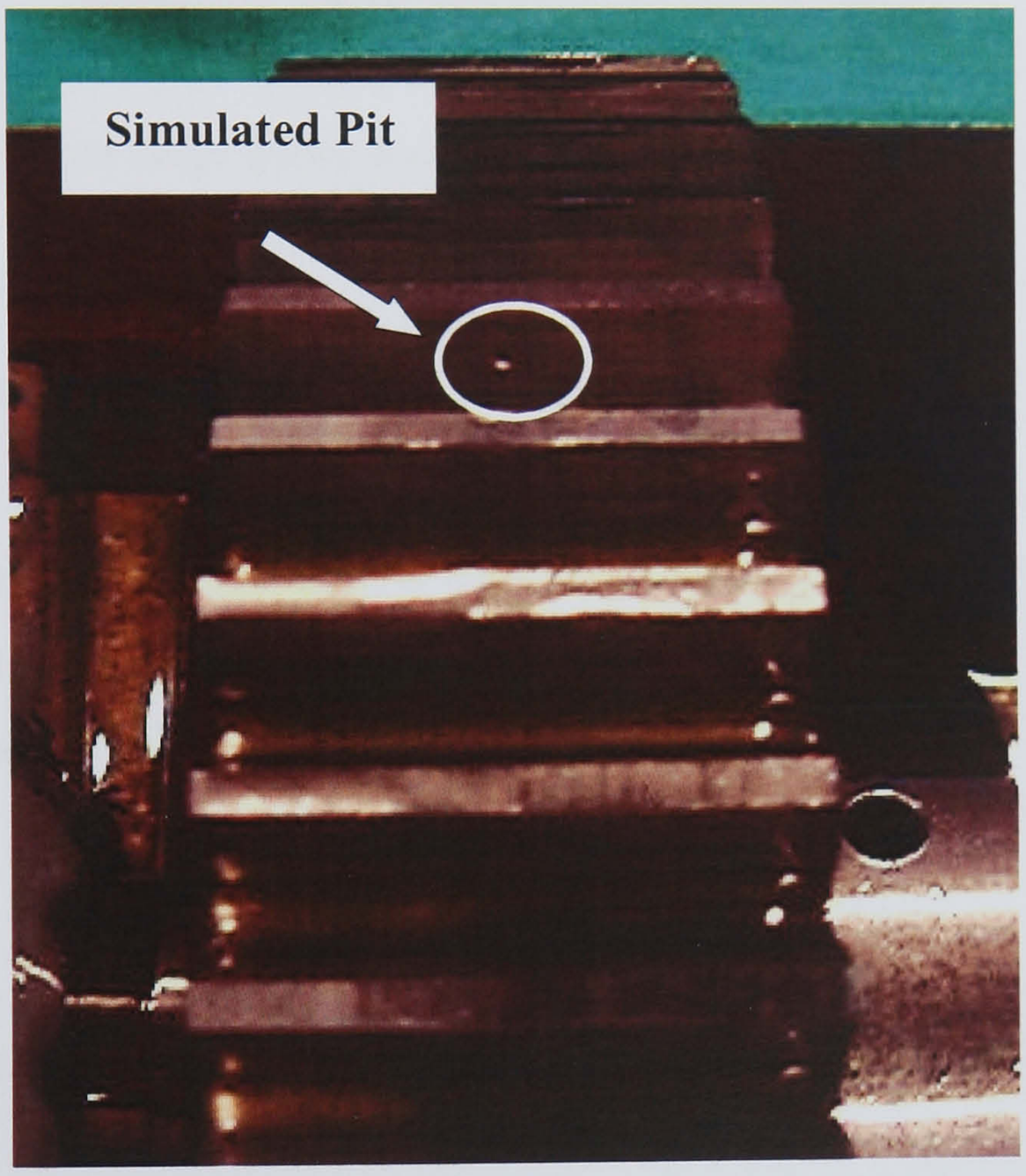

Figure 3.9 Simulated 1 mm diameter pitch-line defect.

Figure 3.10 Simulated large addendum defect.

3.3.2 Influence of operating condition on AE

The primary purpose of the AE source test was to investigate the source of AE during gear mesh and establish the relationships between AE activity levels and changes in speed and applied torque. In order to fulfil the aims of this investigation, a series of tests were undertaken.

3.3.2.1 Influence of operating torque, speed and oil temperatures on AE

In order to study the effect of the operating parameters: applied torques, rotational speeds and oil temperatures, the test gearbox was run under 6 different operating conditions; 2 speeds (745 and 1460 rpm) and 3 applied torque levels (0, 55 and 110 Nm). AE r.m.s data was monitored and recorded continuously via the usage of the software AEWIN at an acquisition interval of 100 ms. The oil temperatures were measured at intervals of 15 minutes as described. For each test, the test gearbox was operated from cold and terminated once the oil temperature had remained constant within $\pm 0.1\ ^{0}C$ for a duration of 1 hour.

It was expected that the oil temperature would exert some influences on AE activity. Hence, to study the significance of applied torque and speed individually on AE activity. a series of isothermal tests needed to be conducted. Due to the space constraint within the test gearbox, it was not possible to install heating coils to maintain a constant oil temperature. To overcome this shortcoming, a set of procedures was devised to achieve near isothermal conditions, and these are detailed in the subsequent paragraphs. In order to study the effect of applied torque on AE activity, the running speed and oil temperature were kept constant. The same set of procedures was applied while investigating the effect of running speed on AE activity with oil temperature kept constant.

3.3.2.2 Constant speed isothermal tests

The test gearbox was run at 745 rpm with a load of 220 Nm far over 5 hours until the oil temperature reached equilibrium, i.e. the oil temperature remained constant within ± 0.1 ^{0}C for a duration of 1 hour. The gearbox was then brought to a stop and the load was re-adjusted to 73 Nm. The gearbox was then re-started and run for 15 minutes whilst continuous AE data, r.m.s., energy and ASL, was recorded. It was again brought to a stop and adjusted to the next load of 147 Nm, and run for a further 15 minutes while data was recorded. These loading procedures were repeated for the subsequent test conditions in the sequence of 220 Nm, 147 Nm and 73 Nm. The prime purpose of this was to ensure repeatability of the AE data recorded during testing. The time taken to set the new torque level was approximately three minutes. Isothermal condition of the tests was ensured by the constant monitoring of oil temperature at 5-minute intervals. The same procedure was repeated at a speed of 1460 rpm. The test condition for 745 rpm was repeated in a separate occasion to ensure the repeatability of the test procedures. In addition, a reverse loading procedures (to the original test) was employed to ensure the consistency of the observations.

3.3.2.3 Constant load isothermal tests

The test gearbox was run at 1460 rpm with a load of 220 Nm far over 5 hours until the oil temperature stabilised within $\pm 0.1\ ^{0}C$ for a duration of 1 hour. The gearbox was then brought to a stop and the lower speed motor (745 rpm) was installed. The gearbox was re-started and run for 15 minutes whilst continuous AE data was recorded. This procedure was repeated for the other two load conditions; 147 and 73 Nm, and speed conditions; 1460 and 2800 rpm. A maximum torque level of 73 Nm was applied for the test speed of 2800 rpm due to the break-up/loss of AE signals as a result of high vibration levels saturating the AE high-bandpass filters on the pre-amplifier. The time taken to strip and replace the motor was approximately four minutes and during this period the acquisition system was paused. Isothermal condition of the tests was ensured by the constant monitoring of oil temperature at 5-minute intervals.

3.3.3 Accelerated gear fatigue tests

The aims of the accelerated gear fatigue tests were to (a) correlate the AE activity with pitting wear progression on the gear teeth surfaces (b) compare the diagnostic capability of the AE technique to the other two damage detection techniques: vibration and SOA (c) explore the prognostic capability of the AE technique. Prior to the start of the fatigue test, the surface durability of the test gears was calculated using a program, Gear Geometry and Stress Analysis Program, developed jointly by Newcastle University Design Unit and the British Mechanical Power Transmission Association's (BMPTA) Gear Research Foundation (GRF). This gear analysis program is intended for gearbox designers and end users who are involved in spur or helical involute gearing. The program consisted of two modules (a) Gear Details Module: drawing data in accordance with the BMPTA's Codes of Practice and (b) Gear Rating Module: calculation of gear tooth contact and bending stresses in accordance with the procedures specified in BS/ISO 6336 [35]. The results from the analysis, presented in Appendix B, revealed that all the three applied torque conditions would lead to pitting damage on the gear teeth surfaces. Figure 3.11 shows the

relationship between the contact stress safety factor and projected gear lives under the three applied torque conditions. The contact stress safety factor is defined as the ratio of calculated contact stress to the allowable contact stress.

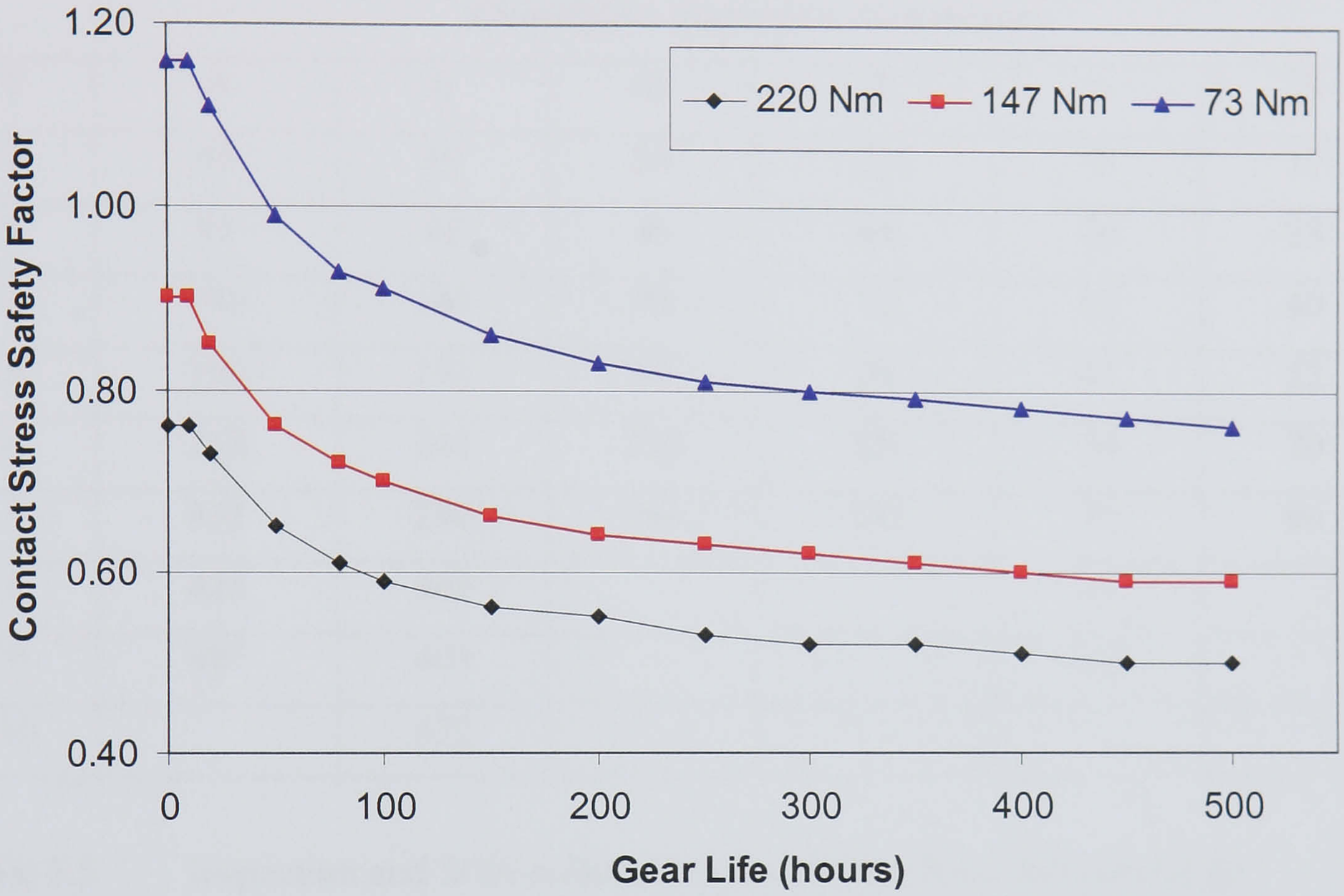

Figure 3.11 Relationships between the contact stress safety factor and gear lives under the applied torque of 220, 147 and 73 Nm for the pinion.

The gear fatigue tests were performed at a rotational speed of 745 rpm and applied torques of 220, 147 and 73 Nm. Two tests were undertaken at each torque to ensure repeatability. At regular intervals (ranging from 15 to 55 hours depending on the applied torque levels), visual inspection of gear surface damage was undertaken, oil sump temperatures were measured and oil samples were drawn for SOA (see table 3.5).

Continuous AE r.m.s values were calculated in real time by the software detailed in Section 3.2.9 with a time interval set at 10 ms and a sampling interval of 90 ms. Raw vibration waveforms, sampled at 8192 Hz, were recorded for a period of 1 second at intervals of 30 minutes. Vibration r.m.s values were calculated over the recorded duration (1-second).

Interval No.	Applied Torque					
	73 Nm		147 Nm		220 Nm	
	Test 1	Test 2	Test 1	Test 2	Test 1	Test 2
	Cumulative inspection time (hours)					
1	0	0	0	0	0	0
2	45	49	24	24	9	17
3	95	96	46	48	20	28
4	145	144	70	72	31	40
5	196	193	94	96	41	52
6	268	241	118	121	54	70
7	353	290	143	145	70	86
8	425	341			91	
9	485	403			116	
10		472				

Table 3.5 Inspection and SOA collection intervals for all the test conditions.

During the inspection interval, gear teeth surfaces on both the pinion and gear were visually inspected for pitting or other abnormalities such as scoring and scuffing. The largest pitted area on any single tooth was recorded. The failure, or test termination, criterion was set at 50% pitted area of any one gear tooth surface area. The visual inspections were performed by two separate inspectors independently and repeated for consistency. This inspection error was determined to be within 5% of pitted area. The inspection results are detailed in Appendix C. In addition, images of the pitting damage were recorded using a digital camera.

After the visual inspection of the gear teeth surfaces, a 60 ml sample of oil was transferred from the oil sump (at the position where the gear meshes) to the oil sample bottle via a syringe. All the oil samples were collected within 20 minutes of gearbox shut down for inspection. Fresh oil was then added to top up to the original level marked on

the wall of the sump. This was to ensure that the volume of oil remained constant throughout all the gear fatigue tests. The analysis was performed on an Inductively Coupled Plasma (ICP) Atomic Emission spectrometer which subjects the oil sample to a high voltage plasma which energises the atomic structure of the metallic elements, causing emission of light. The emitted light is subsequently focused into the optical path of the spectrometer and separated by wavelength, converted to electrical energy and measured. The intensity of the emitted light for any element is proportional to the concentration of wear metal suspended in the lubricating fluid. The ICP used for determining levels of Fe elements in the lubricating fluid had an accuracy of ± 3% at an average precision of 95% confidence level.

Surface texture, which includes the surface roughness and waviness, of the gear teeth was measured after each fatigue test in both longitudinal and transverse directions of the gear tooth. The surface roughness parameters measured consisted of R_a the average roughness, R_q the root-mean-square roughness, the height of the highest peak (P_p) and the depth of the deepest valley (P_v) in the profile roughness over the evaluation length. The measured waviness parameters included W_a the average waviness and W_q the root-mean-square waviness. The texture measurements were performed using a Taylor Hobson form Talysurf 120L profile measuring machine, which has a resolution of 12.8 nm at 10 mm range and a straightness accuracy of 0.2 μm over any 20 mm. Surface textures of two new gear teeth (on the non-working sides) were measured and used as a reference for pitted gear teeth comparisons. After the termination of each fatigue test, the pinion gear tooth with the greatest pitted area was removed for texture measurements. These measurements were subsequently compared with the reference measurement of the undamaged pinion gear tooth.

BAE SYSTEMS

BAE SYSTEMS
Warton visitor information

Warton Site

- ALL non BAE SYSTEMS visitors must report to site reception on their arrival.
- Visitors in possession of an 'Escort Required' pass must be escorted at all times whilst on the site and to the point of egress on completion of the visit.
- Irregular visitors who hold a valid clearance may be issued with a 'Non-Escorted' pass. This will give free access to the site only, not into buildings. It is the responsibility of the host to monitor the movements of the visitor within the building.
- Photographic equipment of any description is not allowed on site unless authorised.
- Mobile phones may be utilised but must be switched off whilst in the hangars or near operational aircraft and airfield services.
- Mobile and Portable Computers are not allowed on site unless authorised.
- Software and data, all computer media must be scanned for viruses. A virus scanning facility is available in reception.

BAE SYSTEMS

BAE SYSTEMS
Warton Aerodrome
Warton,
Preston,
Lancashire
Preston
PR4 1AX

Tel +44 (0) 1772 633333
Fax +44 (0) 1772 634724

Public Transport

Rail Travel. Preston Station. Situated Fishergate Hill in Preston town centre. Take a taxi to Warton Aerodrome.

Air Travel. Manchester Airport is situated just off the M56. Go West on the M56 to Junction 9 and take M6 North until you reach Junction 32. Head West on the M55 until you reach Junction 3, then follow the map below.

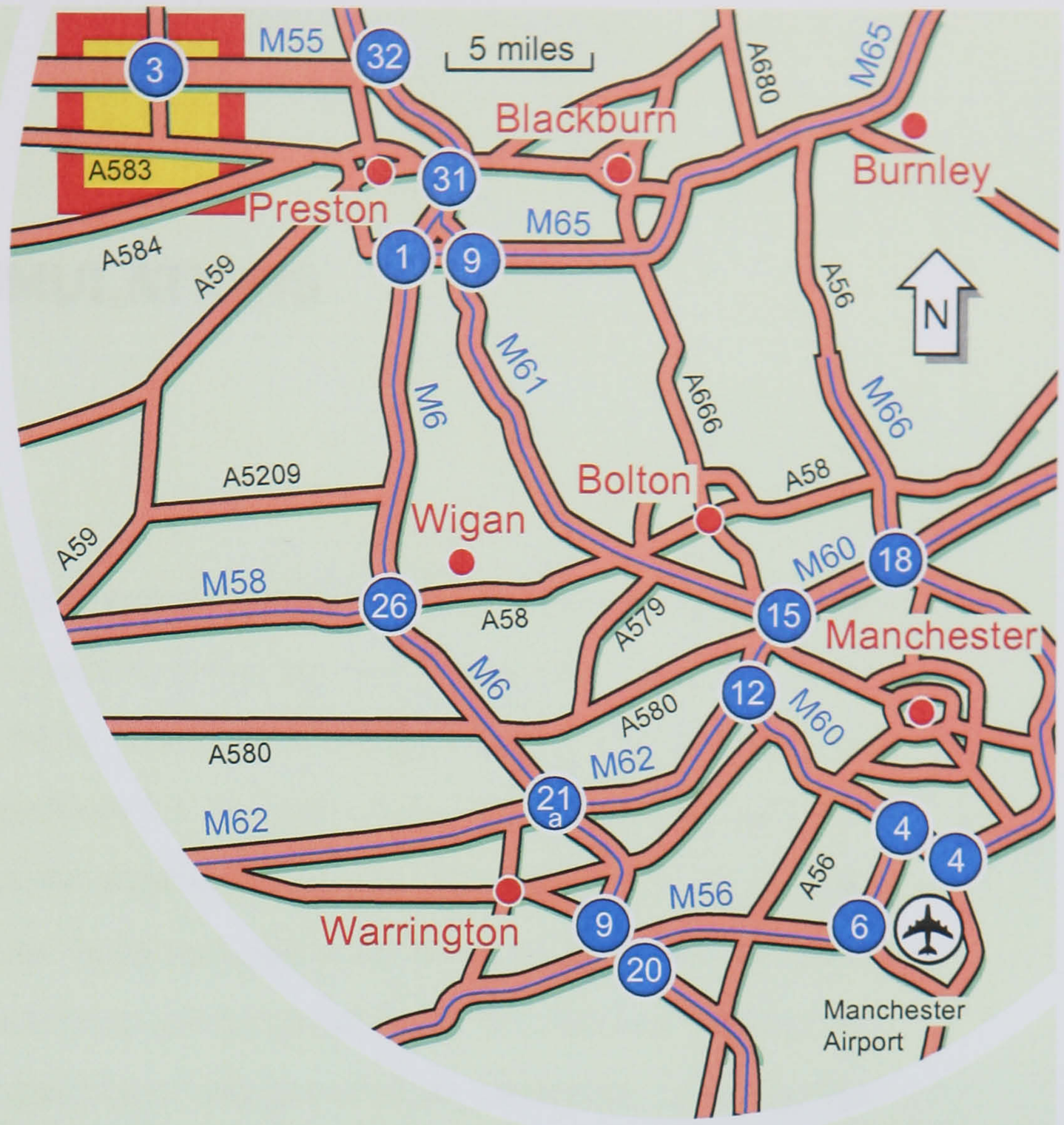

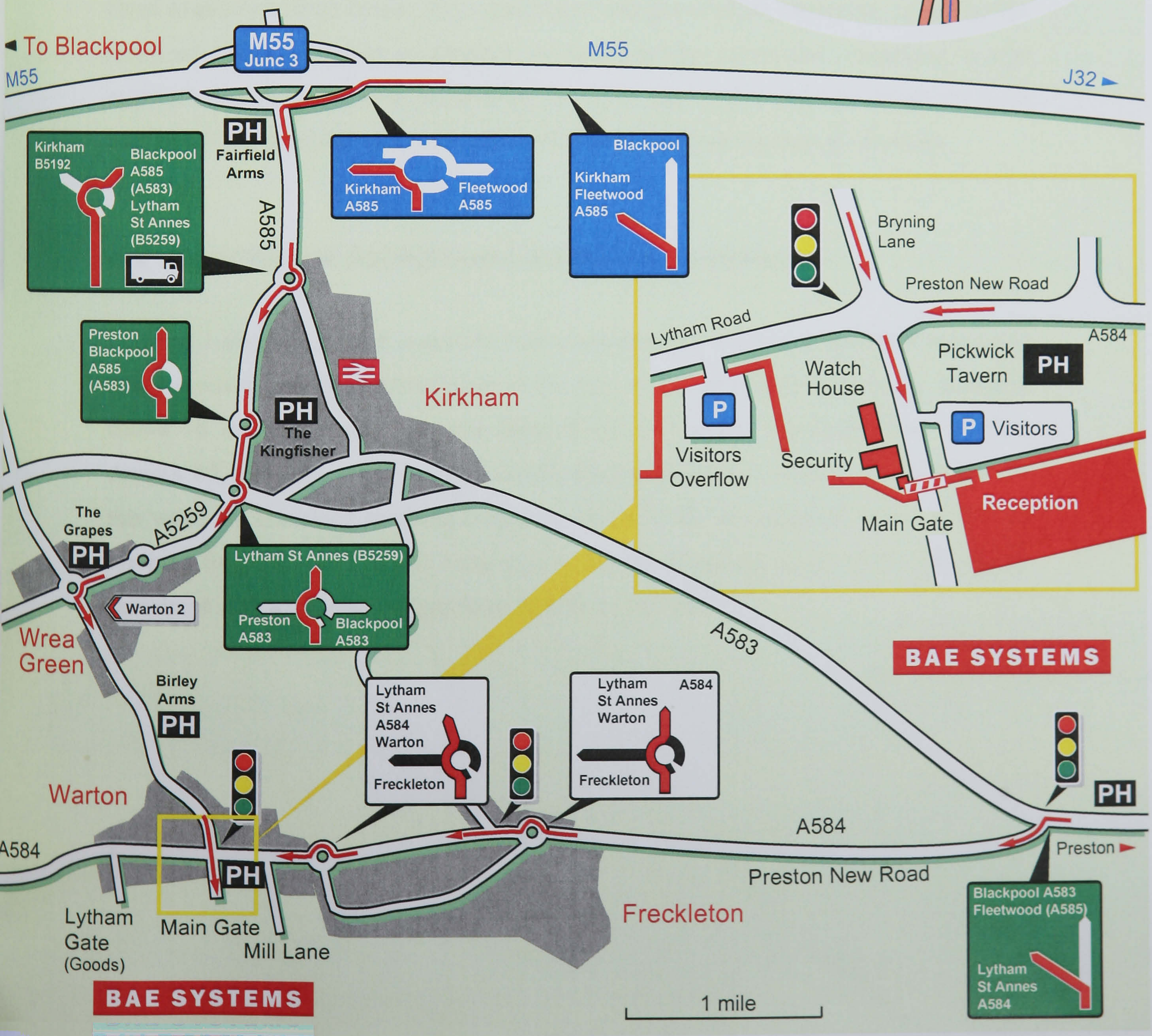

BAE SYSTEMS

4 SEEDED DEFECT SIMULATIONS

4.1 Introduction

Seeded defects of various sizes were introduced on different locations of the pinion gear tooth surface to study the applicability and to assess the defect detection capability of the AE technique. During the seeded defect simulations, various defect analysis methods were explored. Firstly, the AE signatures of 16 gear teeth were recorded using the maximum sampling rate, 10 MHz, of the acquisition system. AE indicators such as r.ms, peak amplitude and crest factor were computed based on the AE signatures recorded within this acquisition window. These were averaged values of the indicators within the fixed acquisition time frame. Any significant changes of these indicators would be the result of defect detection or changes in the operating parameters. Secondly, a new approach was introduced in an attempt to locate the seeded defects, which involved analysis of the basic AE signatures recorded during the seeded defect simulations.

4.2 Operational background noise measurements

Figure 4.1 displays the AE signature with corresponding frequency spectrum associated with operational noise recorded prior to the start of the simulated defect tests. It clearly shows 16 meshing teeth. The gear mesh frequency can be calculated from the time domain AE signal by inverting the periodic time between two subsequent AE bursts. In this case, the estimated meshing frequency was 612 Hz as compared to the computed meshing frequency of 608 Hz. From figure 4.1, the frequency range of the AE signals associated with these tests ranged from 50 kHz to 350 kHz.

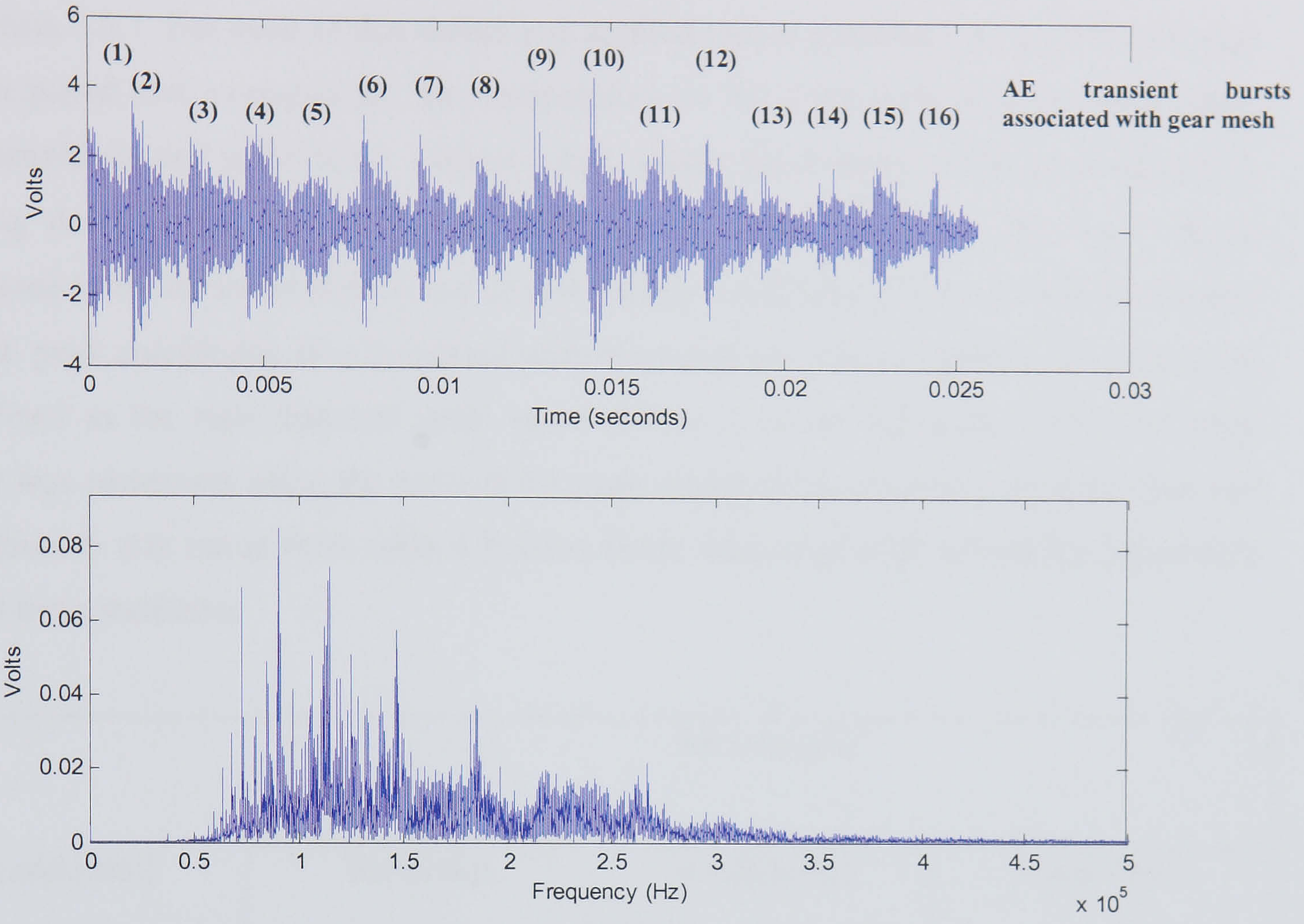

Figure 4.1 Time and frequency domain of an AE signature showing clearly the AE transient response associated with gear meshing of 16 teeth for the rotational speed of 745 rpm (pre-amplification 40dB, 110Nm)

4.3 Defect simulations

For analysis of the AE data obtained from the defect simulations, AE r.m.s and peak amplitude were not only employed to provide a comparison to other published work but principally because of the simplicity and proven robustness of these parameters for machine health diagnosis. In addition, the calculation of crest factor on the same AE data allowed for more understanding of the characteristics of these AE signatures.

The dimensions and locations of the seeded defect on the gear tooth surface are detailed in section 3.3.1. For each of this defect and applied torque condition, a set of 50 AE data was acquired and averaged for the computation of AE indicators such as r.m.s value. peak amplitude and crest factor. Table 4.1 to 4.3 show the changes of AE parameters with varying defect sizes from the defect simulations. From table 4.1, AE r.m.s values decreased with increased defect size for all loaded conditions. Under loaded conditions, the AE peak amplitudes also decreased with increased pit size, see table 4.2. Crest factor is defined as the ratio between peak value and r.m.s of the AE signal [83]. The crest factor was computed using the ratio of the peak amplitude to the r.m.s value of each test condition. It was noted from table 4.3, crest factor decreased with increasing defect size for all test conditions.

Load (Nm)	AE r.m.s (v)		
	No defect	Small defect	Large defect
0	0.1287	0.0848	0.0979
55	0.1007	0.0908	0.0524
110	0.1052	0.1031	0.0444

Table 4.1 AE r.m.s for the various defect sizes and loads

Load (Nm)	AE Peak Amplitude (v)		
	No defect	Small defect	Large defect
0	1.72	1.12	1.23
55	1.15	0.93	0.50
110	1.13	1.05	0.41

Table 4.2 AE peak amplitudes for the various defect sizes and loads

Load (Nm)	Crest Factor		
	No defect	Small defect	Large defect
0	13.36	13.21	12.56
55	11.42	10.24	9.54
110	10.74	10.18	9.23

Table 4.3 Crest factors for the various defect sizes and loads

The observation of decreasing crest factor with increasing defect size may suggest that crest factor could be used as a damage detection indicator. However, a more understanding of the indicator behaviour should be explored before claiming success. In practice, gearboxes are rarely operated under unloaded condition, hence, the focus of the analysis and discussion will be on the loaded test conditions only. Table 4.4 provides the detailed changes in AE r.m.s value and peak amplitude for varying defect sizes at 55 Nm. Both the AE peak amplitude and r.m.s decreased with increasing defect size. In this loaded case, the AE peak amplitude always decreased more than the r.m.s value, implying an overall decrease in crest factor with increased defect size. Similar observations were noted for applied load of 110 Nm, see table 4.5.

	AE Peak amplitude (v)	% difference	AE r.m.s (v)	% difference
No defect	1.15	-	0.1007	-
Small pitch-line defect	0.93	-19.1	0.0908	-9.8
Large addendum defect	0.50	-46.2	0.0524	-42.3

Table 4.4 Percentage difference in AE peak amplitude and r.m.s for different defect sizes at 55 Nm.

	AE Peak amplitude (v)	% difference	AE r.m.s (v)	% difference
No defect	1.13	-	0.1052	-
Small pitch-line defect	1.05	-7.0	0.1031	-2.0
Large addendum defect	0.41	-61.0	0.0444	-57.0

Table 4.5 Percentage difference in AE peak amplitude and r.m.s for different defect sizes at 110 Nm.

These observations do not agree with those of other researchers detailed in chapter 2 [56, 53, 57]. Badi et al [56] observed an increase in crest factor from the seeded defect gear tooth. However, this simulated surface damage was produced by shaving off part of the tooth tip from the side of the gear tooth which differed significantly from simulated pitch-line and addendum defect use in this experiment. Hence, it is not appropriate to compare the results of these simulated defects. For better comparison, Singh et al [53] and Tandon [57] et al undertaken seeded defects at the pitch-line of the gear tooth. Singh observed a single significantly high amplitude transient AE event [53] and correlated it to the detection of the seeded defect. This observation is very different to what was observed in figure 4.1, the transient AE response associated with the meshing gear teeth. This difference in the AE transient response is most likely due to the quality of gear material used. Singh employed a helicopter gear set which is typically hardened and super-finished. The fine surface finished will characteristically produce very low AE operational background noise. With the introduction of the pitch-line pit, a significantly

high amplitude AE transient burst will arise. Tandon and Mata observed increase in AE such as peak amplitude and energy, with increasing defect size [57], which contradicts the results presented in table 4.4 and 4.5. This raises some uncertainties in the effectiveness of the AE indicators employed for the defect simulations. Although the crest factor indicator for these seeded defect simulations revealed changes with increasing defect sizes, but the behaviours of the basic indicators such as the AE r.m.s and peak amplitude were in the opposite trend from those observed in Tandon and Mata [57]. These indifferences in the observations have prompted an exploration of an alternative method not only attempting to detect but to also identify the seeded defect. This proposed approach would be detailed in the following section.

4.4 Seeded defects identification

Based on the sampling rate of 10 MHz, the acquisition time available for recording was 0.0256 seconds which represented 0.31 revolutions (16 teeth) of the pinion at 745 rpm. By employing a trigger mechanism, only AE data from the portion of the pinion where the defect was located was acquired. The trigger system was set such that the defective gear tooth was at the mid point of the acquisition window (0.0256 seconds), see figure 4.2.

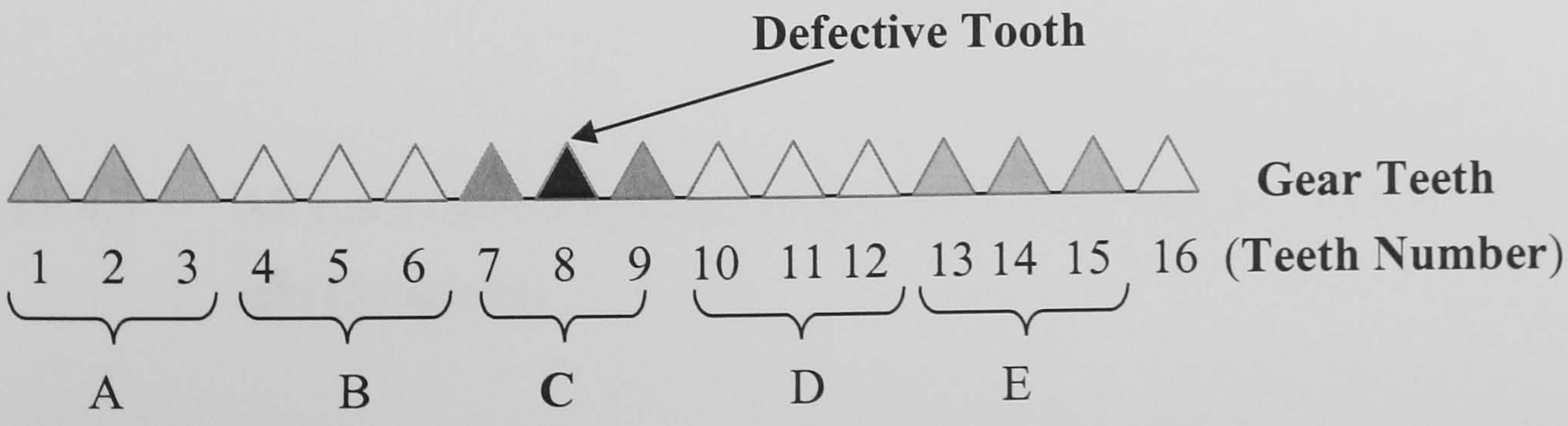

Figure 4.2 Sectioning of gear teeth for analysis, 16 teeth captured over 0.0256 seconds.

For the rotational speeds of 745 rpm, the recorded AE time waveform was divided into five regions, with each region representing 3-teeth, figure 4.2 illustrated the case. The r.m.s value of each region was computed and plotted against the three loading conditions. It was thought that this method of grouping the data would enhance the possibilities of identifying the seeded defect particularly as the defect has been seeded in the centre of the acquisition window.

The result of the undamaged condition gear surface is presented in figure 4.3. It was revealed that there was no particular trend observed from the no defect condition, the AE r.m.s values for the 5 regions appeared to be in a random manner as expected.

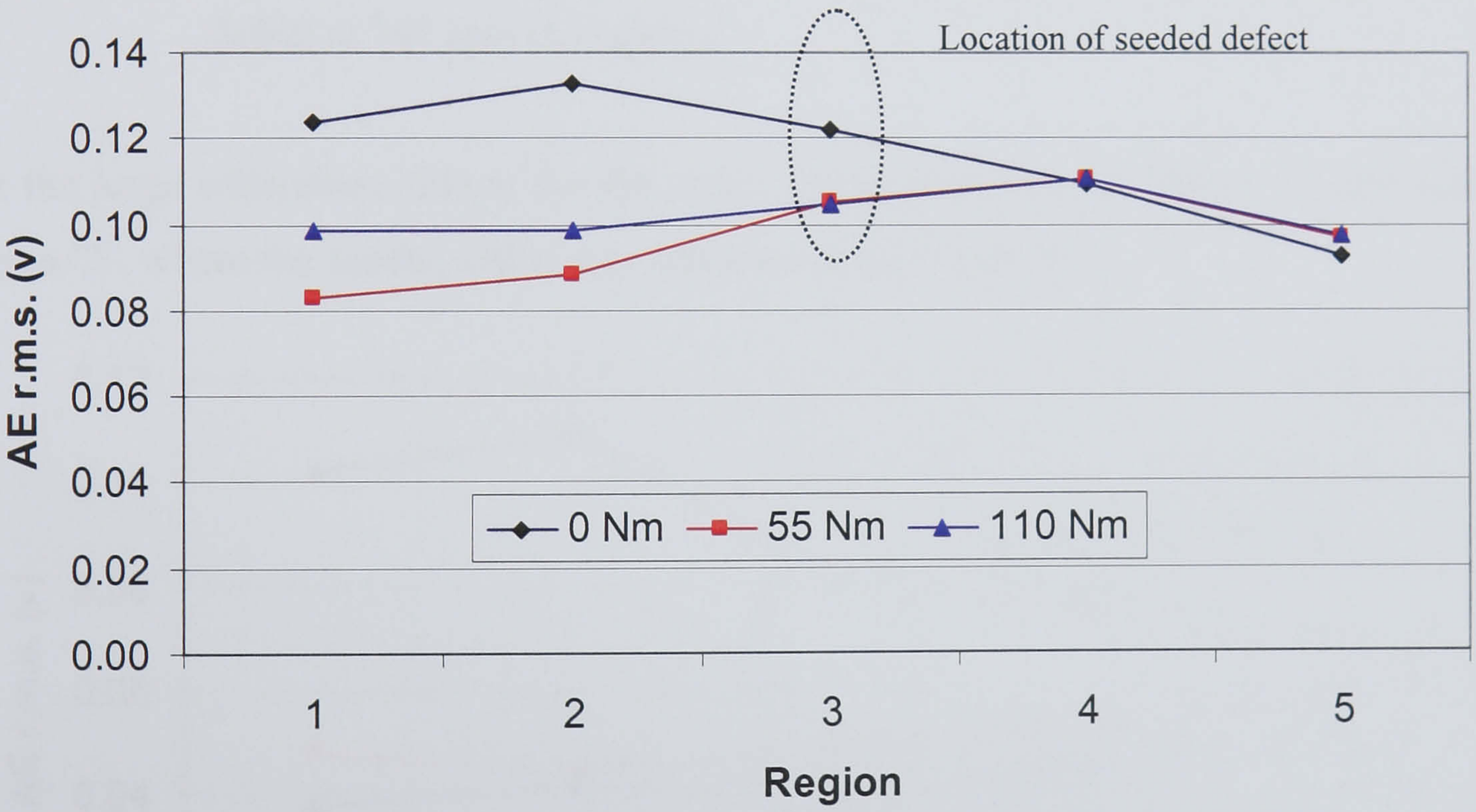

Figure 4.3 AE r.m.s against applied torques for 3-teeth analysis without defect at 745 rpm (5 regions)

For the small pitch-line defect, the AE r.m.s values at the seeded defect location, region '3' were higher than other regions, which may be indicative of the presence of the defect (see figure 4.4).

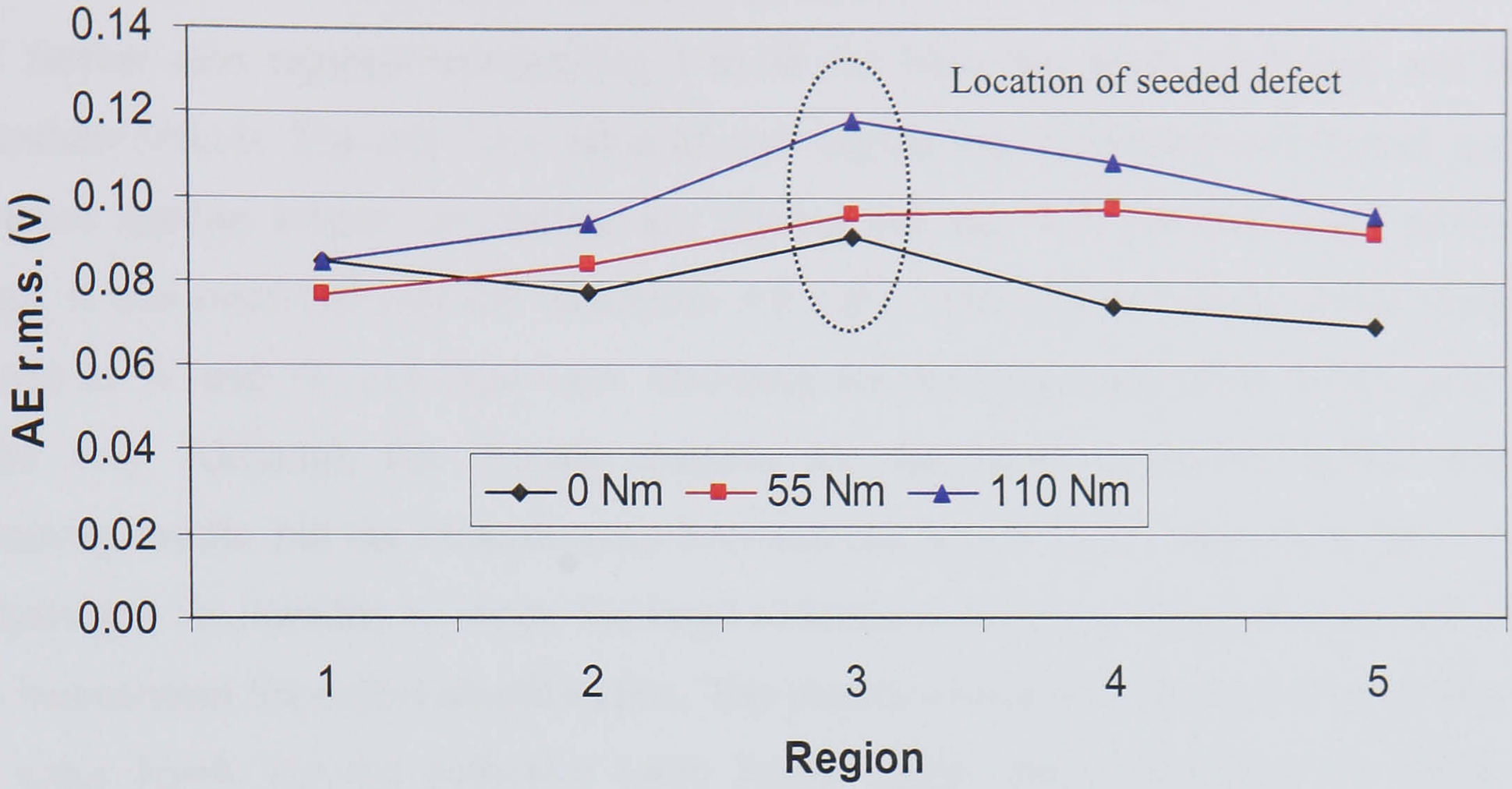

Figure 4.4 AE r.m.s against applied torques for 3-teeth analysis with small pitch-line defect at 745 rpm (5 regions)

For the large addendum defect, the AE r.m.s values were not the highest in the centre region '3', where the seeded defect was introduced, see figure 4.5.

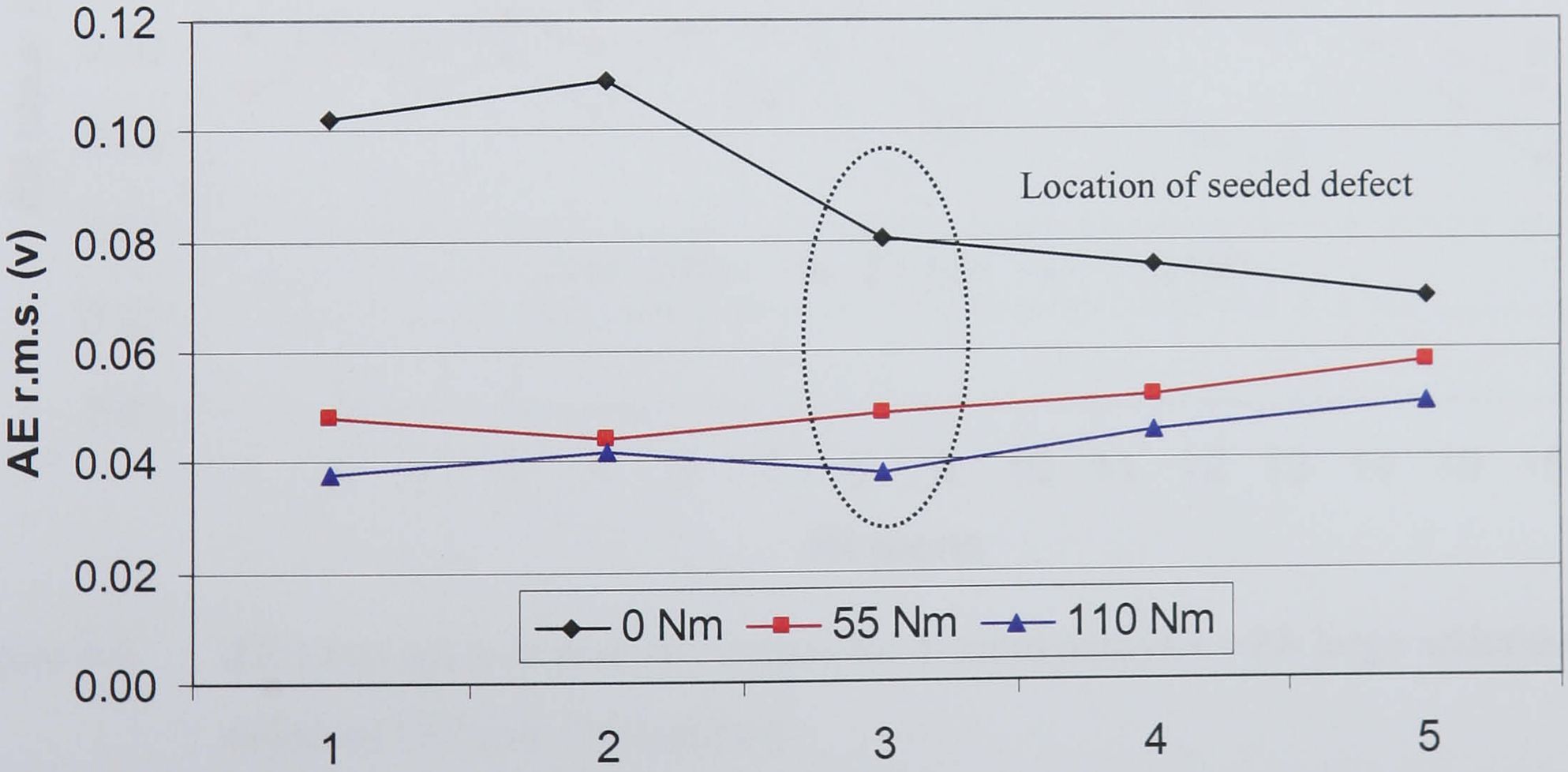

Figure 4.5 AE r.m.s against applied torques for 3-teeth analysis with large addendum defect at 745 rpm (5 regions)

Further analysis was undertaken on the original data. The recorded AE waveform was split further into regions representing 1-tooth for both the small pitch-line and large addendum defects. The AE r.m.s value of each region was computed and plotted against the three applied torque conditions, see figures 4.6 and 4.7. For the small pitch-line defect, it was observed that the maximum AE r.m.s value did not occur at the expected regions of '8' and '9', see figure 4.6. Similarly for the large addendum defect (refers to figure 4.7). Although the 3-teeth analysis for the small pitch-line defect showed promising results, but the inconsistency between the results for a single tooth and 3-teeth analysis and the inability to locate the large addendum defect revealed that this technique was inconsistent for defect identification. The results would have been conclusive had the AE r.m.s levels for the defective tooth being higher than other regions within the acquisition window.

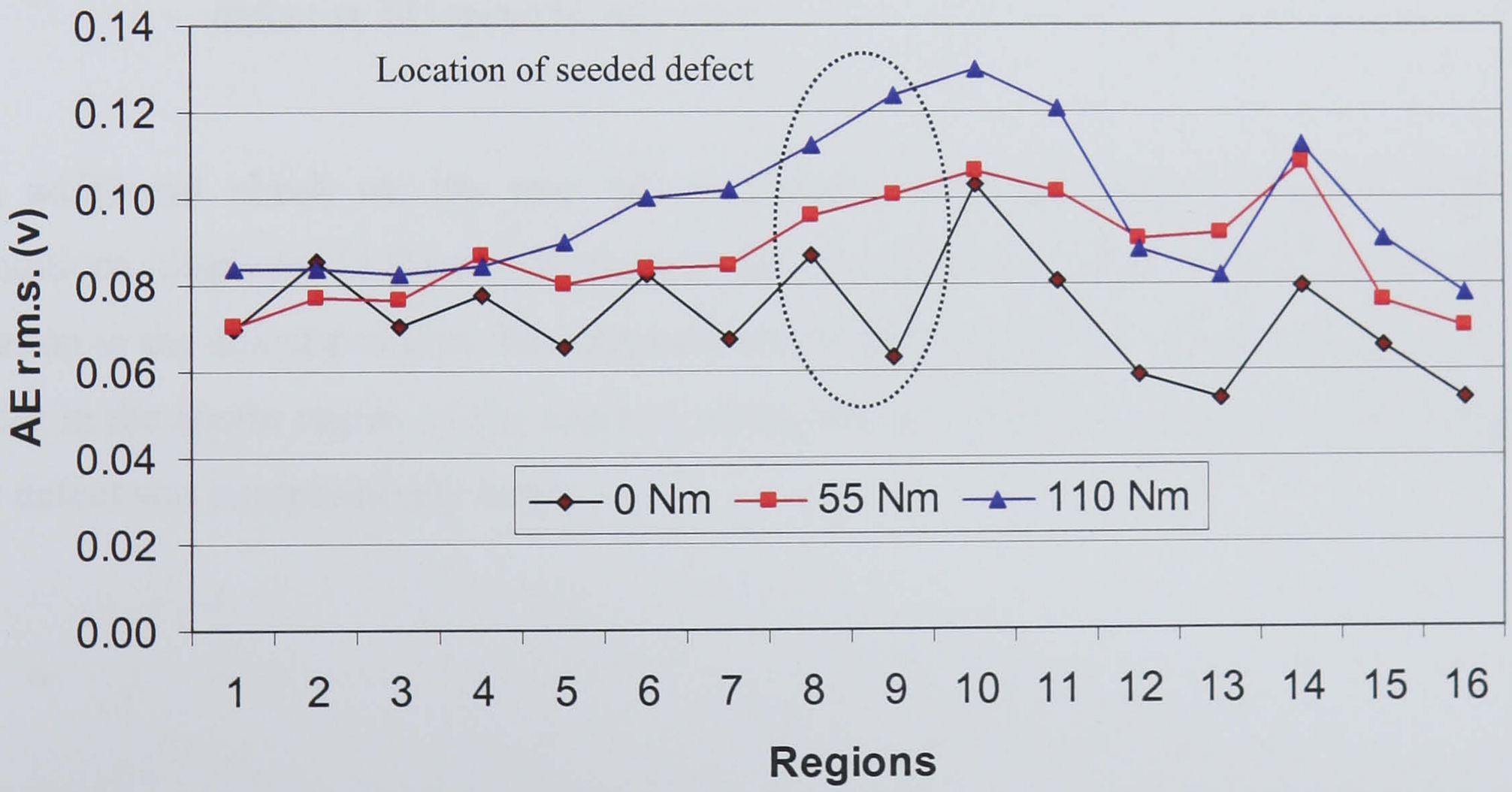

Figure 4.6 AE r.m.s against applied torques for 1-tooth analysis with large addendum defect at 745 rpm (16 regions)

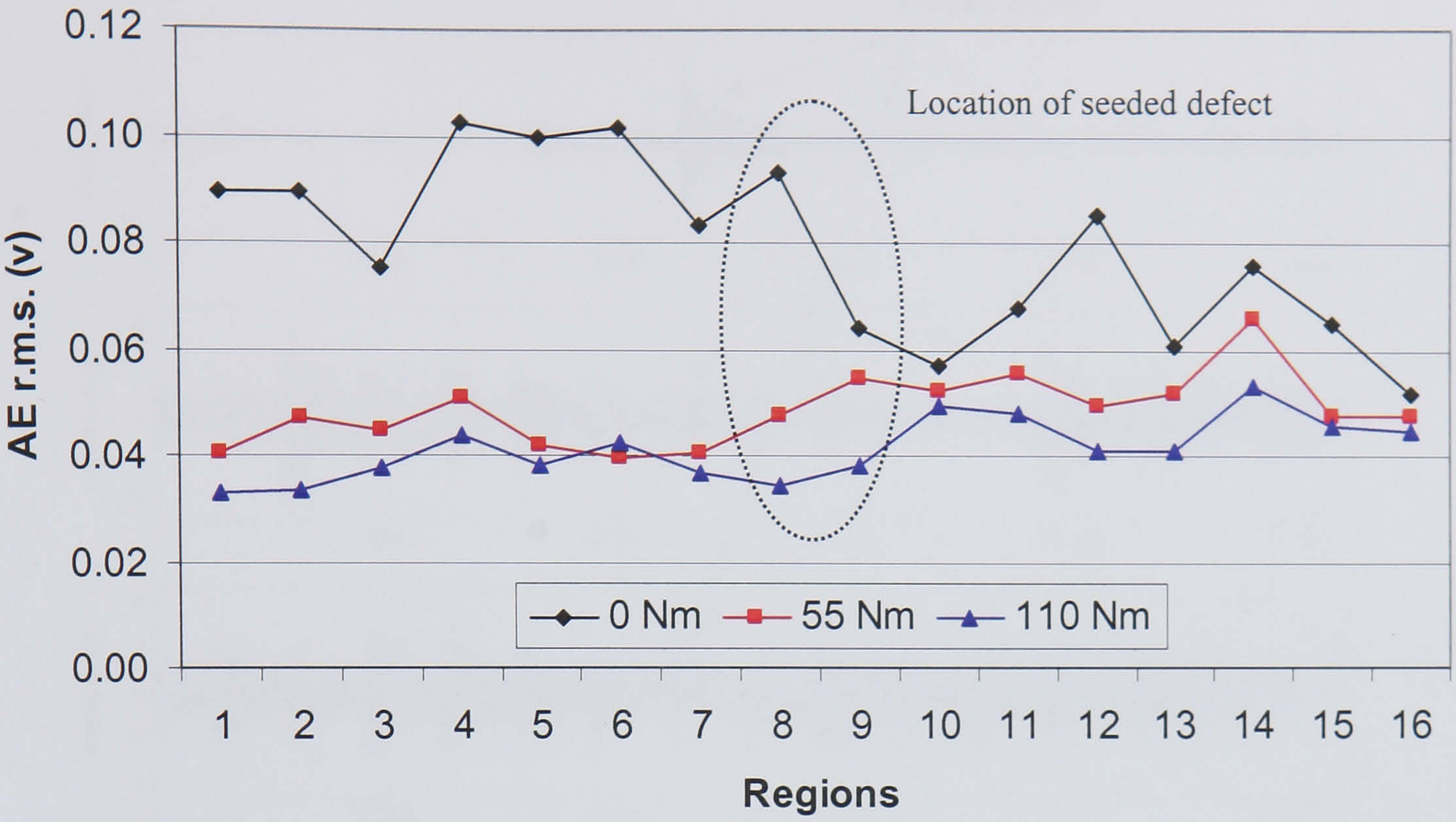

Figure 4.7 AE r.m.s against applied torques for 1-tooth analysis with large addendum defect at 745 rpm (16 regions)

An additional check on the raw AE waveforms from the large addendum defect conditions (displayed in figure 4.8) showed the non-consistent observation of AE burst in relation to the defect position. The biggest burst of the transient AE signal did not always occur in the centre region of the window where the seed defect was located even though the defect was comparatively large.

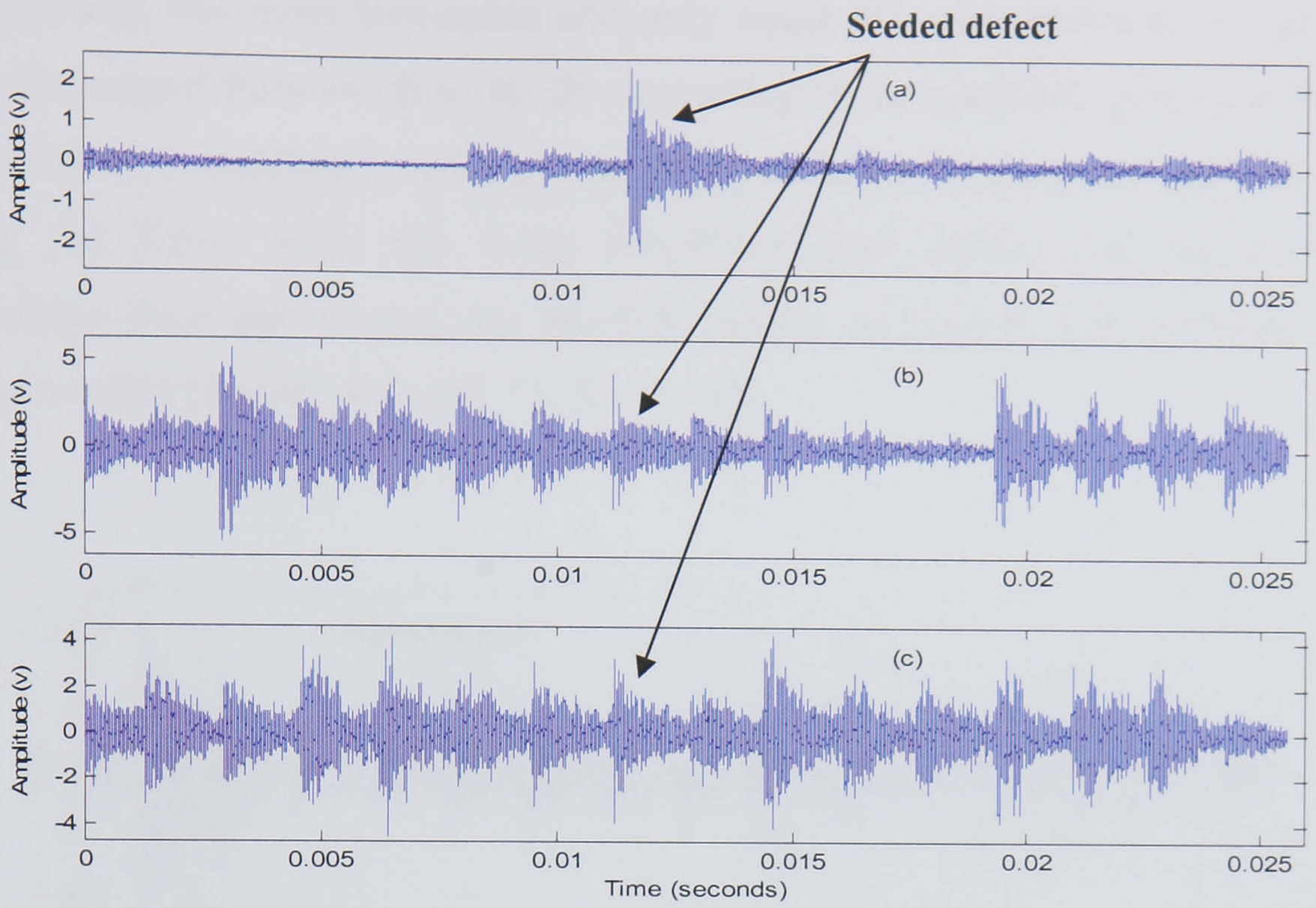

Figure 4.8 Raw AE signal for large addendum defect for (a) no load, (b) 55 Nm load and (c) 110 Nm load at 745 rpm.

4.5 Observations of AE from the bearing housing

Whilst AE signatures recorded on the pinion was triggered when the defect was in the 'gear mesh window', the AE sensor on the bearing casing was synchronised with the AE sensor on the pinion. As such, when the data acquisition system was triggered, both AE sensors captured data simultaneously.

During the seeded defect tests, it was noted that the AE bursts relating to the gear mesh, as detected on the sensor fixed onto the pinion, were also observed from the sensor on the bearing casing, see figures 4.9 and 4.10. However, continuous observations of the AE sensor on the bearing casing showed intermediate loss of the AE bursts associated with the gear mesh. The reason for this is attributed to the position of the bearing ball/roller elements during rotation. It is postulated that when the ball/roller is at bottom dead centre, i.e. directly in the load path, the transmission of the AE bursts to the sensor on the

bearing casing was most favourable and only under this circumstance. As the relative attenuation ranged from 44 dB to 26 dB (depending on the particular gear mesh AE burst, see figure 4.9), in addition to the high probability of loss of transmission path through the bearing, see figure 4.10, this make identifying gear defects and monitoring gear deterioration from the bearing and gearbox casings as fraught with difficulties, again contrary to other investigators [56, 53, 57, 52, 58].

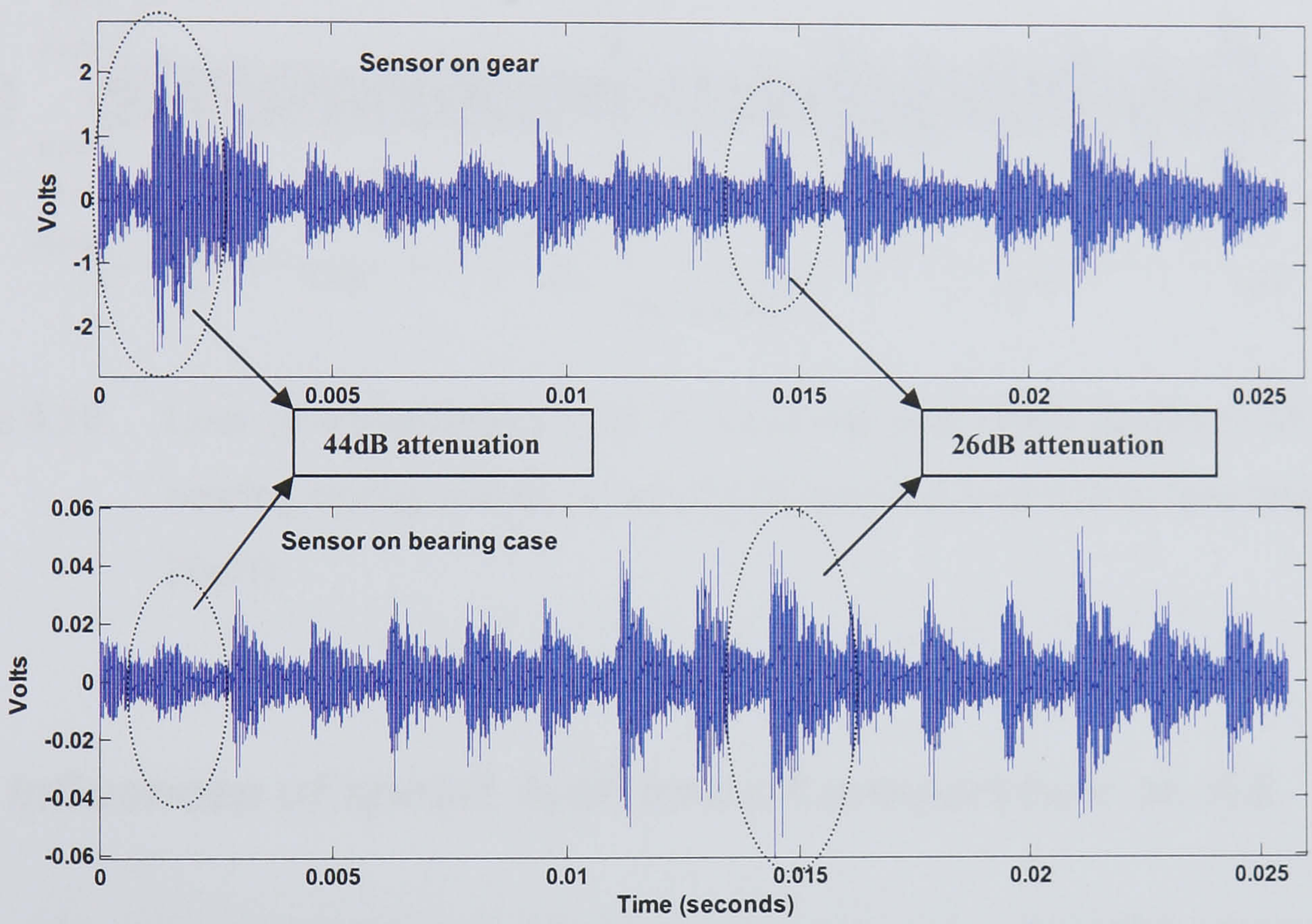

Figure 4.9 AE bursts detected on pinion sensor were observed on bearing casing sensor, speed 745 rpm and load 55 Nm (pre-amplification 40dB).

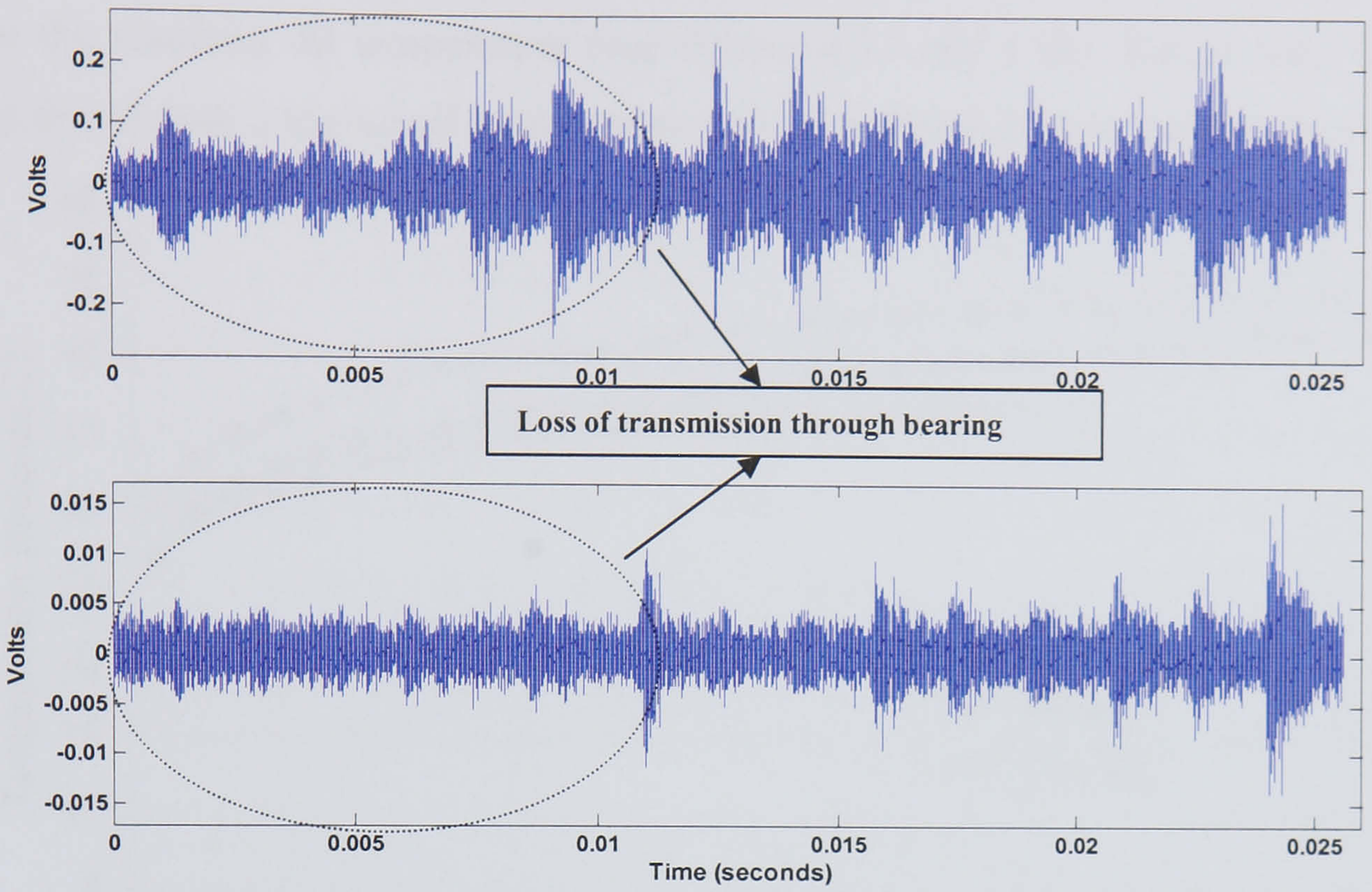

Figure 4.10 Loss of transmission path at particular gear mesh positions observed on bearing casing sensor, at speed 745 rpm and load 55Nm (pre-amplification 20dB).

4.6 Influences of speed, load and oil temperature on AE

The results presented in sections 4.2 and 4.3 thus far were considered unsatisfactory in identifying the seeded defect. Additional tests were performed to explain the discrepancies, particularly as other researchers had supported the applicability of these parameters to gear defect detection. The objective of the new test was to establish if operating conditions such as the oil temperature influenced AE levels. Whilst this would not directly enhance fault identification, it would provide important information on what influences AE activity within the gearbox.

Figures 4.11 and 4.12 illustrates that the gearbox only reached a stabilised temperature in excess of at least 5 hours of continuous running under both speed conditions. The starting points for all the three test conditions investigated were dependent on the ambient

temperatures prior to testing. Under both speed conditions, the higher the applied load the higher the resultant oil temperature (see figures 4.11 and 4.12). For all load conditions, higher speed gave a higher oil temperature, which is clearly illustrated in figure 4.13.

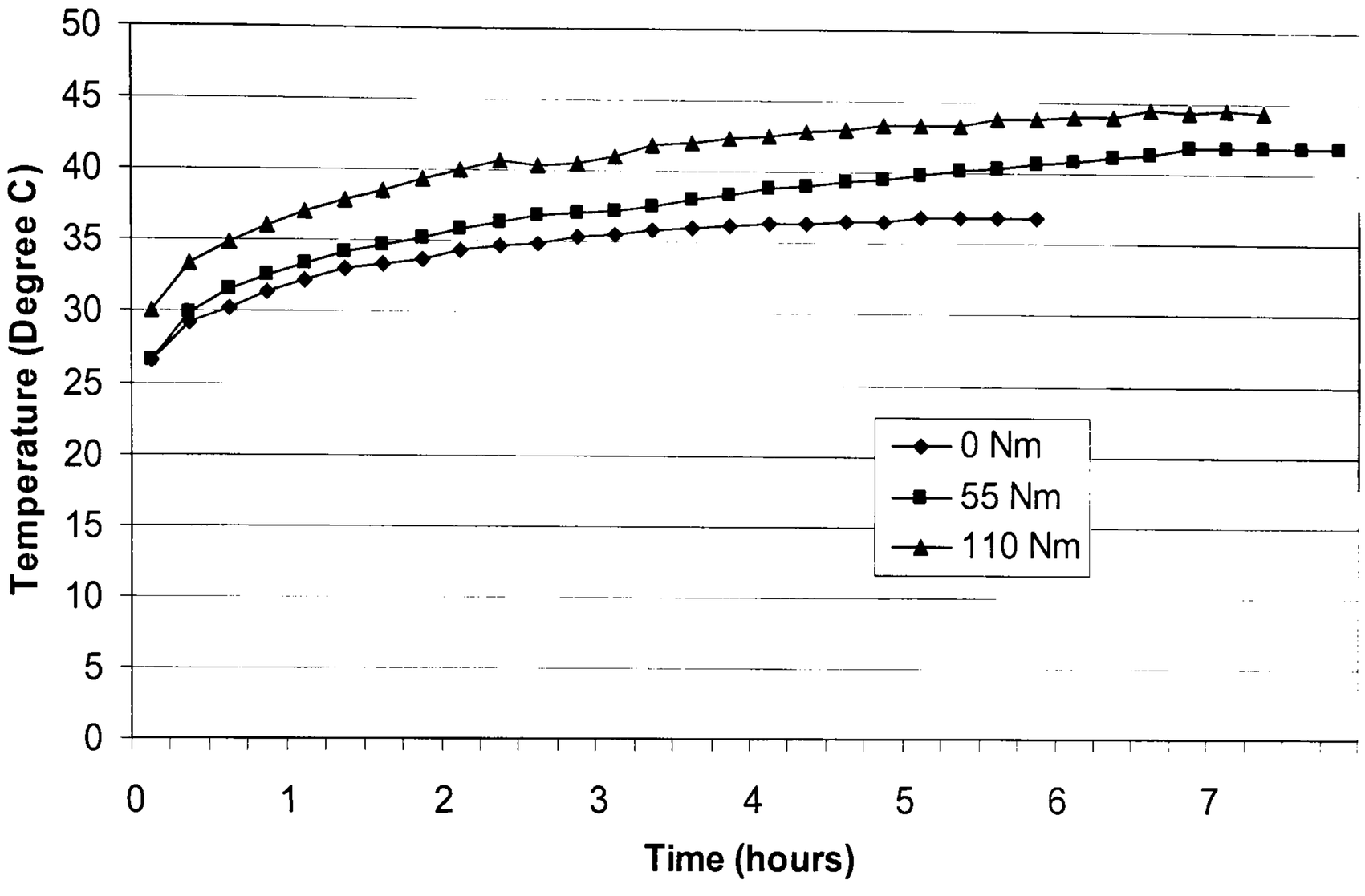

Figure 4.11 The effect of load on oil temperature for speed of 745 rpm.

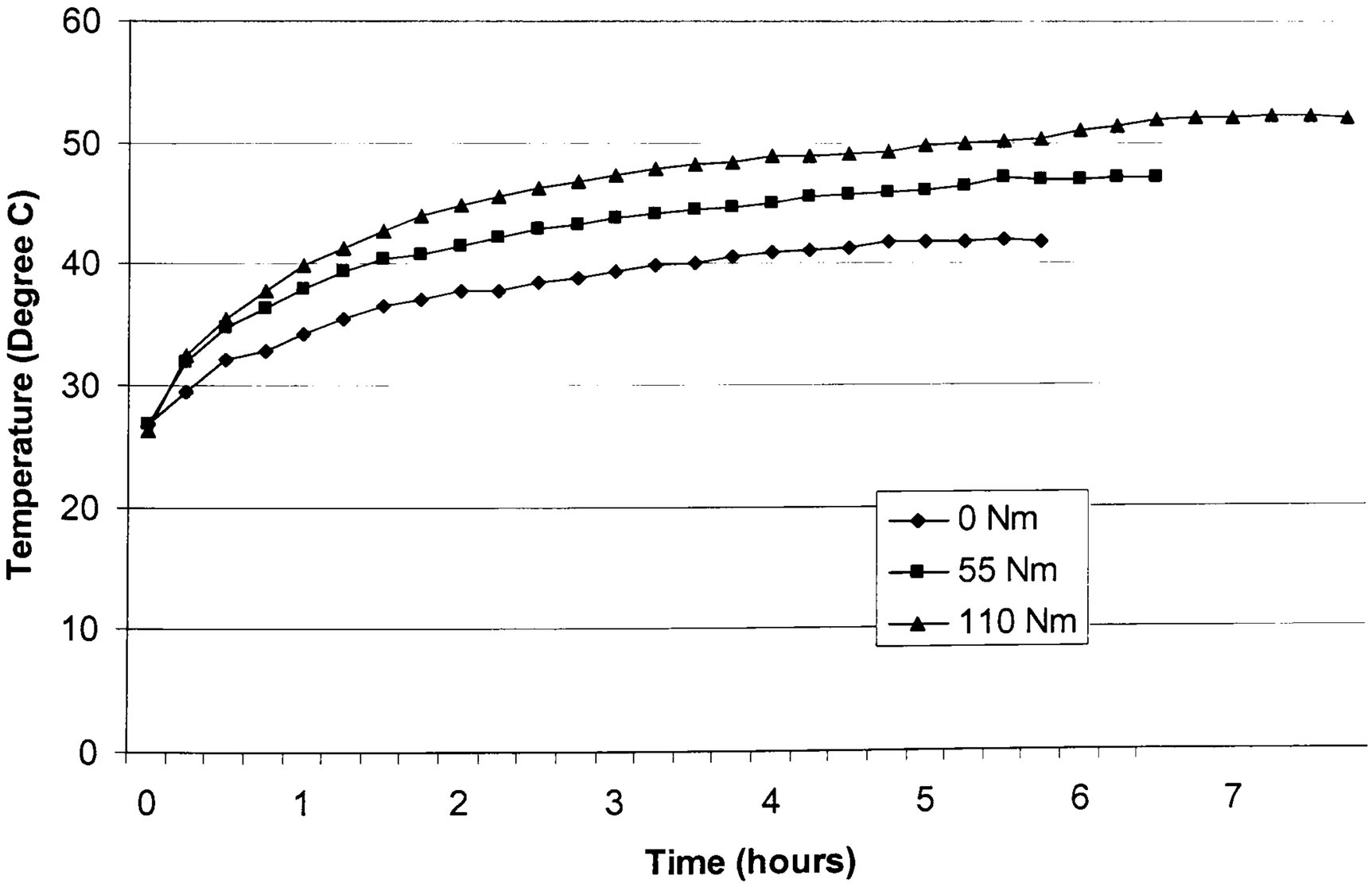

Figure 4.12 The effect of load on oil temperature for speed of 1460 rpm.

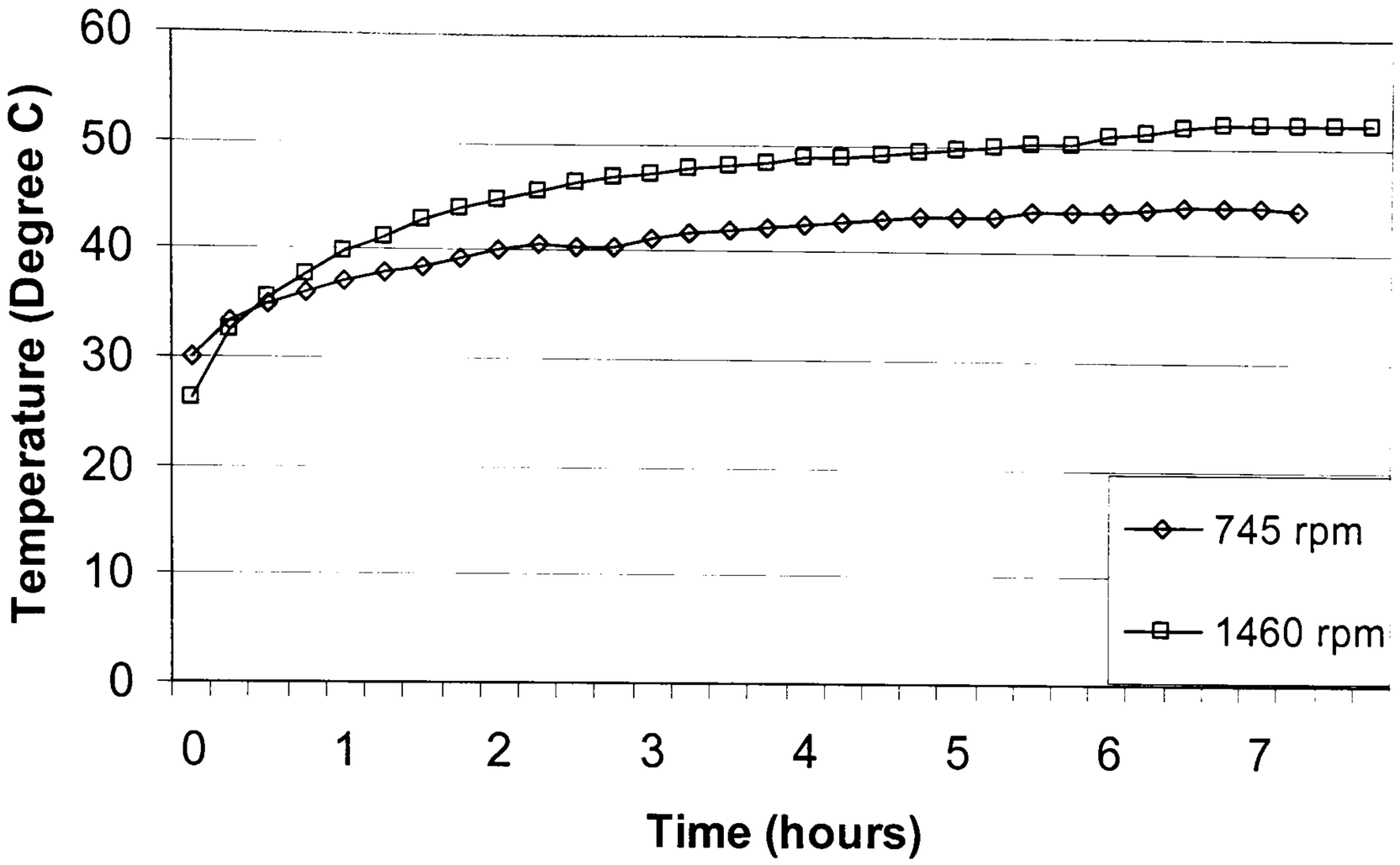

Figure 4.13 The effect of speed on oil temperature under applied load of 110 Nm.

The calculated oil film thickness between the gear teeth surfaces was computed based on the recorded oil temperature and the oil properties, and are depicted in figures 4.14 and 4.15. The detailed derivations of the calculated oil film thickness between the spur gear teeth were shown in Appendix D. The higher load would result in a thinner oil film. A higher operating speed will result in a thicker oil film though an increase in oil temperature will also be experienced. The increase in oil temperature will serve to reduce the film thickness. This decrease in the film thickness is less than the increased in film thickness due to the higher rotational speed. This is clearly shown in figure 4.16.

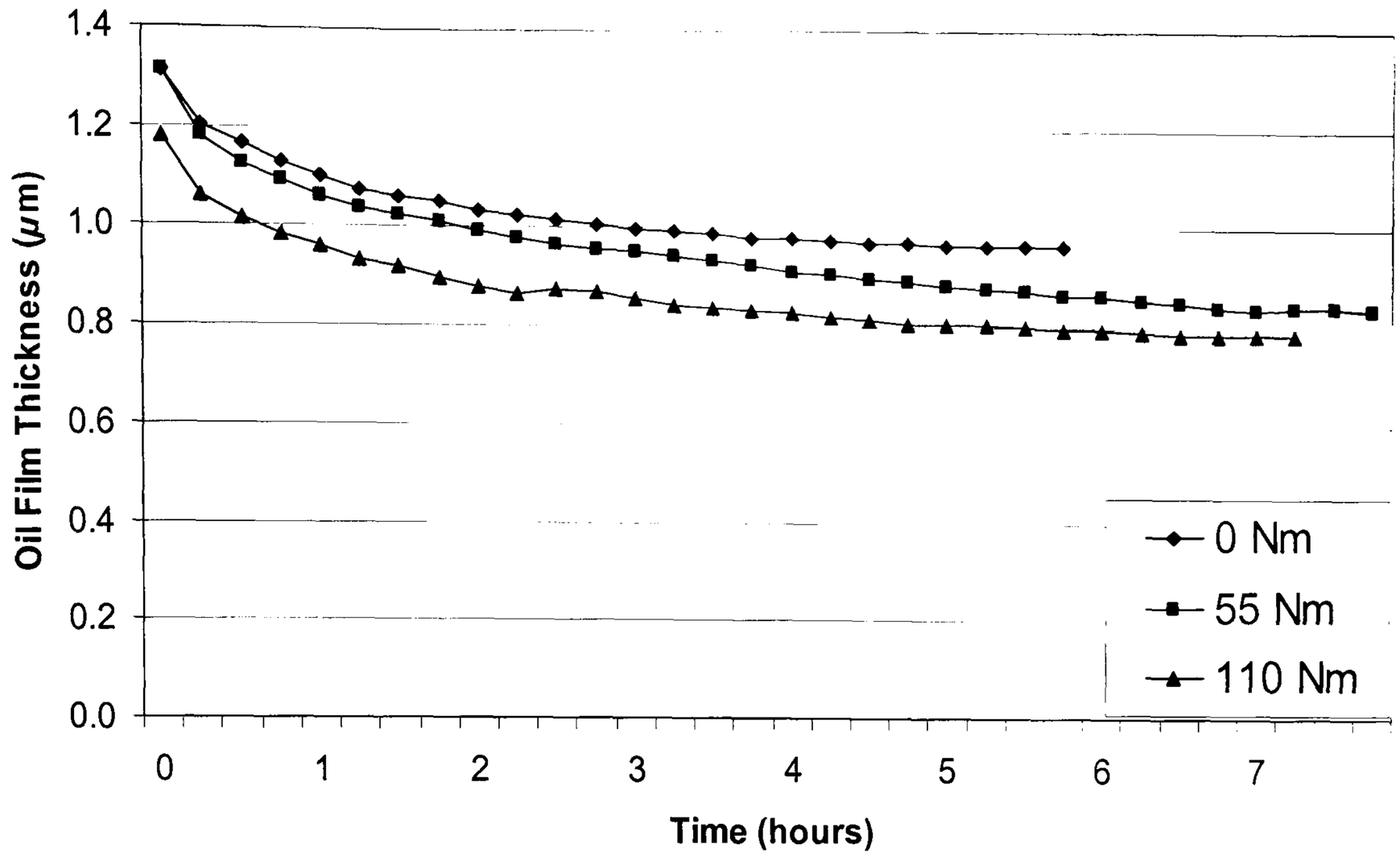

Figure 4.14 The effect of load on oil film thickness for speed of 745 rpm.

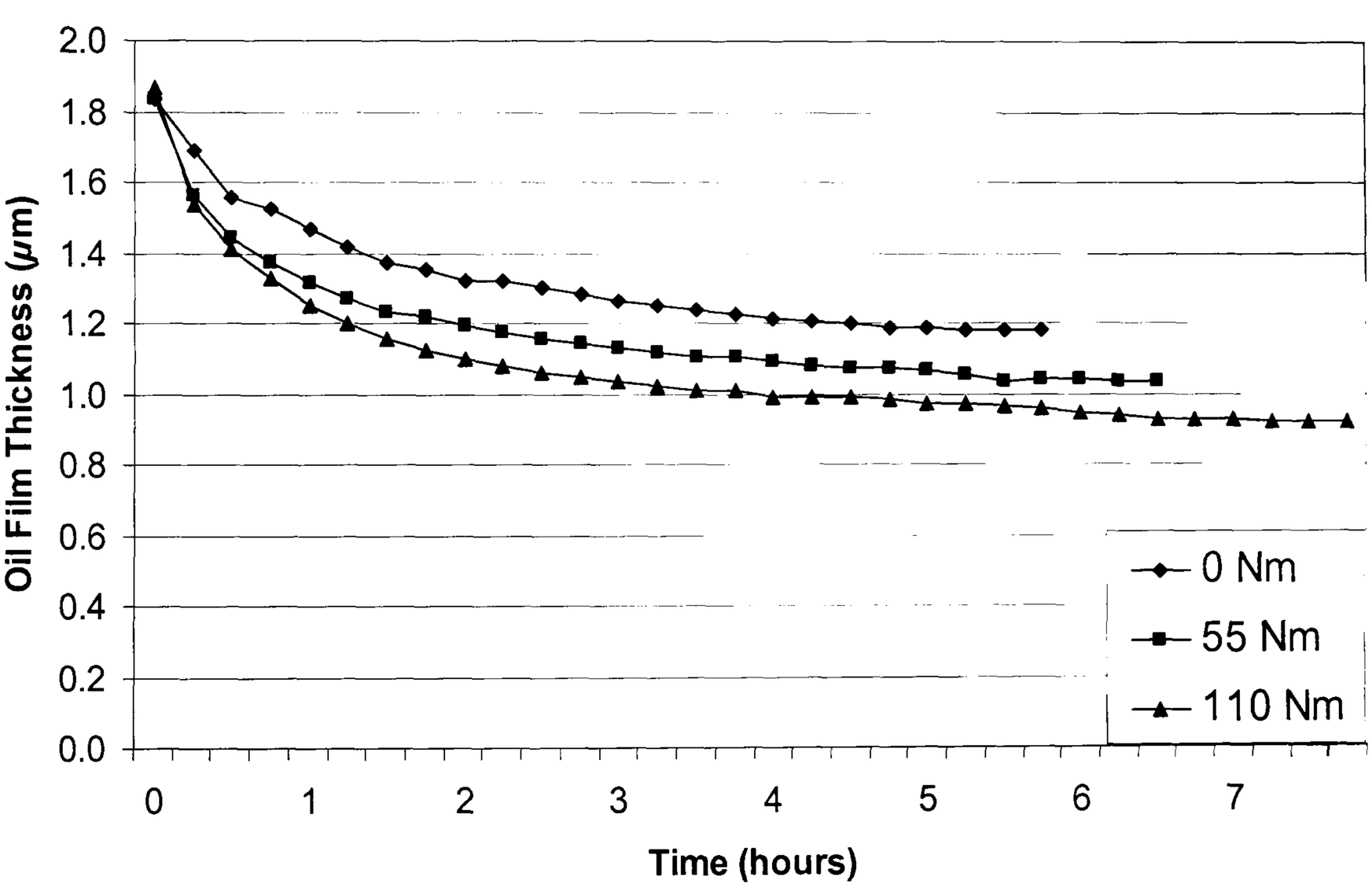

Figure 4.15 The effect of load on oil film thickness for speed of 1460 rpm.

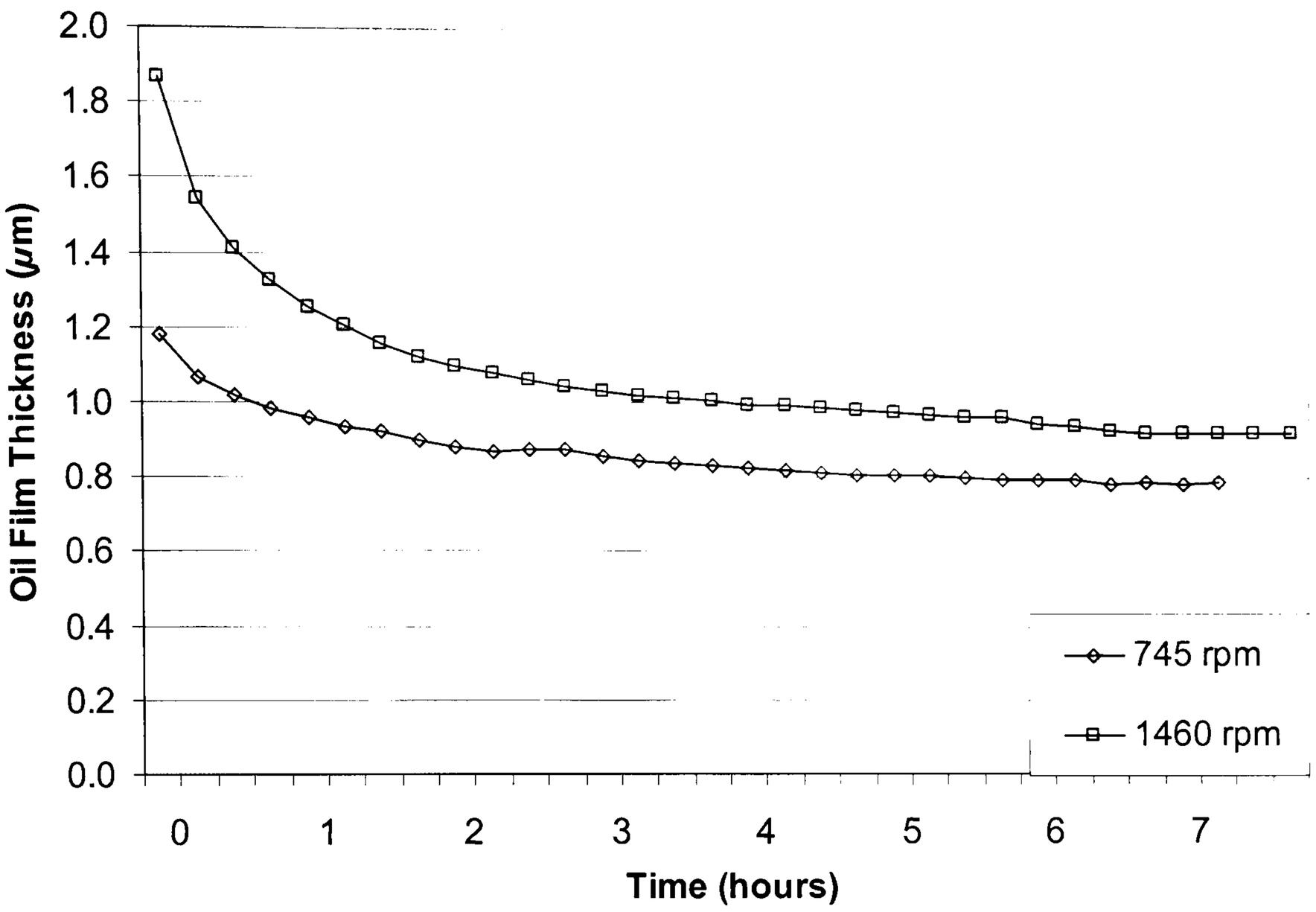

Figure 4.16 The effect of speed on oil film thickness under applied load of 110 Nm.

A smoothing technique was applied to the continuous AE data using moving average of 255 points. From figures 4.17 to 4.20, it was noted that the AE r.m.s and energy levels varied with time as the gear box reached a stabilised temperature. This implied that depending on what time the AE data was collected for a given speed and load condition, the variation in AE activity r.m.s could be as much as 33% (55Nm) and 60% (110Nm) for 745 rpm, and, 125% (55Nm) and 48% (110Nm) at 1460 rpm. The variation for energy ranged from 140% (55Nm) and 107% (110Nm) for 745 rpm, and, 300% (55Nm) and 113% (110Nm) at 1460 rpm. These values were calculated based on the variation between the minimum and maximum AE values (energy, r.m.s) for each test condition. For these particular tests the point at which the AE data for the seeded defect was captured is highlighted in figures 4.17 and 4.19. Thus, the AE signal captured during seeded defect tests were 'snapshots' that are largely influenced by speed, load and oil temperature. As 'snapshots' only provide information at an instance in time, the repeatability of the derived AE parameters will be subjected to considerable variation.

Furthermore, it is postulated the AE r.m.s values for 55Nm and 110Nm fluctuated as a function of increasing oil temperature (figures 4.17 to 4.20) because the gear teeth surfaces attempted to strike a balance between increasing lubricant temperature and decreasing surface roughness (these tests were started from 'cold conditions' and the gears were not run-in). These two factors have opposing effects on the AE levels; the former increases AE levels as oil film thickness reduces and asperity contact increases. The latter reduces the AE levels as the gear teeth surfaces smoothen. Clearly, the initial lubricant temperature and surface roughness of the meshing gear teeth surface will determine the starting level of AE but the running AE levels during temperature changing periods will reflect the balance described above.

The complications of the effect of oil temperature on AE activity have far reaching consequences, particularly as most of the published work to date (detailed in chapter 2) have not take cognisance of this effect. It is fundamentally flawed to compare AE activity from defect free and/or simulated defect conditions under varying loads without accounting for the influence of oil temperature. Whilst researchers [57, 52] have stated that AE indicators such as r.m.s and energy increased with increasing load and speed, none have taken cognisance of the effect of temperature on AE activity. Clearly measuring the load and speed will cause a change in oil temperature. The oil temperature is an influential factor in the AE generation, in addition to the rotational speed and load. This implies that whilst other researchers have stipulated the effect of load/speed on AE activity, the time of data acquisition, in effect the temperature of the lubricating oil, will determine what values of the AE level are obtained. If as observed, the AE parameters continually change for several hours, the data presented by other researchers are subjected to environmental conditions. Even if attempts were undertaken to collect AE data at specified times, the effect of ambient temperature, which will influence the temperature at which the data is collected, could present inconsistencies or repeatability issues. Developing the AE technique as a robust diagnosis tool without taking into consideration of temperature influence, will subject to error. As such a fundamental study into the influence of individual operating parameter, such as oil temperature, speed and

load on AE activity levels is paramount in developing the AE technique for diagnosis and/or prognosis, see chapter 5.

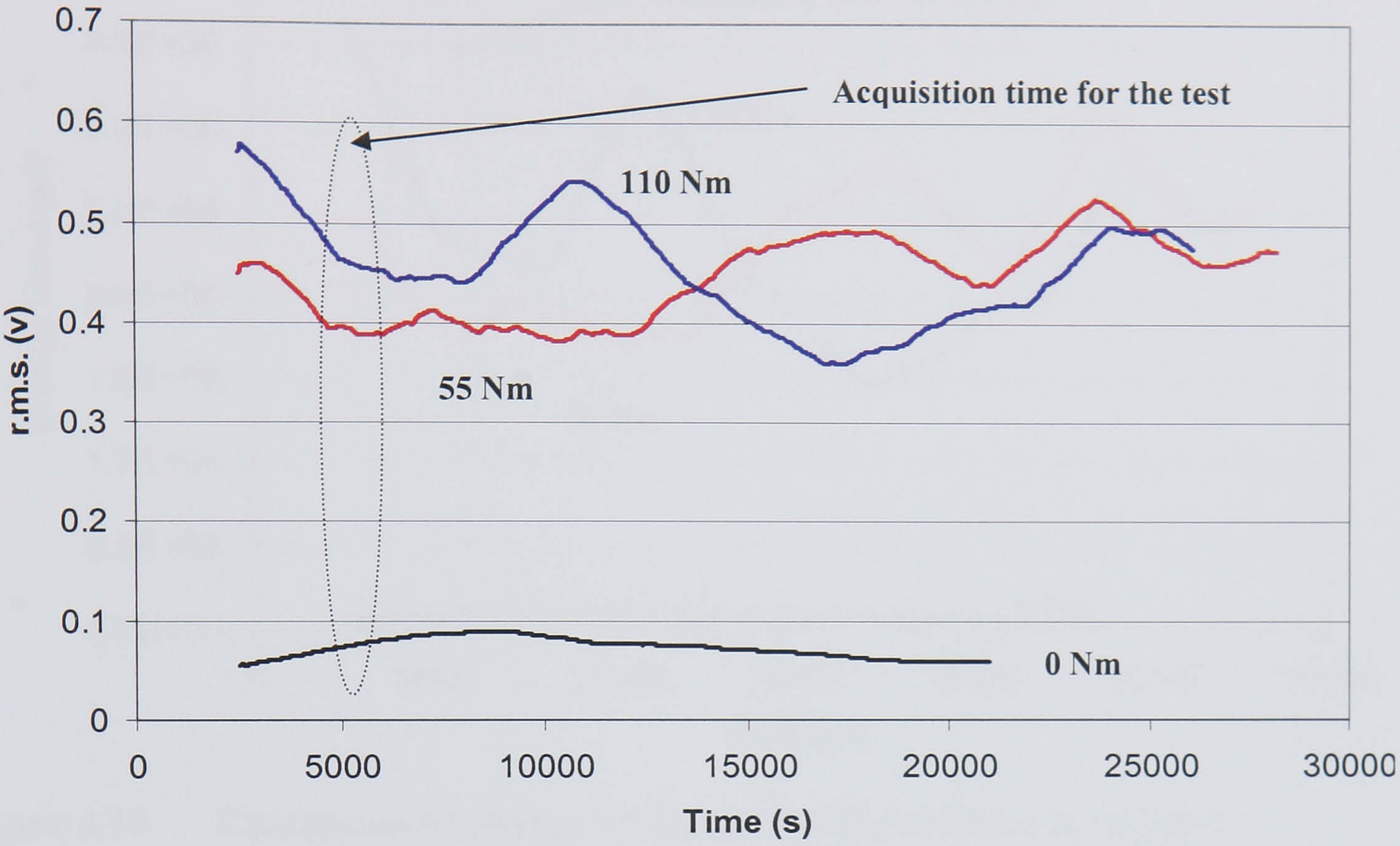

Figure 4.17 Continuous AE r.m.s values under different loads at 745 rpm.

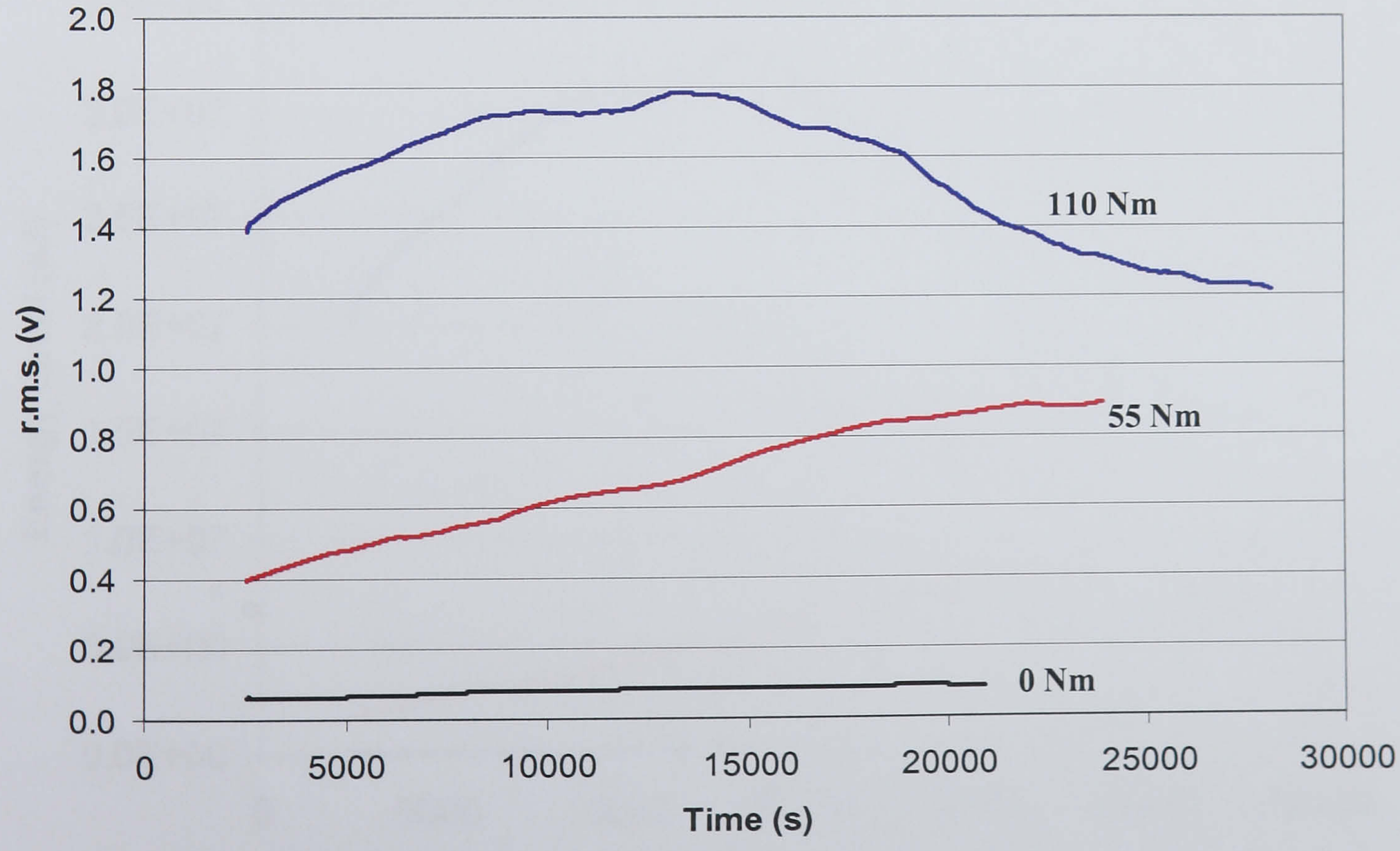

Figure 4.18 Continuous AE r.m.s values under different loads at 1460 rpm.

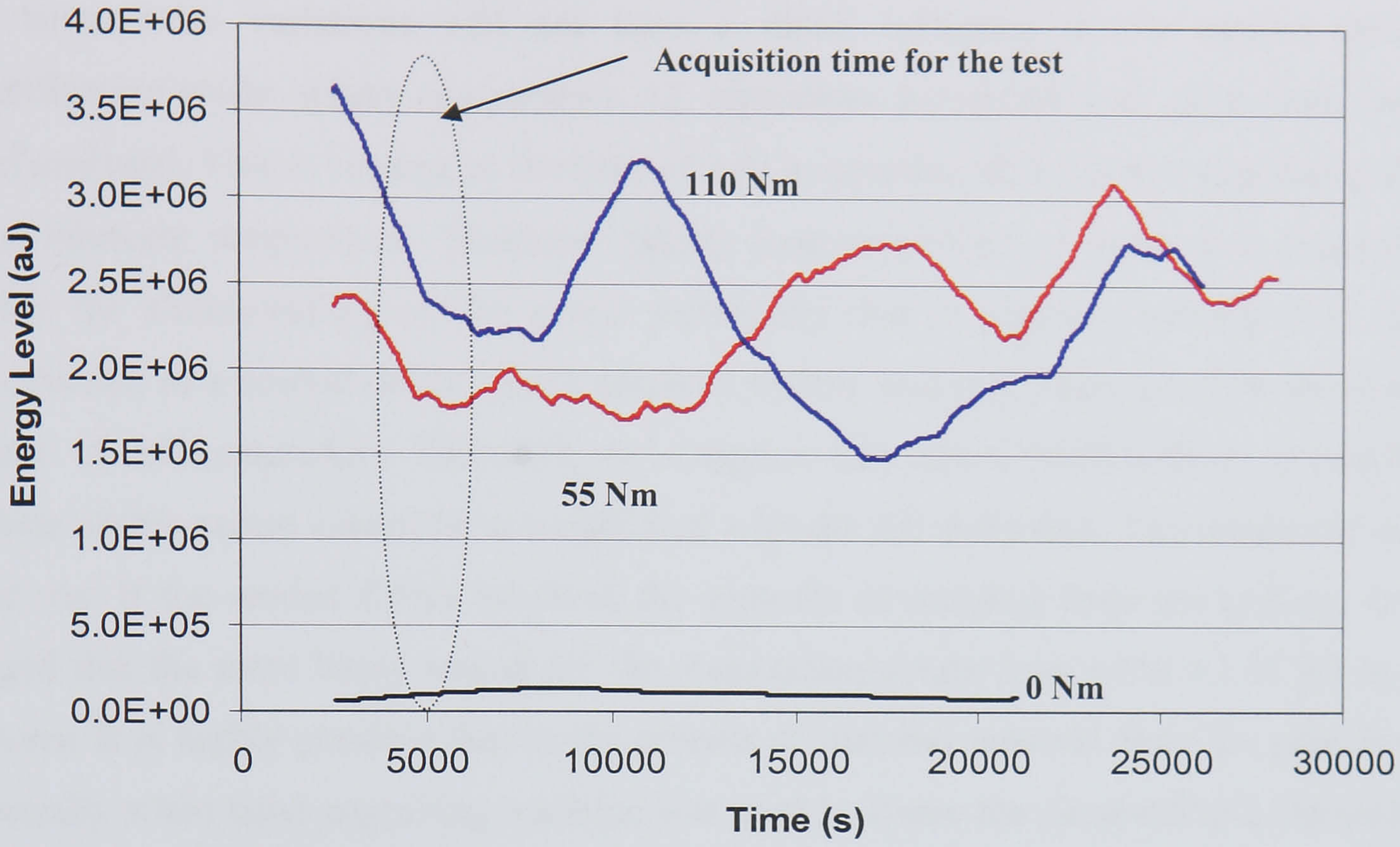

Figure 4.19 Continuous AE energy levels under different loads at 745 rpm.

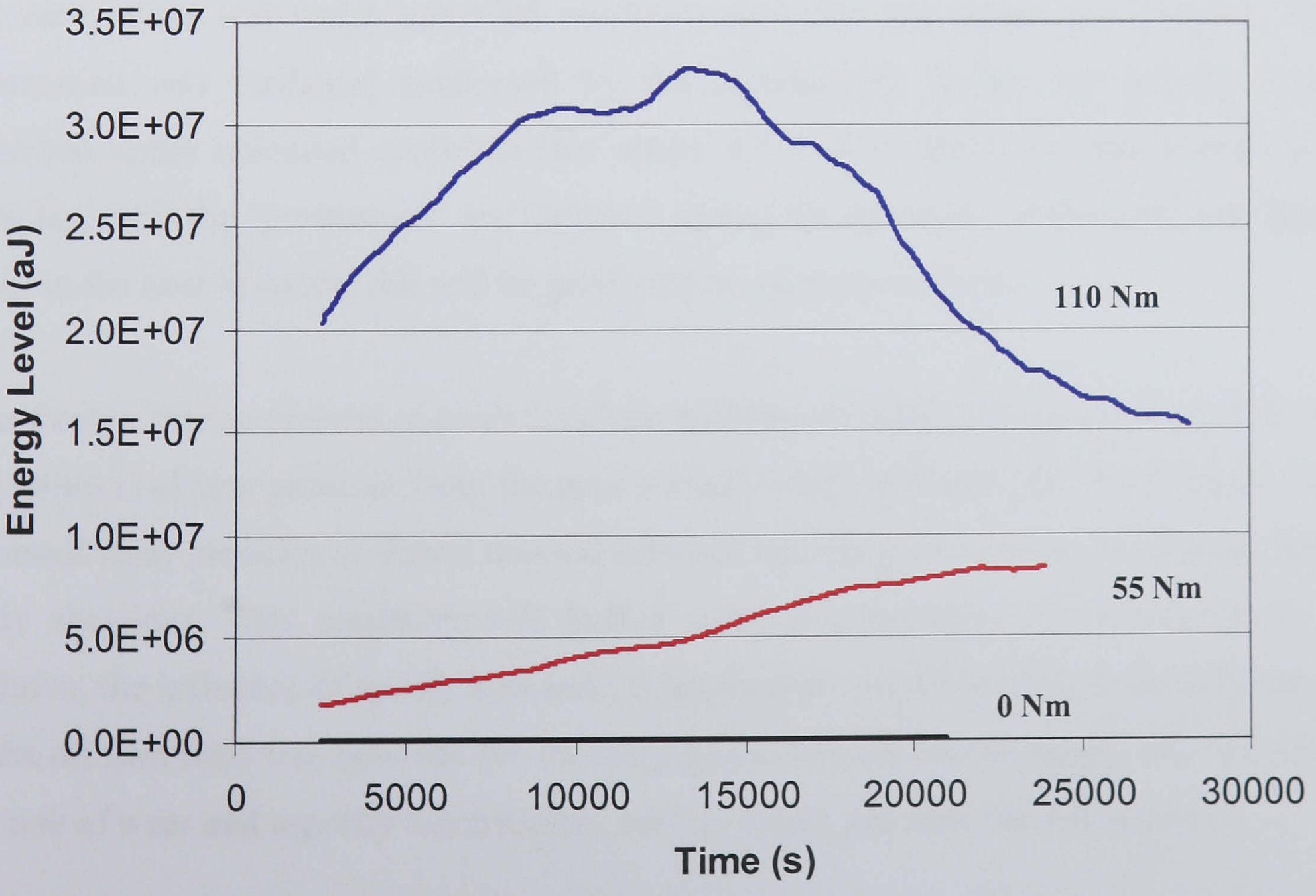

Figure 4.20 Continuous AE energy levels under different loads at 1460 rpm.

Oil temperature variations will not have a direct influence in the seeded defect identification study, where comparative AE signatures associated with each tooth have been analysed. This is because at the time of data acquisition all teeth will experience the same lubricant temperature. However, taking cognisance that AE activity is generated during the sliding/rolling of the gears, principally due to asperity contacts [61], the introduction of a seeded defect which removes surface material, digresses from the basic source of AE generation. Therefore, it is argued that defect identification of seeded defects of this nature cannot be accomplished with the AE technique. This statement will hold true if the seeded defect involved the removal of material from the surface. It is argued that the more likely reason for the observation obtain from table 4.1 to 4.3 is as follows: It is highly possible that in the process of material removal from the gear face, especially when hand engraving machine was used to create the simulated pit, 'mounds' or 'protrusions' will be formed at the boundaries of the seeded defect, see figure 4.21. These were created due to the displacement of material from the region of material removal. It was postulated that these 'protrusions' was responsible for high AE activity at the start of the test under unloaded condition just after the defect was planted. This postulation was furthered confirmed by the significantly higher AE activity levels observed under unloaded condition (see tables 4.1 to 4.3). However, this activity will only last until the 'protrusions' are flattened during the operation of the gear, see figure 4.22. In the later instance, AE will be generated by asperity contacts.

The wear or pitting process of gears involves initiation of micro-cracks, crack growth and the removal of tiny particles from the gear surface which will emit AE. Furthermore, the removed wear particles or debris trapped between mating gear surfaces will create third-body abrasions. This condition will further enhance generation of AE signatures. In addition, the influence of speed, load and oil temperature on AE activity is directly linked to the oil film thickness between the meshing gears. The oil film thickness will influence the rate of wear and asperity deformation, both of which generate the AE activity.

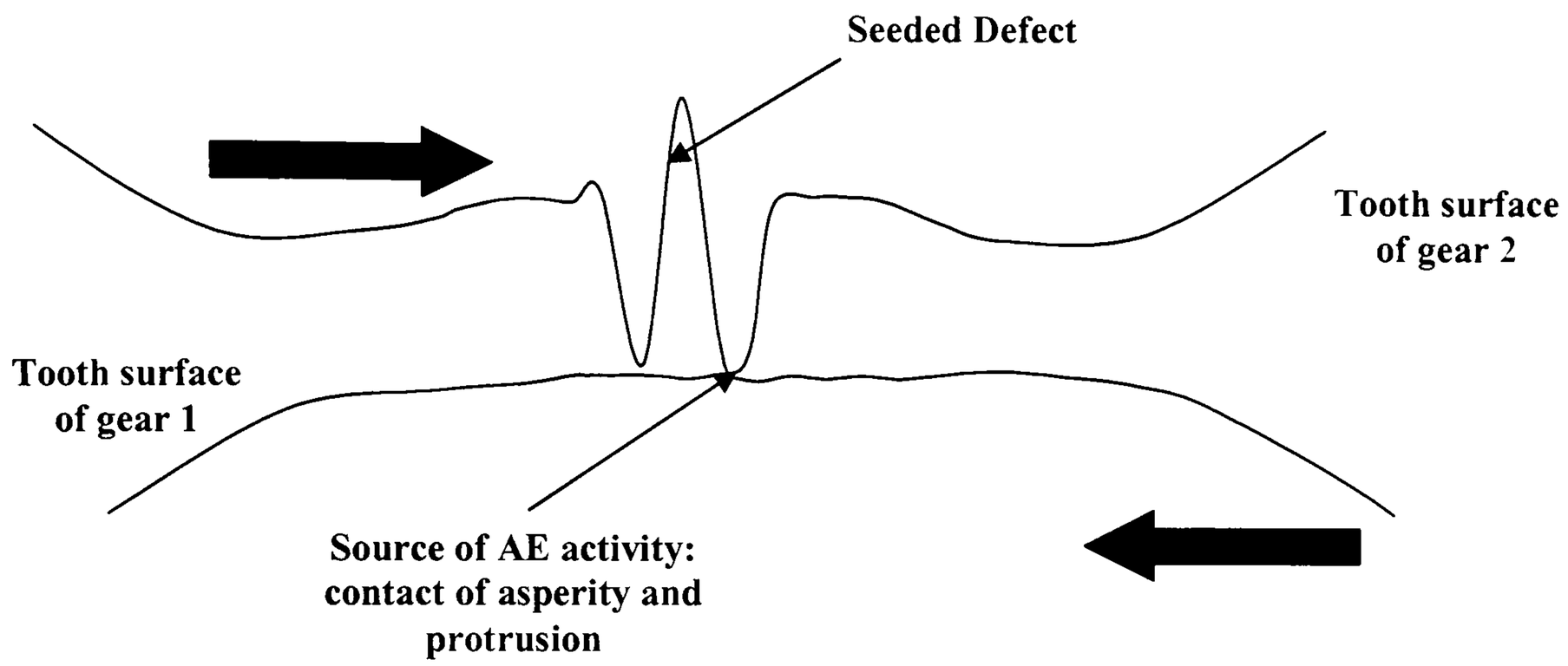

Figure 4.21 Mounds or protrusions of the gear surfaces in contact during rotation.

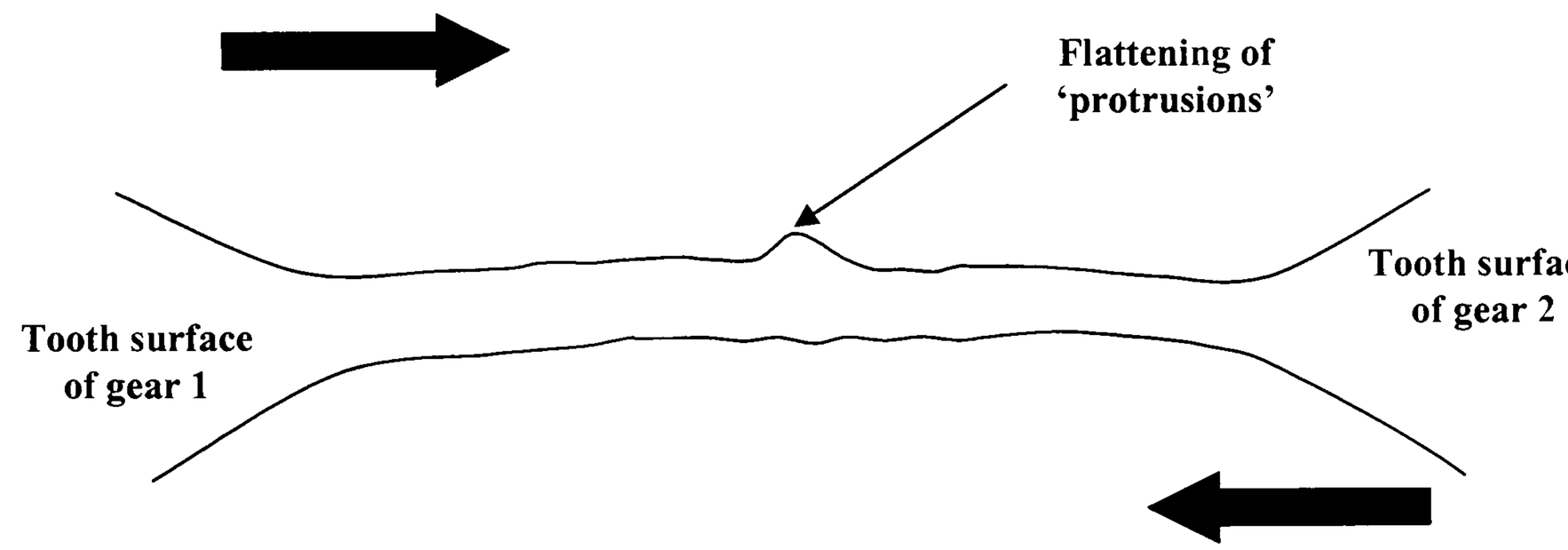

Figure 4.22 Flattened protrusions of gear surfaces.

5 AE SOURCE DURING GEAR MESH

5.1 Influence of operating variables on AE generation

In chapter 4, it was found that operating variables such as speed, load and oil temperature influenced the level of AE activity. However, to study the true effect of varying speed or load on AE level, the oil temperature of the gearbox has to be kept constant (i.e. under isothermal condition) since oil temperature changes with oil film thickness that will affect the surface interactions between the meshing gear teeth and thus the generation of AE signals. Due to the space constraint within the test gearbox, a heating coil could not be employed. The procedure employed in achieving isothermal conditions has been described in chapter 3.3.2.

5.1.1 The effect of load on AE levels under constant speed and temperature

After running in excess of 5 hours at 745 rpm and 220 Nm, the gearbox oil temperature stabilised within $\pm 0.1\ ^0C$ and the gearbox load was adjusted in accordance to the procedures laid out in chapter 3.3.2. In these tests, the average oil temperature was 40.0 ^0C with a maximum temperature difference of $\pm 0.9\ ^0C$. The same procedure was repeated at a speed of 1460 rpm. At a speed of 1460 rpm, the average temperature achieved was 48.0 ^0C with a maximum temperature difference of $\pm 1.6\ ^0C$. The results of these tests are presented in figure 5.1. As mentioned in chapter 3, the test condition at 745 rpm was repeated in a separate occasion. It is important to note that the loading procedures were reversed in this test case to ensure consistency and repeatability of the observations. The result for the repeated test is presented in figure 5.2, but the analysis of this result is not included in section 5.1.3 as the purpose of the repeated test is to ensure consistency in general observation of the AE behaviour. For the repeated test, the gearbox has an average oil temperature and maximum temperature difference of 41.3 ^0C and $\pm 1.5\ ^0C$

respectively. The slight difference in the temperature between the original and repeated test at 745 rpm can be explained by the variation of the ambient temperature. From figures 5.1 and 5.2, it was evident that the observed AE r.m.s values remained relatively constant for the varying load and fixed speed isothermal conditions. Relative changes in AE r.m.s for varying load conditions will be discussed in section 5.1.3.

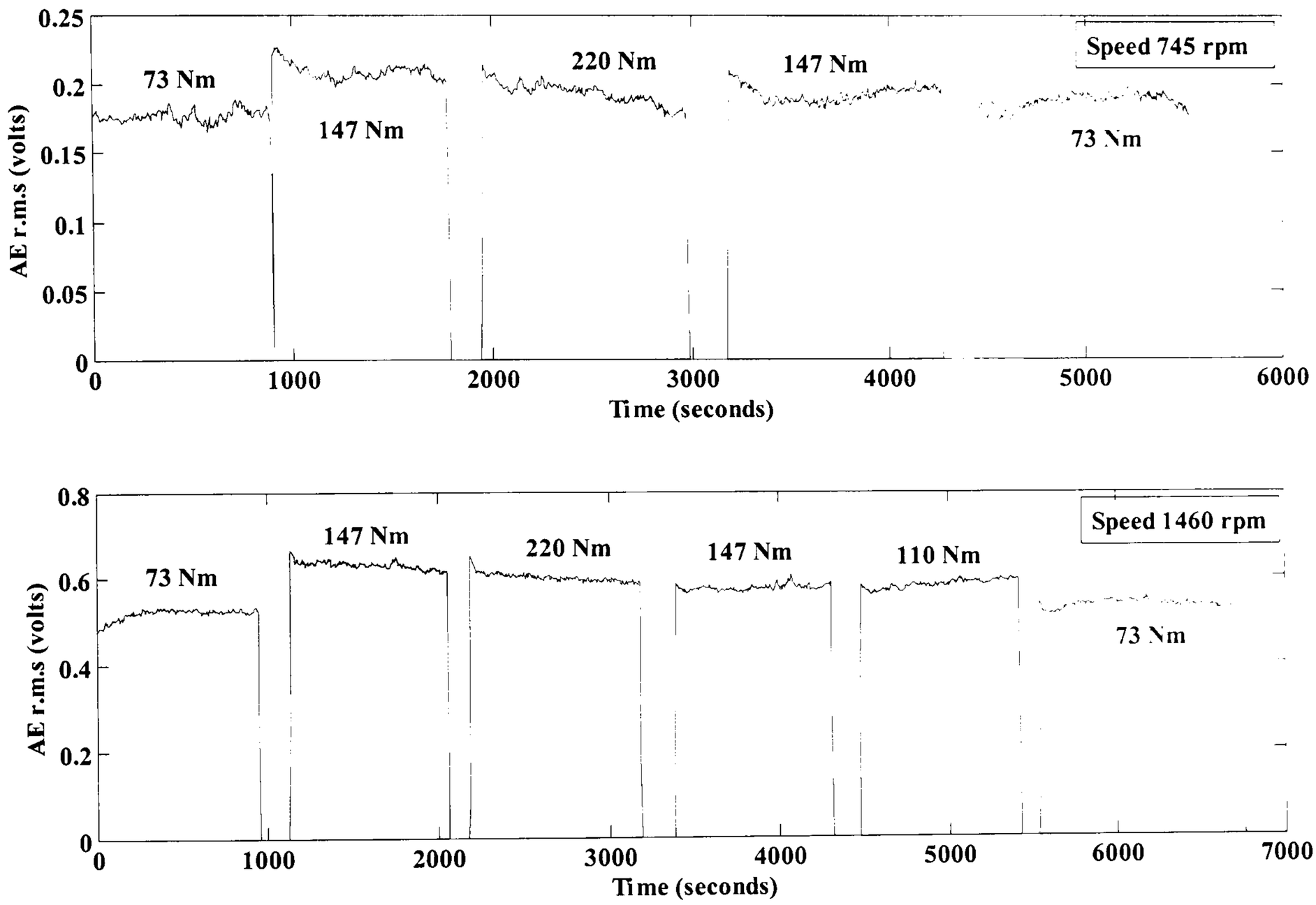

Figure 5.1 AE r.m.s levels at 745rpm and 1460rpm for varying load conditions under near isothermal conditions.

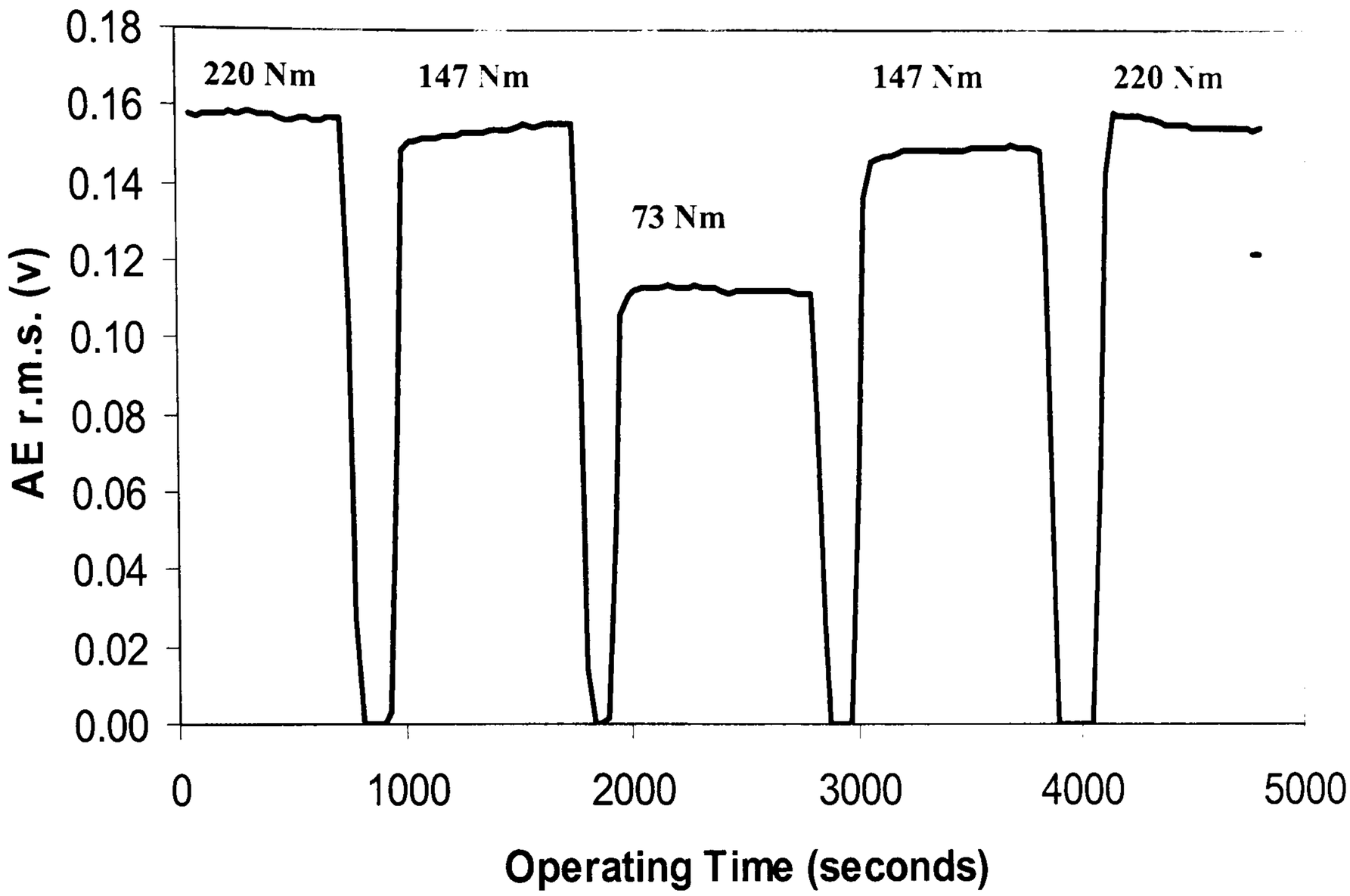

Figure 5.2 AE r.m.s levels at 745 rpm for varying load conditions under near isothermal conditions (repeated test results).

5.1.2 The effect of speed on AE levels under constant load and temperature

The gearbox was run at 1460 rpm with a load of 220 Nm in excess of 5 hours until the oil temperature stabilised at 50.0 ^{0}C. The speed of the gearbox was changed via the procedures detailed in chapter 3. The average oil temperatures were at 49.6 ^{0}C, 47.7 ^{0}C and 45.6 ^{0}C for the respective load condition 220, 147 and 73 Nm. A maximum temperature difference of ±1.0 ^{0}C was recorded for each test condition. Results of the test at the three load conditions investigated are illustrated in figure 5.3. It was observed that changes in speed under fixed load condition had relatively significant changes in measured AE r.m.s values under isothermal conditions in comparison with the changes in load under fixed speed conditions, see section 5.1.3.

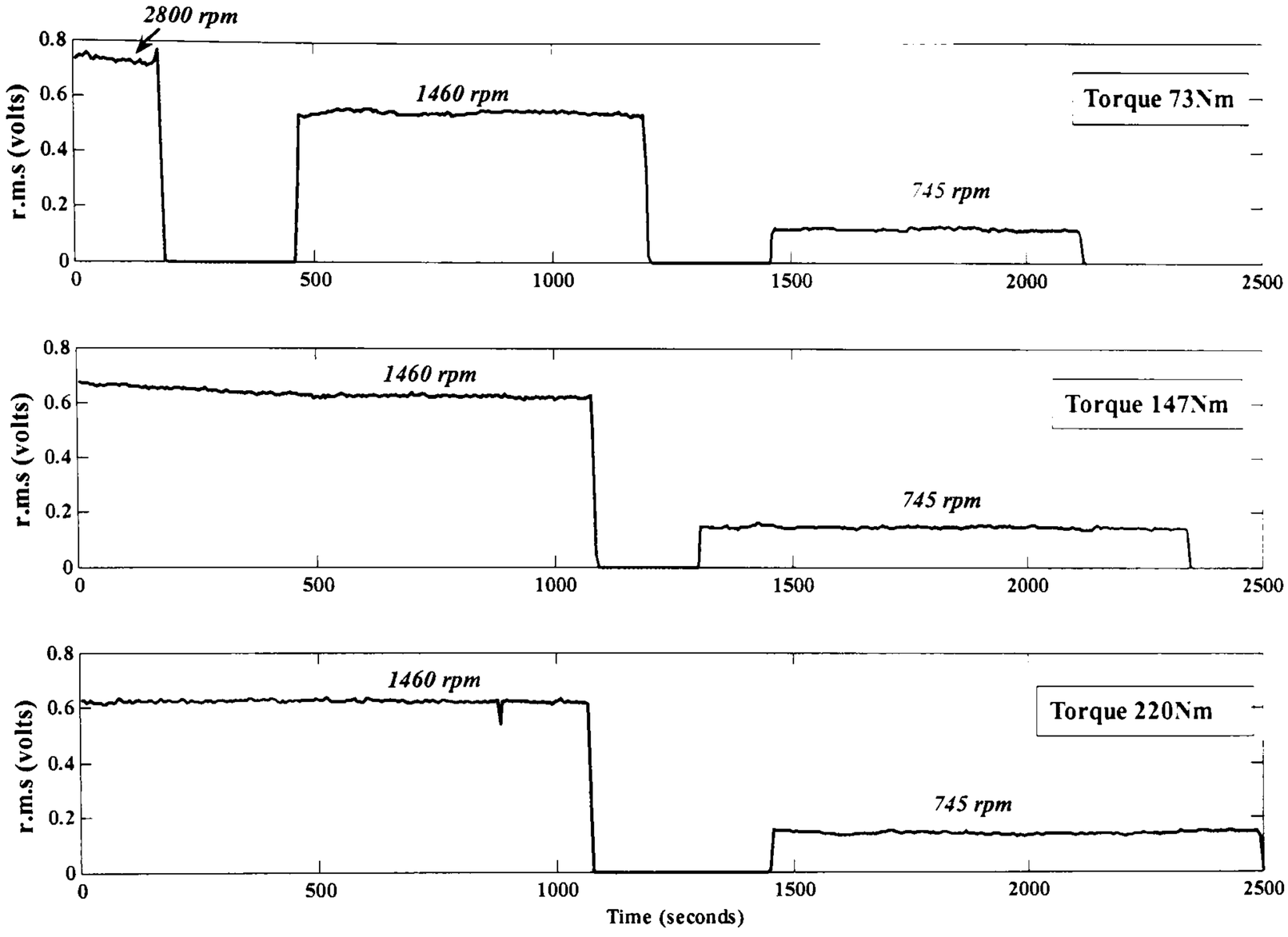

Figure 5.3 AE r.m.s levels for 745, 1460 and 2800 rpm at 73, 147 and 220 Nm.

5.1.3 Influence of operating parameters on AE levels under isothermal condition

The variation in AE r.m.s for each individual test condition was observed by calculating the standard deviation and coefficient of variation (CV); see tables 5.1 and 5.2. In addition, the maximum and minimum r.m.s values for each test condition are also detailed in tables 5.1 and 5.2. CV is defined as the ratio of the standard deviation to the mean [84]. A high CV indicates high variability of the AE r.m.s values. As the CV values calculated ranged from 1% to 5% it was concluded that the variation in AE r.m.s for each test condition was within the range to be expected for experimental analysis. Prior to making comparisons the average values of AE r.m.s associated with each test condition were obtained by averaging all data points for each individual test condition. Percentage changes relative to the mean AE r.m.s value for both the load and speed conditions investigated are summarised in table 5.3. Doubling the rotational speed from 745 to 1460

rpm at load conditions of 220, 147 and 73 Nm resulted in an increase in AE r.m.s value of 329%, 336% and 350% respectively; whereas doubling the load from 73 to 147 Nm at 745 and 1460 rpm resulted in an increase in AE r.m.s of 10% and 14% respectively. In addition, tripling the load from 73 to 220 Nm at 745 and 1460 rpm resulted in a comparable increase as observed when the loads were doubled, 6% and 14% respectively. It was interesting to note that when the speed was doubled from 1460 to 2800 rpm the increase in AE r.m.s was 34%. The reasons for the reduced percentage increase, in comparison to changes between 745 and 1460 rpm, will be detailed later in this chapter.

Load		**Max**	**Min**	**Mean**	**Std**	**CV (%)**
73 Nm						
	2800 rpm	0.8497	0.6505	0.7310	0.0213	2.91
	1460 rpm	0.5841	0.5123	0.5451	0.0100	1.83
	745 rpm	0.1504	0.1000	0.1205	0.0066	5.48
147 Nm						
	1460 rpm	0.6901	0.5968	0.6334	0.0168	2.65
	745 rpm	0.1722	0.1252	0.1447	0.0067	4.63
220 Nm						
	1460 rpm	0.6501	0.5970	0.6232	0.0079	1.27
	745 rpm	0.1638	0.1200	0.1412	0.0068	4.82

Table 5.1 Variation in AE r.m.s under fixed load conditions.

Speed		Max	Min	Mean	Std	CV (%)
745 rpm						
	73 Nm	0.2036	0.1566	0.1772	0.0068	3.84
	147Nm	0.2374	0.1860	0.2093	0.0079	3.77
	220Nm	0.2300	0.1652	0.1937	0.0096	4.96
	147Nm	0.2194	0.1668	0.1931	0.0079	4.09
	73 Nm	0.2174	0.1582	0.1877	0.0081	4.32
1460 rpm						
	73 Nm	0.5536	0.4662	0.5226	0.0136	2.60
	147Nm	0.6856	0.5804	0.6331	0.0114	1.80
	220Nm	0.6644	0.5694	0.6026	0.0121	2.01
	147Nm	0.6190	0.5500	0.5767	0.0093	1.61
	110Nm	0.6140	0.5444	0.5840	0.0116	1.99
	73 Nm	0.5700	0.5012	0.5356	0.0106	1.98

Table 5.2 Variation in AE r.m.s under fixed speed conditions.

	Average increase AE r.m.s (%)
Speed doubled (745 to 1460 rpm) (Load constant at 73 Nm)	350.4
Speed doubled (745 to 1460 rpm) (Load constant at 147 Nm)	336.6
Speed doubled (745 to 1460 rpm) (Load constant at 220 Nm)	329.7
Speed doubled (1460 to 2800 rpm) (Load constant at 73 Nm)	34.1
Load doubled (73 to 147 Nm) (Speed constant at 1460 rpm)	14.3
Load tripled (73 to 220 Nm) (Speed constant at 1460 rpm)	13.9
Load doubled (110 to 220 Nm) (Speed constant at 1460 rpm)	3.2
Load doubled (73 to 147 Nm) (Speed constant at 745 rpm)	10.2
Load tripled (73 to 220 Nm) (Speed constant at 745 rpm)	6.1

Table 5.3 Percentage increase in AE r.m.s for varying speed and load conditions.

From these results it is apparent that load has a relatively small influence on AE levels under conditions of constant temperature. Figures 5.1 and 5.2 depict this observation clearly; however, speed had a significant influence on AE levels, see figure 5.3. This finding has a direct correlation with film thickness levels under elastohydrodynamic lubricating conditions, where the influence of load on film thickness is negligible [32] in comparison to speed.

Under all test conditions observations of the AE waveform revealed AE transient bursts superimposed on a continuous type AE signatures, similar to that highlighted in figure 5.4. After the entire test conditions described, an inspection on the gear surface condition was performed and no visible damage such as scoring or pitting was present. This provided strong evidence that the transient AE bursts were not generated by either wear of gear teeth surface or tip/root interference during gear operation.

5.2 AE source mechanisms during gear mesh

From observations of the AE waveform, identical to that illustrated in figure 5.4, two characteristic types of AE's were present; continuous and burst type emissions. A continuous type AE refers to an AE waveform where the bursts are not discernible [86]. The burst type emission occurred at periods corresponding to the gear mesh frequency. In addition, amplitude variations between each AE transient burst have been observed. These amplitude variations likely to be attributed by the differences in the surface roughness of the meshing gear pair, and the dynamic effect of the gear teeth such as transmission error. The signature of the latter could result in varying dynamic loading for individual meshing pairs. This investigation did not investigate this influence of varying dynamic load on AE amplitude variation. Traditionally, transmission error is the prime source of noise and vibration in the gearboxes. Transmission error will provide a good explanation to the variations in AE signals experienced during the gear fatigue tests under the same test condition in addition to the initial oil temperature and surface roughness effect (see chapter 6.7.1.). In the attempt to investigate the source of the contributors to each type of emission during the gear mesh, three possible sources of AE were identified for investigation; tooth resonance, secondary pressure peak in elastohydrodynamic lubricated gears and asperity contacts.

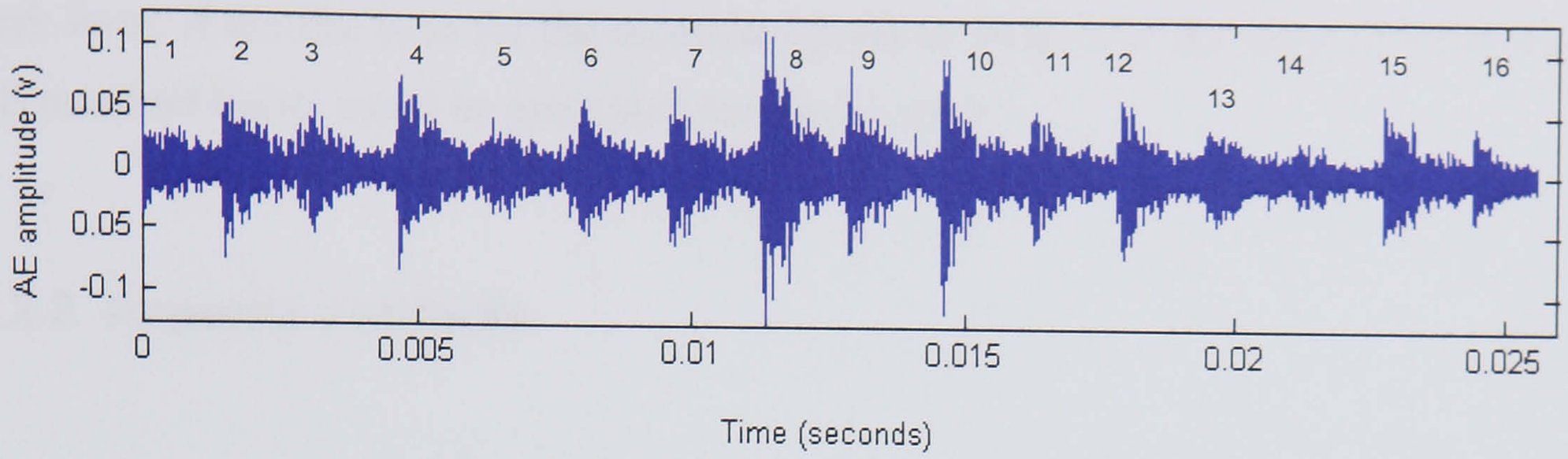

Figure 5.4 AE transient bursts representing sixteen meshing gear pairs [85].

5.2.1 Tooth resonance

The derivation and computation of the tooth resonance frequency is detailed in Appendix E. Estimation of the tooth resonance frequency was calculated at 75 kHz. This is below the frequency range of the AE sensor and high pass filters employed in the experiments and eliminated gear tooth resonance as a source of AE activity in the gear mesh.

5.2.2 Secondary pressure peak in the lubricant

Another possible source of AE during meshing of the test gears could be due to the pressure distribution between the contacting gear teeth surfaces and the lubricating oil film. A known phenomenon of elastohydrodynamic lubrication (EHL) under pure rolling is the secondary pressure peak [32]. This is the occurrence of a local pressure peak far in excess of the Hertzain maximum which effectively reduces the film thickness at that position by approximately a further 25%. The increase in pressure can be abrupt, depending on the surface velocity and material properties. This sudden increase in pressure or decrease in film thickness could be a source of AE activity although it could not be proven this stage; however, by the end of this chapter, and through a process of elimination, a conclusion on the contribution of this phenomenon to AE generation was reached. It may be worth noting that load has minimal influence on the film thickness or

level of secondary peak, but an increase in speed will result in an increase in the pressure peak level. If the rise time for the secondary pressure peak is in the order of 0.8 to 10 μs, AE transient bursts could be generated during the mesh.

5.2.3 Asperity contacts

During the gear mesh a combination of sliding and rolling will occur. As the gear teeth surfaces are limited to manufacturing capabilities asperity contacts will only occur under partial EHL or EHL during meshing on almost all gears, particularly as the calculated oil film thickness, in this instance, is less than the measured composite roughness of 1.9407 μm, see table 5.4. It is known that load has a negligible effect on film thickness under conditions of EHL. This was partly mirrored by the results presented in the earlier section, see figure 5.1, where the AE r.m.s levels remained relatively constant for varying loads, in comparison to speed, see figure 5.3. This similarity in observation, where load has a minimum effect on both the film thickness and AE level, may suggest an existing correlation between them. The small variation in AE r.m.s levels with load is attributed to the small variation in temperature during testing and the relatively small influence of the load on film thickness [30].

Based on the observations by Boness et al [60, 61], sliding between two surfaces will produce a continuous type AE waveform. Hence it was postulated that this type of emission contributes to the underlying operational noise levels. As depicted in figure 5.4, AE transients associated with the gear mesh are superimposed onto this operational noise level. It is worth stating that AE levels are known to increase with sliding speed [60, 61, 87, 62, 63]. An increase in rotational speed, and hence sliding speed of the meshing gears will result in an increase in AE levels on the basis that asperity contact exists during the sliding portion of the mesh cycle [60, 61, 87, 62, 63]. However, an increase in film thickness at the pitch line (rolling portion of the mesh cycle), due to an increase in speed [32], should cause a reduction in AE levels if the main source of the AE burst emission was from asperity contact at the rolling point. A thicker film will result in less asperity

contact, hence less AE activity, as proved by Boness et al [60, 61]. However results presented have shown this not to be the case, an increase in AE levels with increasing speed has been observed.

In order to understand and explain the interactions and relationships between the meshing gear teeth surfaces and the lubricating oil must be explored. The Lamda ratio, λ, or specific film thickness is defined as the ratio of the calculated elastohydrodynamic film thickness to the composite surface roughness, where the composite roughness is defined differently by various researchers; from the mean of the values for the two surfaces to square root of the sum of the squares of the individual surface roughness [10, 11]. In this stance, the latter was used. By employing the specific film thickness parameter, the lubrication regime, film thickness and the extent of asperity contact could be related. As observed in this investigation, that at the speeds of 745 and 1460 rpm, the change in specific film thickness (see table 5.4) was of lesser significant in its influence on AE levels with increasing speed, in comparison to the specific film thickness of 0.8 (2800 rpm, see table 5.4). As such the AE r.m.s levels were seen to rise over 300% with increasing speed, 745 to 1460 rpm. The reason for increased AE levels with speed is attributed to the higher strain rate the asperities experience at higher speeds [12]. An increase in strain rate is known to generate larger amplitude AE response [4]. However, at a rotational speed of 2800 rpm the increase in AE levels were 10-fold less than observed for the speed increase from 745 to 1460 rpm. This would suggest that at this speed the influence of film thickness had caused a reduction in the rate of increase in AE levels. It will be expected that a further increases in speed will actually cause a gradual reduction in AE levels as a full elastohydrodynamic film is approached. This would imply two processes affecting the generation of AE. Firstly, the influence of high strain rates with increasing speeds and a corresponding increase in AE levels. The second involves the influence of film thickness in separating asperities.

73Nm	Temperature (^{o}C)	Kinematics viscosity (mm^2/s)	Calculated Oil film thickness (μm)	Specific film thickness
745rpm	45.4	99.7	0.827	0.426
1460rpm	45.8	97.8	1.146	0.590
2800rpm	45.3	100.2	1.606	0.828
147Nm	**Temperature (^{o}C)**	**Kinematics viscosity (mm^2/s)**	**Calculated Oil film thickness (μm)**	**Specific film thickness**
745rpm	47.3	90.8	0.789	0.406
1460rpm	48.0	87.8	1.086	0.559
220Nm	**Temperature (^{o}C)**	**Kinematics viscosity (mm^2/s)**	**Calculated Oil film thickness (μm)**	**Specific film thickness**
745rpm	48.9	84.1	0.759	0.391
1460rpm	50.3	78.7	1.028	0.530

Table 5.4 Oil film and specific film thickness calculation.

As gears meshed, sliding and rolling of the gear teeth surfaces always occur simultaneously or independently, depending on the position on the line of contact. As depicted in figure 5.4, AE transient bursts associated with gear mesh are superimposed onto the continuous type AE waveforms. These transient AE burst emissions may imply the source of AE at the gear mesh to be either the secondary pressure peak or asperity contact at the pitch line (rolling point). As sliding occurs prior to, and after, the pitch point, any AE activity generated from sliding will not necessarily be associated with the gear mesh frequency but will take the form of a continuous process of sliding, particularly as the contact ratio was 1.77. The results of tests with fixed load and temperature, but varying speed, supports the idea that the secondary peak could also be a

contributor to the burst emission, as the peak amplitude of the pressure peak is known to increase with speed. In an attempt to differentiate between the secondary pressure peak, sliding and rolling asperity contact as the source of the transient AE burst a couple of experiments were undertaken. The first involved running a set of gears to destruction under dry conditions while the second involved running a damaged set of gears (loss of profile) under lubricated condition.

5.2.4 Observations of AE under dry conditions

This test was run under dry conditions with the same experimental set-up are of those previously employed; speed 745 rpm, load 220 Nm. The gear teeth surface and gearbox housing were cleaned with 'Acetone' thoroughly in an attempt to achieve fully dry running conditions. However, irrespective of the effort to ensure a clean gear surface it is highly probable that a thin film of oil/acetone will exist on the gear surface at the start of the tests. As the gearbox ran up, the lubrication condition at the meshing face will rapidly develop from partial EHL to boundary lubrication and finally dry conditions will be attained. This is primarily due to the temperature increase under operation. It took approximately 9-minutes from the start of the test until shutdown. During this period continuous AE r.m.s data and AE waveforms were recorded at various stages during the 9-minute period, see figure 5.5.

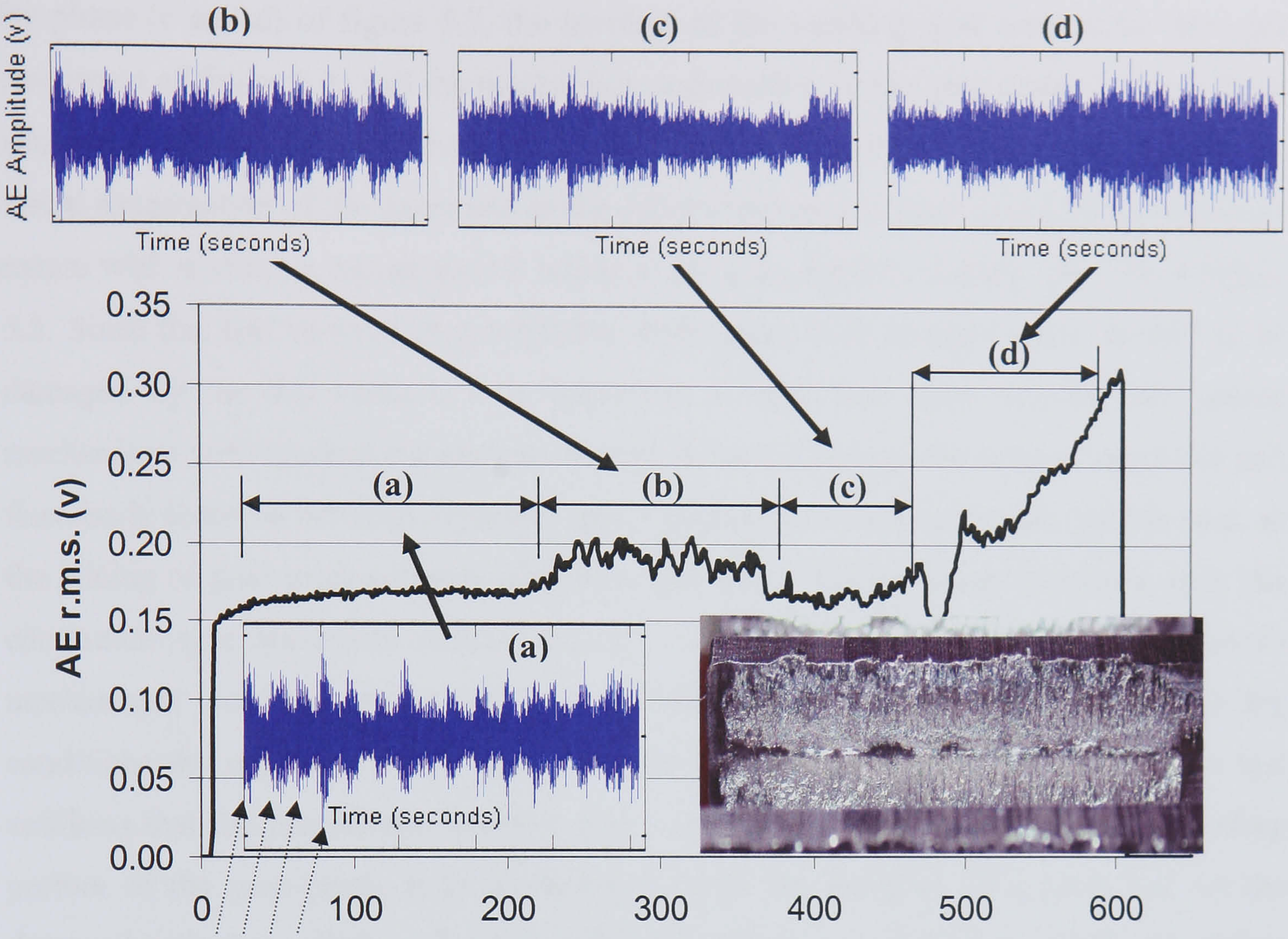

Figure 5.5 AE r.m.s levels for the 'dry run' test with associated AE time waveforms.

Figure 5.5 shows the AE waveform at several stages during the test condition. Plot (a) represents the period during which the film on the gear surface was gradually drying out. The transient burst associated with the gear mesh are visible. Five minutes into the run, the transient bursts were barely visible as the waveform approached a continuous type AE response; see plot (b). After a further 2-minute run, the AE transients associated with the gear mesh were no longer visible; see plot (c). By this stage, it is anticipated that the gears were operating under dry conditions. After a further two minutes the AE r.m.s data (figure 5.5) showed a steady rise in AE r.m.s levels suggesting that the gears were being damaged. A continuous type AE waveform was now evident, see plot (d). The test rig was stopped due to the excessive vibration levels and a visual examination of the gears was undertaken, see insert in figure 5.5.

By phase (c and d) of figure 5.5, the involute of the meshing gear teeth were damaged (see insert of figure 5.5) and the mechanism responsible for the gear damage was sliding, which was also dominant in the generation of AE. This conclusion was reached based on visual examination of the gears and as the AE waveform was dominantly of a continuous nature with minimum transients AE bursts at the gear mesh frequency, plot (d) of figure 5.5. Since this test was ran in a condition where gear teeth surfaces were allowed to be damaged by the dry contact, it is important to note that other possible AE source mechanisms with random transient burst type emission such as fractural of asperities and third-body abrasion between asperities and wear particles may be present. In this case, as the sliding of gear teeth surfaces dominates the entire AE waveform spectrum, only the continuous type waveform existed and the AE waveforms generated by other source mechanisms were masked within the dominant waveform due to sliding. Under dry conditions the influence of the secondary pressure peak will be non-existent. This test confirms that the continuous emission type waveforms are a direct result of the sliding portion of the gear mesh. It is interesting to note the presence of a pitch line on the damaged gear face, albeit undulating and non-uniform across the face width; see figure 5.5.

5.2.5 Observations of AE due to loss of gear profile

The next test involved running the damaged gear (loss of involute profile) for a prolonged period, approximately 30-minutes, whilst observing changes in AE waveform. The same test conditions as applied in the previous test were employed. In addition, as the pitch line on the gear face was still evident after considerable wear, as observed in figure 5.6, it was thought that the inclusion of a lubricant towards the end of the test might give an indication of the influence of the secondary pressure peak on the generation of transient AE's. Again the test rig was cleaned with 'Acetone' to achieve an oil free environment. At the start of the tests AE transient burst were observed, as noted in the previous test. Again after a few minutes an intermediate stage between burst type emissions superimposed on operational noise to continuous type emissions was evident, see figure

5.7, plot (a). A couple of minutes later a continuous type waveform was evident, see figure 5.7 plot (b), though some transient AE bursts were still evident. Unlike the previous tests where the experiment was stopped at this stage due to excessive vibrations, the rig was allowed to continue operating.

Figure 5.6 Damage gear teeth surface showing loss of involute profile with the presence of the pitch-line.

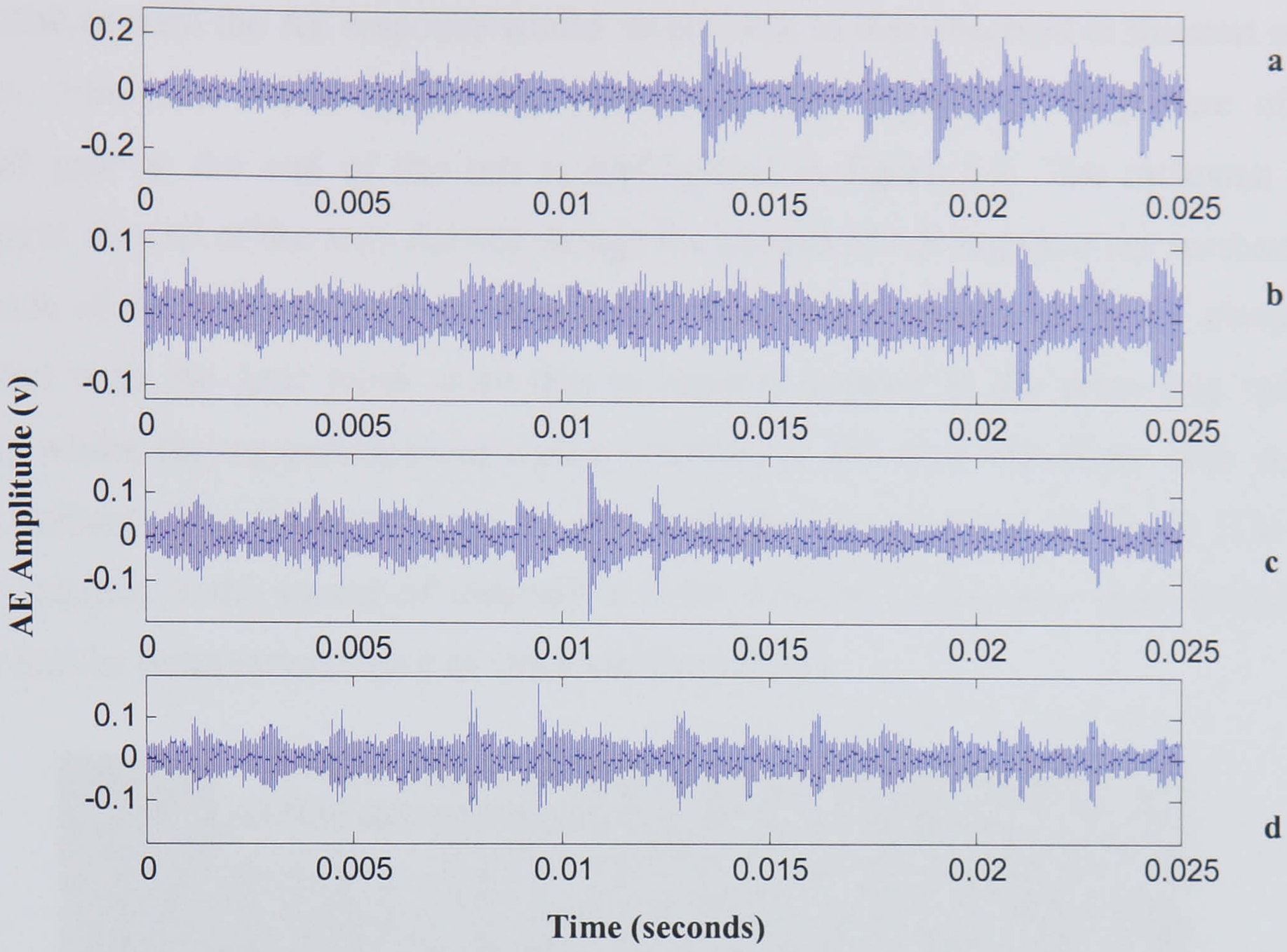

Figure 5.7 Illustration of AE waveforms at varying stages during the second dry test run (loss of gear profile test). (a) AE waveforms at the start of the test (b) Continuous type AE waveform dominates after several minutes of operation with increased vibration levels (c and d) AE waveforms reverted back to as observed during the start of the test where the vibration level was subsided.

Very interestingly it was noted that the gradual rise in vibration subsided and at the same time the AE waveform revealed AE transient bursts as at the start of the test, see plots (c and d) of figure 5.7. With prolonged running a gradual rise in vibration was noted and the AE waveform gradually reverted back to a continuous type. This cycle was noted throughout the test period. The rise in vibration was attributed to be associated with the damaging of the gear faces. Under this regime it would be expected that continuous type AE's would dominate due to the collation of numerous AE transients during this period. The transients will be associated with the breakage of asperities during the sliding process, and, the removal of material from the gear face. On the contrary, a reduction in vibration levels will imply a condition where the gears were no longer in the damaging

regime and as such the AE response would revert back to that observed at the start of the test, i.e., transients superimposed on continuous type signatures. A picture of the damaged gear at the end of the test is highlighted in figure 5.8. The inclusion of a lubricant at the end of the tests did not change the pattern of AE response nor increase the magnitude of the transient AE type response. This clearly showed that the AE transients associated with the gear mesh were due to asperity contact at the pitch line (rolling contact) whilst the operational/underlying continuous AE type waveform was due to sliding contact. The findings agree in part with the observations of Smith [13] that asperity contact is the source of transient activity detected at the gear mesh frequency, though Smiths observations were at vibration frequencies.

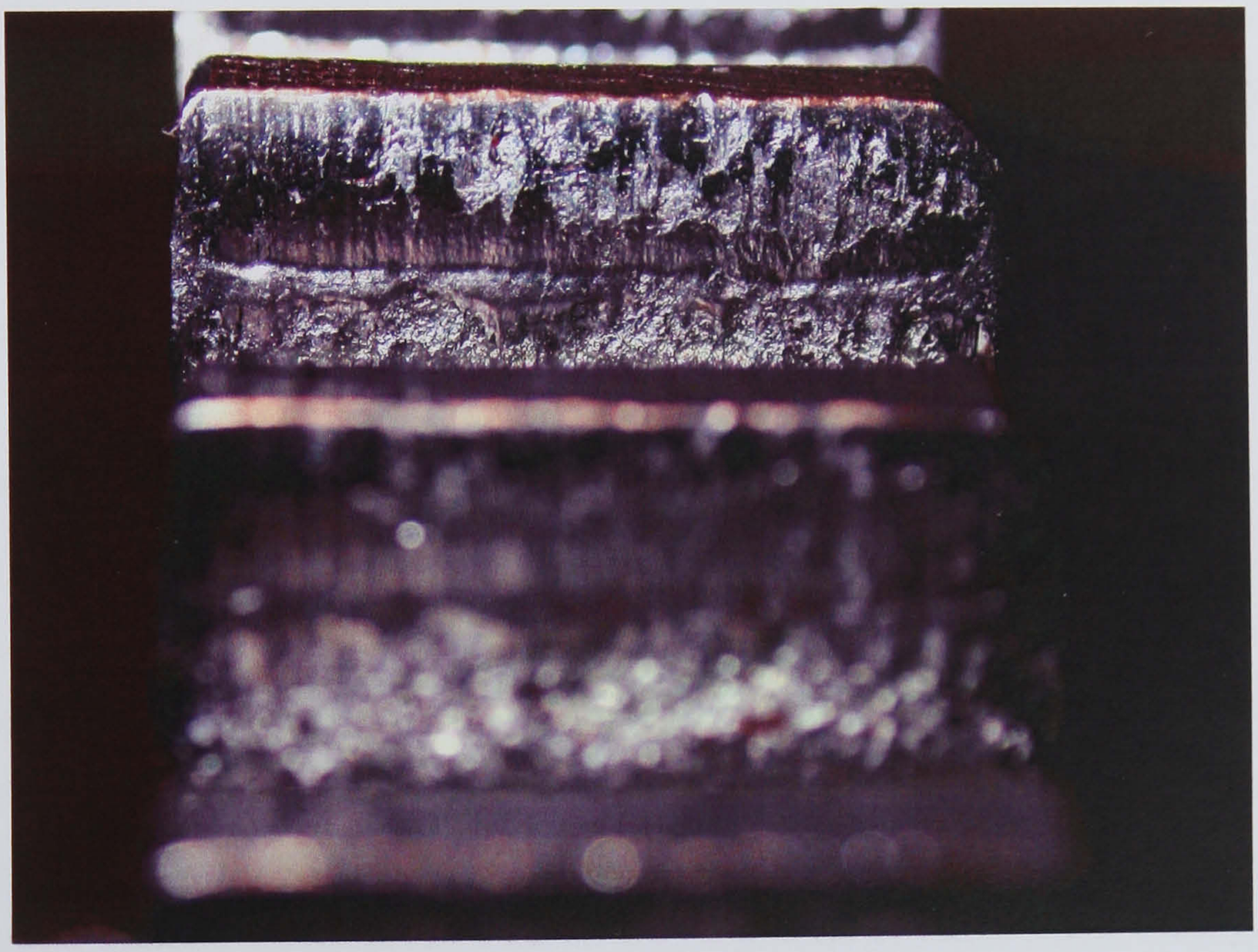

Figure 5.8 Damage gear teeth surface after dry run for 30-minutes (For loss of gear profile test).

5.3 Conclusions

In summary the following conclusions could be drawn from the observations and results of the tests detailed in this chapter:

I. Load had minimal influence on levels of AE activity under isothermal conditions
II. Speed had a significant influence on AE activity levels under isothermal conditions
III. Sliding contact was responsible for generating continuous type AE waveform
IV. Rolling contact generated AE transients at the gear mesh frequency
V. It has been shown that the main source of AE is due to asperity contact under sliding and rolling.
VI. It is postulated that two processes affect the generation of AE; influence of high strain rates and film thickness in separating asperities
VII. The secondary pressure peak had no influence on AE transient bursts generated at the gear mesh frequency

Since asperity contacts were the prime source of AE generation during gear mesh. AE technique offers the potential for assessing the level of asperity contact under a variety of operation conditions (speed, surface roughness, lubricant temperature, etc) in real time. As the amount of asperity contact is influenced by the lubricant film thickness and surface roughness, opportunities are presented for AE technique to be employed as a useful tool in detecting lubricating film breakdown and/or degradation of contact surfaces.

6 COMPARATIVE STUDY ON THE DIAGNOSTIC AND PROGNOSTIC CAPABILITIES OF AE, VIBRATION AND SOA TECHNIQUES

6.1 Introduction

This chapter describes an experimental investigation on spur gears in which natural pitting was allowed to occur. Throughout the test period, AE, vibration and spectrometric oil samples were monitored continuously in order to correlate and compare these techniques to natural life degradation of the gears.

6.2 Pitting rates

Figure 6.1 shows percentage of the gear surface pitted area plotted against the test operating time. For each torque condition a linear equation was fitted to both sets of data. The worst fit was at 73 Nm with a correlation coefficient value (R^2) of 0.8696. The gradient values of the equations fitted to each data set represent the pitting rates at each applied torque. These values were 0.45, 0.35 and 0.10 (%/hr) for 220, 147 and 73 Nm respectively. The highest gear teeth pitting rate was observed at 220 Nm (figure 6.1). With decreasing torque levels, the rate of pitting decreased.

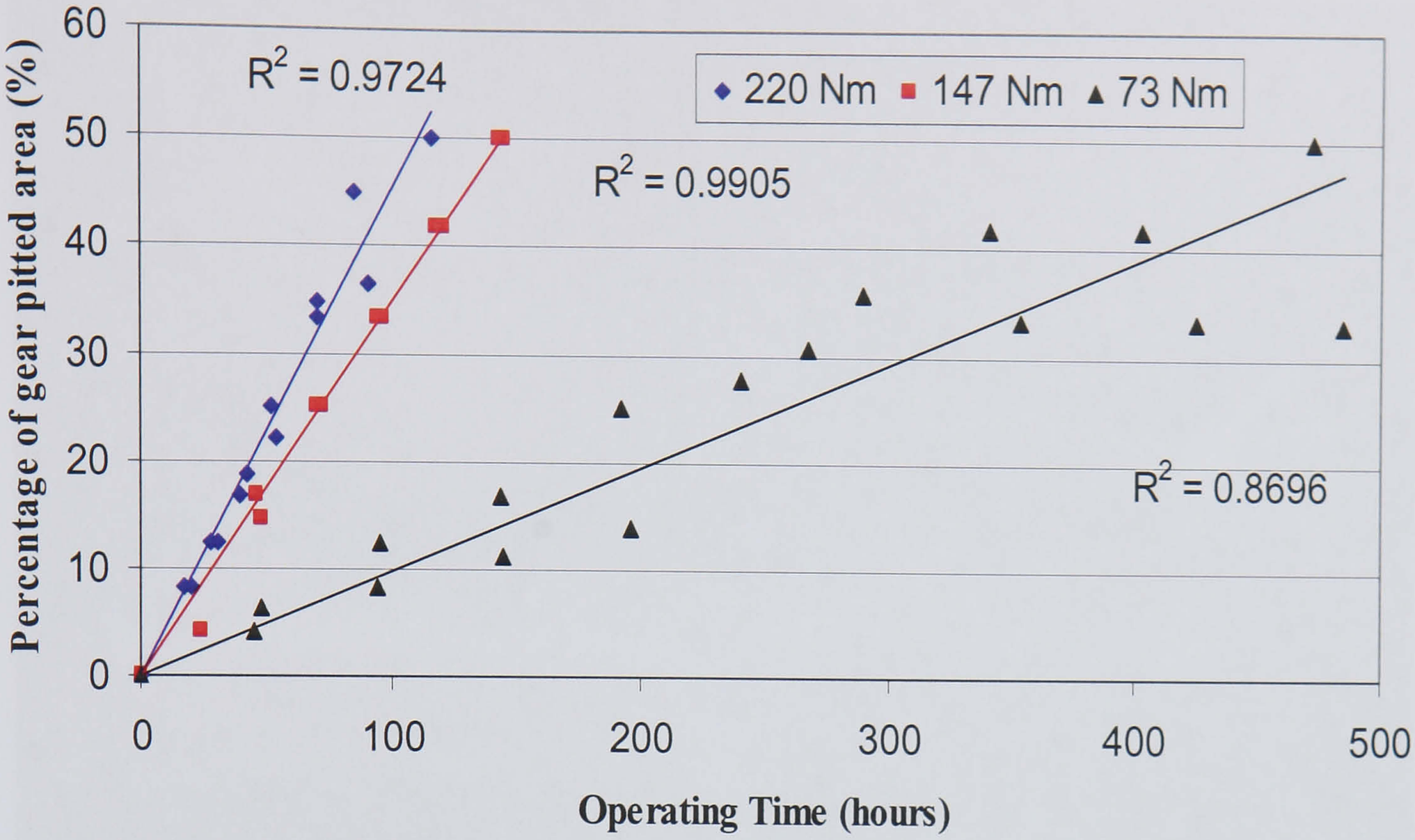

Figure 6.1 Pitting rates of the test gear under 220, 147 and 73 Nm at 745 rpm.

The observed pitting progression for all test conditions are summarised in Appendix F which lists all detailed observations of pitting, pitting rates and location of pitting in relation to the gear face location (dedendum, pitch-line and addendum) as a function of operating time. The experiments revealed that pitting occurred from the dedendum and moved towards the pitch-line. Pitting occurred in dedendum area is due to the existent of high sub-surface stress when the rolling and sliding motions of the gear teeth are in the opposite direction. This phenomenon was illustrated in chapter 1. For the higher applied torque conditions (220 and 147 Nm), the pitting always occurred across the face width and was evident on most of the gear teeth. For the light torque condition (73 Nm), pits spread across the face width of the gear teeth at a much slower rate and was localised to only a few teeth. With prolonged operation time, the pitting spread across to other gear teeth. Figures 6.2 to 6.4 show the progression of gear tooth pitting from 6.3% to 41.7% of gear pitted area, under the test condition of 73 Nm and 745 rpm.

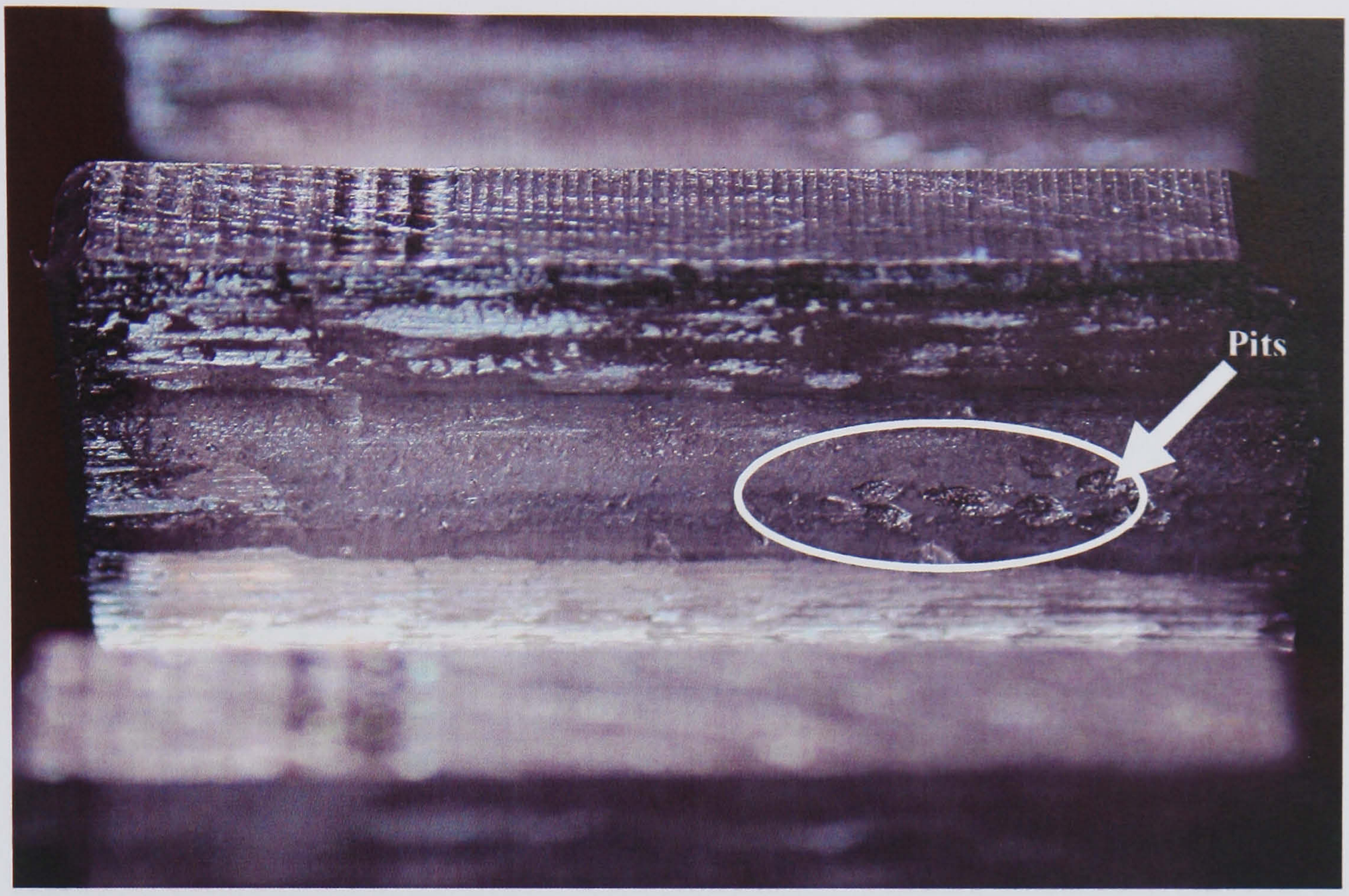

Figure 6.2 6.3% of gear pitted area at 48.5 hours of operating time; 73 Nm and 745 rpm.

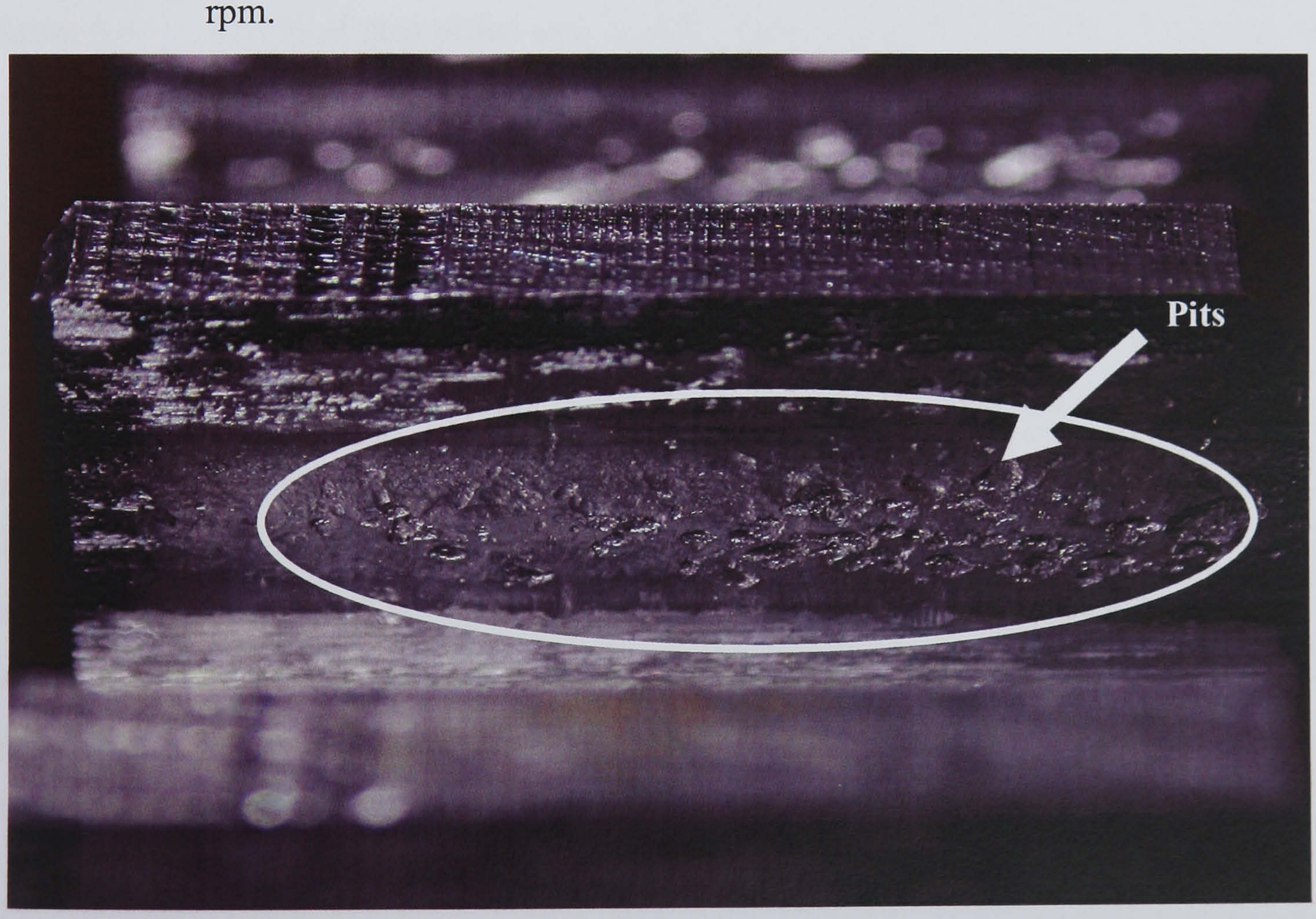

Figure 6.3 27.8% of gear pitted area at 240.5 hours of operating time; 73 Nm and 745 rpm.

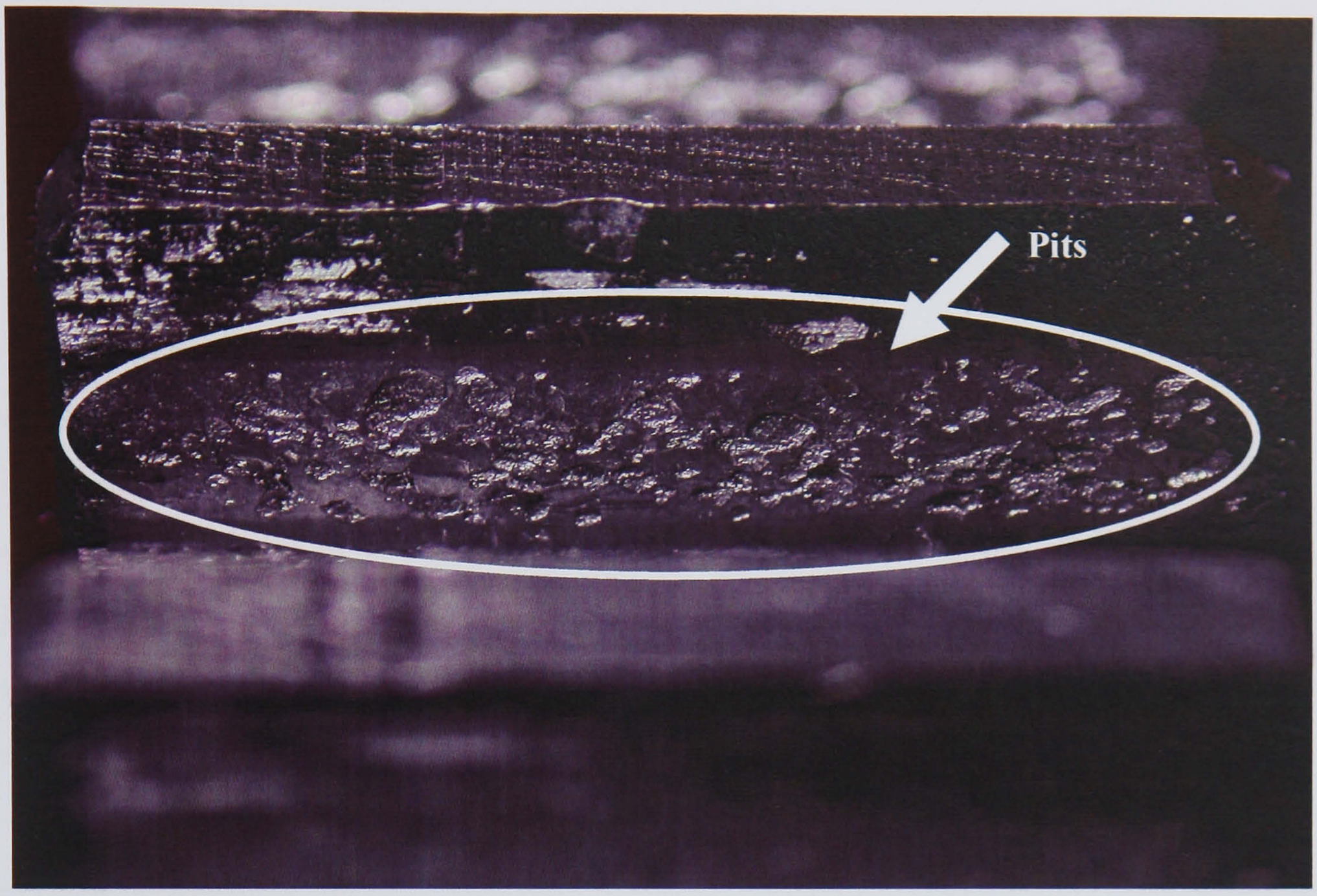

Figure 6.4 41.7% of gear pitted area at 402.5 hours of operating time; 73 Nm and 745 rpm.

6.3 Oil temperature result

The oil sump temperature of the test gearbox was recorded at regular intervals as detailed in chapter 3 and the results are presented in table 6.1 and figure 6.5. From the result detailed in table 6.1, the average oil sump temperatures for 220, 147 and 73 Nm applied load conditions were 63.4, 49.9 and 38.3 ^{0}C respectively. In addition the average ambient temperatures during the tests remained constant at 23.5, 23.1 and 20.7 ^{0}C for applied load of 220, 147 and 73 Nm respectively. This result was as expected since higher applied load will produce a higher oil sump temperature.

Interval No.	Applied Torque					
	73 Nm		147 Nm		220 Nm	
	Test 1	Test 2	Test 1	Test 2	Test 1	Test 2
	Oil temperatures at respective cumulative inspection times (^{0}C)					
1	19.7	21.7	24.1	22.1	23.1	23.8
2	36.5	37.4	48.0	44.5	60.9	60.5
3	36.3	37.0	50.2	46.7	64.1	61.9
4	38.2	37.6	51.7	48.3	63.8	62.9
5	37.8	39.4	52.8	50.3	65.3	63.8
6	36.2	37.9	54.3	51.3	65.2	63.1
7	36.4	40.2	49.9	51.0	66.0	63.9
8	35.7	41.9			63.0	
9	35.9	40.5			64.0	
10		48.0				

Table 6.1 Oil temperatures at respective inspection intervals for all the test conditions.

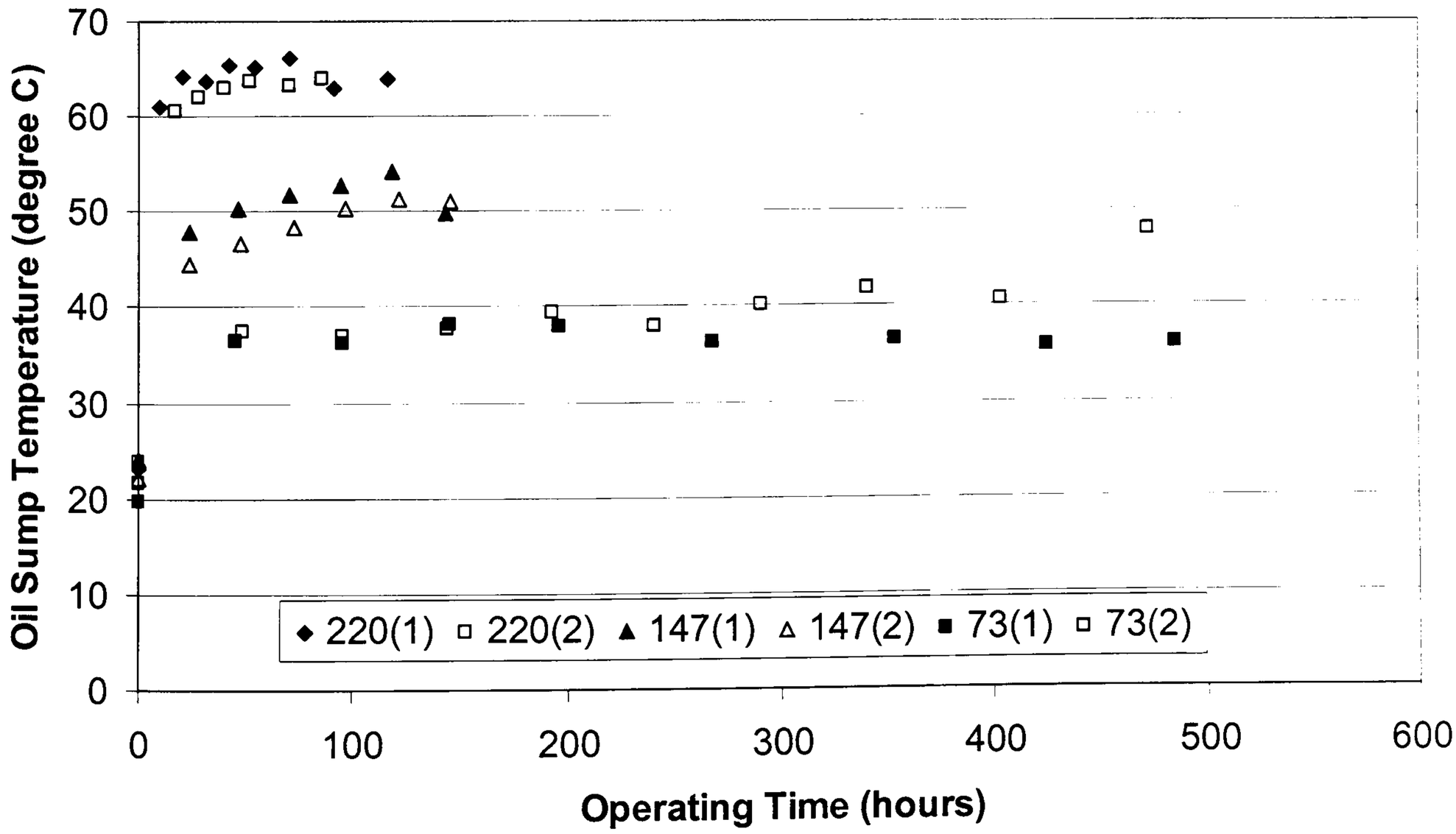

Figure 6.5 Oil temperatures at respective inspection intervals for all the test conditions.

6.4 Monitoring parameters results

6.4.1 AE response

All original data from AE, SOA and vibration are presented in figures 6.6 to 6.23. A few general observations on all torque levels were noted. From figures 6.6, 6.8 and 6.10, at each applied torque level, it can be seen that despite the application of the same torque, both tests started at different normalised AE r.m.s values. However, in one of the tests the AE r.m.s initially decreased, whereas in the other it increased from the start. For the 220 Nm load case, after approximately 15 hours the AE levels in both tests increased at very similar rates (gradients) but different absolute AE r.m.s values. For 147 and 73 Nm, similar observations were noted, and the 2 tests at each torque level assumed the same gradient after approximately 20 and 60 operating hours respectively. Figures 6.7, 6.9 and 6.11 highlight plots of AE r.m.s versus the percentage of gear pitted area illustrating a linear relationship between the two for both tests at all applied torque levels.

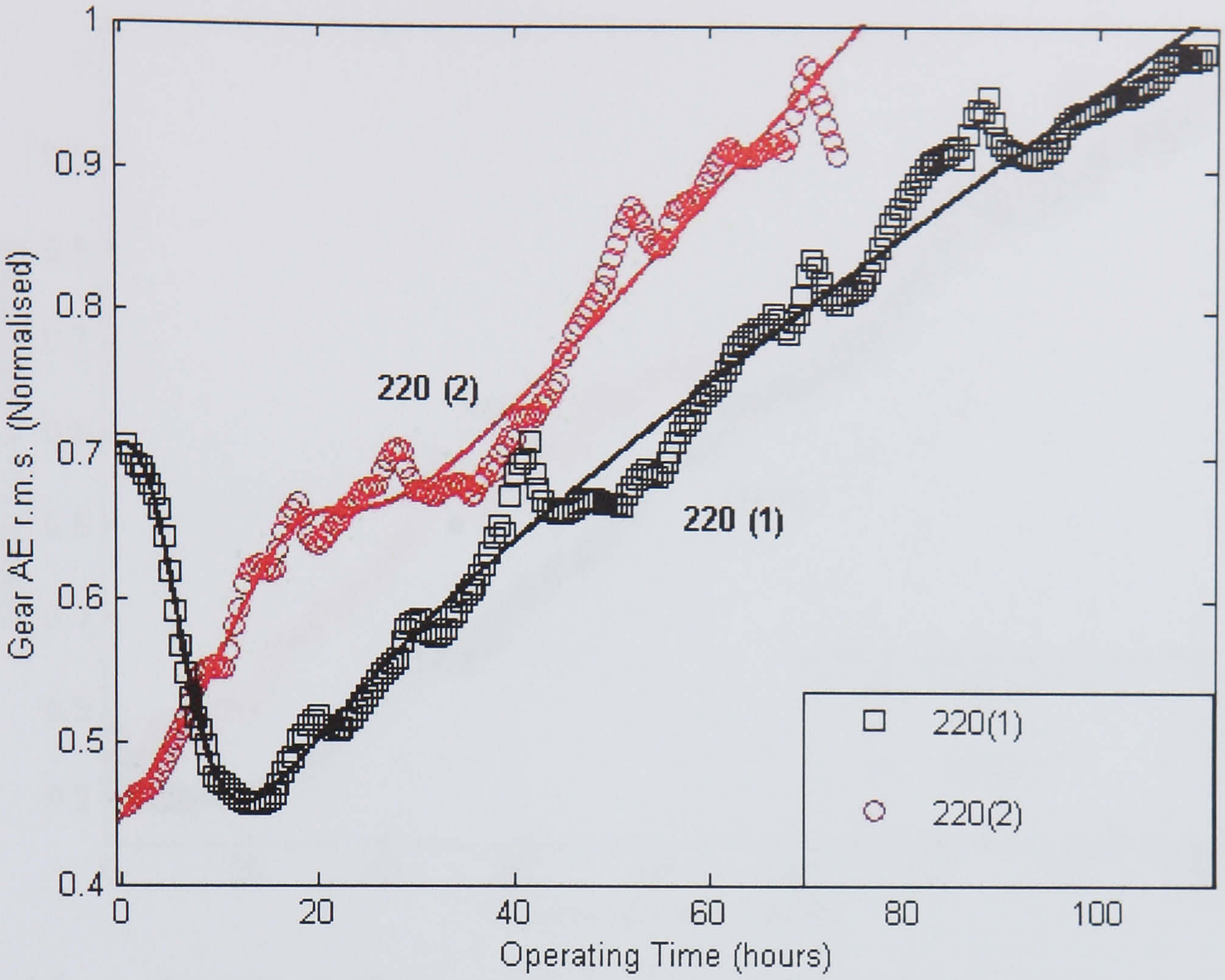

Figure 6.6 Normalised AE r.m.s against operating time at 220 Nm; 745 rpm

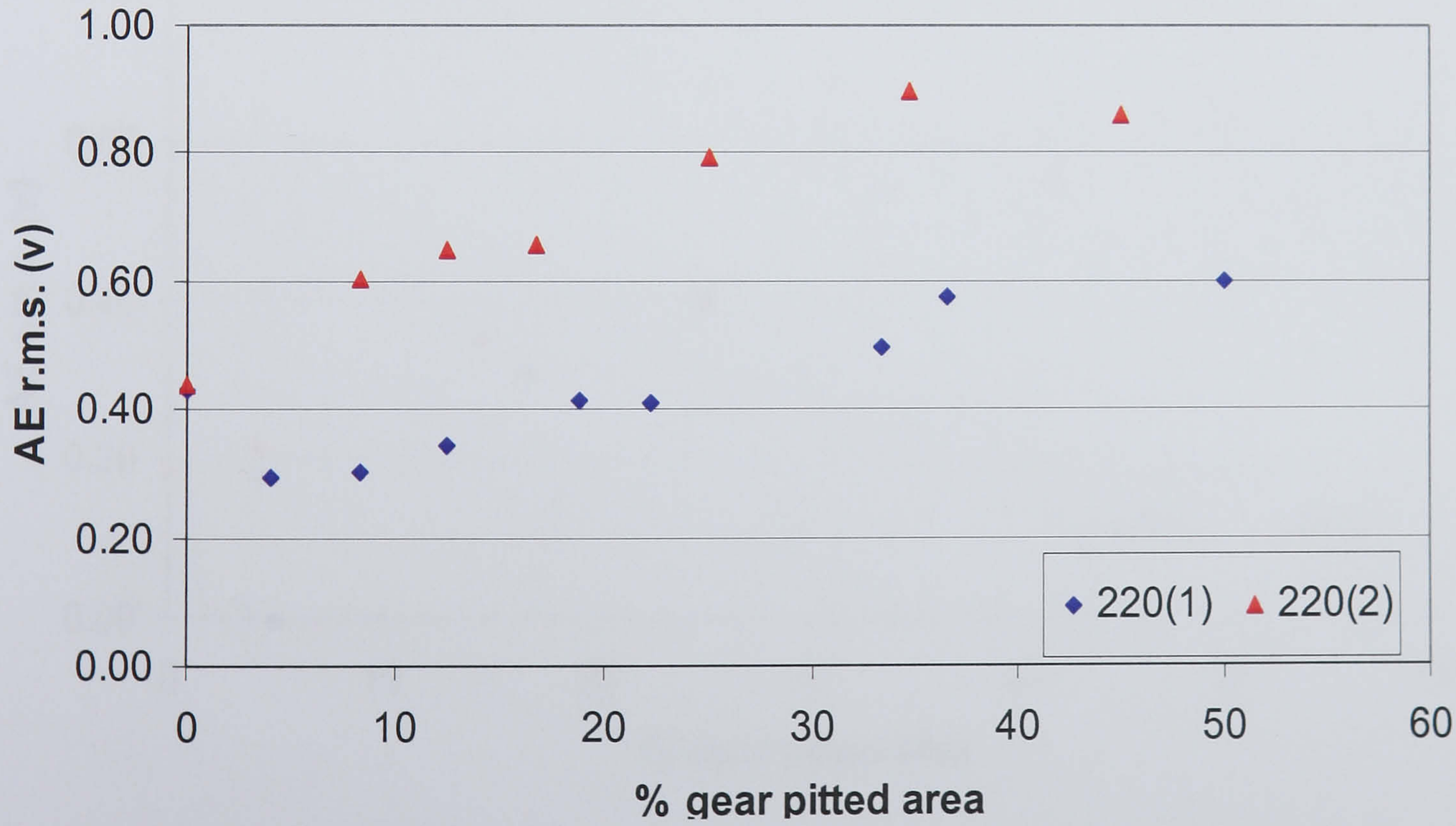

Figure 6.7 AE r.m.s against percentage of gear pitted area at 220 Nm; 745 rpm

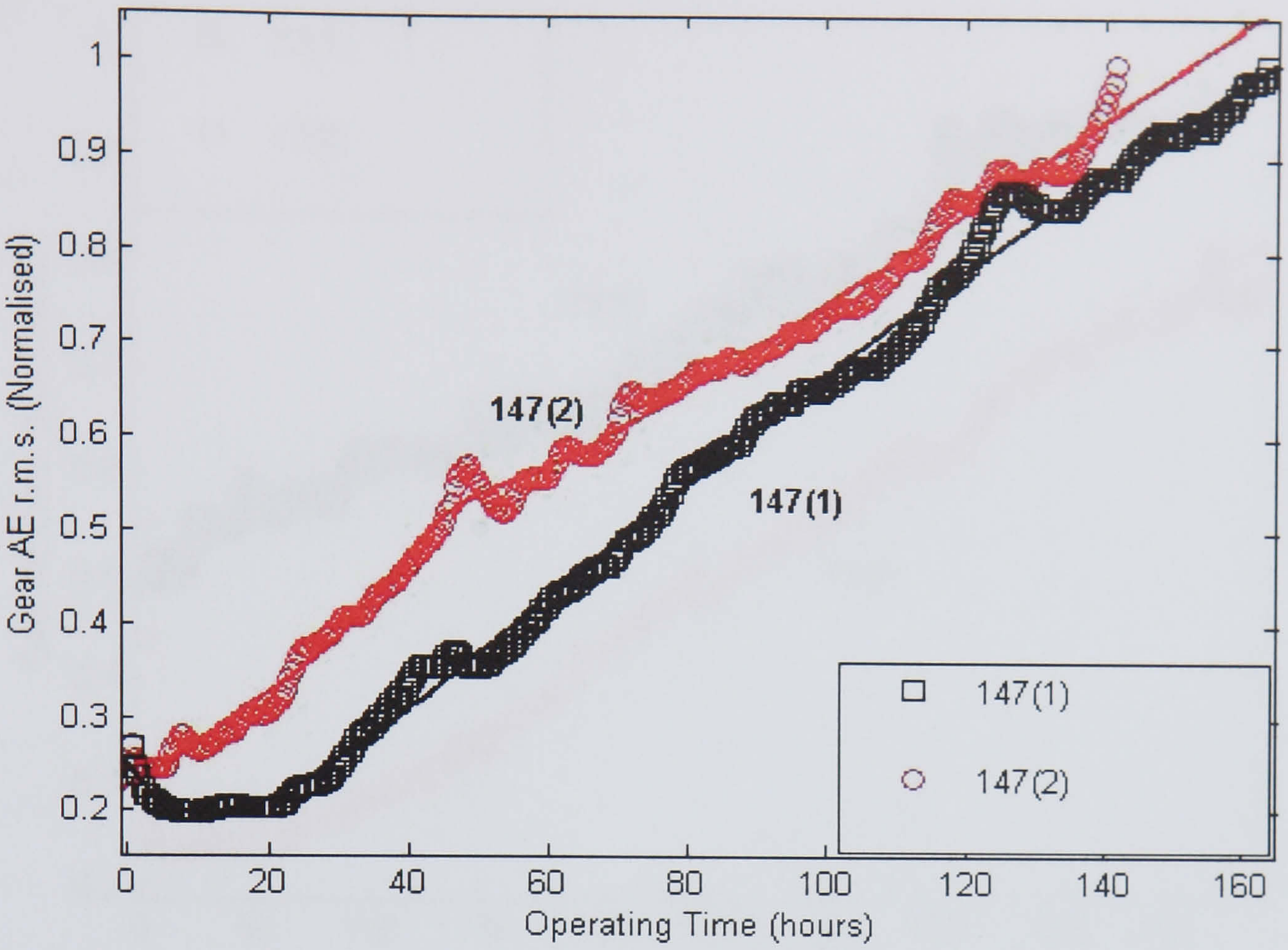

Figure 6.8 Normalised AE r.m.s against operating time at 147 Nm; 745 rpm

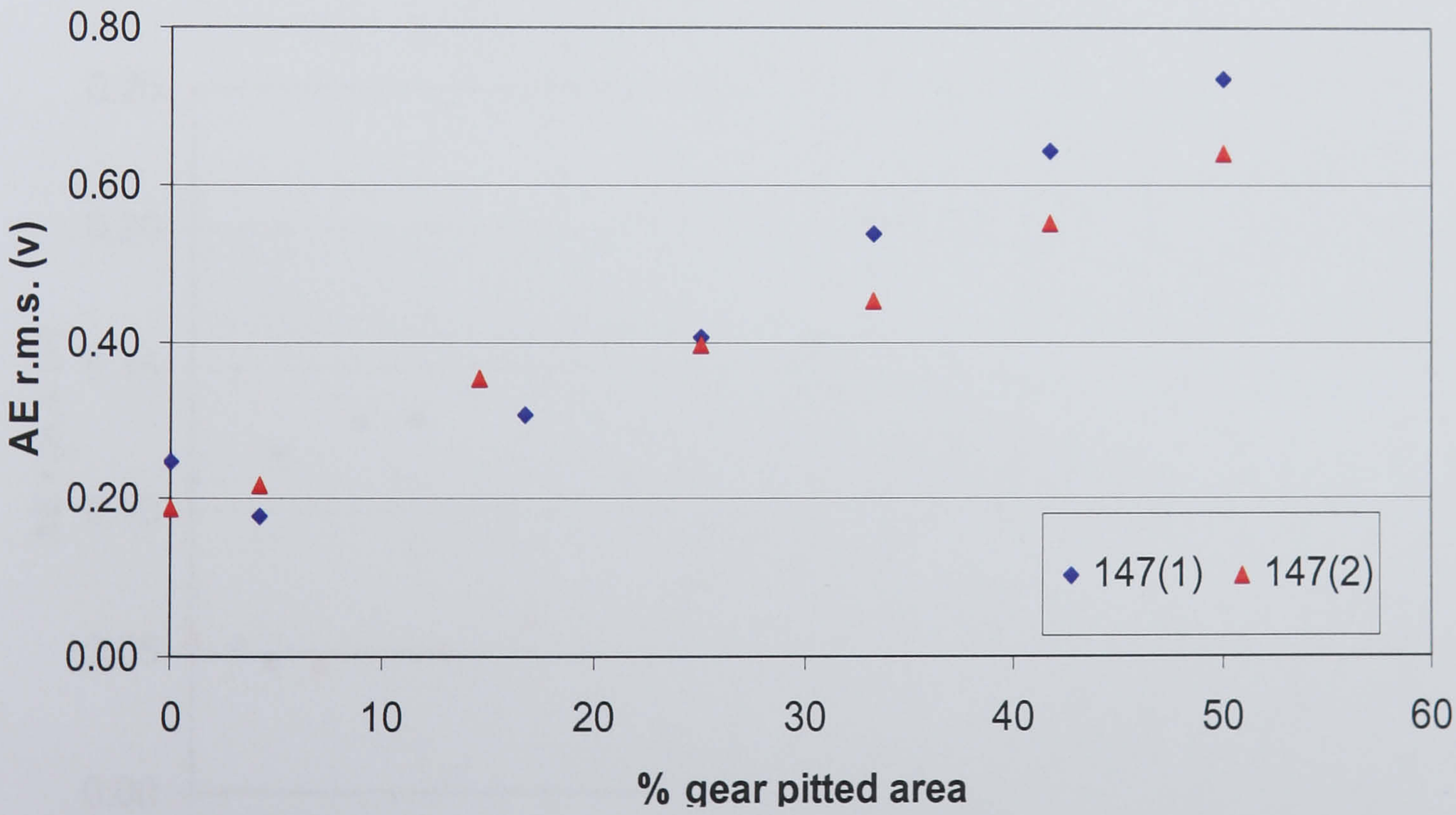

Figure 6.9 AE r.m.s against percentage of gear pitted area at 147 Nm; 745 rpm

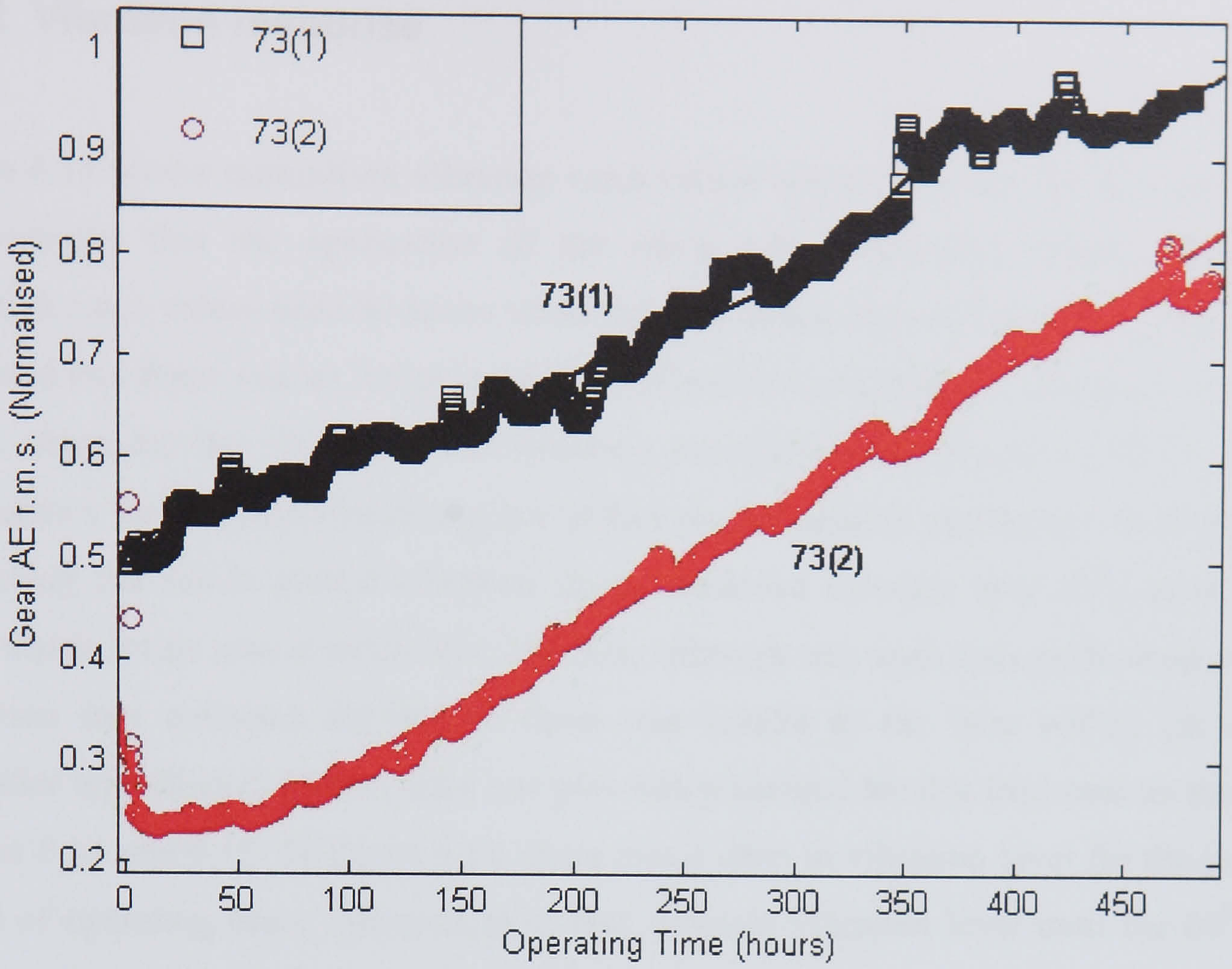

Figure 6.10 Normalised AE r.m.s against operating time at 73 Nm; 745 rpm

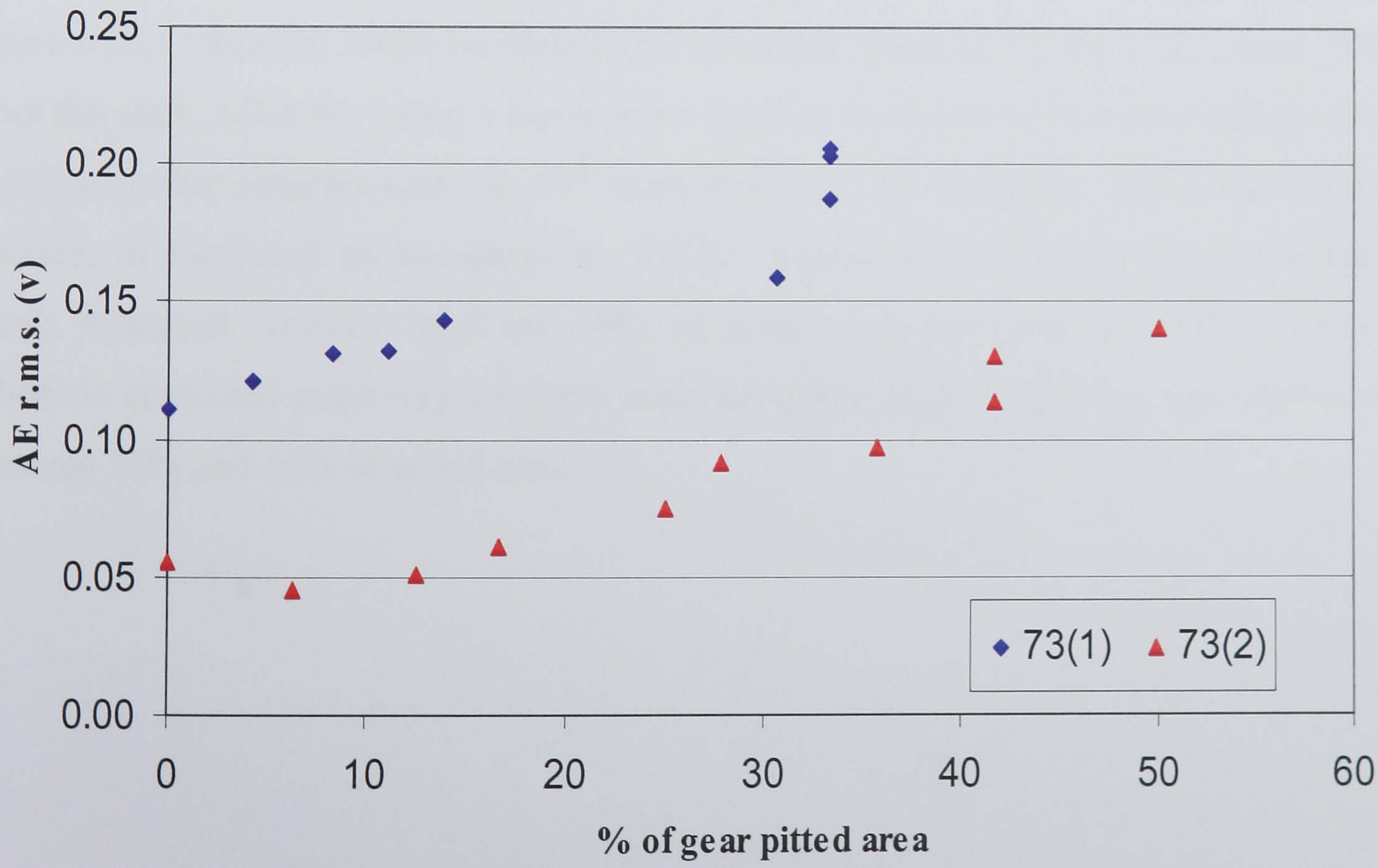

Figure 6.11 AE r.m.s against percentage of gear pitted area at 73 Nm; 745 rpm

6.4.2 Vibration response

Figure 6.12 shows normalised vibration r.m.s values against time for the 220 Nm test. It demonstrates that the application of the same torque produced similar normalised vibration r.m.s values until 60 hours when the tests departed from each other. Also it was observed that there was an initial increase of vibration level from 0 to between 10 and 15 hours, thereafter the vibration level remained relatively constant until 60 hours. Figure 6.13 shows the original vibration r.m.s values plotted against percentage of pitted area. Following the run-in period vibration levels remained constant until 25% pitted area, after which levels rose steadily. For 147 Nm, although two tests were performed, but the vibration data collected for one of them was invalid as the wire within the charge amplifier was shorted. Hence, only one plot was presented for this load case as shown in figures 6.14 and 6.15. In figure 6.14, there was a drop in vibration level for the initial 2 hours of operating time, followed by a near constant vibration level until the 60^{th} hour where the vibration level starts to increase. Figure 6.15 revealed a near constant vibration level with increasing percentage of gear pitted area until 25% pitted area. For the 73 Nm load case, the two tests showed different initial trends for the first 5 operating hours (see figure 6.16); vibration levels increased and decreased respectively for '73(1)' and '73(2)' from the start. After the initial 5 hours, the vibration levels for both tests levelled off and remained rather constant until the 50^{th} operating hour. As observed, '73(1)' has a greater gradient of increased as compared to '73(2)'. Figure 6.17 revealed that the vibration levels remained constant until the 10% of pitted area was reached. These levels of vibration remained relatively constant until advanced stage of pitting was achieved at between 30% and 40% of pitted area.

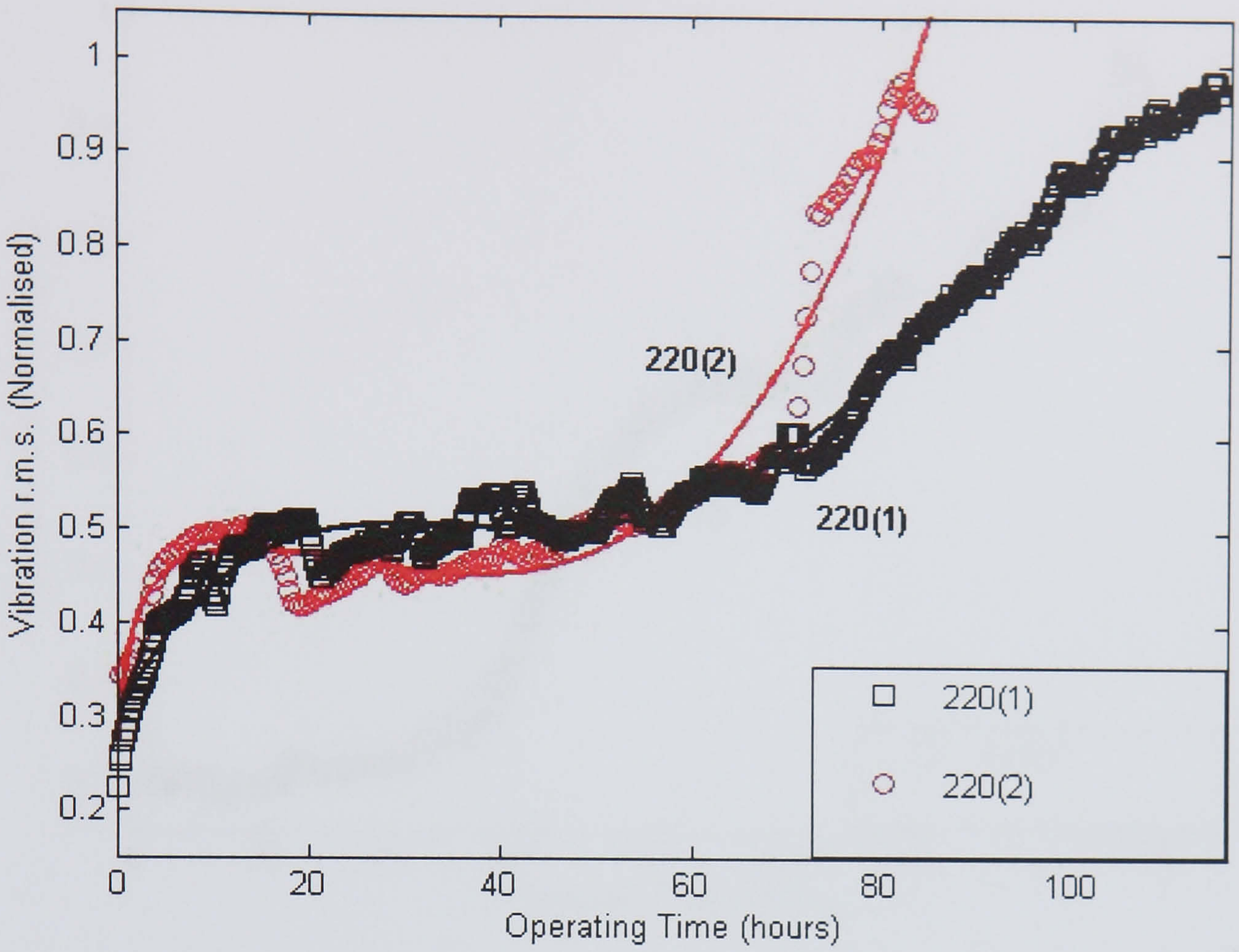

Figure 6.12 Normalised vibration r.m.s against operating time at 220 Nm; 745 rpm

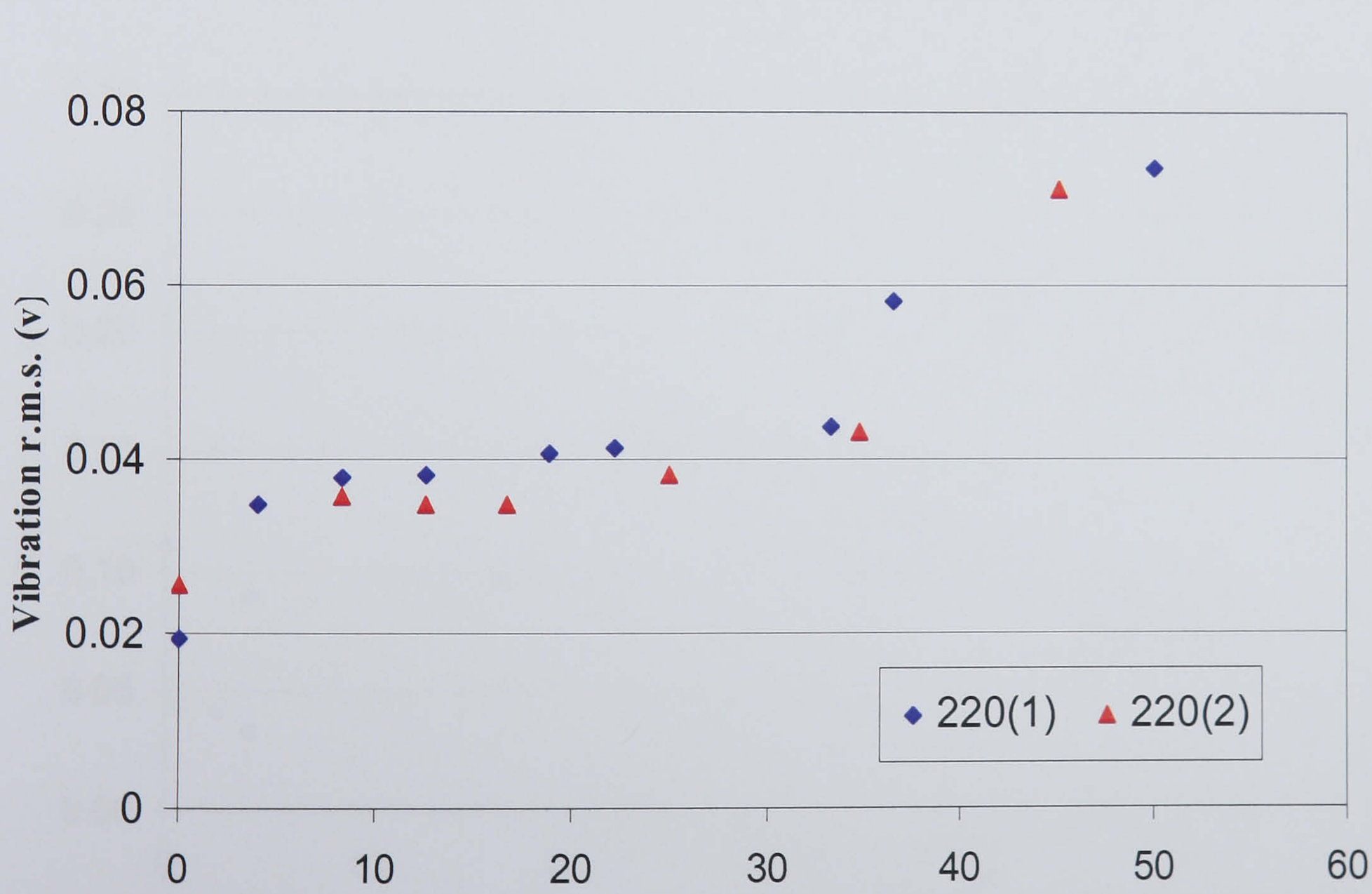

Figure 6.13 Vibration r.m.s against percentage of gear pitted area pitted area; 220 Nm, 745 rpm (Accelerometer calibrated to 0.1 v equivalents to 1 g).

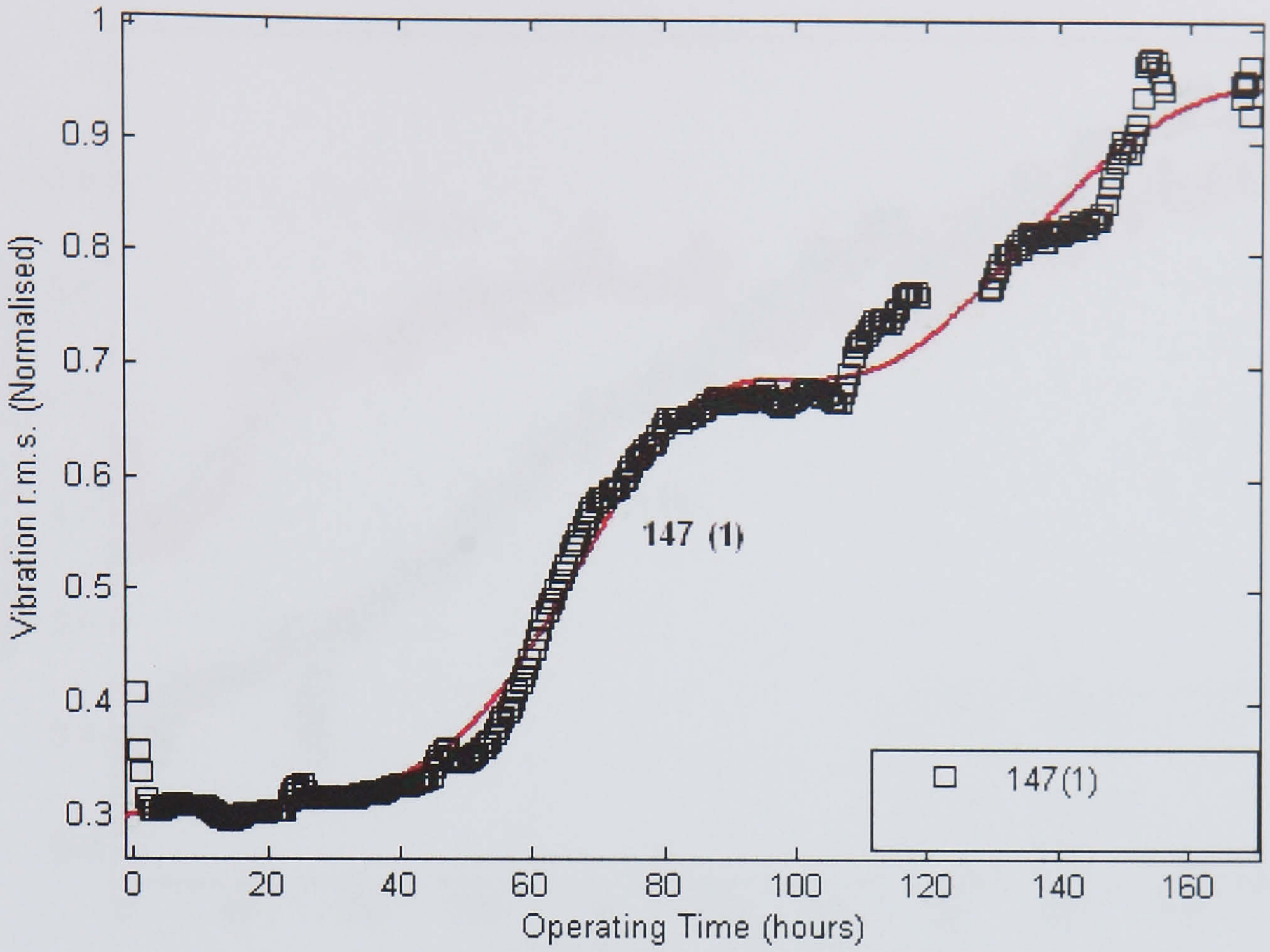

Figure 6.14 Normalised vibration r.m.s against operating time at 147 Nm; 745 rpm

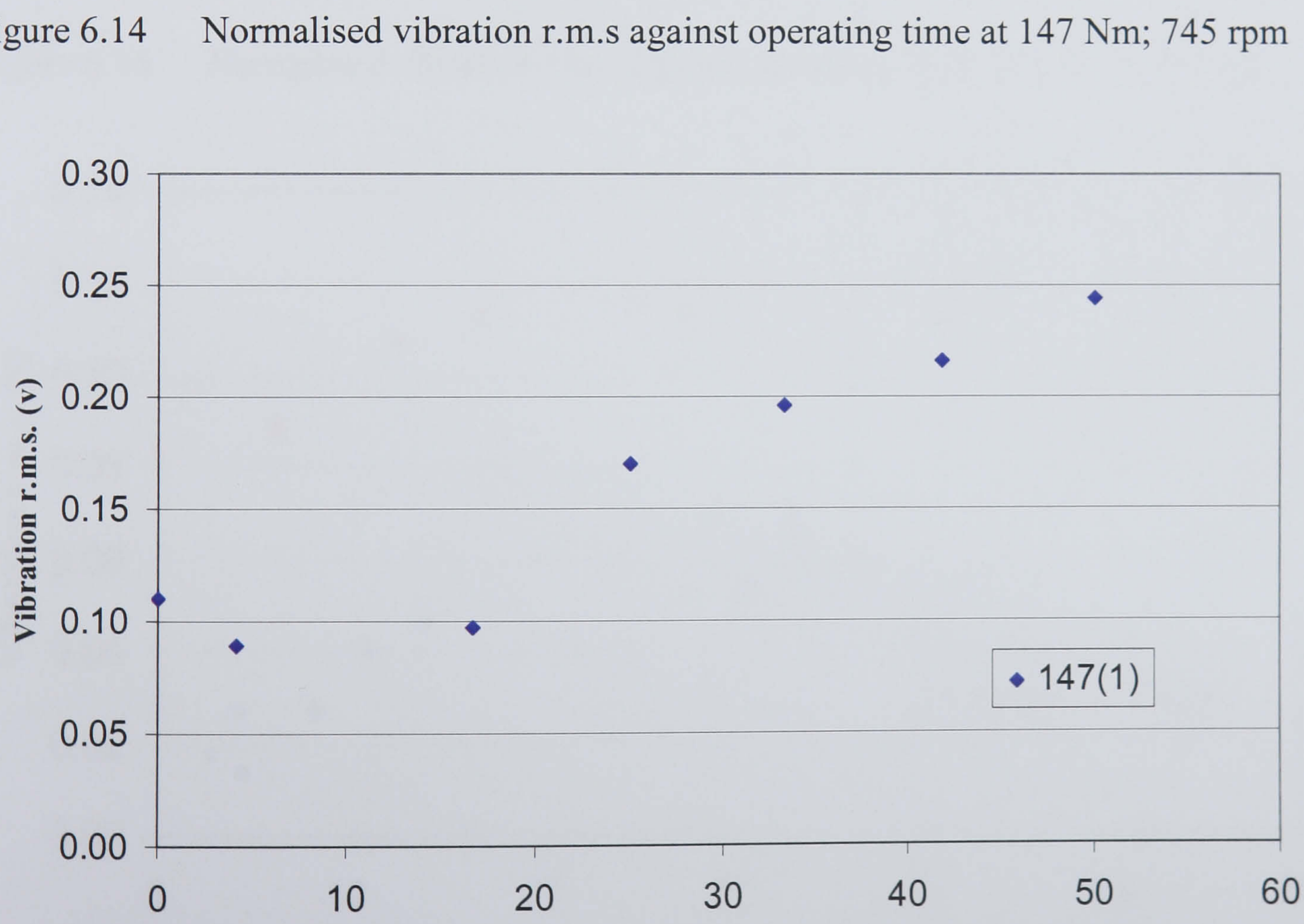

Figure 6.15 Vibration r.m.s against percentage of gear pitted area; 147 Nm, 745 rpm (Accelerometer calibrated to 1 v equivalents to 1 g).

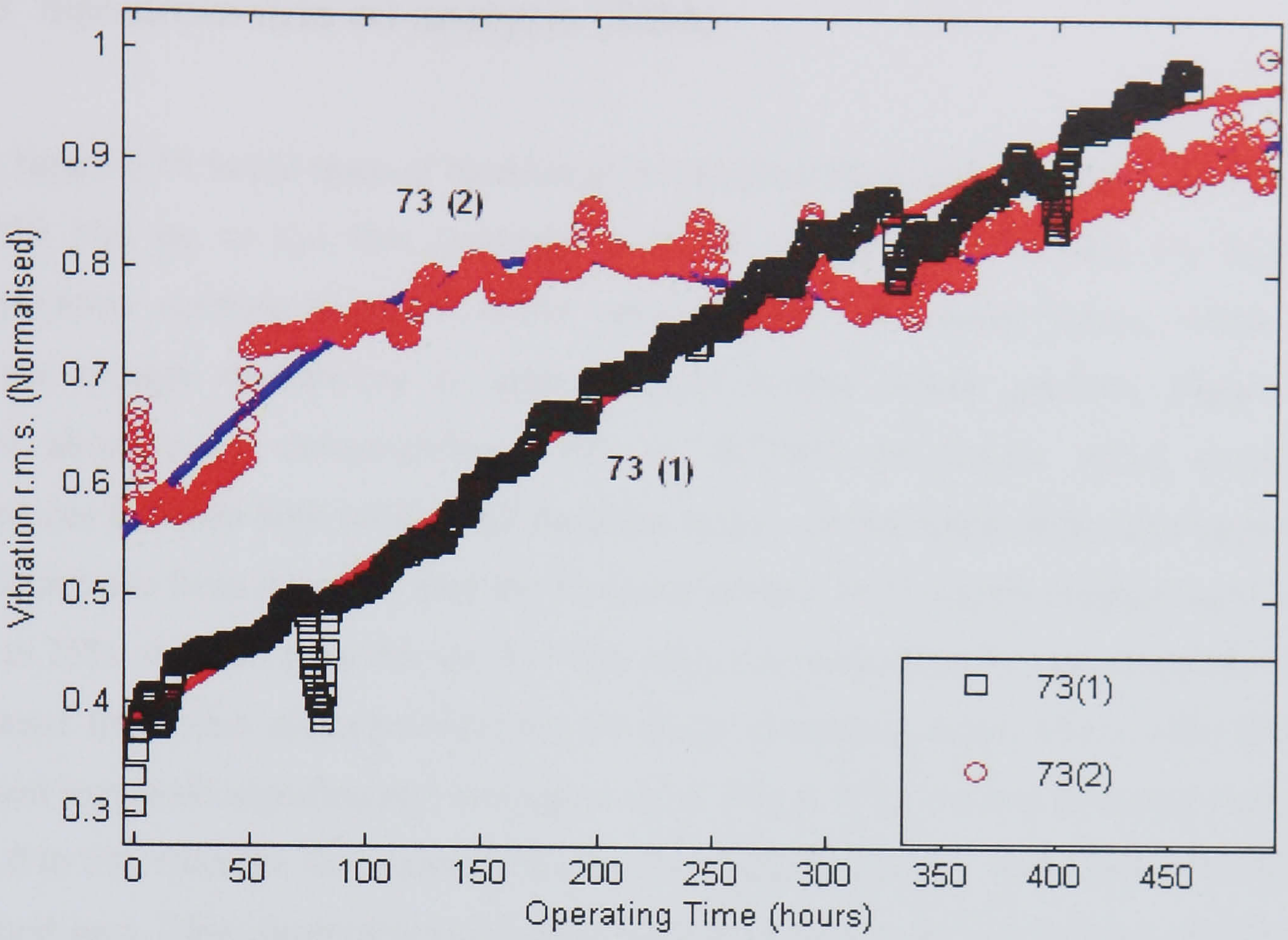

Figure 6.16 Normalised vibration r.m.s against operating time at 73 Nm; 745 rpm

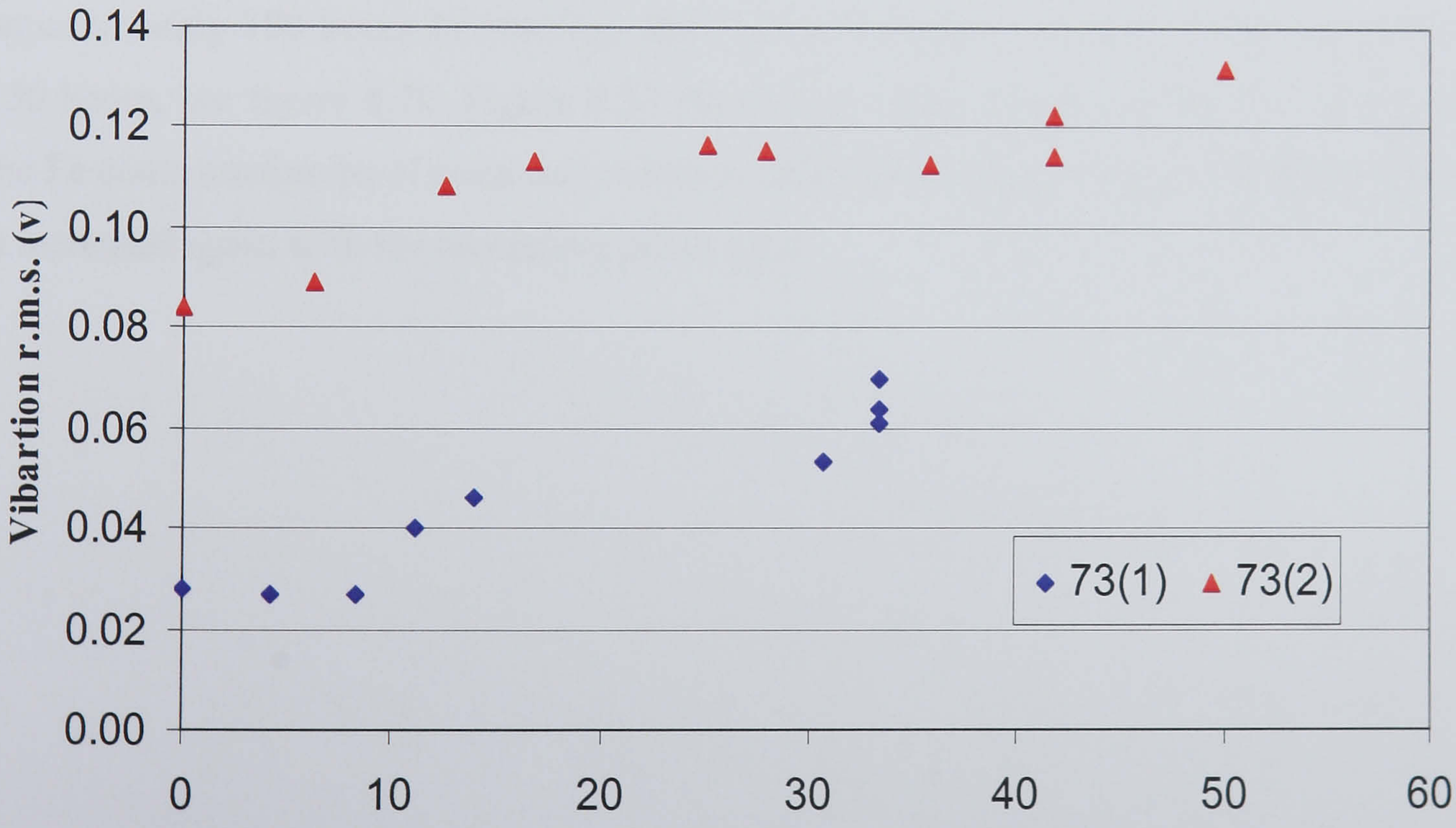

Figure 6.17 Vibration r.m.s against percentage of gear pitted area; 73 Nm, 745 rpm (Accelerometer calibrated to 1 v equivalents to 1 g).

6.4.3 Spectrometric oil analysis (SOA)

From figure 6.18 initial rates of increase of normalised SOA were similar in the two tests for 220 Nm up to the first readings at 9 and 17 hours. After that the SOA Fe concentration reading remained rather constant until 50 running hours, where they diverged though maintaining an approximately similar overall gradient. Figure 6.19 shows absolute Fe concentration levels at different percentage pitted areas; the differences between both tests under the same torque can be noted. Both tests showed an initial increase from 0 to 5%, then the Fe concentration level remain constant until about 20% to 25% of pitted area. For the 147 Nm tests, the normalised Fe concentration values increased from start till approximately 50 hours of running time, where after that the gradient increased significantly, see figure 6.20. Figure 6.21 showed an initial increased from 0 to 5%, then the Fe concentration level remained constant until about 20% to 25% of pitted area. This observation coincided with what had been noted under the 220 Nm load condition, refers to figure 6.19. For the lightest load case at 73 Nm, a similar observation was noted. The normalised Fe concentration values increased from start till approximately 100 hours of running, after that it remained constant for the next 100 to 150 hours, see figure 6.22. Figure 6.23 showed an initial increase from 0 to 10%, then, the Fe concentration level remained constant until about 20% to 30% of pitted area before it increased again with the increasing pitted area.

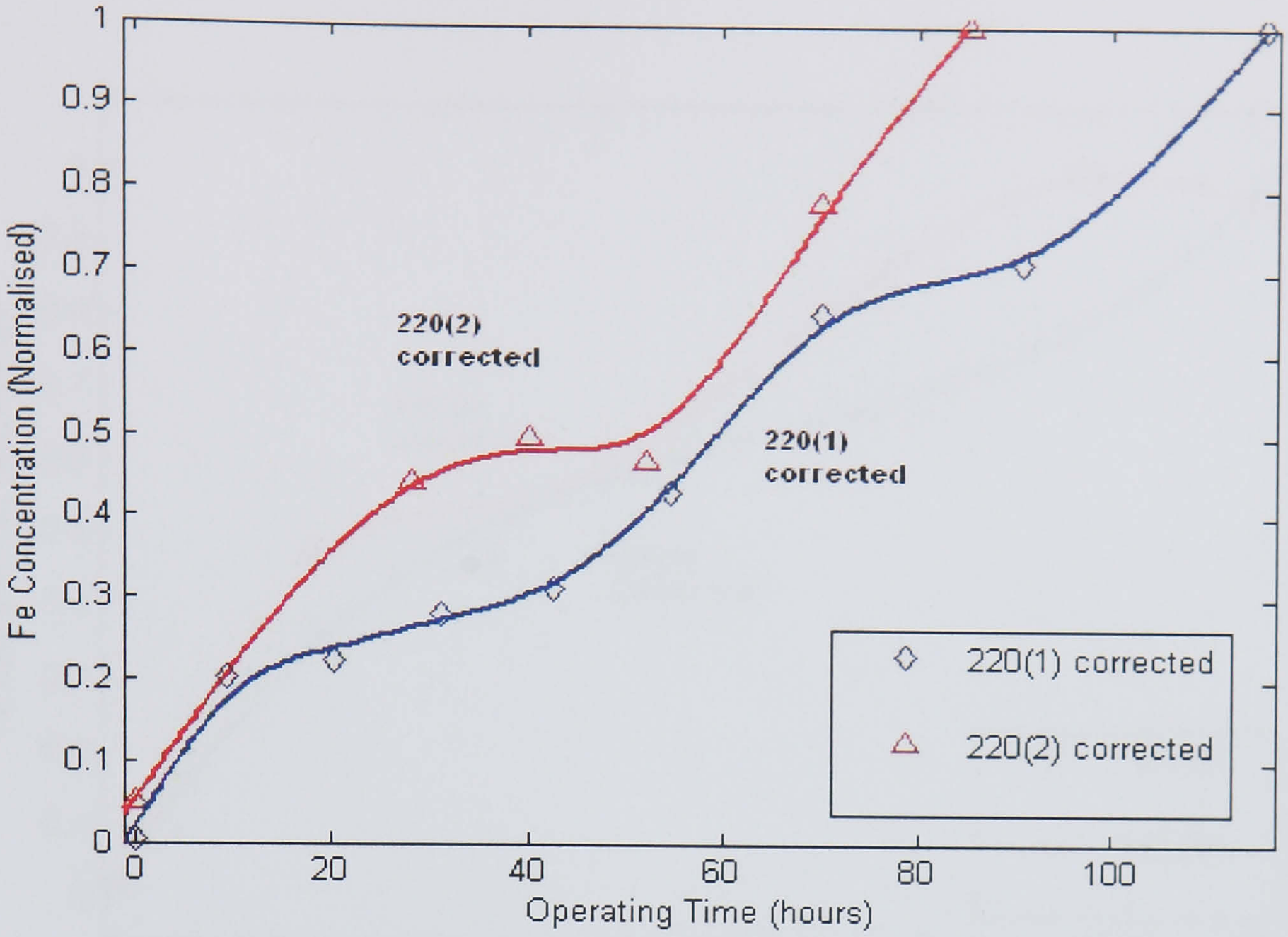

Figure 6.18 Normalised Fe concentration with correction against operating time at 220 Nm; 745 rpm

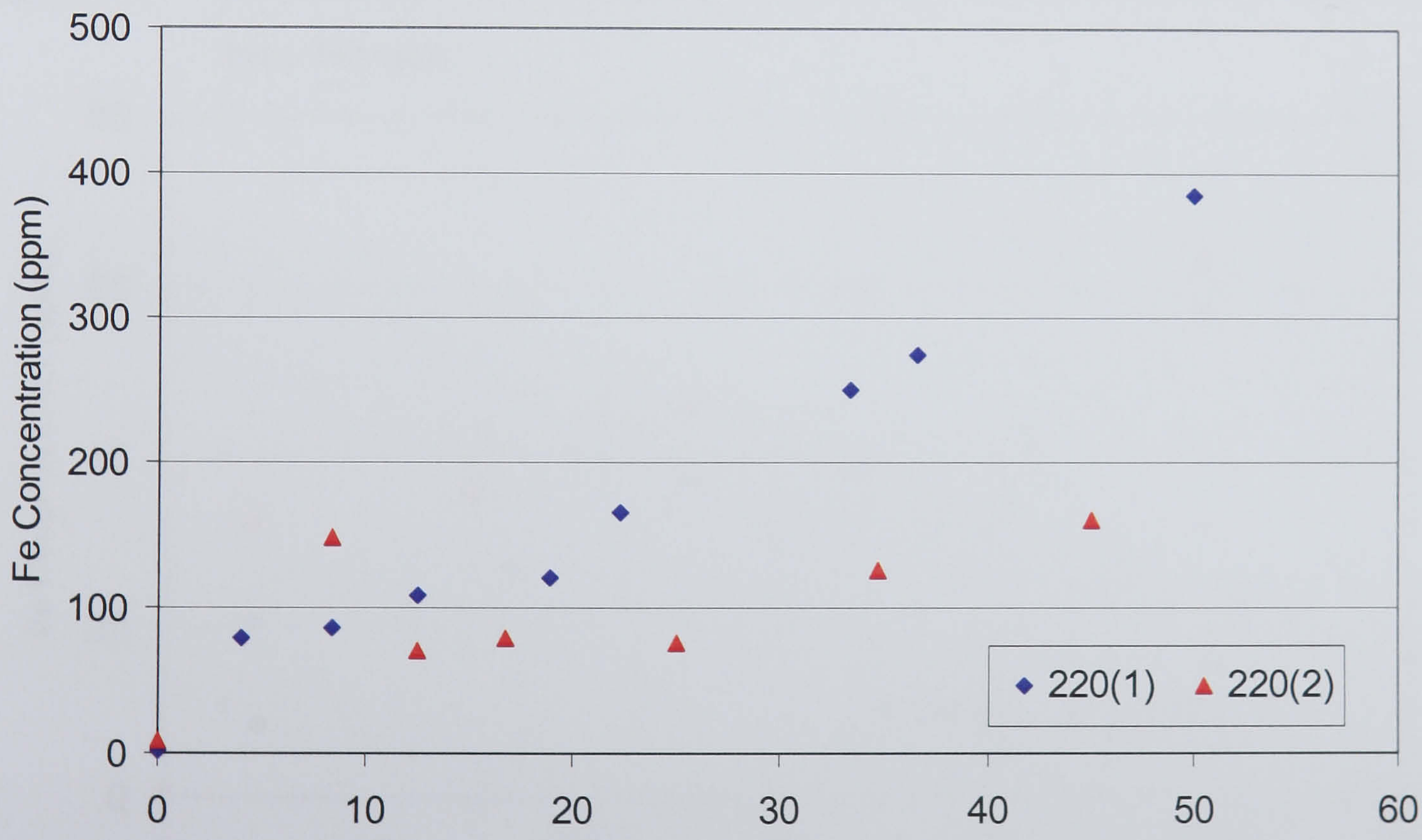

Figure 6.19 Fe concentration with correction against percentage of gear pitted area; 220 Nm, 745 rpm

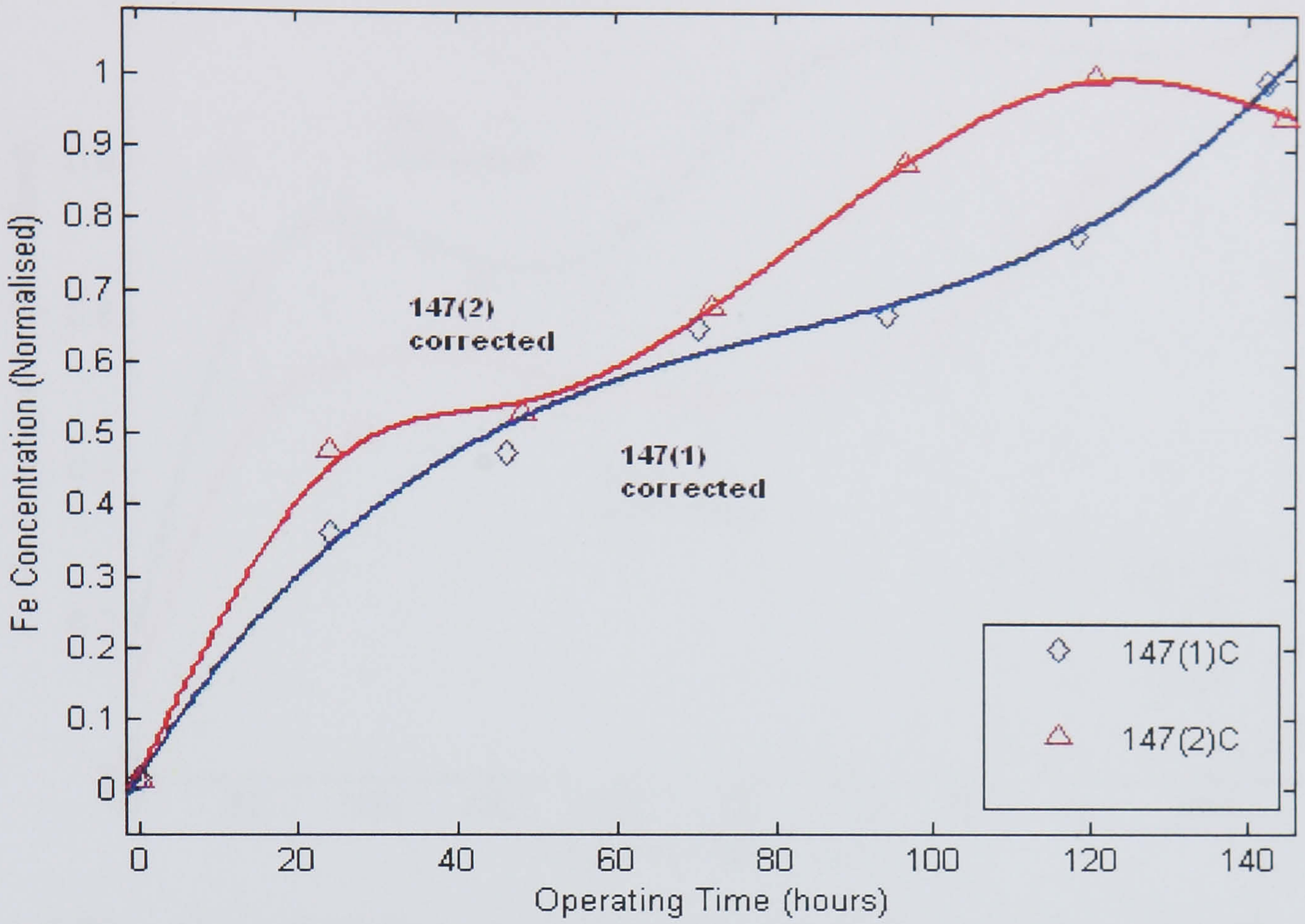

Figure 6.20 Normalised Fe concentration with correction against operating time at 147 Nm; 745 rpm

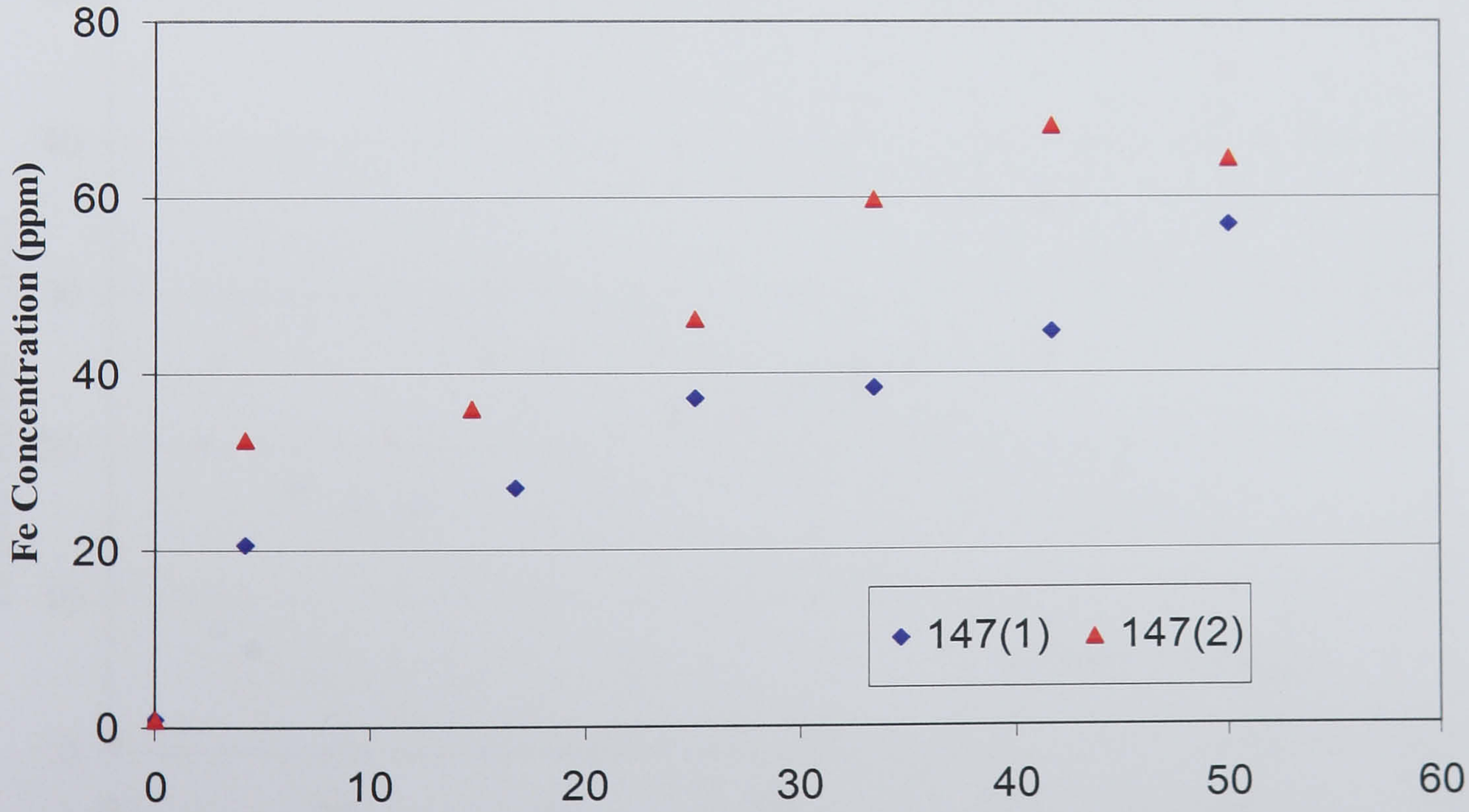

Figure 6.21 Fe concentration with correction against percentage of gear pitted area; 147 Nm, 745 rpm

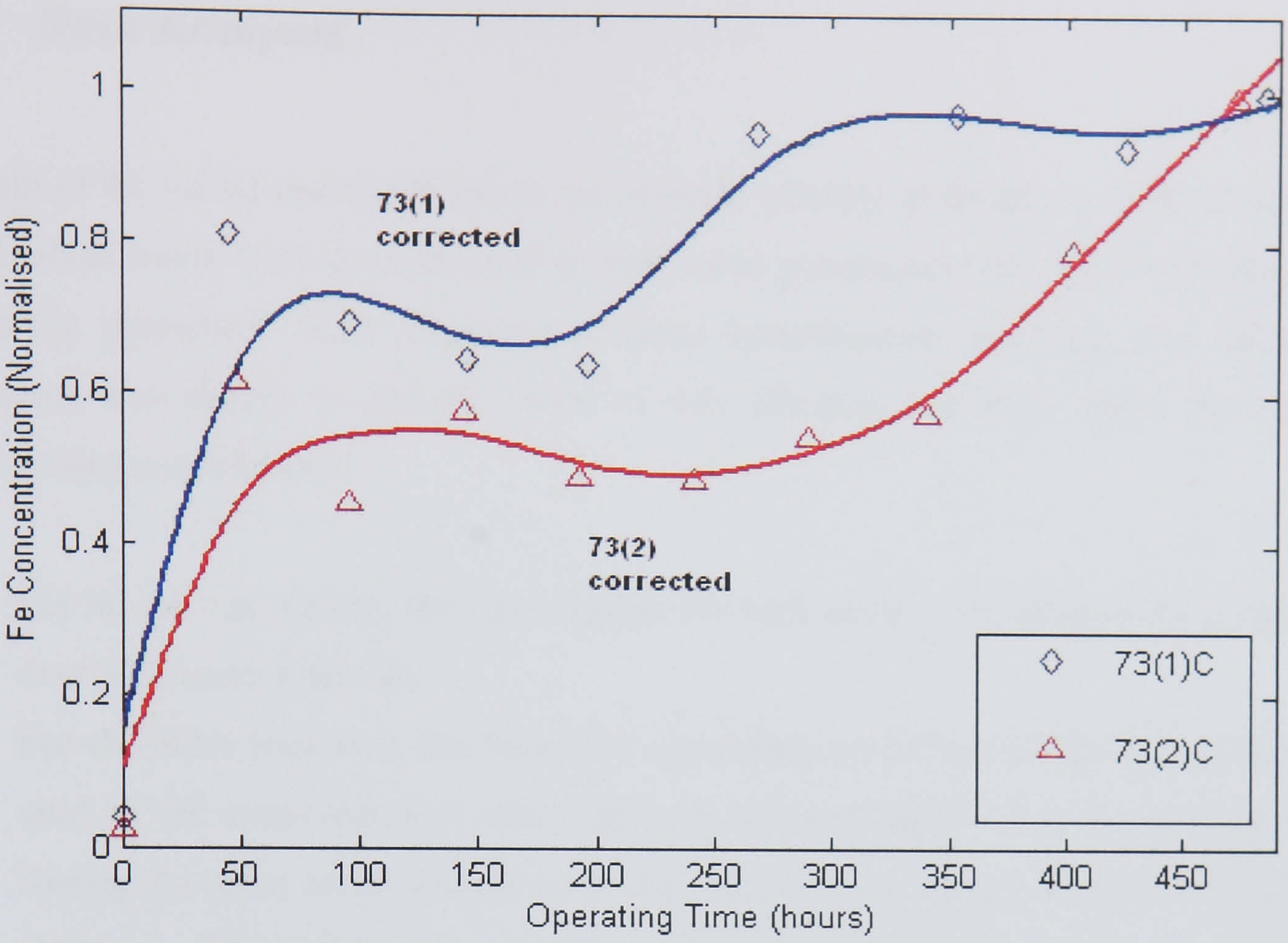

Figure 6.22 Normalised Fe concentration with correction against operating time at 73 Nm; 745 rpm

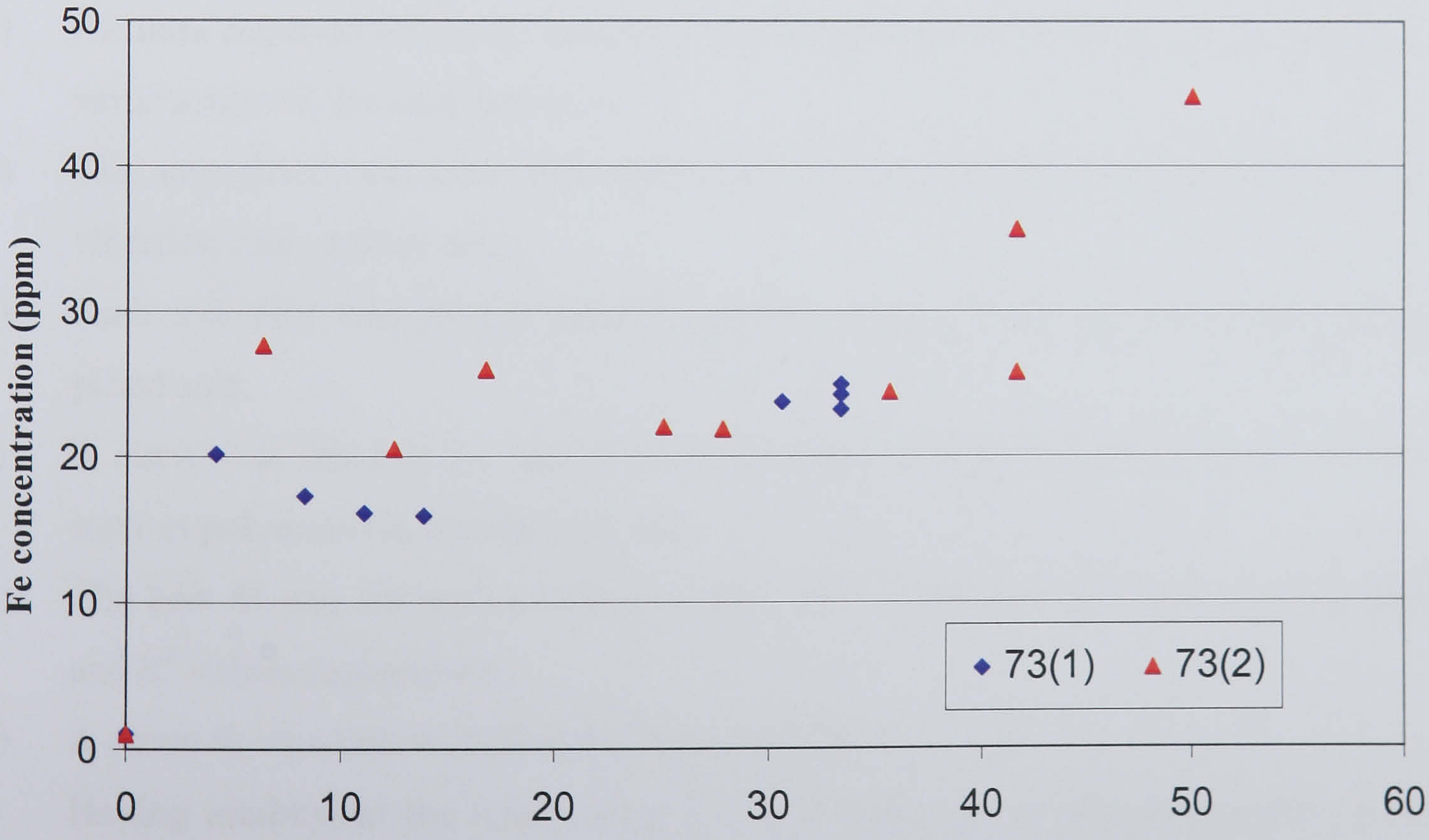

Figure 6.23 Fe concentration with correction against percentage of gear pitted area; 73 Nm, 745 rpm

6.5 *Data Analysis*

In light of the varied test conditions it was thought prudent to develop a method whereby all absolute levels from the indicators or monitored parameters (AE, SOA and vibration) could be presented. After exploring various normalisation methods, the following technique was chosen to present trends of AE, vibration and SOA under the various applied torque conditions.

a) For all AE r.m.s plots, the r.m.s values for each point were obtained by averaging over 30 minute-intervals.

b) For the SOA indicator, the Iron (Fe) concentration in part-per-million (ppm) was used as the main indicator since the gear surface material was made from steel. During the tests, an oil sample of 60 ml was taken at regular intervals (detailed in chapter 3. After the sample was taken, fresh oil of equivalent volume was replaced into the gearbox. This will influence SOA measurements and as such, a correction of the Fe concentration was employed by using an expression detailed in chapter 2.

c) All data acquired for every indicator was normalised with respect to the maximum value achieved for each test case.

d) The normalised data were smoothed with a moving average of 5-points for AE and vibration r.m.s values only.

e) Each indicator was plotted against gearbox running time and percentage of gear pitted area.

f) A curve was fitted to the data points (see steps –c and -d) using various functions such as polynomials, exponential, etc.

g) The best fit was chosen as close to 'zero' and '1' for sum of squares errors (SSE) and R^2 values respectively.

h) A curve fit equation was obtained from the best fit.

i) Having established the relationship for each indicator, as described above, it was now possible to make direct comparisons. Hence by using the equation obtained from step-h, a representation of the trends of each indicator, for all torque

conditions, was obtained at incremental intervals of 10 hours, see figures 6.24, 6.27 and 6.29.

j) The same procedures were used to represent the indicator trends against gear pitted area at step increments of 5% gear pitted area, see figures 6.26, 6.28 and 6.30.

k) As two tests were undertaken at each applied torque condition, the trends presented, as obtained from steps -i and -j, were the averaged values for both tests at each torque level.

l) Figures 6.24 to 6.30 (except figure 6.25) presented were based on the steps described above.

6.6 AE and pitting

In relating AE activity to pitting rates, cognisance of the effects of surface roughness, lubrication regime, friction and the slide-to-roll ratio of the meshing gears must be considered. In the literature review of AE from sliding friction and wear, Dornfeld, Jiaa and Handy [87, 63] stated that AE is sensitive to the surface conditions of the sliding material pair based on several researchers' work; (a) Suh defined asperity deformation as the main determinant of friction in metal to metal contact and (b) Diei proposed a relationship between AE r.m.s in term of voltages and the rate of frictional energy dissipation from sliding contact of parts of materials. Furthermore, the relationship between AE and wear of mating surfaces was presented by McBride et al [88] where it was stated that '*This paper shows that asperity contact can be detected by acoustic emission measurements, and that such measurements can provide a vital understanding of the complex wear processes in both dry and lubricated situations'*. Tan et al [89] concluded that the source of AE during the gear mesh could be attributed to asperity contact. In the work of Xiao et al [90], rough friction was investigated via the usage of lubricated sliding roller surfaces which simulate the real gear teeth surfaces. Based on the results obtained from the grounded roller surface (made from hardened steel), he noted that friction coefficient of mating surfaces increased with increasing average surface roughness. Wang and Hsu [91] investigated the friction and wear process of asperity

contacts during sliding by performing multi-scratch tests on ball-to-ball test apparatus. The test results revealed that the friction coefficient increases with the increased number of scratches.

The detail results for the surface roughness measurements on both the undamaged and damaged gear teeth surfaces are presented in Appendix G. Table 6.2 provides a summary of the gear teeth roughness measured in both radial and axial direction of the gear for all test conditions. From table 6.2, it could be concluded that the both surface roughness of the gear teeth in the radial and the axial directions were higher for the pitted condition in comparison to the undamaged condition. Coupled with the observations of AE activity and pitting progression during this investigation, and conclusions of the various researchers detailed above, it was proposed that AE levels will increase with increasing gear pitted area. A consequence of the increase in pitted area is an increase of surface roughness and friction, leading to an increase in AE levels. This deduction was confirmed by the observations from figures 6.6 to 6.11 which show AE levels increasing with operating time/gear pitted area.

	Average Ra (μm) (Radial direction)	Average Ra (μm) (Axial direction)
Undamaged Gear Surface (reference)	1.3723	0.6660
50% pitted area gear surface for 220 Nm	2.5242	2.5290
50% pitted area gear surface for 147 Nm	2.7771	1.7070
50% pitted area gear surface for 73 Nm	1.8275	1.7960

Table 6.2 Average surface roughness of pinion gear teeth for undamaged and 50% gear pitted area under various load condition.

6.7 Diagnostics and prognostics capabilities

In assessing the diagnostics and prognostics capabilities of the AE, SOA and vibration monitoring techniques for gear teeth surface pitting wear, the following questions arise:

1) Which is the best indicator for monitoring pit growth?
2) How does load affect the various indicators?
3) What is the prognostic potential of these techniques?

6.7.1 Which is the best indicator for monitoring pit growth?

Clearly, there existed an initial period during which the gear teeth surface smoothened out, oil sump temperatures increased and dynamic stabilisation of the rotating systems (such as bearing, alignments etc) took place. Because of the complexity involved during this process, it was deemed inappropriate to relate any of the monitoring indicators to this period; 0 to 15hrs. However, after this initial period defined as wear-in, the monitoring indicators behaved differently with pit progressions. As discussed earlier, AE r.m.s level exhibits a linear relationship with running time after this initial period, which was not necessarily the case for vibration and SOA observations.

6.7.1.1 The AE technique

Throughout the duration of the tests it is believed that there are two processes affecting the generation of AE. Firstly, the wear-in process which causes a smoothing of surface roughness with a consequent decrease in AE levels. The second involves the increased surface roughness due to pitting progression/development which will increase surface roughness and AE levels. At the beginning of the tests AE levels will also be influenced by the oil film temperature and dynamic characteristics of the test-rig arrangement. Increasing oil temperature will lead to a reduction of oil film thickness; this encourages

more asperity contacts resulting in increased AE levels. On the other hand, the smoothing of the gear teeth surfaces due to the wear-in process will reduce surface roughness which will result in lower AE levels. Furthermore, it was postulated that the factors that determine the onset value of the AE level are the initial surface roughness of the gear teeth surfaces, assembly of the gear components and bearings which affects the transmission error and vibrational behaviour of the gearbox, and, the initial oil temperature.

The two test results at 220 Nm, see figure 6.6, exhibited different trends at the start of the tests; '220(1)' showed decreasing AE levels up to 15 hours operational time, whereas AE level for '220(2)' increased from the start of the test. It was postulated that the difference is due to the balancing process between increasing oil temperature and reducing surface roughness of the gear teeth, which have opposing effects on AE levels. In addition, it cannot be guaranteed that the exact positioning of the gear wheels and clearances within the gearbox were identical for each test condition; best practice was followed. For this particular test, from about 15 hours, 8% of gear pitted area; the AE r.m.s values increased linearly with increasing running time and pitted area. An important point to note; both test cases exhibit similar gradient from 8% pitted area or 15 hours running time onward. Similarly, for the 147 and 73 Nm tests (see figures 6.8 to 6.11), the AE levels exhibit different behaviours during the start of the test as highlighted for the load case of 220 Nm. However, after the initial 20 hours of running time or approximately 10% of gear pitted area, the AE level increased with both the operating time and percentage of pitted area. Inaddition, for both test cases under each applied load condition, the gradient are similar.

The linear relationship between AE levels and pit growth rate at all torque conditions was encouraging and emphasised the sensitivity of the AE technique.

6.7.1.2 The Vibration technique

Figure 6.12 shows the plot for vibration r.m.s against gearbox operating time under an applied torque of 220 Nm. Vibration levels increased from 0 to between 10 to 15 hours, which was indicative of increasing oil temperature (see table 6.1) and decreasing oil film thickness. As oil film thickness reduced, the damping effect of the oil film between the meshing gear teeth surfaces will reduce resulting in increasing vibration levels. A plateau was observed for the vibration r.m.s between 15 to 55 hours of the running time, even though gear surface pitted area increased to 25%, see figure 6.13. This showed that vibration technique was unable to monitor the pit grow process until the pit development was advanced. Hence at this point, it can be concluded that AE technique has an advantage over vibration technique in terms of pit growth monitoring. Observations of vibration response at 147 and 73 Nm, see figures 6.14 to 6.17, reiterated the observations detailed above. In summary, the vibration response increased when a minimum of 25% pitted area was reached, which is attributed to alterations in the stiffness of the gear due to modification of the Hertzian contact zone and changes in geometric profile. It must be noted that for this particular investigation the gearbox configuration is very simple, on real operational gearboxes as used on helicopters, the detection of pitting would occur later in operational life. This conclusion is attributed to the increased background noise levels and highly complex transmission path from the gears to the accelerometer.

6.7.1.3 Fe Concentration

As mentioned earlier it is believed that there are two processes operating during the tests. Firstly, the wear-in progress which causes the smoothing of the gear teeth surfaces, and secondly, the increased surface roughness due to pitting progression/development. At the beginning of the tests SOA levels will also be influenced by oil film temperature. An increase in oil temperature will led to a reduction of oil film thickness which will result in increased asperity contact hence increased Fe concentration levels. On the other hand, the smoothing of the gear teeth surface due to the wear-in progress will also result in Fe

particle production. Typically the concentration levels increased with operational time and level of applied torque (see figures 6.18 to 6.21). However, this was not exactly true for the test condition of 73 Nm, see figures 6.22 and 6.23. As the pit rate at 73 Nm test condition is significantly lower than the other applied torque conditions, the concentration of pit particles within the SOA detectable range may not increase consistently with the operating time. However, when all Fe concentration data are plotted against percentage pitting, see figure 6.30, more consistent behaviour was obtained after 20% gear pitted area. Normalised Fe concentration increased linearly for all torque values. The unique observation of Fe concentration levels for the first 15 hrs at 73 Nm is attributed to the particle generation during wear-in. From this observation it was envisaged that for the torque conditions where pit development is slow, wear-in will dominate over particles generated from pits until such a time that pit progress advances.

At the higher applied torque (220 Nm) the averaged absolute value of the Fe concentration was significantly higher than at 147 and 74 Nm; 146.5 ppm compared to 43.5 and 24.5 ppm respectively.

6.7.2 How does load affect the various indicators?

The influence of torque on these monitoring indicators could provide valuable information on the potential, or limitation, in applying these techniques in practical situations where environmental and operational factors come into play. The load dependency of each indicator was investigated in terms of gearbox operating/running time and percentage of gear pitted area.

6.7.2.1 Gear AE r.m.s

From figure 6.24 at any particular given operating time, the greater the applied torque the greater the normalised AE r.m.s value. Furthermore, the higher applied torque condition

always produced a greater rate of AE generation, which is evident in figures 6.24 and 6.25. This is due to the higher pitting rates (detailed in figure 6.1) and smaller oil film thickness. Absolute values of AE plotted against operating time are presented in figure 6.25. The absolute values do showed higher AE r.m.s levels for higher torque levels which were as expected. It is also important to note that theses were performed at different starting oil temperatures and initial surface roughness, and these initial conditions may vary the results. Coupled with these effects are the variation in pitting rates, surface roughness, oil sump temperatures and especially the set-up of the test-rig (clearances, alignment, backlash, etc) all having an influence on the starting level of AE activity.

An interesting observation from figure 6.26 was that whilst the rate of pitting accelerated at higher torques, the gradients for normalised AE r.m.s values against percentage of gear surface pitted area were similar for the various applied torque conditions; 0.014, 0.013 and 0.010 at 220, 147 and 73 Nm respectively. This implied that irrespective of the applied torque the gradient was nearly constant, or, the amount of pitting as a function of normalised AE r.m.s levels was independent of applied torque. This observation will hold true if the type and progression of surface damage, in this instance pitting wear, is consistent throughout all applied torque conditions which was supported by the results from visual inspection of the gear teeth surfaces. For example, the gradient of the plots illustrated in figure 6.26 will not be constant if a much higher torque had been applied resulting in occurrence of other types of surface damage such as scuffing. Furthermore, this observation revealed that the AE technique had a good sensitivity to percentage pitted gear area at all torque levels following the wear-in period from 5% gear pitted area onwards.

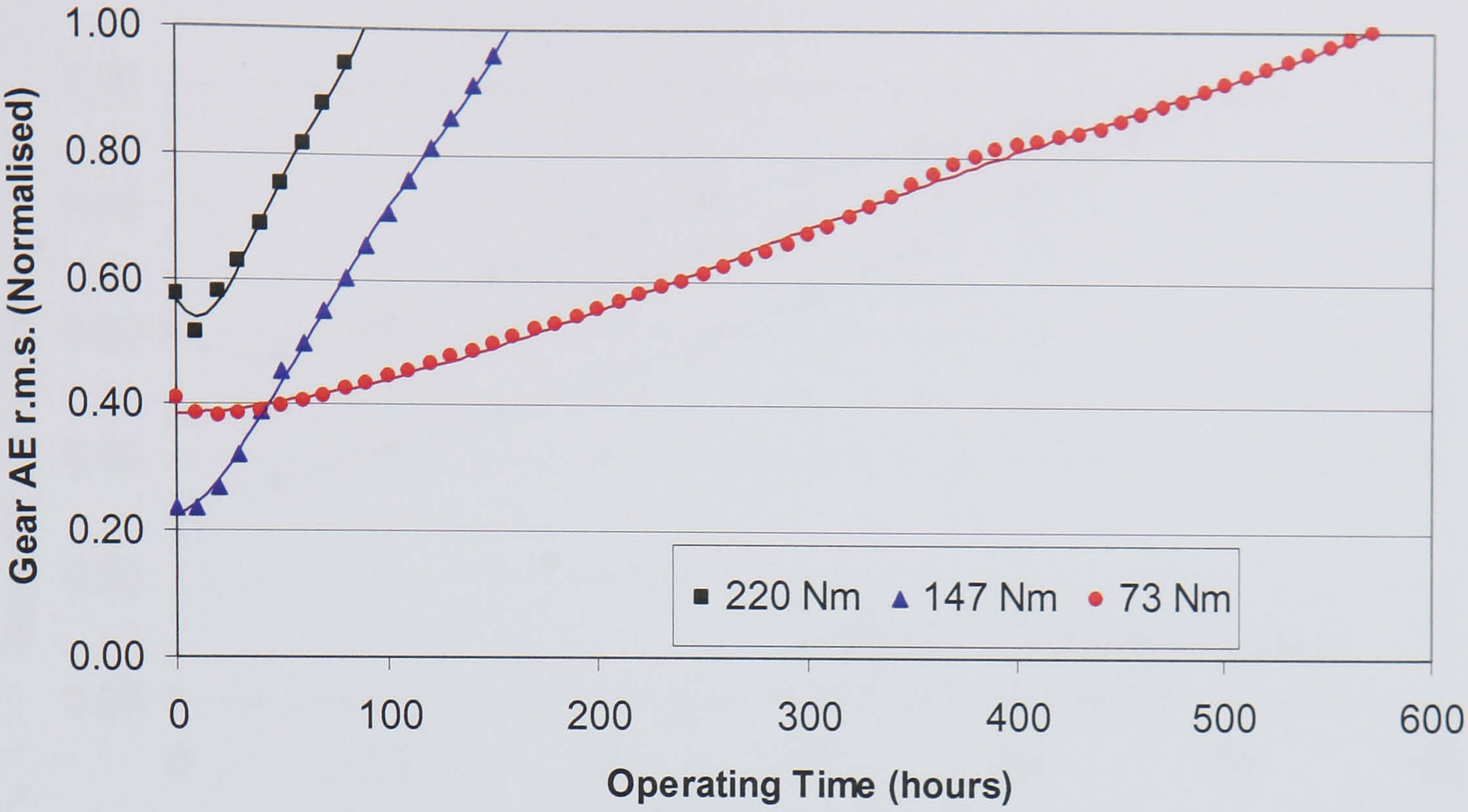

Figure 6.24 Normalised AE r.m.s against gearbox operating time for various torque conditions at 745 rpm.

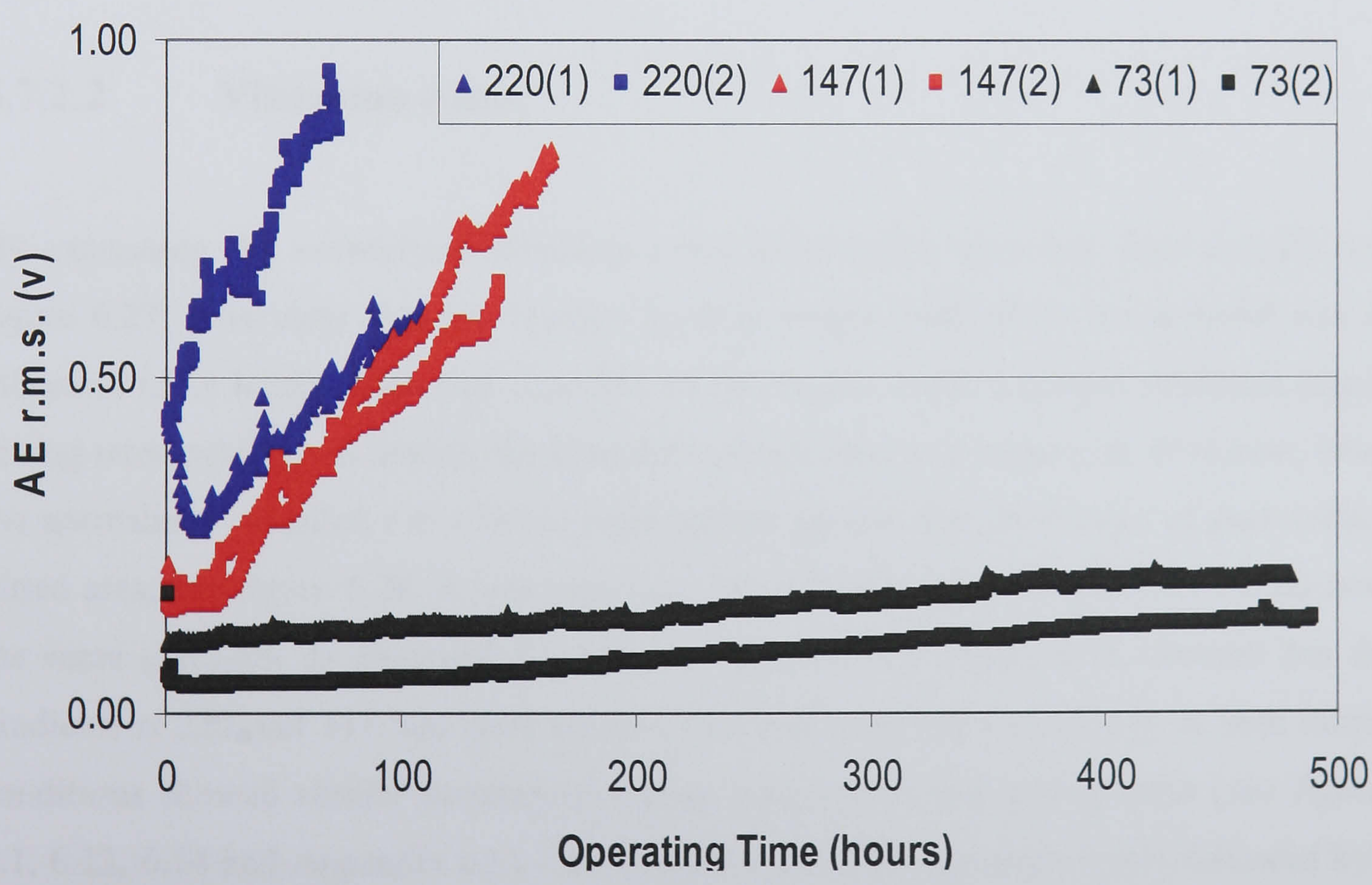

Figure 6.25 Absolute AE r.m.s values for all load conditions.

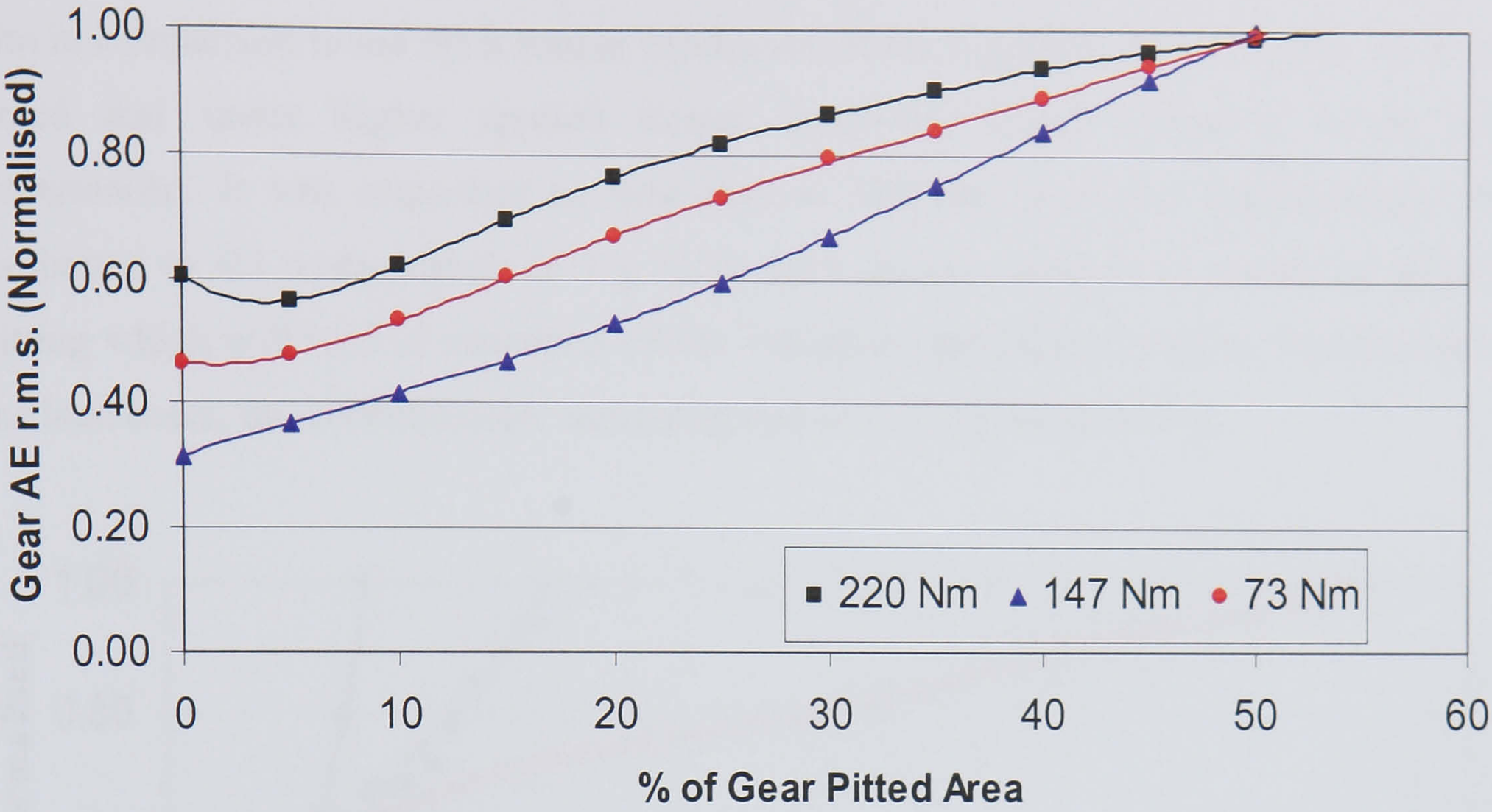

Figure 6.26 Normalised AE r.m.s against gear pitted area for various torque conditions at 745 rpm.

6.7.2.2 Vibration r.m.s

By examining the normalised vibration r.m.s level under operating time domain, see figure 6.27, it is clear that the highest applied torque resulted in the steepest rise in vibration r.m.s levels. This was expected as the higher applied torque produced higher pitting rates, which will modify the Hertzian contact zone at a faster rate. However, when the normalised vibration r.m.s levels were plotted against the percentage of gear surface pitted area, see figure 6.28, it was expected that all three torque conditions would have the same gradients as observed for AE (see figure 6.26). Figure 6.28 showed that the gradients at 220 and 147 Nm were similar, this was expected particularly as both torque conditions showed similar patterns of pitting progression and pitting rates (see figures 6.1, 6.12, 6.14 and Appendix 6A), i.e., a relative period of constant levels followed by a steep rise before termination of the tests. This pattern was also observed for one of the tests at 73 Nm, see figure 6.16 [73(2)], however, the pattern was not mirrored for the other test at 73 Nm. As the results presented were averaged for both tests under the same

torque condition, the results presented in figure 6.28 showed a different gradient at 73 Nm in comparison to the other torque conditions. From figures 6.13, 6.15 and 6.17, it was noted that under higher applied torque condition, higher vibration levels were experienced. It was important to note that at 220 Nm load, the accelerometer was calibrated to 0.1 v equivalent to 1 g to prevent excess vibration at advanced stage of pitting which will lead to saturation of the vibration acquisition systems. For the rest of the load cases, the accelerometer was calibrated to 1 v equivalent to 1 g.

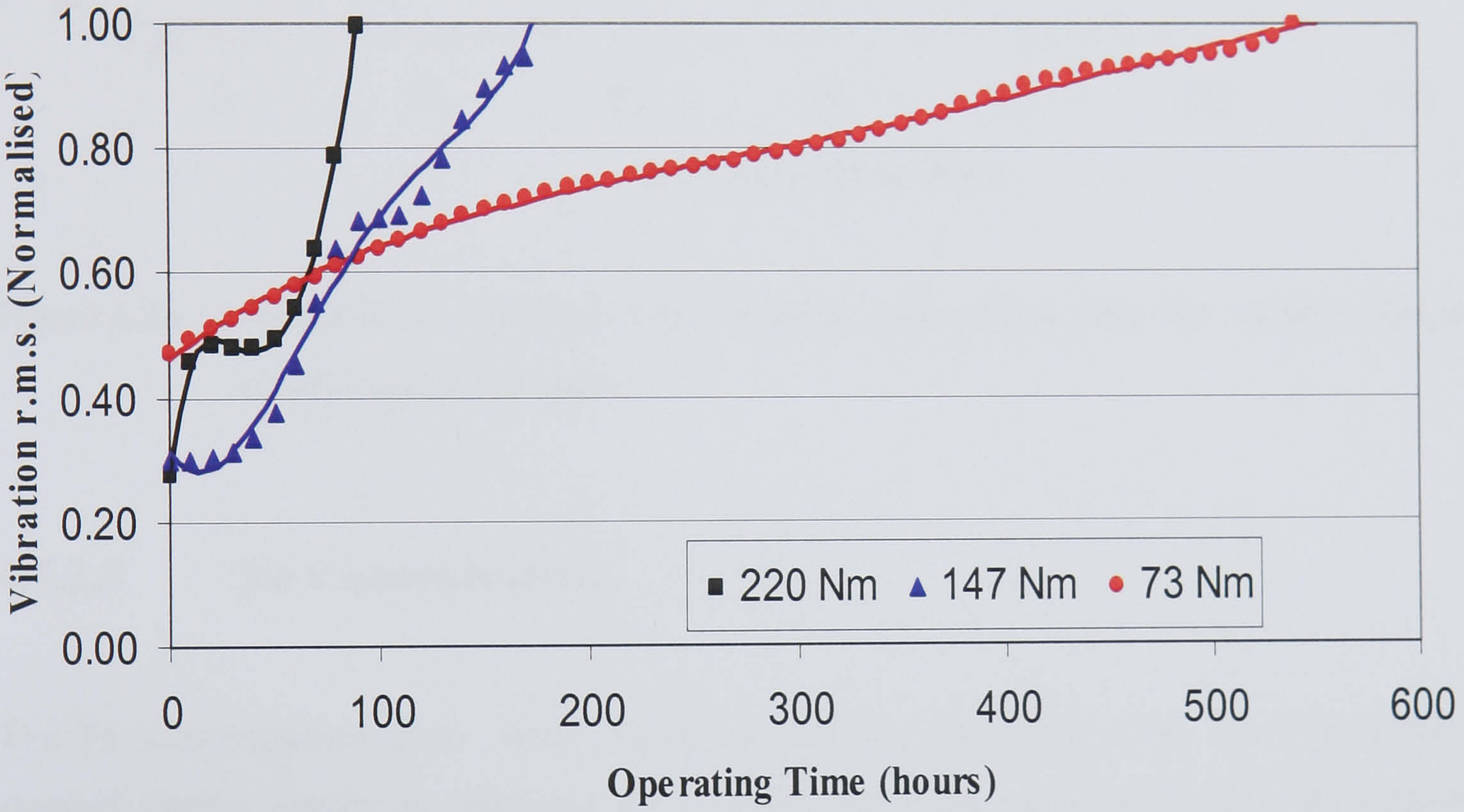

Figure 6.27 Normalised vibration r.m.s against gearbox operating time for various torque conditions at 745 rpm

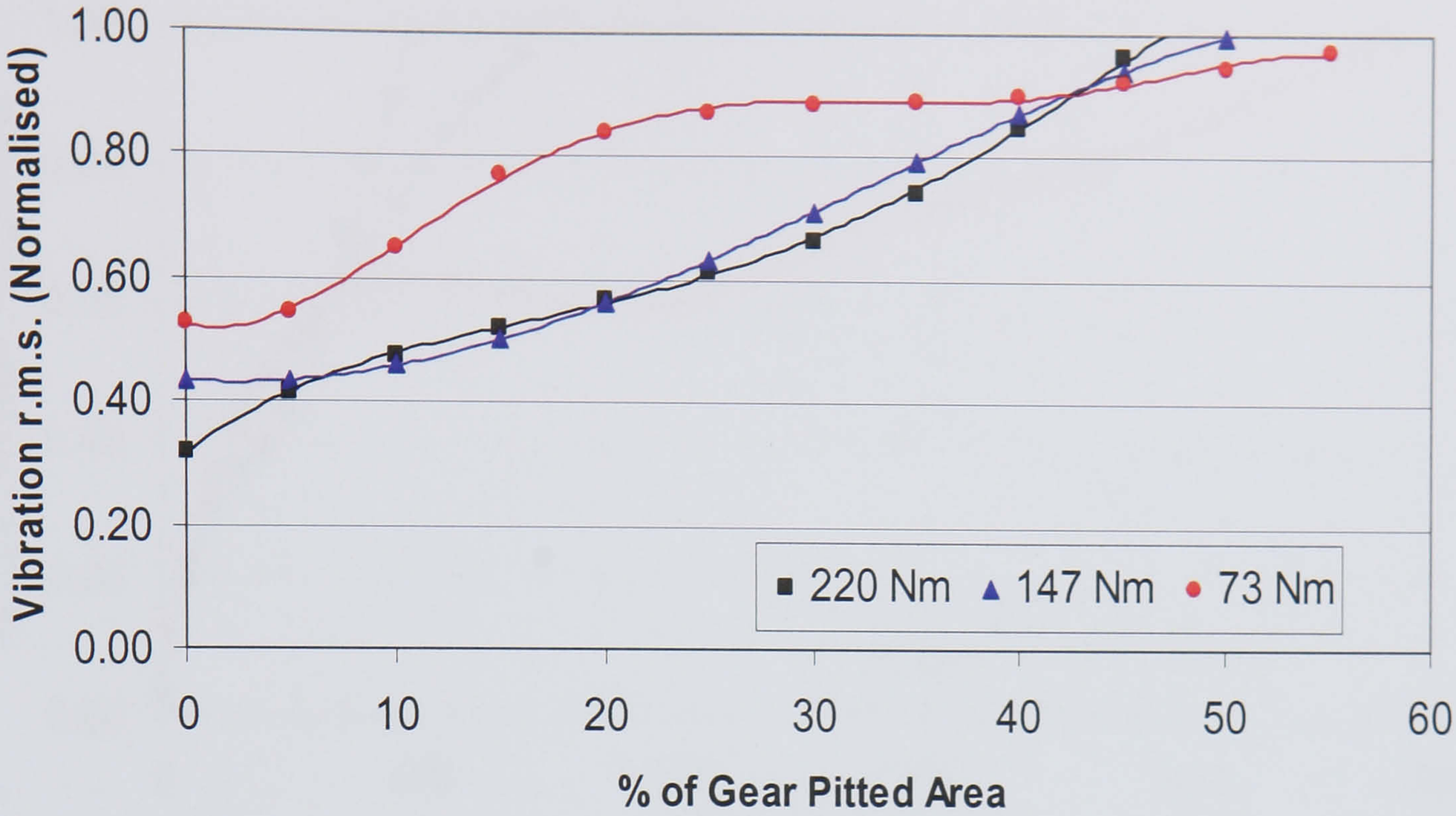

Figure 6.28 Normalised vibration r.m.s against gear pitted area for various torque conditions at 745 rpm.

6.7.2.3 Fe Concentration

The Fe concentration plots with respect to gearbox operating time, see figure 6.29, showed similar results as observed for AE and vibration r.m.s; the higher the applied torque, the steeper the gradients. This was the consequence of higher pitting rate producing greater amount of wear particles at a quicker rate. This was further supported by the observation; the higher the applied torque, the greater the averaged absolute value of the Fe concentration (refers to figures 6.19, 6.21 and 6.23). It is important to note that at the torque value of 73 Nm a period existed where Fe concentration changed relatively slower with respect to the running time. Figure 6.30 showed similar results to the vibration; similar gradients at 220 and 147 Nm, though after 15% pitted area, all torque conditions displayed near identical gradients (0.014, 0.010, and 0.010 at 220, 147 and 73 Nm respectively).

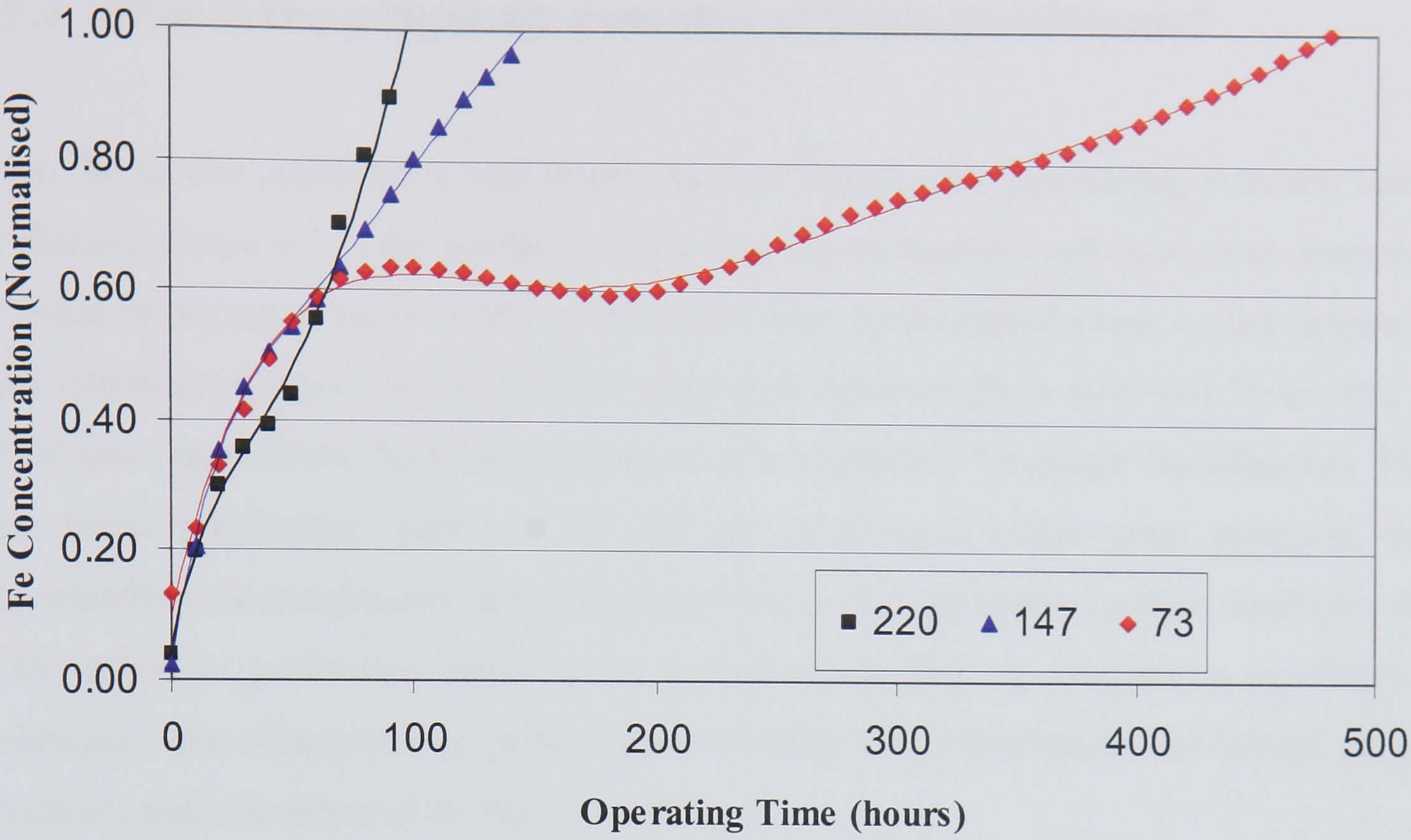

Figure 6.29 Normalised Fe concentration against gearbox operating time for various torque conditions at 745 rpm.

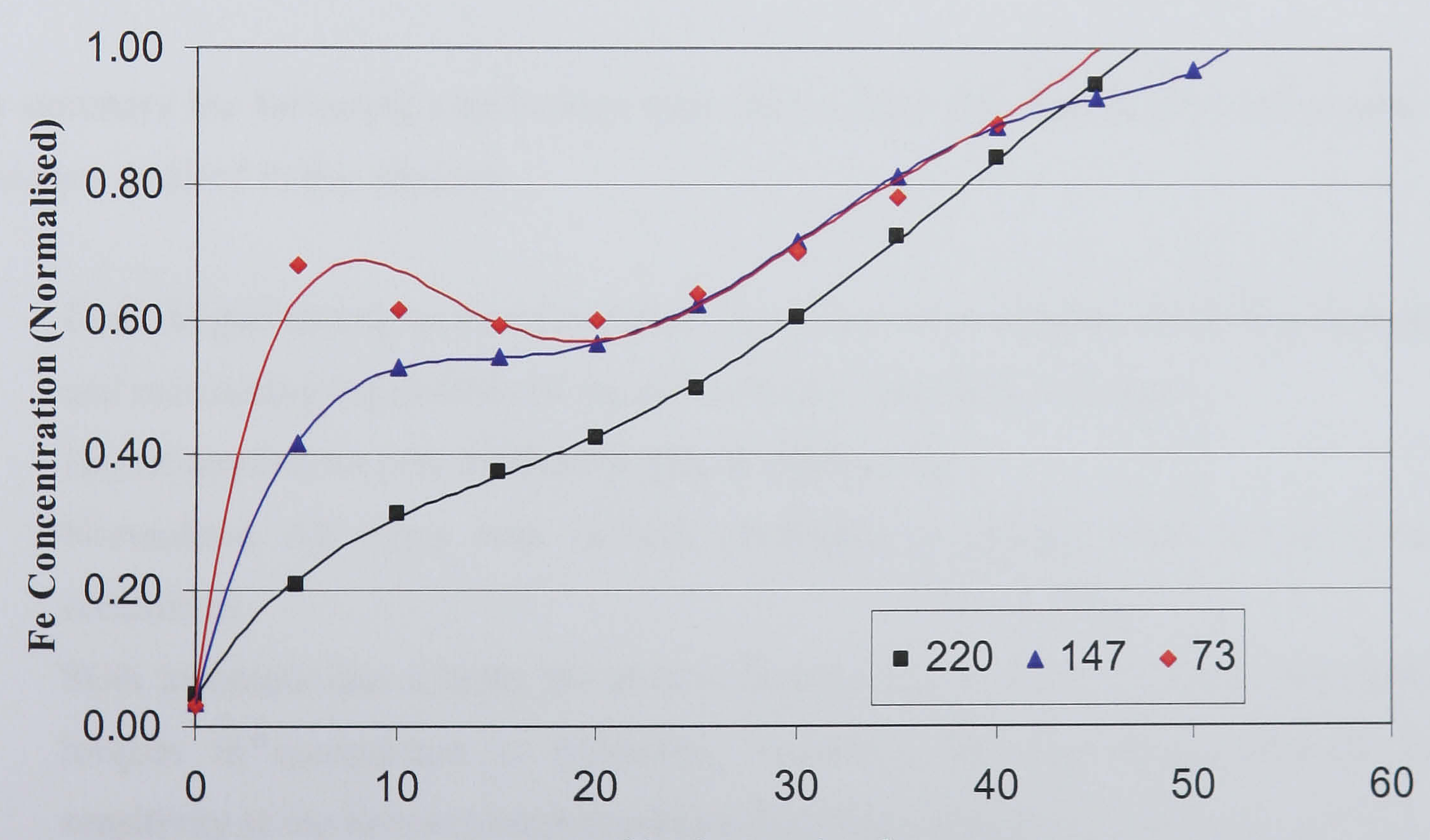

Figure 6.30 Normalised Fe concentration against gear pitted area for various torque conditions at 745 rpm.

6.7.3 What is the prognosis potential of these techniques?

From the results presented it was clearly evident that the AE monitoring indicator could be linearly correlated to the gearbox pitting rates for all torque conditions, with detection of onset of pitting as early as 8% of the pitted area. This offered much earlier diagnosis than vibration analysis and SOA where only after between 25 to 40% and 20 to 30% of pitted area respectively did these techniques offer capability for defect identification. This near linear relationship between AE and pit progression offers great potential, and opportunities, for prognostics in rotating machinery. At high applied torque condition, the SOA technique performed better in pit growth monitoring in comparison to vibration technique. The disappointing performance of SOA and vibration at the lowest torque condition was not mirrored by the AE technique.

6.8 Conclusions

In summary the following conclusions were drawn from the observations and results of the tests detailed in this chapter:

I. Gear fatigue testing was performed on spur gears to investigate the pitting detection and monitoring capabilities of the AE, vibration and SOA techniques.
II. Higher applied torques resulted in greater pitting rate.
III. Normalised AE r.m.s was linearly correlated to pitting rates for all torque conditions.
IV. SOA technique has a better pit growth monitoring capability at the higher applied torques in comparison to vibration. However, both techniques showed less sensitivity at the lowest torque condition than AE technique.
V. For all 3 indicators; Fe concentration, AE and vibration r.m.s, the rate of change of these parameters with respect to gearbox operating time increased with increasing applied torque.

VI. The rate of change of the normalised AE values with respect to percentage of gear pitted area remained constant regardless of the applied torque. SOA had similar trends after 15% of gear pitted area whilst vibration monitoring had similar gradients at 220 and 147 Nm.

VII. For all 3 indicators; Fe concentration, AE and vibration r.m.s, the higher the applied load, the greater the response in term of absolute amplitude from the indicators.

VIII. The linear relationship between AE, gearbox running time and pit progression implied that the AE technique offers good potential for prognostic capabilities for health monitoring of rotating machines.

7 RELATIONSHIP BETWEEN AE ACTIVITY AND GEAR TEETH PITTING PROGRESSION

Published research relating AE activity to the amount of wear involving dry or lubricated sliding surfaces is limited to slider/disk/roller configurations. There has been no published attempt to relate the amount of gear surface pitting wear to the level of AE activity. This chapter provides a brief review of research into formulating the relationships between dry/lubricated sliding surface wear and AE activity levels. By employing these relationships and the experimental data presented in chapter 6, a model was devised to predict the amount of gear surface pitting wear using the AE activity level. Although the model revealed inconsistencies during this first attempt, it helped to expose the difficulties and the potential problem areas in achieving an accurate model. The shortcomings of this model will be discussed and recommendations will be made to improve it.

7.1 Background

Matsuoka et al [92] employed the AE technique for monitoring wear on a slider/disk configuration. Using this technique, AE transducers were mounted directly onto both the arm with the slider and disk to measure their contact behaviour. It is important to note that this set-up is similar to AE transducer mounted on the pinion of the test gearbox. Based on past research, Matsuoka obtained a relationship between AE r.m.s and wear.

$$V_{volts} = \alpha\sqrt{kNV_{slidingspeed}} + \beta \qquad (7.1)$$

where V_{volts} is the AE r.m.s. (volts)

$V_{sliding\ speed}$ is the sliding speed (m/s)

α and β (volts) are constants

k is the wear coefficient

Using Archard's equation, the wear coefficient could be expressed as

$$k = \frac{V_{volume} H}{Nx} \tag{7.2}$$

where V_{volume} is the volume of material removed (m^3)

H is the hardness of the material (Pa or $\frac{N}{m^2}$)

x is the sliding distance (m)

N is the normal force (N)

Employing the experimental apparatus detailed in [92], Matsuoka determined α and β experimentally for several sets of measured wear volume and corresponding AE r.m.s voltage. Using the experimental results and equations 7.1 and 7.2, Matsuoka concluded that the AE technique is able to predict the wear status for both the sliding surfaces, in this instance, the slider and disk. In another investigation Jiaa and Dornfeld on *'Experimental studies of sliding friction and wear via AE signal analysis'* [63], a power function relation between AE r.m.s. voltage and the rate of frictional energy dissipation during sliding contact proposed by Diei was presented in the following form:

$$V_{volts} = (k\eta\tau_s A_a V)^{m/2} \tag{7.3}$$

Where k and m are constants that characterised the AE acquisition systems

τ_s is the shear strength of the contacting material surfaces ($\frac{N}{m^2}$)

η is the constant function of the surface roughness of the contacting surfaces

$V_{sliding\ speed}$ is the sliding speed (m/s)

A_a is the apparent contact area (m^2)

A close examination on the both sides of the equations 7.1 and 7.3 revealed that they are dimensionally balanced in term of units. The left hand sides of the equations have the

final unit of voltage which is proportional to the square root of power which was evident on the right hand sides of equation 7.1 and 7.3. The major difference between these two equations is; in equation 7.1, the AE r.m.s value was related directly to wear volume whereas equation 7.3 is concerned with the relationship between friction and AE signal levels.

In order to determine the relationship between AE and wear and friction, Lingard et al [93] performed an investigation of AE in sliding friction and wear of metallic materials. Their experimental work was conducted using a two-disc machine under dry sliding conditions. It was found that there was no obvious relationship between AE and wear even with the various variations in operating parameters such as load, speed and running time. However, Lingard et al did not preclude the possibility of an AE-wear relationship in view of other researchers' work. This possibility was evident in the case of the pitting wear of the test gear teeth as shown in chapter 6. A relationship between cumulative AE count and frictional work was proposed by Lingard as he expects the AE to be influenced more by the friction rather than wear parameters based on the experimental results obtained. The proposed empirical equation takes the following form:

$$\sum C = b(W_f)^a \tag{7.4}$$

Where ΣC is the cumulative AE count

b is a constant characterised by the AE transducer properties and settings

a is the exponential constant determined by the sliding surfaces

W_f is the frictional work done between the sliding surfaces

Another empirical relationship between AE r.m.s signals and wear status from sliding metallic contacts under both lubricated and dry conditions was proposed by Boness et al [60, 61]. Based on the assumption that the AE r.m.s voltage at any particular instant measures the instantaneous wear rate, Boness et al suggested that the total wear for a given contact time will be proportional to the integral of the AE r.m.s voltage over that given contact time. In this case, the integral value of AE r.m.s voltage was computed

using trapezoidal summing process over the given contact time. For simplification purpose, Boness fitted the experimental data using several power laws to establish the empirical relationship between AE r.m.s voltage and wear scar volume, which was presented in the following form:

$$\text{Wear scar volume } (mm^3) = \text{constant} \times \int (\text{R.M.S})^n \, dt \qquad (7.5)$$

Where n are 0.1, 0.5 and 1.5 for initial wear (lubricated), adhesive wear (dry) and abrasion (dry) respectively. In addition, it is important to take note that Boness observed and established that both the measured wear scar volume and the corresponding integrated AE r.m.s signal were independent of the lubricant viscosity and thus the oil film thickness. This observation is opposite to what has been established in the AE generation between meshing gear teeth where lubricant properties do influence AE activity levels. Since both equations 7.4 and 7.5 were derived from experimental results empirically, these equations were only accurate and applicable to the specific test conditions entailed in [93, 60, 61]. It is also very important to note that equations 7.4 and 7.5 were not dimensionally equivalent on both sides of the equations.

7.2 AE r.m.s voltage and wear volume of gear teeth surfaces

As discussed in the previous section, there are typically two types of engineering models; empirical and theoretical, to relate AE r.m.s signal to the amount of wear between sliding surfaces. However, an universal model is not to be expected. For those operating conditions under which the wear regimes and behaviours were stable, empirical models may be developed as illustrated in equations 7.3 and 7.4. Furthermore, for cases that the mechanics of wear and AE generation, and their influencing factors could be understood or determined, a theoretical model could be developed together with the empirical data to enhance a more accurate prediction model. There have been many attempts by researchers to attain an accurate prediction model to relate AE r.m.s level to sliding wear. However, limited success has been achieved [94] on pin or slider on disk or cylinder

machines. Furthermore, to date, there is limited literature on the relationship between AE levels and pitting gear wear on gears. This will be the first documented work that has attempted to relate AE r.m.s voltage to pitting wear progressions on gear teeth flanks. The objective of this section is to derive a simple theoretical model, enhanced by experimental data, to predict the behaviour of AE r.m.s with respect to the pitting wear on the gear teeth surfaces or visa versa.

There are many factors that influence pitting wear on gear teeth flanks and the generation of AE signals from meshing gear teeth. In general, there are two levels of variables in a pitting wear system; the macroscopic parameters and the microscopic processes in the contact zone during pit development. The proposed pitting wear model will attempt to link the macroscopic level of wear, simply in terms of the amount of material lost during pit progressions, to the operating parameters of the gearbox such as applied load, rotational speed, oil viscosity, oil temperature or oil film thickness. In this case, macroscopic parameters were chosen due to the lack of information and data on the microscopic processes during the accelerated gear fatigue tests. In order to proceed to formulate this model, factors affecting both the pitting wear progressions and AE generation during the pit progressions must be identified and examined. These factors are listed in table 7.1.

Influencing Factors	**Remarks**
Speed (Sliding/rolling)	Operating parameter of gearbox
Applied load/torque	Operating parameter of gearbox
Oil temperature	All these parameters are related to asperity contact
Oil viscosity	
Oil film thickness	
Surface roughness	All these parameters are affected by pit progression and related also to asperity contacts
Friction	

Table 7.1 Factors affecting pitting wear progressions and AE generation during the wear processes.

In table 7.1, both the rotational speed and applied load are the operating variables of the test gearbox that could influence both the AE generation and pitting wear. As detailed in Annex F, the pits always start from the dedendum and move towards the pitch-line. Hence, in this proposed prediction model, the average sliding speed from the pinion's lowest contact point to the pitch-line would be employed. The applied load parameter was included directly into this model; in term of the Hertzian contact stress acting on the gear teeth surfaces. As shown in table 7.1, the oil temperature, viscosity and film thickness, surface roughness of gear teeth surfaces and friction between gear teeth surfaces were classified under the same category; in general they are the gearbox operating parameters, and all of them would affect the amount of asperity-to-asperity contact. As presented in chapter 5, asperity contact is the prime source of AE during gear mesh; hence, these parameters definitely have an effect on the AE level generated. In this instance, due to the requirement to balance the proposed model equation dimensional, oil film thickness will be employed. The last category that would go into the proposed model equation is the pit progression. Pit progression is a measure of the status of the damaged gear teeth surface and certainly has an influence on both the surface roughness and friction of the gear teeth surfaces, thus the AE activity level. As observed in chapter 6, the pit development has two stages; (a) before onset of pitting and (b) after onset of pitting. This pit development characteristic was also reflected in the corresponding AE behaviours described in chapter 6. In the accelerated gear fatigue tests, the test set-up could not measure both the surface roughness and the friction between the meshing gear teeth continuously and in-situ, although theses two factors changed with the pit progression. The only form of measurement on the pit progression during the accelerated gear fatigue tests was the visual inspection on the gear teeth surfaces in terms of percentage of gear pitted area. However, this parameter could only provide 2-dimensional damage information; hence the depth of the pit and the volume of material removed from the gear teeth surfaces were not available. Therefore, in this instance, pit progression would be most suitably represented in term of wear volume removed from the gear surface material through the SOA data collected.

After examining all the factors and other researchers' work (from equations 7.1 to 7.5), the pitting wear model equation to relate AE r.m.s. voltage and volume of material removed from the gear teeth surfaces is proposed to take the following form:

$$V_{volts} = \alpha \sqrt{\frac{V_{slidingspeed} S_{contact} V_{volume}}{h}} + \beta \qquad (7.6)$$

Where $V_{sliding\ speed}$ is the pinion average sliding speed from the lowest contact point to the pitch-line (m/s)

$S_{contact}$ is the calculated contact stress (N/m^2)

V_{volume} is the volume of material removed from the gear teeth surfaces (m^3)

h is the calculated oil film thickness (m)

It could be observed that equation 7.6 is dimensionally balanced between the left hand side of the equation (in voltage, which is directly proportional to) and the right hand side (in square root of power). In order to ascertain whether the relationships between the parameters of the equation are logical and reasonable; a closer examination was undertaken. Firstly, an increase in sliding speed would increase the AE r.m.s due to higher strain rate encountered by the two surfaces, this was clearly explained in chapters 2 and 5. Secondly, as highlighted in chapter 5, asperity contact is the prime source of AE generation. An increase in applied load, thus the contact stress, will expect to increase the AE r.m.s level since more asperities would come into contact during the gear mesh. Thirdly, as the oil film thickness increased, lesser asperity contact will come into contact, therefore, one would expect AE r.m.s level to reduce which is evident in equation 7.6. Finally, it is logical to expect AE r.m.s level increased with pitting progression, which has been proven in chapter 6 where AE r.m.s increased with percentage of gear pitted area. However, in this wear model, the pitting progression will be in term of wear volume removed from the gear teeth surfaces.

Furthermore, the more deterministic model of Matsuoka et al [92] will be computed and used as a reference to compare with the proposed model (equation 7.6). By combining equations 7.1 and 7.2, the final form of Matsuoka's model will be as follows:

$$V_{volts} = \alpha \sqrt{\frac{V_{slidingspeed} HV_{volume}}{x}} + \beta \qquad (7.7)$$

In the subsequent sub-sections, the determination of each parameter for equations 7.6 and 7.7 will be presented and discussed.

7.2.1 Determination of wear volume

In the accelerated gear fatigue tests presented in chapter 6, the pit progressions of the damaged gear teeth were assessed by visual inspection in term of percentage of gear pitted area. Although this assessment is 2-dimensional (2D); more accurate assessment in terms of volume of material removed from the gear teeth surfaces were met with difficulties. It was not advisable to remove the test gear set for surface damage assessment, as this will alter the dynamic characteristics of the gearbox. The option of including an oil filter in the test gearbox to capture the wear debris removed from the gear teeth surfaces during pit progressions was explored. However, due to the space constraint in the test gearbox, installation of a filtration system was unachievable.

An alternative method has to be explored to convert the gear teeth damaged assessment from 2D to 3D, i.e. from percentage of gear pitted area to volume of material removed. Since the amount of material removed from the gear teeth surfaces were unable to be measured real time during pit progressions, an approximation of the wear volume may be determined based on the SOA results presented in chapter 6. As detailed in chapter 2, the SOA technique is able to detect wear material of size up to 10 μm. Hence, the Fe concentration in the used oil obtained from the SOA technique could provide an estimate on the amount of wear material removed from the damaged gear teeth surfaces.

In chapter 6, the Fe concentration obtained from the SOA technique was computed in term of ppm. However, ppm could be measured either with the ratio of mass-to-mass or mass-to-volume of the sample. In this instance, the Fe concentration in ppm was measured in mass-to-mass ratio. In order to determine the actual mass of Fe elements present in the lubricating oil of the test gearbox, equation 7.8 was employed.

$$Fe(mass) = \frac{Fe(ppm)x\ mass\ of\ sample}{10^6} \tag{7.8}$$

where Fe(wt) is the mass of Fe in the sample (kg)

Fe(ppm) is the Fe concentration in ppm

Mass of the sample used in the laboratory analysis is 0.000247 kg

Since the pitting damage on the gear teeth surfaces was to be measured in terms of wear volume. Dividing equation 7.8 by the density of Fe, which is 7930 kg/m^3, the volume of material removed from the pitting gear teeth surfaces could be obtained using equation 7.9.

$$Fe(volume) = \frac{Fe(mass)}{7930} \tag{7.9}$$

where Fe(volume) is the volume of Fe (m^3)

The total volume of Fe present at the inspection interval (provided in chapter 3) will be the sum of the volumes of the Fe present from the start of the gear fatigue test till this particular inspection interval.

7.2.2 Average sliding speed

The sliding speed of any gear pair could be computed using the formulae provided in Drago [24, chapter 3]. For the rotational speed of 745 rpm, the pinion sliding speeds at various positions, such as pinion lowest point of contact, pitch point and highest point of contact were calculated and presented in table 7.2. The negative sign for the sliding speed at pinion lowest point of contact indicates that the sliding direction is opposite to that of rolling.

Pinion positions	**Pinion sliding speed (m/s)**
Lowest point of contact (at the dedendum)	-1.09
Pitch point (at pitch-line)	0.00
Highest point of contact (at the addendum)	1.05

Table 7.2 Pinion sliding speeds at the respective pinion-wheel contact positions.

7.2.3 Calculated oil film thickness

Using the oil film thickness calculation derived in Appendix D and the oil temperatures recorded for the accelerated gear fatigue tests presented in chapter 6, the oil film thickness for each applied load condition is depicted in table 7.3.

Applied load (Nm)	Average Oil temperature (^{o}C)	Composite surface roughness (μm)	Kinematics viscosity (mm^2/s)	Calculated oil film thickness (μm)
73	28.3	2.58	147.79	1.01
147	49.9	3.93	86.69	0.77
220	63.4	3.57	50.88	0.59

Table 7.3 Oil temperature, kinematics viscosity, film thickness and specific film thickness parameters at final wear stage (50% gear pitted area) for all load conditions.

7.2.4 Contact stress computation

The contact area between non-conformal surfaces such as bearings, gears and cams are usually very small and thus high pressure will be yielded in the contact zone. This high pressure can be determined by formulae utilising the theory of elasticity developed by Hertz in 1881 [33]. This high pressure usually been referred as Hertzian contact stress. In lubricated contact, the contact stresses are affected by both the sliding and rolling motion and the lubricating film separating the contact surfaces. However, the effect of sliding between the two contacting surfaces will result in frictional force that causes shear stress along the interface of the contacting surfaces. This phenomenon will provide the opportunity for crack formation and subsequently surface damages.

The contact between a pair of spur gear could be simplified into contact between two parallel cylinders as illustrated in [33, chapter 7]. The formulae for the contact stresses, dimension and contact parameters are presented in table 7.4 and 7.5. The resultant contact width and stresses are computed and depicted in table 7.6.

Contact width (m)	Max. contact stress (N/m^2)	Avg. contact stress (N/m^2)	Max. shear stress (N/m^2)
$b_{contact} = \sqrt{\frac{4FR}{\pi dE}}$	$P_{\max} = \frac{F}{\pi b_{contact} l}$	$P_{avg} = \frac{F}{4 b_{contact} l}$	$\tau_{\max} = 0.304 P_{\max}$ at a depth of $0.786 b_{contact}$

Table 7.4 The formula for contact stresses and width between two parallel cylinders [33].

Where $\frac{1}{E} = \frac{1}{2}(\frac{1-\upsilon_1^{\,2}}{E_1} + \frac{1-\upsilon_2^{\,2}}{E_2})$

υ_1, υ_2 is the Poisson's ratio of the gear pair

E_1, E_2 is the Young's elastic modulus of the gear material

$\frac{1}{R} = \frac{1}{R_1} + \frac{1}{R_2}$

R_1, R_2 is the pitch radius of the pinion and wheel respectively

l is the face width of the pinion

F is the contact load which acts normal to the gear contact surface

R_1	0.0735 m
R_2	0.0975 m
R	0.0419 m
E_1, E_2	205×10^9 N/m^2
υ_1,υ_2	0.3
E	225×10^9 N/m^2
l	0.015 m
F	Applied torque/R_1 N

Table 7.5 The parameters to determine contact stresses and width between the gear teeth surfaces.

Applied torque (Nm)	Contact width (m)	Max. contact stress (N/m^2)	Avg. contact stress (N/m^2)	Max. shear stress (N/m^2)
220	$2.17x10^{-4}$	$2.92x10^{8}$	$2.30x10^{8}$	$8.88x10^{7}$
147	$1.78x10^{-4}$	$2.39x10^{8}$	$1.88x10^{8}$	$7.26x10^{7}$
73	$1.25x10^{-4}$	$1.68x10^{8}$	$1.32x10^{8}$	$5.12x10^{7}$

Table 7.6 The resultant contact stresses and width between the gear teeth surfaces.

7.2.5 Computation of Matsuoka's model

Based on the model derived by Matsuoka, equation 7.7 will require two input parameters; sliding distance, x and gear teeth surface hardness, H. The effective contact length is approximated to the sliding distance between the two mating gears. Drago [24] proposes a method to calculate the sliding distance (equation 3.87); this was employed to determine the distance x (0.0153 m). In order to complete the formulation of equation 7.7, the measured hardness of the gear teeth surface is required. In order to balance both sides of equation 7.7, the measured hardness of 137 Hv was converted to 465.8 MN/m^2 through the following equation documented by John [95].

$$\text{Tensile Strength} = H_D \text{ X } 3.4 \tag{7.10}$$

With the relevant gearbox data such as the gear teeth surface hardness, sliding distance and rotational speed, equation 7.7, which entailed the relationship between AE r.m.s and wear volume using Matsuoka's model, is simplified into the following form.

$$V_{volts} = 128027\alpha\sqrt{V_{volume}} + \beta \tag{7.11}$$

7.3 Discussion of proposed model

Using the proposed model equation 7.6 and the gearbox operating parameters derived in tables 7.2 to 7.6, the relationship between AE r.m.s and wear volume was computed at each applied load level. The results are as shown in table 7.7:

Applied Load (Nm)	Equations
220	$V_{r.m.s.} = \alpha(1.64x10^{7})\sqrt{W_{vol.}} + \beta$
147	$V_{r.m.s.} = \alpha(1.30x10^{7})\sqrt{W_{vol.}} + \beta$
73	$V_{r.m.s.} = \alpha(0.95x10^{7})\sqrt{W_{vol.}} + \beta$

Table 7.7 The equation that entailed the relationship between AE r.m.s and wear volume using the proposed model at each applied load level.

In order to determine the values for α and β, experimental data would be required. The AE r.m.s and Fe concentration values for each applied load condition based on the accelerated gear fatigue tests (shown in chapter 6) were utilised to provide AE r.m.s against square root of wear volume plots. The square root of the wear volume is determined by employing the procedures entailed in chapter 7.2.1. The resulting plots were presented in figures 7.1 to 7.3. For simplification purpose, linear equation was fitted through each set of test data. The worst fit was from 220 Nm with a R^2 value of 0.61. Under each applied load condition; a mid-point value was obtained by averaging the AE r.m.s. values obtained from the two linear equations at a step increment of square root of wear volume. With these mid-point values, a straight line could be drawn in between the two sets of data as shown in figure 7.4 for each applied load level.

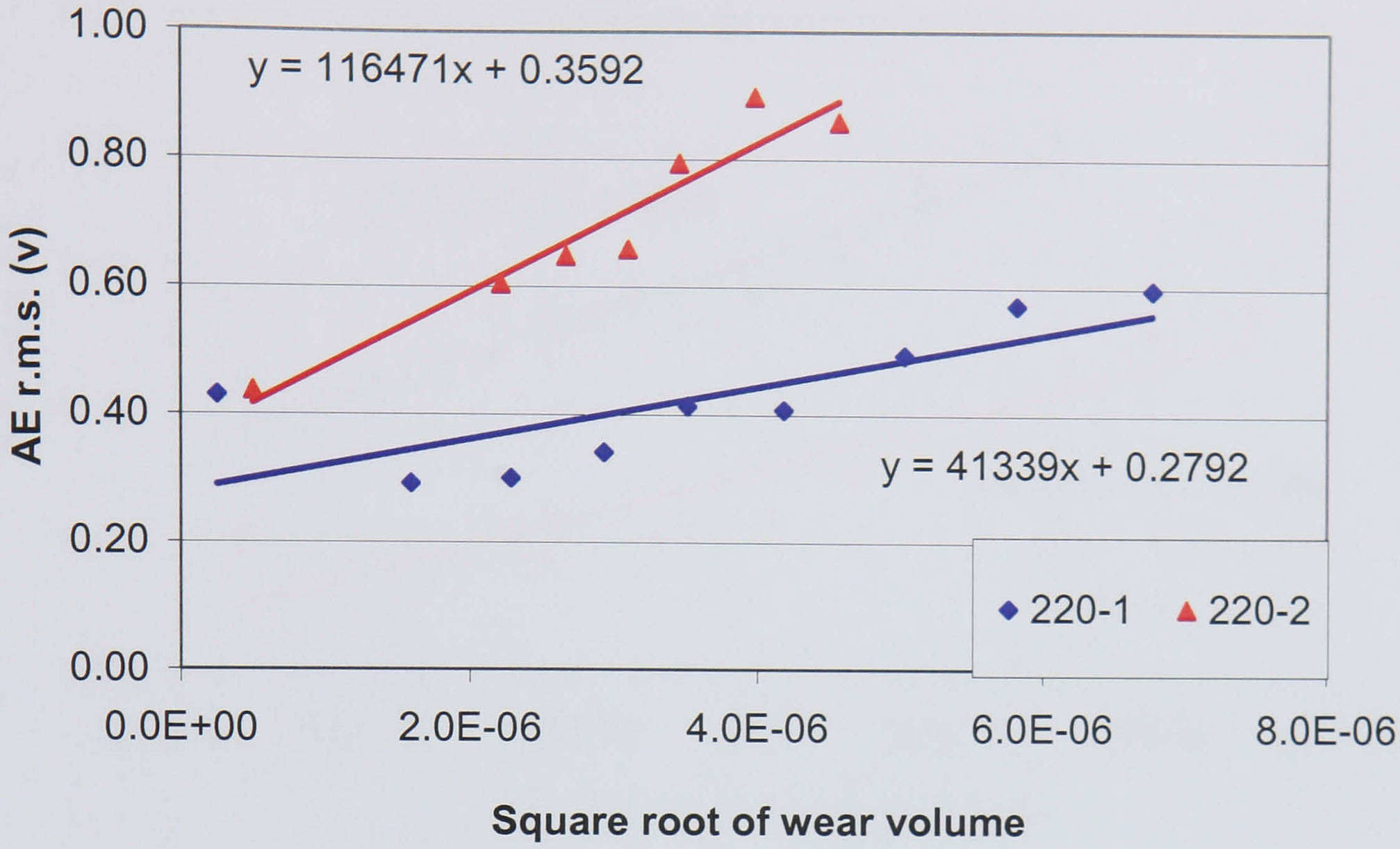

Figure 7.1 AE r.m.s against square root of wear volume plots for 220 Nm; 745 rpm

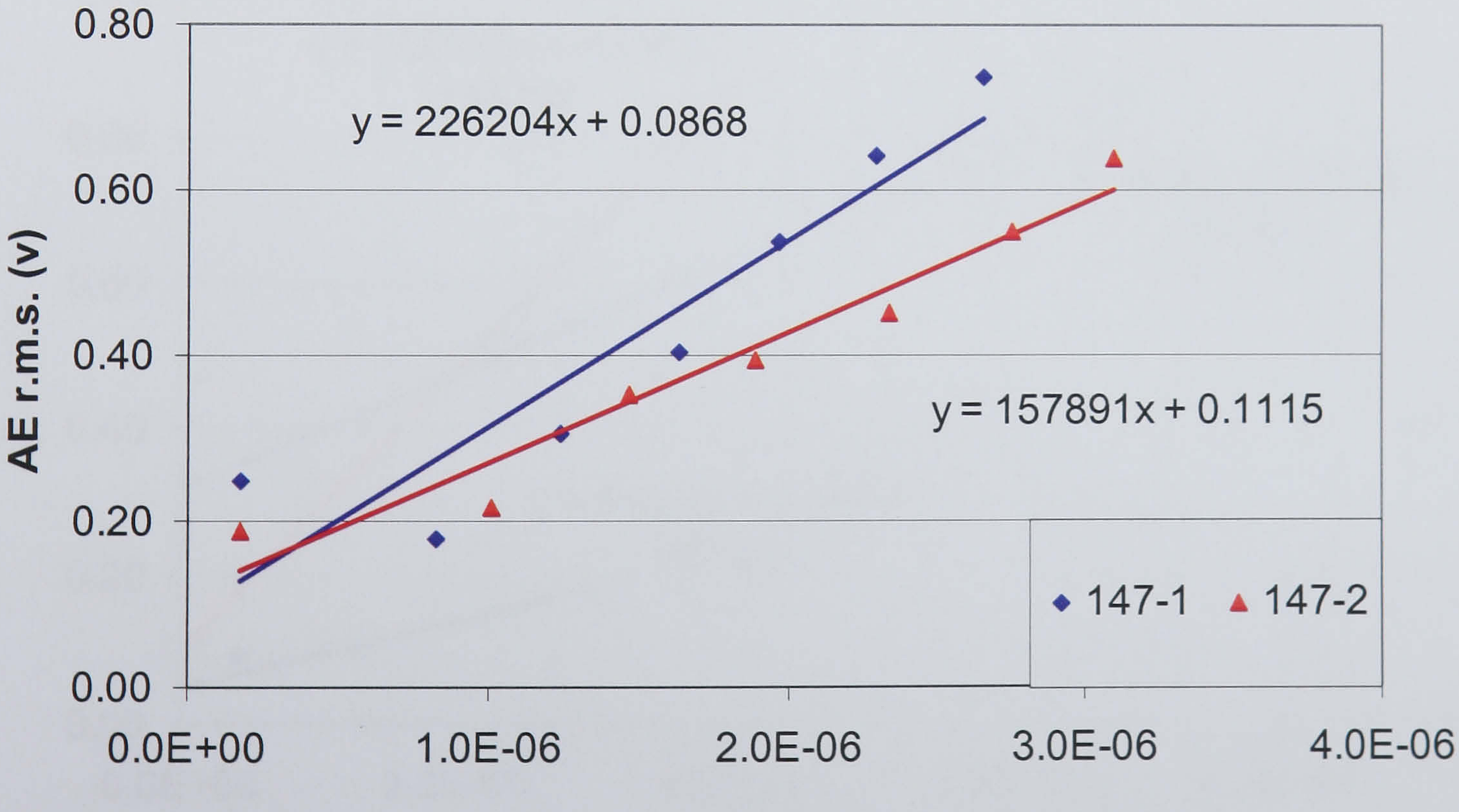

Figure 7.2 AE r.m.s against square root of wear volume plots for 147 Nm; 745 rpm

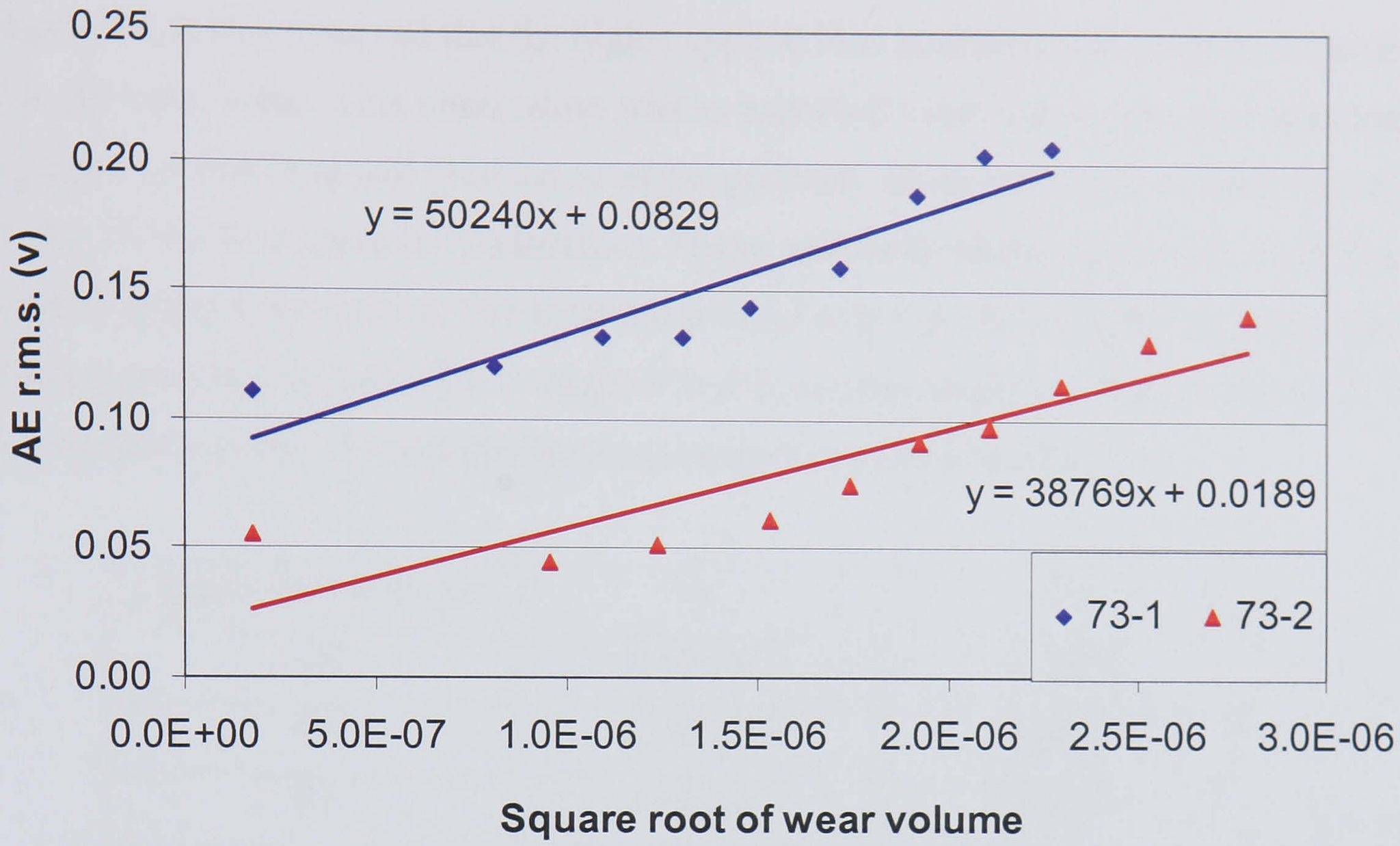

Figure 7.3 AE r.m.s against square root of wear volume plots for 73 Nm; 745 rpm

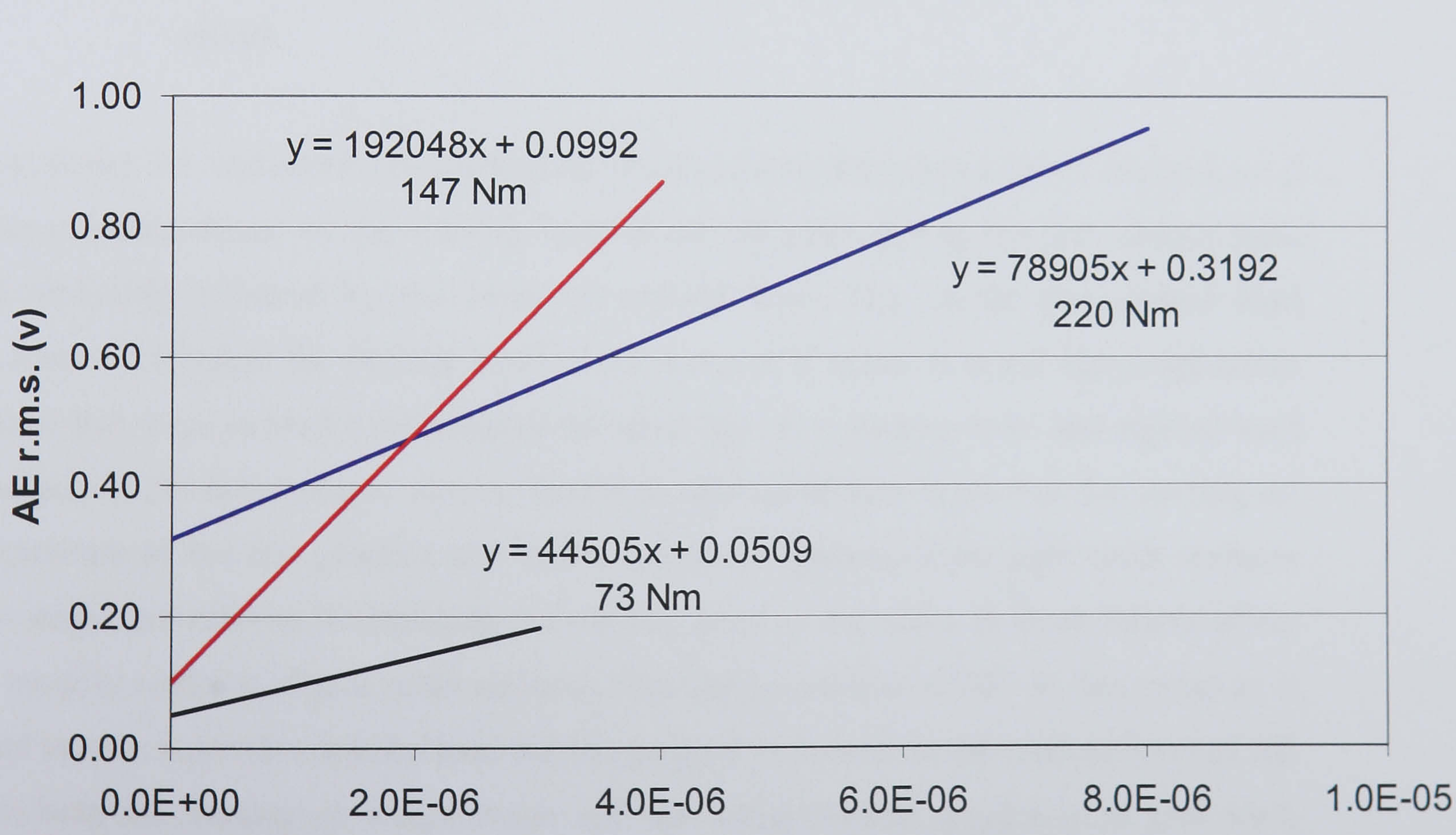

Figure 7.4 AE r.m.s against square root of wear volume plots for all 3 load levels at 745 rpm

In figure 7.4, it was observed that the higher applied load condition always gives a higher initial AE r.m.s value. This observation was as expected. However, it was also expected that higher applied load will produce a steeper gradient, which were only evident for 220 Nm and 73 Nm load cases in this instance. These indifferent observations will be further discussed in the later section. For determination of α and β, the equation for each load condition presented in table 7.7 is equated to the corresponding equation in figure 7.4. The respective results for each applied load case were depicted in table 7.8.

Applied Load (Nm)	α	β
220	4.81×10^{-3}	0.3192
147	14.77×10^{-3}	0.0992
73	4.68×10^{-3}	0.0509

Table 7.8 The values of α and β at the respective applied load condition for proposed model.

From figure 7.4 and table 7.8, it could be observed that the y-intercept of the plot, or β value was determined by the starting level of the AE r.m.s during the gear fatigue tests and obviously affected by the level of applied load. The higher the applied load conditions the higher the starting level of AE r.m.s or β value. It is not inappropriate to assume that there existed a relationship between AE r.m.s starting level and applied load condition in the macroscopic senses. However, one could not forget that the starting oil temperature of the test gearbox and initial surface roughness of the gear teeth surfaces have important roles in determining the starting level of AE r.m.s as these factors affect the asperity contacts of gear teeth surfaces, thus the generation of AE. In this instance, it could be concluded that applied load has the greatest influence on the starting level of AE since both the starting oil temperatures and the initial surface roughness of gear teeth were rather constant for all the gear fatigue test cases. However, more detailed investigation should be conducted to understand and determine the underlying factors in the microscopic processes that influence these behaviours.

α is the change in AE activity with respect to the change in amount of material, in terms of volume, removed from the meshing gear teeth surfaces. From table 7.8, the computed α values for the load cases of 220 Nm and 73 Nm were 4.81×10^{-3} and 4.68×10^{-3} respectively, which the difference between them was well within 3%. This observation suggested that α is independent of applied load and coincided with the observation drawn in chapter 5; applied load has minimum influence on AE r.m.s as compared to the operational speed of the gearbox. However, it is also important to note that α value for the intermediate load case of 147 Nm deviated significantly from those of 220 and 73 Nm. This result was also mirrored in figure 7.4 where the 147 Nm plot exhibited a much stepper gradient. For better understanding of the results and possible reason behind the inconsistency observed. The following aspects identified as possible AE sources during the gear fatigue tests were put through for closer examination: (a) the amount or volume of material removed from the gear teeth surfaces and (b) the asperity contacts between gear teeth surfaces during gear mesh.

Firstly, the results for the rate of volume of material removed from gear teeth surfaces were investigated. This volume is based on the SOA results presented in chapter 7.2.1. In order to determine the rate of material removed, the volume of material removed was plotted against the gearbox operating time as shown in figure 7.5. Figure 7.5 revealed that the higher the applied load, the higher the volume of material removal and the steeper the gradients of the plots. These observations were deemed logical and would not contribute to the inconsistent result obtained for 147 Nm load case.

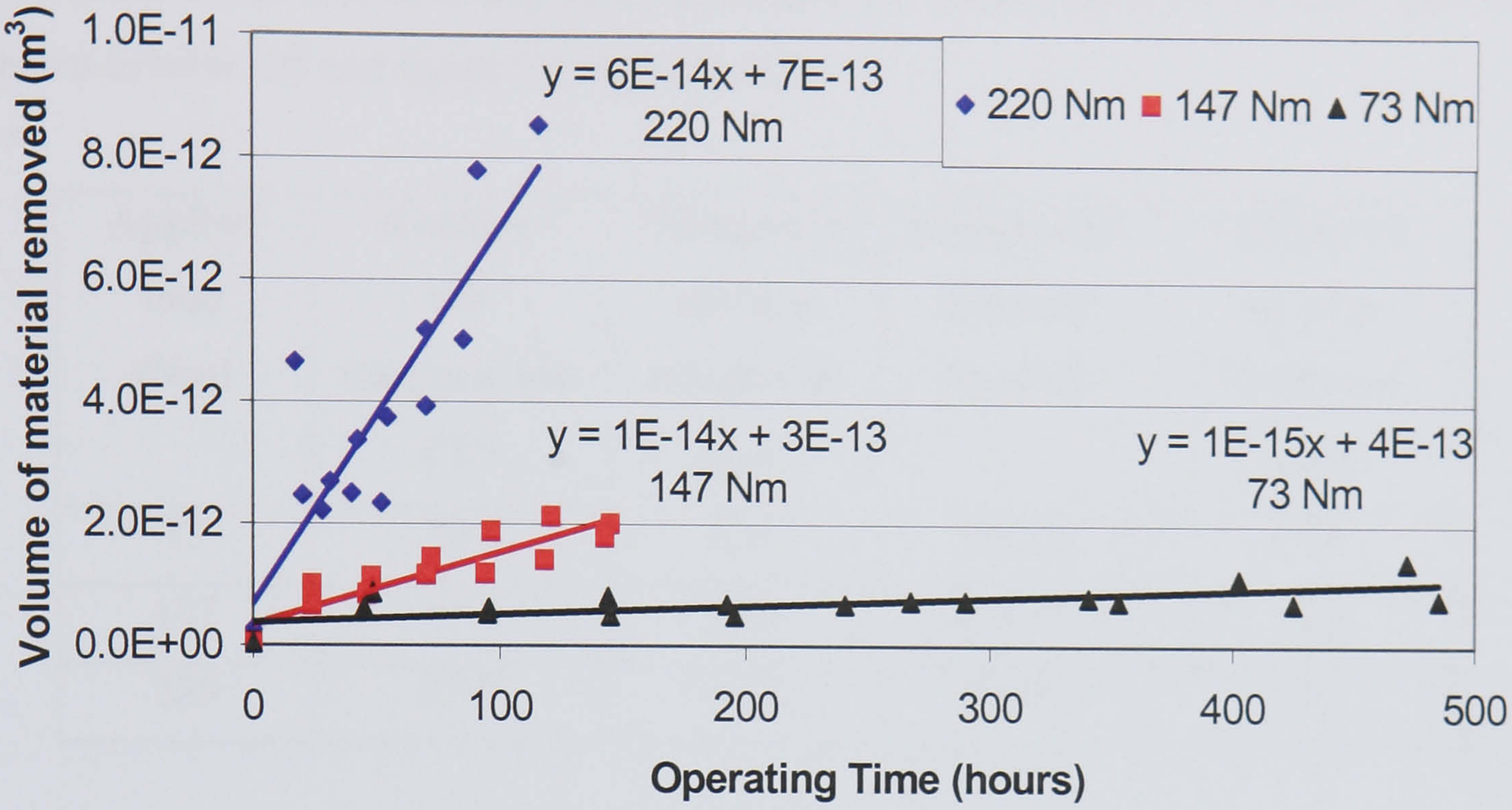

Figure 7.5 Volume of material removed from gear teeth surface (based on SOA results) against gearbox operating time.

Secondly, as detailed in chapter 5, the possible source of AE generation between a pair of undamaged meshing gear teeth is the asperity contacts between the gear teeth surfaces. Hence, the amplitude of AE generated should be related to the oil temperature, surface roughness and oil film thickness. As highlighted in chapter 5, the oil temperature, surface roughness and oil film thickness could be related to the extent of asperity contacts and thus the level of AE activity generated. These parameters at both the initial and final test conditions: undamaged and final damage at 50% gear pitted area, were computed for all applied load cases. The results were tabled in table 7.3 and 7.9 respectively. From table 7.3, it was observed that the starting oil temperature and initial composite surface roughness of the test gear teeth were similar for all test conditions. The slight difference was most likely attributed to the small variation in the starting oil temperatures.

From table 7.9, it was observed that the oil temperatures increased with increasing load, thus producing a thinner oil film. But it is important to note that the 147 Nm load

condition had the highest composite surface roughness, this may be a factor that contributed to the inconsistency of α value, and the steeper plots for 147 Nm load case (shown in table 7.8 and figure 7.4 respectively).

Applied load (Nm)	**Average Oil temperature (^{o}C)**	**Composite surface roughness (μm)**	**Kinematics viscosity (mm^2/s)**	**Calculated oil film thickness (μm)**
73	20.7	1.94	393.32	1.64
147	23.1	1.94	339.40	1.52
220	23.5	1.94	331.32	1.51

Table 7.9 Oil temperature, kinematics viscosity, film thickness and specific film thickness parameters during start up phase for all load conditions.

It was understood that surface roughness alters the characteristics of the contacts, thus not only affecting the film thickness and pressure distribution but also the friction in EHL conjunction [31]. Although this research area spurs vast interests in many researchers, to date, severe difficulties were encountered when prediction of the influence of surface roughness on EHL condition was attempted. The major set backs are the high level of discretisation to account for all the details present in the random roughness texture and coupled with the transient nature of the problem, till today, all the micro-EHL solution was computational based [31]. Currently, researchers could only relate surface roughness to friction rather than fluid film thickness. As shown by Xiao [90], Wang [91] and Lipp [29], friction will increase with increasing surface roughness. Furthermore, Dornfeld and Hardy expected AE would be less sensitive to surfaces with lower surface roughness [87]. This expectation was echoed by; (a) Diei (stated in Jiaa and Dornfeld [63]), who proposed a power relationship between AE r.m.s and the rate of frictional energy dissipation, and (b) Lingard and Ng [93] who suggested that AE would be more likely to relate to frictional force.

All these evident and studies pointed towards an existing relationship such that AE r.m.s is directly related to surface roughness and friction. Hence, this may provide an explanation on the inconsistent observation for 147 Nm load case. Inaddition, coupling with little published information on fundamental studies of the source of AE from sliding friction and wear processes [93]. These areas are identified as a novel field for future exploration. It was proposed that more fundamental studies on meshing gear teeth to be performed to better understand the relationship between AE, sliding friction, surface roughness, wear, EHL and their influences on the level of AE generated.

To determinate the values of α and β for Matsuoka's model, equation 7.11 is equated to the corresponding equation at each applied load condition depicted in figure 7.4. The results for each applied load case were presented in table 7.10.

Applied Load (Nm)	α	β
220	0.62	0.3192
147	1.50	0.0992
73	0.35	0.0509

Table 7.10 The values of α and β at the respective applied load condition for Matsuoka's model.

Comparing tables 7.8 and 7.10, the values of β are the same for both models. This implied that β is empirically determined by gear fatigue test data and is independent of the characteristics of the model used. Obviously from table 7.10, α varies with the applied load condition for Matsuoka's model, such that higher applied load produced higher α value except for the 147 Nm load case. By ignoring the results from 147 Nm applied load case for both models in order to have a fairer comparison, the observation from Matsuoka's model contradicts the characteristic of α in the proposed model where α is observed to be independent of the applied load. A closer examination on equation 7.7 revealed that with sliding speed, sliding distance and hardness of gear teeth surface constant, this equation is dominated by pitting wear rate which varies with applied load

condition, see figure 7.5. This provides a reasonable explanation to the observation of α varying with applied load. As discussed at the earlier part of this section, the possible AE sources during the gear fatigue tests were identified as the amount or volume of material removed from the gear teeth surfaces and the asperity contacts between gear teeth surfaces during gear mesh. Matsuoka's model (equation 7.7) only considered the relationship of AE activity with the volume of material removed and ignored the asperity contacts between the meshing gear pair. On the other hand, the proposed model given in equation 7.6 considered two possible AE sources during gear fatigue tests. In this instance, the proposed model can be considered as more representative of the actual gear operating condition in comparison to Matsuoka's model. Even with the distinctive observation of AE activity varies with pitting wear rate (see figure 7.5 and equation 7.7), the proposed model revealed that α is independent of applied load condition, supporting the conclusion drawn from chapter 5. This further strengthened the argument that asperity contacts are the prime source of AE generation even with the present of pitting wear.

Although the proposed model equation 7.6 did provide some insights of AE r.m.s response to the pitting progression in term of the macroscopic parameters, there are still some shortcomings presence in this model. Firstly, the assessment on the wear status based on the volume of material removed from the gear teeth surfaces using SOA results may not be an accurate method. The SOA results only capture wear debris data of size up to 10 μm [96]. But the typical sizes of wear debris produced by non-conformal rolling-sliding actions of the gear teeth are between 10 and 1000 μm [77]. Hence, information on the wear debris of size ranges from 10 to 1000 μm would be important in determining the volume of material removed from the gear teeth surfaces accurately. This is particularly so for wear debris size of less than 100 μm as particles in this size range usually occur during normal wear condition and would increase in size and quantity with the onset of accelerated wear [97, 98]. This observation is clearly illustrated in a typical wear debris production history shown in figure 7.6. Hence, different debris collection methods and analysis techniques, without removal or disturbance of the gearbox that would affect its

dynamic characteristics, must be explored. In general, there are various methods of debris collection for a gearbox self-contained lubricating oil system:

(a) oil sampling method, which was utilised in the gear fatigue tests as shown in chapter 6 (all size ranges depending on the sampling equipment)
(b) filtration system which will capture wear debris of size greater than the size of filter mesh or membrane (typically between 10 to 50 μm [96])
(c) on-line inductance sensor which will capture wear debris data using inductance concept (typically between 100 to 300 μm [97 and 99]
(d) magnetic debris collection through the usage of magnetic plug or chip detector (typically more than 200 μm [97])

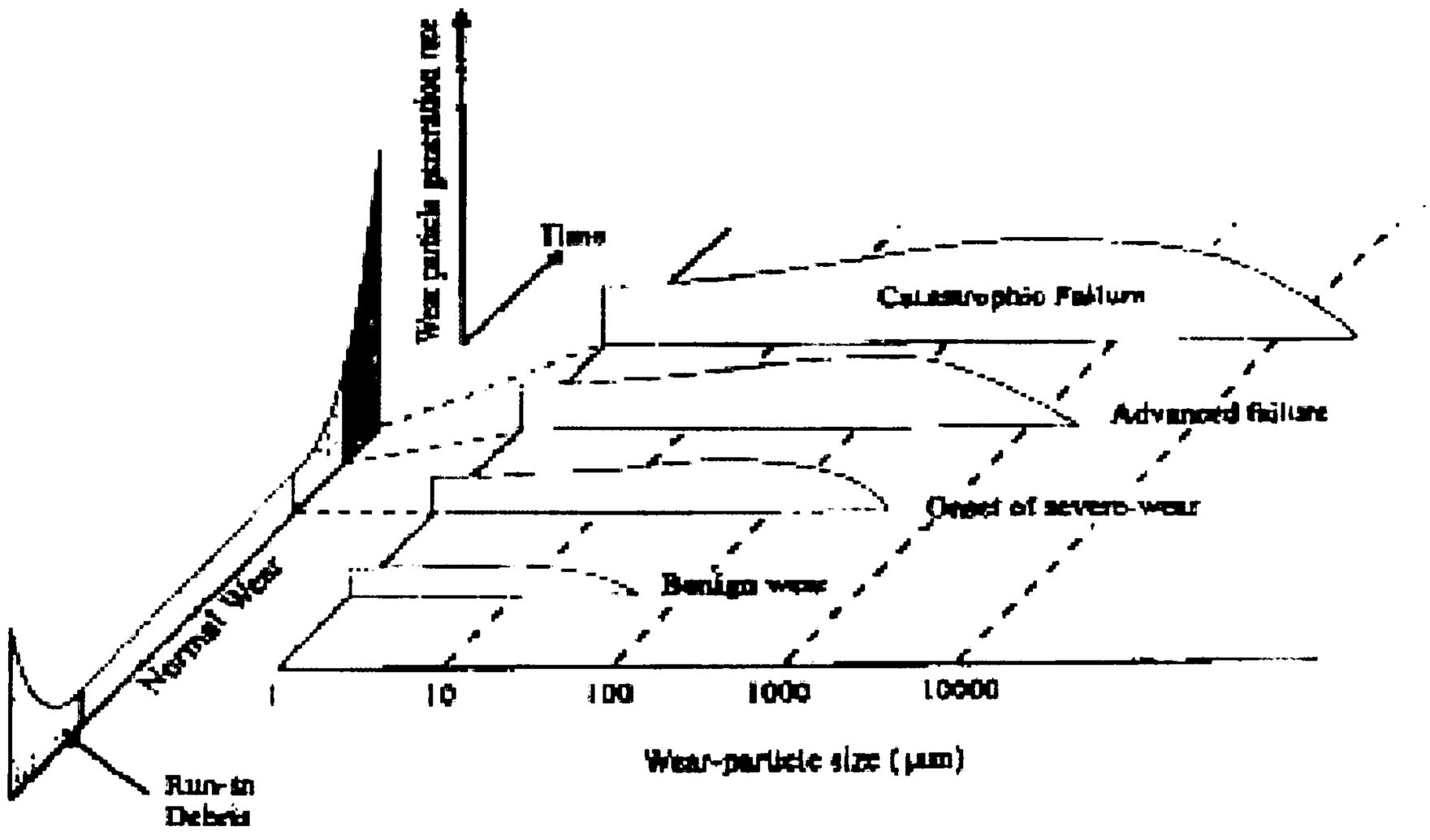

Figure 7.6 Wear debris production history [97].

By employing these debris collection methodologies, the full size range of wear debris could be captured within the circulating oil lubrication systems. However, in order to analyse these full range of wear debris collected, different analysis techniques should be employed to better estimate the volume of material removed from the damaged gear teeth

surfaces. The current gear fatigue test set-up mentioned in chapter 2.3 provides information on both elemental analysis of the wear particles and its concentration (of size less than 10μm) present in the oil sample using SOA technique. Inaddition, this oil sample could be further analysed employing Ferrography Analysis technique which will detect wear particles up to 100 μm [98]. This technique is a microscopic examination of wear particles suspended in the lubrication fluid and allows wear particles to be separated from the lubrication fluid using magnetic means. There are two types of ferrographs that were used to evaluate wear particles. Firstly, the analytical ferrograph that allows visual analysis of wear particles in order to identify the type and characteristics of the wear. Secondly, the direct ferrograph that sets the numerical baseline values for normal and accelerated wear conditions [75]. Furthermore, with the inclusion of the on-line inductance sensor, the analysis of the wear particles of size between 100 to 300 μm could be done real time without interfering operation of the gearbox. This sensor could detect metallic particles especially the Fe element and define the particles by size [97, 98]. Currently, there are existing commercial off-the-shelf systems such as MetalSCAN available to perform this particular task. When the debris flowed through the sensor employed by the MetalSCAN system, it records the debris size and mass via the usage of magnetic field. Lastly, for those larger wear particles that would be arrested by the magnetic chip detector systems, three analysis techniques could be applied. They are namely; microscope analysis, scanning electron microscope (SEM) analysis and image analysis, which would provide characteristic data of the wear debris such as size, shape and quantity [100]. With these wear debris collection methods and analysis technique in place, the volume of material removed from the gear teeth surfaces could be better and accurately accounted for.

For broader application of the model, wider operating range need to be expanded and more operating parameters must be explored. As discussed in the chapter 5, gearbox operational speed does have an effect on the AE generation and the corresponding r.m.s level. Although changes in sliding speed was taken into account in equation 7.6, but the accelerated gear fatigue tests were conducted at single speed condition with varying loads. Thus, a series of accelerated gear fatigue tests under different operating speed

should be undertaken to improve the accuracy and consistency of the model. In order to refine and further verify the proposed model, the proportion of the extent of the various parameters should be determined. For instance, chapter 5 showed that the operating speeds of the gearbox has a much significant influence on the AE level compared to the applied load when the gearbox oil temperature was kept constant. This effect was not taken into account while formulating equation 7.6 since the extent of the influence on the generation of AE by these two operating parameters was not known. Adjustments to the existing test set-up or employing new test set-up, and further experimental work should be conducted to provide a better understanding of the relationship between the macroscopic operating parameters and their respective influences over the AE level.

Current stage of investigation linked the AE r.m.s value only to the macroscopic parameters of the test gearbox. It will be fundamentally beneficial to investigate the microscopic processes within the wear zones and those that contributed to the generation of AE and their corresponding levels. These proposed studies would not only meet with technical difficulties but also the financial ones. Based on the literature review entailed in chapter 2, AE not only has close relationship with pitting wear, but also the oil film thickness, contact pressure, surface temperature and frictional behaviours between the gear surfaces. However, the measurements of these parameters without removal of the gearbox assemblies may meet with difficulties using current available technologies and given the space constraints within the gearbox. For instance, in-situ measurements on oil film thickness, surface roughness or pit size could be done through optical method such as air-borne laser system. But installation of such expensive system within or outside the gearbox may prove to be dangerous and restrictive due to high level of vibration, high rotational speed and high temperature environment. Thus, alternative test set-up such as pin on disk or slider on cylinder should be considered and performance of tests on this type of set-up could be utilised to understand the effect of each influential factor and the cross effect between them in the generation of AE. Although these testing set-up and methods could not fully represent the real gear contact conditions and behaviours, it will be the closest simulation one can achieved until technologies allow us to perform the in-

situ measurements on the respective factors safely and accurately on operating gearbox with minimum disruptions.

7.4 Conclusions

1. A proposed model that relates AE r.m.s to the volume of material removed from the gear teeth surfaces (based on SOA results) was presented.
2. Experimental results from the gear fatigue tests were employed to determine the 2 unknown parameters, α and β, of the proposed model equation.
3. The y-intercept of the AE r.m.s against square root of wear volume plot or the β value of the proposed model equation was determined by the starting level of the AE during gear fatigue test.
4. β increases with increasing applied load.
5. The gradient of the AE r.m.s against square root of wear volume plot determined the α value of the proposed model equation.
6. α is observed to be independent of applied load condition except for 147 Nm load case. This observation coincided with the observation drawn in chapter 5; applied load has minimum influence on AE r.m.s as compared to the operational speed of the gearbox.
7. Due to spatial constraints in the test gearbox and technological constraints in measurements techniques, alternative experimental test set-ups were suggested to simulate real gear operating and contact conditions and behaviours in understanding the fundamental relationship between AE activity and the microscopic processes of gear pitting wear and contacts.

8 CONCLUSIONS AND RECOMMENDATIONS

This research work introduced and explored a new technique, AE, in the field of condition monitoring in spur gearbox. The AE technique was put through a series of tests, such as seeded defect simulations and gear fatigue tests, to verify the defect detection capability and the weakness in applying this new technique. The performance of the AE technique is measured against the project objectives set out in chapter 1.3. In this chapter, conclusions and recommendations will be made accordingly to each objective detailed in chapter 1.3.

Seeded defect simulations were always used to study the viability of new condition monitoring technique, especially when applied in the field of rotating machinery. This approach was evident during the introduction of vibration monitoring technique on helicopter HUMS; UK MOD had worked with the various helicopter manufacturers to perform seeded defect tests on rotating components to verify the capability and applicability of this technique on the helicopter platform [101]. For this project, the seeded defect simulations detailed in chapter 4 not only highlighted the inconsistency in defect detection employing AE technique but also the existent of relationship between AE and the various gearbox operating parameters. Although the employment of AE indicators such as crest factor does exhibits a change with respect to the changing defect size, conclusion has been drawn that this result was inconsistent with other researchers' work.

Several areas have been identified for further improvement for better and more consistent results. Firstly, the data acquisition capability of the test set up could be further enhanced since the employed sampling rate of 10 MHz could only resolute to approximately 16 pinion gear teeth based on a rotational speed of 745 rpm. With the advancements in electronic devices, a higher sampling rate could possibly be expected. Ideally, the sampling rate should be able to resolute to each individual tooth of the gear so that their corresponding AE signature can be investigated and more useful information can be extracted from the raw AE signal. Furthermore, to ensure the mating teeth from the

meshing gear pair is always the same pair, both pinion and wheel should have the same number of teeth. Hence, under this circumstance, the raw AE signature obtained could be easily identified to the particular pair of meshing teeth, and variation in AE signature due to mating of different gear teeth between the pinion and wheel would be eliminated. This methodology would provide a more consistence comparison between the various AE signatures produced under different operational or defect conditions since the same pair of gear teeth is always in contact within a single revolution of the pinion and wheel.

Another key factor that may account for the inconsistency of the AE indicator is the finishing quality of the gear teeth surface, which the observations of the seeded defect simulations were compared with Singh [53] investigation employing seeded defect on fine finished helicopter gear teeth surfaces (see chapter 4.3). The higher quality surface finish of the gear teeth would produce very low AE background noise, which would generate prominent AE burst signature with the introduction of seeded defect when compared to the usage of normal surface finished grounded gear in this case. This prominent AE signature could further improve the seeded defect identification capability of the AE technique. The introduction of fine quality surface finished gear and same number of gear teeth for both the pinion and wheel, would be interesting to observe for the possible change in the AE behaviour when the seeded defects are planted on one gear tooth or both the mating gear teeth. Under this test configuration, one could simulate the scenario where natural pitting occurs first on one gear tooth, then developed onto the corresponding mating gear tooth while changes in the AE activities are recorded for further analysis.

The practical aspect of applying this new condition monitoring technique was also been investigated. With the AE sensor mounted on the pinion shaft bearing block, significant attenuation of AE signal was experienced. This observation posed a challenge to monitor the condition of the spur gears from a stationary member of the gearbox. As most gearboxes have compact interior structures, mounting of sensor on or near the gear itself posed a constraint. Furthermore, the consequence of a detached sensor falling into the gearbox may lead to catastrophic failure, especially in aviation gearbox, fatalities may

occur. Another challenge faced by mounting the sensor on the rotating gear, is the transferring of AE signal from the sensor to the processor. In this case, slip ring has to be employed to perform the transferring of signal from the rotating gear. The usage of slip ring not only added more components into the gearbox but also increased the complexity of the monitoring systems. Hence, with the current available technologies, mounting the sensor on the stationary member of the gearbox is still the more viable approach. However, more research work in reducing attenuation and improving sensor technologies must be explored before a practical working system can be materialised.

In chapter 4.6, it was concluded that there exists a relationship between AE activities and the gearbox operational parameters such as rotational speed, applied torque/load and the gearbox oil sump temperature for continuous running of undamaged gear pair. Hence, further investigations were performed to study the effect of individual operating parameter on AE activity. The results obtained under this experimental work were discussed and highlighted in chapter 5.1. The applied load had minimal influence on the level of AE activity under constant speed and isothermal conditions, while operating speed had a much more significant effect on AE activity under constant load isothermal conditions. It was deemed that the installation of a heating coil assembly within the gearbox oil sump would provide a more consistent constant oil temperature as compared to the procedures laid out in chapter 3.3.2. However, in this instance, the space constraint within the test gearbox prevented the installation of such heating coil assembly. The introduction of the heating coil assembly would ensure that the test gearbox experiences minimum temperature variation so as to provide more consistent results.

In addition, it would also allow a longer running period for the test gearbox without the need to worry about change in oil temperature, thus, more observations can be made in comparison to the current test set up and procedures. The most important breakthrough of employing the heating coil assembly would be the ability to study the effect of oil temperature or the oil film thickness on generation of AE signal while maintaining constant operating speed and applied load. The raw AE signal captured can be further

analysed to understand the influence of changing oil film thickness over both the AE burst and continuous signatures recorded.

Chapter 5.2 investigated the source mechanism of AE during gear mesh. The results obtained from the investigation suggested that the main source of AE is due to asperity contact under the sliding and rolling motions of the meshing gear teeth surfaces. As the amount of asperity contact is influenced by the lubricant film thickness and surface roughness, this suggestion will not be conclusive since these two parameters were not experimentally measured during operation of the gears; the concluding remarks in chapter 5.3 are based on theoretical prediction of the film thickness. Although there are existing technologies that will enable the measurement of both the lubricant film thickness and gear teeth surface roughness, it would be important to note that these measurements should be undertaken without disturbing the dynamics of the gearbox. This investigation did not investigate this influence of varying dynamic load on AE amplitude variation. These types of measurement would pose a physical constraint in the currently deployed test gearbox. A new test gearbox has to be used to accommodate the new film thickness and surface roughness measurement machines. At the same time, test procedures have to be reviewed to perform the measurements without removal of any test gearbox component. These new test set up and procedures would further ensure more consistent results which may be utilised.

Introduction of these two measuring machines allowed the researcher to vary the oil temperature and monitor the surface roughness of the gear teeth surfaces to simulate various lubricating regimes, such as EHL, partial EHL and boundary lubrication and determining their corresponding specific film thickness, λ, more accurately. With these experimentally determined λ values, the lubricating regimes can be more accurately defined, which enable a correlation between AE activity and lubricating regimes to be established. Furthermore, it is recommended that super finished or high quality finished gears to be used for this investigation as these gears can minimise the operational background noise during gear mesh, and thus, made analysis of the AE signatures more obvious and easier.

The gear fatigue testing was performed on the test gearbox to study the pitting detection and monitoring capabilities of the AE, vibration and SOA techniques. From the results presented in chapter 6, it was clearly evident that AE monitoring indicator can be linearly correlated to the gearbox pitting rates for all torque conditions, with detection of onset pitting as early as 8% of the pitted gear working face area. This offered much earlier diagnosis than vibration analysis and SOA techniques where only after between 20 to 40% of pitted gear working face did these techniques offer capability for defect identification. This near linear relationship between AE and pit progression offers great potential and opportunities for prognostics in rotating machinery. Building on this statement, very recently, Price et al [102] investigated the detection of severe sliding and pitting with AE. Price's experimental results presented were based on a 'four-ball machine' test rig. It was observed that scuffing and pitting were easily detected by observing changes in AE energy, principally due to changes in contact friction. More interestingly, Price noted changes in the frequency patterns of the measured AE signals prior to pitting and stated that AE monitoring was capable of detecting wear events prior to either vibration monitoring or wear debris analysis. However, under the experimental work detailed in chapter 6, it is prudent to point out that the AE and vibration sensors were located at different locations, with the former nearer to the source of signal generation (i.e. at the gear mesh). Although argument on the fairness in the comparison between AE and vibration analysis techniques would arise due to the difference in the sensor mounting locations, it was expected that AE technique would still outperform vibration technique in surface defect detection. This expectation was furthered confirmed and proven by Price [102], Singh [53], Raad [54] and Tandon [57] where all these researchers concluded that AE technique is able to detect the surface defect in advance of vibration analysis technique with both the AE and vibration sensors mounted on the same location. Minor modifications can be done on the current experimental set up to mount both the AE and vibration sensors either on the pinion or the pinion shaft bearing housing of the test gearbox.

Chapter 7 illustrated the proposal to formulae a model to predict the amount of gear surface pitting wear using AE activity by combining experimental results obtained in chapter 6 and theoretical model derived from literature reviews. Inconsistencies have been surfaced for this first attempt to model and relate these two parameters. The key factors driving the model: the amount or volume of material removed from the gear teeth surfaces and the asperity contacts between gear teeth surfaces during gear mesh have been highlighted and discussed. A comparison with Matsuoka's model had also been made and deliberated. Furthermore, the difficulties and problematic areas in achieving a more accurate model were also highlighted in details and recommendations have been made in chapters 7.3 to fine-tune the model for future applications.

In conclusion, this project has allowed one to go through the processes of verifying and exploring the diagnostic and prognostic potential and capability of a new condition monitoring technique. These processes could be used as guidelines for exploring future condition monitoring technique or new/difference types of rotating machinery. The lessons learnt and recommendations highlighted in this project have been implemented in a new on-going project where a new gearbox has been built to study the applicability of AE technique in monitoring the conditions of a helical gear pair. With the on-going research of exploring and verify AE technique as a new condition monitoring tool for gearbox and other rotating machinery, it is believed one day, AE technique would be like vibration analysis technique being commonly and effectively employed in the condition monitoring applications.

REFERENCES

1. Vinall, P.D. Airworthiness of helicopter. *Symposium on Helicopter Transmissions- Royal Aeronautical Society. London, UK.* 1-29. 1980.
2. DiPasquale, F. Application of quantitative debris monitoring to gear systems. AIAA-88-2982. 1988.
3. Choy, F.K., Mugler, D.H. and Zhou, J. Damage identification of a gear transmission using vibration signatures. Journal of Mechanical Design. **125**. 394-403. 2003.
4. Decker, H.J. Crack detection for aerospace quality spur gear. NASA/TM-2002-211492. 2002.
5. Pusey, H.C. and Pusey, S.C. A critical link: Diagnosis to prognosis. . *MFPT 51 meeting proceeding. Virginia Beach, VA, USA.* 93-102. 1997.
6. Irving, P.E., Place, S., Strutt, J.E. and Allsopp, K. *International Symposium on Condition Base Maintenance. Pisa, Italy.* 2000.

Dempsey, P.J. Gear damage detection using oil debris analysis. *International Congress on Condition Monitoring and Diagnostic Engineering Management (COMADEM'2001). Manchester, UK.* 433-440. 2001.

8. Dempsey, P.J. A comparison of vibration and oil debris gear damage detection methods applied to pitting damage. NASA/TM-2000-210371. 2000.
9. Astridge, D.G. Health monitoring of helicopter gearboxes. *8th European Rotorcraft Forum. Ai-en-Provence, France.* 7.3.1-7.3.13. 1982.
10. Hodges, D. and Pearce, J. Gearbox condition monitoring. *IMechE Conference Transactions, Gearing and Gearbox Practice Today. London, UK.* S318. 1995.
11. Collier-Marsh, M.E. and Astridge, D.G. Operational experience with the advance transmission health monitoring techniques on the Westland 30 Helicopter. *11th European Rotorcraft Forum. London, England.* 48.1-48.12. 1985.
12. Horsley, D. Introduction of HUMS to the RAF. *Australian DSTO HUMS Workshop. Melbourne, Australia.* 1999.

13. Augustin, M.J. Specifying HUMS to meet enhanced safety and reduced operating cost requirements. *American Helicopter Society 54th Annual Forum. Washington, DC, USA.* 1998.

14. Larder, B.D. Helicopter HUM/FDR: Benefits and developments. *American Helicopter Society 55th Annual Forum. Montreal, Quebec, Canada.* 1999.

15. Larder, B.D. An analysis of HUMS vibration diagnostic capabilities. *American Helicopter Society 53rd Annual Forum. Virginia Beach, Virginia, USA.* 1997.

16. Engel, S.J., Gilmartin, B.J., Bongort, K. and Hess, A. Prognostics, the real issues involved with predicting life remaining. IEEE. 457-469. 2000.

17. Irving, P.E. and Hudson, R.A. The contribution of HUMS to calculations of damage state and future life of helicopter components under safe life and damage tolerant designs. *RTO AVT Specialists' Metting on "Exploitation of Structural Loads/Health Data for Reduced Life Cycle Costs". Brussels, Belgium.* RTO MP-7. 1998.

18. Leblanc, J.F.A., Dube, J.R.F. and Devereux, B. Helicopter gearbox vibration analysis in the Canadian Forces – applications and lessons. *1st International Conference for Gearbox Noise and Vibration. IMechE. Cambridge, UK.* 173-177. 1990.

19. Troyer, D.D. Effective integration of vibration analysis and oil analysis. *International Conference on Condition Monitoring. Swansea, UK.* 411-420. 1999.

20. Peng, Z. and Kessissoglou, N. An integrated approach to fault diagnosis of machinery using wear debris and vibration analysis. *Wear.* 255. 1221-1232. 2003.

21. Barnes, J.A. and Starr, A.G. The application of oil debris monitoring and vibration analysis to monitor wear in spur gear. *International Congress on Condition Monitoring and Diagnostic Engineering Management (COMADEM'2001). Manchester, UK.* 953-958. 2001.

22. Vizintin, J. Application of vibration and wear particles analysis to condition monitoring of rotating machinery. *International Conference on Condition Monitoring. Oxford, UK.* 169-185. 2003.

23. Astridge, D. and Savage, M. Rotorcraft Drivetrain Life Safety and Reliability. AGARD-R-775. 1-77. 1990.

24. Drago, R.J. *Fundamentals of gear design*. Butterworth Publisher. Boston, USA. 1988.

25. Oila, A. and Bull, S.J. Assessment of the factors influencing micropitting in rolling/sliding contacts. Wear. 258. 1510-1524. 2004.

26. Olver, A.V., Tiew, L.K., Medina, S. and Choo, J.W. Direct observation of a micropit in an ealstohydrodynamic contact. Wear. **256**. 168-175. 2004.

27. Ding Y. and Rieger, N.F. Spalling formation mechanism for gears. Wear. **254**. 1307-1317. 2003.

28. Fernandes, P.J.L. and McDuling, C. Surface contact fatigue failures in gears. Engineering failure Analysis. **4(2)**. 99-107. 1997.

29. Lipp, K. and Hoffmann, G. Design for rolling contact fatigue. *MFPT 56 meeting proceeding. Virginia Beach, VA, USA*. 5-28 to 5-52. 14-19 April 2002.

30. Dowson, D. Elastohydrodynamic and micro-ealstohydrodynamic lubrication. Wear. **190**. 125-138. 1995.

31. Dowson, D. and Ehret, P. Past, present and future studies in elastohydrodynamics. Journal of Engineering Tribology. **213**. 317-333. 1999.

32. Dowson, D. and Higginson, G.R. *Elastohydrodynamic Lubrication*. 1st edition. Pergamon Press. Oxford, UK. 1977.

33. Stachowiak, G.W. and Batchelor, A.W. *Engineering Tribology*. 2nd ed. Butterworth Publisher. Boston, USA. 2001.

34. British Standard. Spur and helical gears. Part 3. Method for calculation of contact and root bending stress limitations for metallic involute gears. BS 436: Part 3: 1986.

35. International Standard. Calculation of load capacity of spur and helical gear. Part 2: Calculation of surface durability (pitting). 1SO 6336-2. 1996.

36. American National Standard. Fundamental rating factors and calculation methods for involute spur and helical gear teeth. ANSI/AGMA 2101-C95. 1995.

37. Coy, J.J., Townsend, D.P. and Zaretsky, E.V. Analysis of dynamic capacity of low-contact-ratio spur gears using Lundberg-Palmgren Theory. NASA TN D-8029. 1975.

38. Coy, J.J., Townsend, D.P. and Zaretsky, E.V. Dynamic capacity and surface fatigue for spur and helical gears. Journal of Lubrication Technology. **98(2)**. 267-276. 1976.

39. Townsend, D.P., Coy, J.J. and Zaretsky, E.V. Experimental and analytical load-life relation for AISI 9310 steel spur gears. Journal of Mechanical Design. **100(1)**. 54-60. 1978.

40. Coy, J.J., Townsend, D.P. and Zaretsky, E.V. An update on the life analysis of spur gears. Advanced Power Transmission Technology. NASA CP2210. 421-433. 1982.

41. Coy, J.J., Townsend, D.P. and Zaretsky, E.V. Gearing. NASA Reference Publication 1152. 1995. Holroyd, T. *Acoustic Emission & Ultrasonic.* 1st edition. Coxmoor Publishing Company's. Oxford, UK. 2000.

42. Holroyd, T. *Acoustic Emission & Ultrasonic.* 1st edition. Coxmoor Publishing Company's. Oxford, UK. 2000.

43. Drouillard, T.F. Introduction to Acoustic Emission. Material Evaluation. **46**. 174-180. 1988.

44. Henning, D. Josef Kaiser: His achievements in Acoustic Emission research. Material Evaluation. **46**. 193- 195. 1988.

45. Tensi, H.M. The Kaiser-effect and its scientific background. *26th European Conference on Acoustic Emission Testing. Berlin, Germany.* 1-17. 15-17 September 2004.

46. Matthews, J.R. and Hay, D.R. *Nondestructive Testing Monographs & Tracts Volume 2.* Acoustic Emission evaluation. Gordon & Breach science Publishers. USA. 1983.

47. Scott, I.G. *Basic Acoustic Emission*. Gordon & Breach science Publishers. Switzerland. 1991.

48. Miyachika, K., Oda, S. and Koide, T. Acoustic Emission of bending fatigue process of spur gear teeth. Journal of Acoustic Emission. **13(1/2)**. S47-S53. 1995.

49. Miyachika, K., Zheng, Y., Tsubokura, K., Oda, S., Kanayama, Y., Koide, T., Namba, C. and Hayashi, T. Acoustic Emission of bending fatigue process of

super-carburised spur gear teeth. *Progress in Acoustic Emission XI. The Japanese Society for NDI*. 304-310. 2002.

50. Singh, A., Houser, D. R., and Vijayakar, S. Detecting Gear Tooth Breakage Using Acoustic Emission: A Feasibility and Sensor Placement Study. Journal of Mechanical Design. **121**. 587-593. 1999.

51. Wheitner, J., Houser, D. and Blazakis, C. Gear tooth bending fatigue crack detection by Acoustic Emissions and tooth compliance. ASME technical paper 93FTM9. 1-7. 1993.

52. Siores, E. and Negro, A.A. Condition Monitoring of a Gear Box Using Acoustic Emission Testing. Material Evaluation. 183-187. 1997.

53. Singh, A., Houser, D. R., and Vijayakar, S. Early Detection of Gear Pitting. *Power Transmission and Gearing Conference, ASME*. **DE-Vol. 88**, 673-678. 1996.

54. Raad, A., Zhang, F., Randall, B. and Sidahmed, M. On the comparison of the use of AE and vibration analysis for early gear fault detection. *The 8th Western Pacific Acoustics Conference. Melbourne, Australia.* 7-9 April 2003.

55. Sentoku, H. AE in Tooth Surface Failure Process of Spur Gears. *Progress in Acoustic Emission IX. AEWG & AE Group*. S19-S24. 1998.

56. Badi, M.N.M., Engin, S.N. and Schonfeld, D. Fault classification of a model drive-line using time domain data. *COMADEM 1996. Sheffield, UK*. 43-50. 1996.

57. Tandon, N. and Mata, S. Detection of Defects in Gears by Acoustic Emission Measurements. Journal of Acoustic Emission. **17(1-2).** 23-27. 1999.

58. Al-Balushi, K. R. and Samanta, B. Gear Faults Diagnosis Using Energy-Based Features of Acoustic Emission. Journal of Systems and Control Engineering. **216**. 249-263. 2002.

59. Toutountzakis, T. and Mba, D. Observation of Acoustic Emission Activity During Gear Defect Diagnosis. NDT and E International. **36(7).** 471-477. 2003.

60. Boness, R. J., McBride S.L., and Sobczyk, M. Wear studies using Acoustic Emission techniques. Tribology International. **23(5)**. 291-295. 1990.

61. Boness, R.J. and McBride, S.L. Adhesive and abrasive wear studies using acoustic emission techniques. Wear. **149**. 41-53. 1991.

62. Sarychev, G. A, and Shchavelin, V. M. Acoustic emission method for research and control of friction pairs. Tribology International. **24(1)**. 11-16. 1991.

63. Jiaa, C. L. and Dornfeld, D. A. Experimental studies of sliding friction and wear via acoustic emission signal analysis. Wear. **139**. 403-424. 1990.

64. Mechefske, C.K. and Sun, G. Monitoring sliding wear using acoustic emission. *Condition Monitoring and Diagnostic Engineering Management. Manchester, UK*. 57-65. 2001.

65. Smith, J.D. A new diagnostic technique for asperity contact. Tribology International. **26.** 25-27. 1993.

66. Samuel, P.D. and Pines, D.J. A review of vibration-based techniques for helicopter transmission diagnostics. Journal of Sound and Vibration. **282**. 475-508. 2005.

67. Lebold, M., McClintic, K., Campbell, R., Byington, C. and Maynard, K. Review of vibration analysis methods for gearbox diagnostics and prognostics. *MFPT 54th meeting proceeding. Virginia Beach, VA, USA*. 623-634. 2000.

68. Staszewski, W.J. Gearbox vibration diagnostics- an overview. *COMADEM 1996. Sheffield, UK*. 95-111. 1996.

69. Giurgiutiu, V., Cuc, A. and Goodman, P. Review of vibration based helicopter health and usage monitoring methods. *MFPT 55th meeting proceeding. Virginia Beach, VA, USA*. 69-80. 2001.

70. Drosjack, M.J. and Houser, D.R. An experimental and theoretical study of the effects of simulated pitch line pitting on the vibration of a geared system. ASME report 77-DET-123. 1977.

71. Yesilyurt, I., Gu, F.S. and Ball, A.D. Gear tooth stiffness reduction measurement using modal analysis and its use in wear fault severity assessment of spur gears. NDT & E International. **36**. 357-372. 2003.

72. Choy, F.K., Polyshchuk, V., Zakrajsek, J.J., Handschuh, R.F. and Townsend, D.P. Analysis of the effects of surface pitting and wear on the vibration of a gear transmission. Tribology International. **29(1)**. 77-83. 1996.

73. Lukas, M. and Yurko, R.J. Current technology in oil analysis spectrometers and what we may expect in the future. *MFPT 50th meeting proceeding. Virginia Beach, VA, USA.* 161-171. 1996.

74. Tindall, G.S. The prediction of helicopter component failure using the Army Oil Analysis Program versus the high/fine filtration of lubricating oil. *American Helicopter Society 54th Forum. Washington, DC, USA.* 1998.

75. Joint Oil Analysis Program Manual. NAVAIR 17-15-50.1. TM 38-301-1. T.O. 33-1-37-1.

76. Lukas, M. and Anderson, D.P. Laboratory used oil analysis methods. Journal of the Society of Tribologists and Lubrication Engineers- Lubrication Engineering. 31-35. October 1998.

77. Price, A.L. and Roylance, B.J. Detection and diagnosis of wear through oil and wear debris analysis. *Handbook of Condition Monitoring. Edited by A. Davis.* Chapman and Hall. London, UK. 1998.

78. Fitch, J.C. Elements of a successful oil analysis program-Part II. Journal of the Society of Tribologists and Lubrication Engineers- Lubrication Engineering. 15-17. October 1998.

79. Davis, A.M. Fundamental principles in setting alarms and limits in wear debris analysis. Practicing Oil Analysis- The Magazine for Analysis and Management of Lubricant. *http://www.practicingoilanalysis.com/*

80. Fitch, J.C. Best practices in maximising fault detection in rotating equipment using wear debris analysis. *International Conference on Condition Monitoring. Swansea, UK.* 65-75. 1999.

81. Vayionas, P.V. Design and build of a gearbox test rig for condition monitoring through vibration analysis. *MSc Thesis*. 1991.

82. EN-BS 1330-9:2000.

83. Decker, H.J. and Lewicki, D.G. Spriral bevel pinion crack detection in a helicopter gearbox. NASA/TM-2003-212327. 2003.

84. Chatfield, C. Statistics for technology. A course in applied statistic. 3rd ed. Chapman and Hall Ltd. London, UK. 1983.

85. Toutountzakis, T., Tan, C.K. and Mba, D. Application of acoustic emission to seeded defect gear fault detection. NDT & E International. **38**. 27-36. 2005.

86. Non-destructive testing handbook, Volume 5 – Acoustic Emissions. Published by the American Society of Non-destructive testing. ISBN 0-931403-02-2.

87. Dornfeld, D. and Handy, C. Slip detection using acoustic emission signal analysis. IEEE International Conference on Robotics and Automation. **Vol. 4**, 1868-1875. 1987.

88. MacBride, S.L., Bones, R.J., Sobczyk, M and Viner, M.R. Acoustics emission from lubricated and rubbing surfaces. Journal of Acoustic Emission. **8(1-2)**. 192-196. 1989.

89. Tan, C.K. and Mba, D.U. Identification of the Acoustic Emission source during a comparative study on diagnosis of a spur gearbox. Tribology International. **38**. 469-480. 2005.

90. Xiao, L., Rosen, B.G., Amini, N. And Nilsson, P.H. A study on the effect of surface topography on rough friction in roller contact. Wear. **254(11).** 1162-1169. 2003.

91. Wang, Y.L. and Hsu, S.M. Lubricated friction and wear simulation of multi-scratches in asperity-asperity contact. Wear. **217**. 104-109. 1998.

92. Matsuoka, K., Taniguchi, K. and Nakakita, M. In-situ wear monitoring of slider and disk using acoustic emission. Journal of Tribology. **123**. 175-180. 2001.

93. Lingard, S. and Ng, K.K. An investigation of acoustic emission in sliding friction and wear of metals. Wear. **130**. 367-379. 1989.

94. Borland, D.W. and Bian, S. Unlubricated sliding wear of steels: towards an alternative wear equation. Wear. **209**. 171-178. 1997.

95. John, V. Testing of materials. 1st ed. Macmillan Education Ltd. Hampshire, UK. 1992.

96. Fisher, G. and Donahue, A. Filter debris analysis as a first-line condition monitoring too1. Lubrication Engineering. 18-22. 2000.

97. Edmonds, J., Resner, M.S. and Shkarlet, K. Detection of precursor wear debris in lubrication systems. IEEE. 73-77. 2000.

98. Davies, A. and Drake, P.R. Commercial applications of wear debris analysis. *Handbook of Condition Monitoring*. Edited by A. Davis. Chapman and Hall. London, UK 1998.

99. Bassett, D. PHM 'Failure monitoring/condition assessment' technologies and product. *AHS International Forum 60, Baltimore, MD. 8-10th June*. 2004.

100. Davies, A. Wear particles collection and evaluation. *Handbook of Condition Monitoring*. Edited by A. Davis. Chapman and Hall. London, UK 1998.

101. Jackson, C.E.P. and White, C.J. Detection of faults in complex gearbox by analysis of vibration. Westland Helicopter Limited. Report RP 372.

102. Price, E.D., Lees, A.W. and Friswell, M.I. Detection of severe sliding and pitting fatigue wear regimes through the use of broadband acoustic emission. Engineering Tribology. **219(12)**. 85-98. 2005

103. Alexander, D.L. The viscosity of lubricants. Lubrication. **78(3)**. 1992.

104. Timeshenko, S.and Baud R.V. The strength of gear teeth. Mechanical Engineering. **48**. 1105-1110. 1926.

105. Attia, A.Y. Deflection of spur gear teeth cut in thin rims. Journal of Engineering for Industrial. 333-341. 1964.

Appendix A

Back-to-Back Gearbox Maximum Applied Torque Calculations

The test gearbox was designed and fabricated by Vayionas in 1991 and the maximum applied torque to the test gearbox was calculated to be 267 Nm [81]. Employing the same method of calculation but only differs in the way where strain measurements were performed. Vayionas computed the applied torque to the gearbox by measuring the strains on the gearbox input shaft (using Wheatstone half bridge configuration). While in this instance, fibre optic was employed. Followings are the procedures to obtain the maximum applied torque to the gearbox using fibre optic strain measurements.

Before the start of the measurements, a pre-strain of 65 μm was recorded. The fibre optic measuring systems was then set to zero. The torque was applied to the gearbox by turning the torque bolt at a step increment of quarter turn until the torque bolt was fully engaged into the load plate. The measurements were repeated by releasing the torque bolt at a quarter turn at each time. The strain measurement results are presented in figure A1.

From figure A1, a maximum strain of 460 μm was recorded.

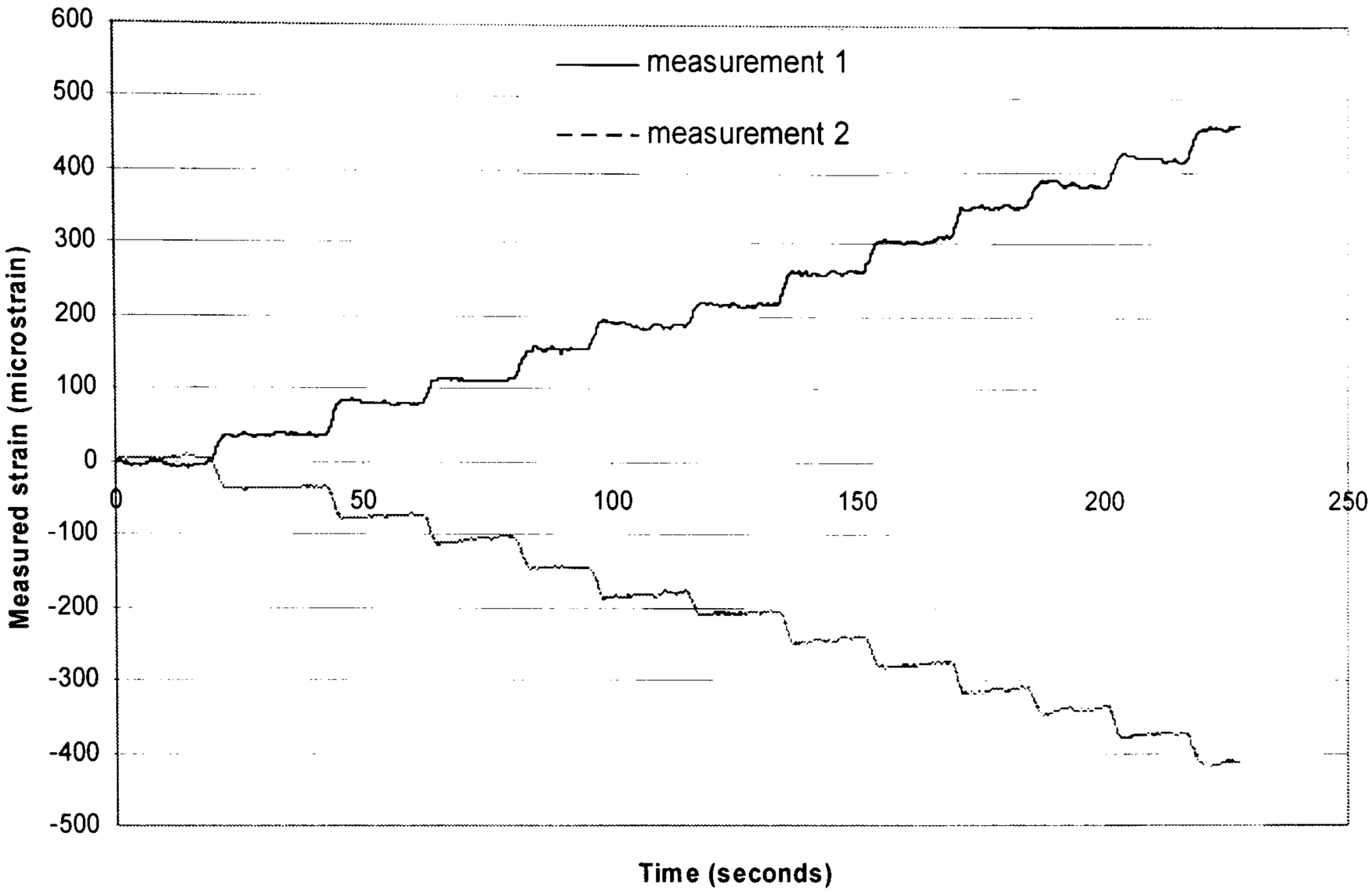

Figure A1 Measured strains using fibre optic.

Hence, with the pre-load, the test gearbox could be loaded up to 525 μm.

Employing the same torsion theory as Vayionas [81], the maximum applied torque, T_{max}, could be calculated using equations A.1 to A.3. Using the input shaft material and geometrical data (see table A1), the maximum applied torque was determined to be 260 Nm.

$$T_{\max} = \frac{J\tau_{\max}}{r} \tag{A.1}$$

$$J = \frac{\pi d^4}{32} \tag{A.2}$$

$$\tau_{\max} = 2\varepsilon G \tag{A.3}$$

Where J is the polar moment of inertia

d is the shaft diameter

r is the shaft radius

G is the shear modulus of steel

τ_{max} is the maximum shear stress

ε is the measured strain

d	0.025 m
G	8.08×10^{10} N/m^2

Table A1 Material and geometrical parameters of the input shaft.

Appendix B

Gear Pitting Prediction Results

The British Gear Association (BGA) has developed a complex program to calculate the load capacity of gear in term of contact stress based on BS436 part 3 [34]. This program will be employed for this investigation to ascertain whether pitting will occur for the accelerated gear fatigue tests. The permissible and actual contact stresses can be calculated based on equations (1) and (2) of BS436 part 3 respectively. In these equations, effects such as material and processing, tooth profile, contact ratio, lubricant etc present themselves as correction factors in determining the contact stresses. The effect and computation of each correction factor is illustrated in [34].

The surface durability of the test gears was calculated using a program, Gear Geometry and Stress Analysis Program, developed jointly by Newcastle University Design Unit and the British Mechanical Power Transmission Association's (BMPTA) Gear Research Foundation (GRF). This gear analysis program is intended for gearbox designers and end users who are involved in spur or helical involute gearing. The program consisted of two modules (a) Gear Details Module: drawing data in accordance with the BMPTA's Codes of Practice and (b) Gear Rating Module: calculation of gear tooth contact and bending stresses in accordance with the procedures specified in BS/ISO 6336 [35].

```
**********************************
*      D E S I G N    U N I T    *
*      Gear Technology Centre    *
* User          Cranfield University*
* Organisation Cranfield University*
* Rating to ISO 6336    1 Apr 2005 *
* DU/GRF  ISO Rating  Version 3·5  *
**********************************
file not named
```

pinion material	St						
wheel material	St						
hardness	HV	137	137				
material quality		MQ	MQ				
roughns flnk/µm	Rz	18.0	18.0				
roughns root/µm	Rz	18.0	18.0				
viscosity @ 40C	nu	136					
pitting permitted?		yes	yes				
reversing duty?		no	no				

number of teeth	z	49	65	applicatn factr	KA	1.000	
normal module	mn	3.000		required life/h		0	
transvrs module	mt	3.000		load cycles	NL	0.00E0	0.00E
gear ratio	u	1.327		mesh power/kW	P	5.70	
centres	a	171.00		torque/Nm	T	73.0	96.
facewidth	b	15.00	30.00	tr tang force/N	Ft	993.2	
reference diam	d	147.00	195.00	speed/RPM	n	745.0	561.
base diameter	db	138.13	183.24	pitch line speed/m/s		5.73	
tip diameter	da	153.00	201.00	tip relief/µm	Ca	14	
root diameter	df	139.50	187.50	helix modifictn	none		
tooth depth	h	6.750	6.750	fav contact pattn posn		verifctn?	n
internal diameter		0.0	0.0	wheel web thickness		0.00	
norm pres angle	alphan	20.0000		pinion offset	s	0.000	
transv pres ang	alphat	20.0000					
wkng tr pr ang	alphawt	20.0000					
ref helix angle	beta	0.0000					
base helix ang	betab	0.0000					
prof shift coef	x	0.000	0.000	hx dev elast/µm	fsh	0	
sum of "" coefs	Sigx	0.000		quality grade	q	10	10
bsc rack dedend	hfP/mn	1.250	1.250	hx dev manuf/µm	fma	36	
bsc rk root rad	rofP/mn	0.250	0.250	init'l misal/µm	Fbetax	36	
residual protub	Spr/mn	0.000	0.000	run-in misal/µm	Fbetay	1	
root chord lgth	sFn/mn	2.177	2.227	stiff/(N/mm/µm)	cgamma	20.45	
bending mom arm	hFa/mn	0.958	0.980				
root radius	roF/mn	0.424	0.399				
tr contct ratio	epsalpha	1.774		overlap ratio	epsbeta	0.000	

FACTORS

resonance ratio	N	0.183		dynamic fct	Kv	1.495	
TOOTH FLANK				**TOOTH ROOT**			
face load factr	KHbeta	1.078		face load factr	KFbeta	1.054	1.0
transv load fct	KHalpha	1.348		transv load fct	KFalpha	1.486	
zone factor	ZH	2.495		form factor	YF	1.221	1.1
elasticity fctr	ZE	189.812		stress conc fct	YS	2.286	2.3
single pair fct	ZB/ZD	1.006	1.000	notch parameter	qs	2.567	2.7
cont ratio fctr	Zepsilon	0.861		cont ratio fctr	Yepsilon	0.673	
helix ang factr	Zbeta	1.000		helix ang factr	Ybeta	1.000	
life factor	ZN	1.600	1.600	life factor	YN	1.600	1.6
lub inf fct	ZLZVZR	1.000	1.000	notch sensy fct	YdrelT	1.128	1.1
work-hardng fct	ZW	1.196		surface factor	YRrelT	1.000	1.0
size factor	ZX	1.000		size factor	YX	1.000	1.0
CONTACT STRESS (N/mm²)				**BENDING STRESS (N/mm²)**			
allw stress num	sgHlm	327.0	327.0	allw stress num	sigFE	174.0	174.
permiss stress	sigHP	625.7	625.7	permiss stress	sigFP	224.3	232.
"" (reference)	" ref	286.7	286.7	"" (reference)	" ref	121.8	122.
contact stress	sigH	537.6	534.3	root stress	sigF	144.2	104.
safety factor	SH	1.16	1.17	safety factor	SF	2.18	3.1
min safety fctr	SHmin	1.00		min safety fctr	SFmin	1.40	

```
**********************************
*      D E S I G N    U N I T    *
*      Gear Technology Centre    *
* User          Cranfield University*
* Organisation Cranfield University*
* Rating to ISO 6336    1 Apr 2005 *
* DU/GRF  ISO Rating  Version 3·5  *
**********************************
file not named
```

pinion material	St							
wheel material	St							
hardness	HV	137	137					
material quality		MQ	MQ					
roughns flnk/µm	Rz	18.0	18.0					
roughns root/µm	Rz	18.0	18.0					
viscosity @ 40C	nu	136						
pitting permitted?		yes	yes					
reversing duty?		no	no					
applicatn factr	KA	1.000						
required life/h		10						
load cycles	NL	4.47E5	3.37E					
mesh power/kW	P	5.70						
torque/Nm	T	73.0	96.					
tr tang force/N	Ft	993.2						
speed/RPM	n	745.0	561.					
pitch line speed/m/s		5.73						
tip relief/µm	Ca	14						
helix modifictn	none							
fav contact pattn posn		verifctn?	n					
wheel web thickness		0.00						
pinion offset	s	0.000						

number of teeth	z	49	65					
normal module	mn	3.000						
transvrs module	mt	3.000						
gear ratio	u	1.327						
centres	a	171.00						
facewidth	b	15.00	30.00					
reference diam	d	147.00	195.00					
base diameter	db	138.13	183.24					
tip diameter	da	153.00	201.00					
root diameter	df	139.50	187.50					
tooth depth	h	6.750	6.750					
internal diameter		0.0	0.0					
norm pres angle	alphan	20.0000						
transv pres ang	alphat	20.0000						
wkng tr pr ang	alphawt	20.0000						
ref helix angle	beta	0.0000						
base helix ang	betab	0.0000						
prof shift coef	x	0.000	0.000					
sum of "" coefs	Sigx	0.000						
bsc rack dedend	hfP/mn	1.250	1.250					
bsc rk root rad	rofP/mn	0.250	0.250					
residual protub	Spr/mn	0.000	0.000					
root chord lgth	sFn/mn	2.177	2.227					
bending mom arm	hFa/mn	0.958	0.980					
root radius	roF/mn	0.424	0.399					
tr contct ratio	epsalpha	1.774						
hx dev elast/µm	fsh	0						
quality grade	q	10	10					
hx dev manuf/µm	fma	36						
init'l misal/µm	Fbetax	36						
run-in misal/µm	Fbetay	1						
stiff/(N/mm/µm)	cgamma	20.45						
overlap ratio	epsbeta	0.000						

FACTORS

resonance ratio	N	0.183		dynamic fct	Kv	1.495		
TOOTH FLANK				**TOOTH ROOT**				
face load factr	KHbeta	1.078		face load factr	KFbeta	1.054	1.0	
transv load fct	KHalpha	1.348		transv load fct	KFalpha	1.486		
zone factor	ZH	2.495		form factor	YF	1.221	1.1	
elasticity fctr	ZE	189.812		stress conc fct	YS	2.286	2.3	
single pair fct	ZB/ZD	1.006	1.000	notch parameter	qs	2.567	2.7	
cont ratio fctr	Zepsilon	0.861		cont ratio fctr	Yepsilon	0.673		
helix ang factr	Zbeta	1.000		helix ang factr	Ybeta	1.000		
life factor	ZN	1.600	1.600	life factor	YN	1.118	1.1	
lub inf fct	ZLZVZR	1.000	1.000	notch sensy fct	YdrelT	1.031	1.0	
work-hardng fct	ZW	1.196		surface factor	YRrelT	0.983	0.9	
size factor	ZX	1.000		size factor	YX	1.000	1.0	
CONTACT STRESS (N/mm²)				**BENDING STRESS (N/mm²)**				
allw stress num	sgHlm	327.0	327.0	allw stress num	sigFE	174.0	174.	
permiss stress	sigHP	625.7	625.7	permiss stress	sigFP	140.8	146.	
"" (reference)	" ref	286.7	286.7	"" (reference)	" ref	121.8	122.	
contact stress	sigH	537.6	534.3	root stress	sigF	144.2	104.	
safety factor	SH	1.16	1.17	safety factor	SF	1.37	1.9	
min safety fctr	SHmin	1.00		min safety fctr	SFmin	1.40		

```
**********************************
*      D E S I G N    U N I T    *
*      Gear Technology Centre    *
* User          Cranfield University*
* Organisation Cranfield University*
* Rating to ISO 6336    1 Apr 2005 *
* DU/GRF  ISO Rating  Version 3·5  *
**********************************
file not named
```

pinion material	St		
wheel material	St		
hardness	HV	137	137
material quality		MQ	MQ
roughns flnk/µm	Rz	18.0	18.0
roughns root/µm	Rz	18.0	18.0
viscosity @ 40C	nu	136	
pitting permitted?		yes	yes
reversing duty?		no	no

number of teeth	z	49	65
normal module	mn	3.000	
transvrs module	mt	3.000	
gear ratio	u	1.327	
centres	a	171.00	
facewidth	b	15.00	30.00
reference diam	d	147.00	195.00
base diameter	db	138.13	183.24
tip diameter	da	153.00	201.00
root diameter	df	139.50	187.50
tooth depth	h	6.750	6.750
internal diameter		0.0	0.0
norm pres angle	alphan	20.0000	
transv pres ang	alphat	20.0000	
wkng tr pr ang	alphawt	20.0000	
ref helix angle	beta	0.0000	
base helix ang	betab	0.0000	
prof shift coef	x	0.000	0.000
sum of "" coefs	Sigx	0.000	
bsc rack dedend	hfP/mn	1.250	1.250
bsc rk root rad	rofP/mn	0.250	0.250
residual protub	Spr/mn	0.000	0.000
root chord lgth	sFn/mn	2.177	2.227
bending mom arm	hFa/mn	0.958	0.980
root radius	roF/mn	0.424	0.399
tr contct ratio	epsalpha	1.774	

applicatn factr	KA	1.000	
required life/h		20	
load cycles	NL	8.94E5	6.74E
mesh power/kW	P	5.70	
torque/Nm	T	73.0	96.
tr tang force/N	Ft	993.2	
speed/RPM	n	745.0	561.
pitch line speed/m/s		5.73	
tip relief/µm	Ca	14	
helix modifictn	none		
fav contact pattn posn verifctn?		n	
wheel web thickness		0.00	
pinion offset	s	0.000	
hx dev elast/µm	fsh	0	
quality grade	q	10	10
hx dev manuf/µm	fma	36	
init'l misal/µm	Fbetax	36	
run-in misal/µm	Fbetay	1	
stiff/(N/mm/µm)	cgamma	20.45	
overlap ratio	epsbeta	0.000	

FACTORS

resonance ratio	N	0.183	
dynamic fct	Kv	1.495	

TOOTH FLANK

face load factr	KHbeta	1.078	
transv load fct	KHalpha	1.348	
zone factor	ZH	2.495	
elasticity fctr	ZE	189.812	
single pair fct	ZB/ZD	1.006	1.000
cont ratio fctr	Zepsilon	0.861	
helix ang factr	Zbeta	1.000	
life factor	ZN	1.554	1.586
lub inf fct	ZLZVZR	0.979	0.994
work-hardng fct	ZW	1.196	
size factor	ZX	1.000	

TOOTH ROOT

face load factr	KFbeta	1.054	1.0
transv load fct	KFalpha	1.486	
form factor	YF	1.221	1.1
stress conc fct	YS	2.286	2.3
notch parameter	qs	2.567	2.7
cont ratio fctr	Yepsilon	0.673	
helix ang factr	Ybeta	1.000	
life factor	YN	1.074	1.0
notch sensy fct	YdrelT	1.020	1.0
surface factor	YRrelT	0.981	0.9
size factor	YX	1.000	1.0

CONTACT STRESS (N/mm²)

allw stress num	sgHlm	327.0	327.0
permiss stress	sigHP	595.0	616.6
"" (reference)	" ref	286.7	286.7
contact stress	sigH	537.6	534.3
safety factor	SH	1.11	1.15
min safety fctr	SHmin	1.00	

BENDING STRESS (N/mm²)

allw stress num	sigFE	174.0	174.
permiss stress	sigFP	133.6	138.
"" (reference)	" ref	121.8	122.
root stress	sigF	144.2	104.
safety factor	SF	1.30	1.8
min safety fctr	SFmin	1.40	

```
**********************************
*      D E S I G N    U N I T    *
*      Gear Technology Centre    *
* User          Cranfield University*
* Organisation Cranfield University*
* Rating to ISO 6336    1 Apr 2005 *
* DU/GRF  ISO Rating  Version 3·5  *
**********************************
file not named
```

pinion material	St						
wheel material	St						
hardness	HV	137	137				
material quality		MQ	MQ				
roughns flnk/µm	Rz	18.0	18.0				
roughns root/µm	Rz	18.0	18.0				
viscosity @ 40C	nu	136					
pitting permitted?		yes	yes				
reversing duty?		no	no				

number of teeth	z	49	65	applicatn factr	KA	1.000	
normal module	mn	3.000		required life/h		50	
transvrs module	mt	3.000		load cycles	NL	2.24E6	1.68E
gear ratio	u	1.327		mesh power/kW	P	5.70	
centres	a	171.00		torque/Nm	T	73.0	96.
facewidth	b	15.00	30.00	tr tang force/N	Ft	993.2	
reference diam	d	147.00	195.00	speed/RPM	n	745.0	561.
base diameter	db	138.13	183.24	pitch line speed/m/s		5.73	
tip diameter	da	153.00	201.00	tip relief/µm	Ca	14	
root diameter	df	139.50	187.50	helix modifictn	none		
tooth depth	h	6.750	6.750	fav contact pattn posn	verifctn?		n
internal diameter		0.0	0.0	wheel web thickness		0.00	
norm pres angle	alphan	20.0000		pinion offset	s	0.000	
transv pres ang	alphat	20.0000					
wkng tr pr ang	alphawt	20.0000					
ref helix angle	beta	0.0000					
base helix ang	betab	0.0000					
prof shift coef	x	0.000	0.000	hx dev elast/µm	fsh	0	
sum of "" coefs	Sigx	0.000		quality grade	q	10	10
bsc rack dedend	hfP/mn	1.250	1.250	hx dev manuf/µm	fma	36	
bsc rk root rad	rofP/mn	0.250	0.250	init'l misal/µm	Fbetax	36	
residual protub	Spr/mn	0.000	0.000	run-in misal/µm	Fbetay	1	
root chord lgth	sFn/mn	2.177	2.227	stiff/(N/mm/µm)	cgamma	20.45	
bending mom arm	hFa/mn	0.958	0.980				
root radius	roF/mn	0.424	0.399				
tr contct ratio	epsalpha	1.774		overlap ratio	epsbeta	0.000	

FACTORS

resonance ratio	N	0.183		dynamic fct	Kv	1.495	
TOOTH FLANK				TOOTH ROOT			
face load factr	KHbeta	1.078		face load factr	KFbeta	1.054	1.0
transv load fct	KHalpha	1.348		transv load fct	KFalpha	1.486	
zone factor	ZH	2.495		form factor	YF	1.221	1.1
elasticity fctr	ZE	189.812		stress conc fct	YS	2.286	2.3
single pair fct	ZB/ZD	1.006	1.000	notch parameter	qs	2.567	2.7
cont ratio fctr	Zepsilon	0.861		cont ratio fctr	Yepsilon	0.673	
helix ang factr	Zbeta	1.000		helix ang factr	Ybeta	1.000	
life factor	ZN	1.452	1.483	life factor	YN	1.017	1.0
lub inf fct	ZLZVZR	0.934	0.948	notch sensy fct	YdrelT	1.007	1.0
work-hardng fct	ZW	1.196		surface factor	YRrelT	0.978	0.9
size factor	ZX	1.000		size factor	YX	1.000	1.0
CONTACT STRESS (N/mm²)				BENDING STRESS (N/mm²)			
allw stress num	sgHlm	327.0	327.0	allw stress num	sigFE	174.0	174.
permiss stress	sigHP	530.4	549.5	permiss stress	sigFP	124.5	128.
"" (reference)	" ref	286.7	286.7	"" (reference)	" ref	121.8	122.
contact stress	sigH	537.6	534.3	root stress	sigF	144.2	104.
safety factor	SH	0.99	1.03	safety factor	SF	1.21	1.7
min safety fctr	SHmin	1.00		min safety fctr	SFmin	1.40	

```
**********************************
*      D E S I G N    U N I T    *
*      Gear Technology Centre    *
* User          Cranfield University*
* Organisation Cranfield University*
* Rating to ISO 6336    1 Apr 2005 *
* DU/GRF  ISO Rating  Version 3·5  *
**********************************
file not named
```

pinion material	St		
wheel material	St		
hardness	HV	137	137
material quality		MQ	MQ
roughns flnk/µm	Rz	18.0	18.0
roughns root/µm	Rz	18.0	18.0
viscosity @ 40C	nu	136	
pitting permitted?		yes	yes
reversing duty?		no	no

number of teeth	z	49	65
normal module	mn	3.000	
transvrs module	mt	3.000	
gear ratio	u	1.327	
centres	a	171.00	
facewidth	b	15.00	30.00
reference diam	d	147.00	195.00
base diameter	db	138.13	183.24
tip diameter	da	153.00	201.00
root diameter	df	139.50	187.50
tooth depth	h	6.750	6.750
internal diameter		0.0	0.0
norm pres angle	alphan	20.0000	
transv pres ang	alphat	20.0000	
wkng tr pr ang	alphawt	20.0000	
ref helix angle	beta	0.0000	
base helix ang	betab	0.0000	
prof shift coef	x	0.000	0.000
sum of "" coefs	Sigx	0.000	
bsc rack dedend	hfP/mn	1.250	1.250
bsc rk root rad	rofP/mn	0.250	0.250
residual protub	Spr/mn	0.000	0.000
root chord lgth	sFn/mn	2.177	2.227
bending mom arm	hFa/mn	0.958	0.980
root radius	roF/mn	0.424	0.399
tr contct ratio	epsalpha	1.774	

applicatn factr	KA	1.000	
required life/h		80	
load cycles	NL	3.58E6	2.70E
mesh power/kW	P	5.70	
torque/Nm	T	73.0	96.
tr tang force/N	Ft	993.2	
speed/RPM	n	745.0	561.
pitch line speed/m/s		5.73	
tip relief/µm	Ca	14	
helix modifictn	none		
fav contact pattn posn verifctn?		n	
wheel web thickness		0.00	
pinion offset	s	0.000	
hx dev elast/µm	fsh	0	
quality grade	q	10	10
hx dev manuf/µm	fma	36	
init'l misal/µm	Fbetax	36	
run-in misal/µm	Fbetay	1	
stiff/(N/mm/µm)	cgamma	20.45	
overlap ratio	epsbeta	0.000	

FACTORS

resonance ratio	N	0.183	
dynamic fct	Kv	1.495	

TOOTH FLANK

face load factr	KHbeta	1.078	
transv load fct	KHalpha	1.348	
zone factor	ZH	2.495	
elasticity fctr	ZE	189.812	
single pair fct	ZB/ZD	1.006	1.000
cont ratio fctr	Zepsilon	0.861	
helix ang factr	Zbeta	1.000	
life factor	ZN	1.403	1.432
lub inf fct	ZLZVZR	0.912	0.925
work-hardng fct	ZW	1.196	
size factor	ZX	1.000	

TOOTH ROOT

face load factr	KFbeta	1.054	1.0
transv load fct	KFalpha	1.486	
form factor	YF	1.221	1.1
stress conc fct	YS	2.286	2.3
notch parameter	qs	2.567	2.7
cont ratio fctr	Yepsilon	0.673	
helix ang factr	Ybeta	1.000	
life factor	YN	0.998	1.0
notch sensy fct	YdrelT	1.002	1.0
surface factor	YRrelT	0.977	0.9
size factor	YX	1.000	1.0

CONTACT STRESS (N/mm²)

allw stress num	sgHlm	327.0	327.0
permiss stress	sigHP	500.3	518.2
"" (reference)	" ref	286.7	286.7
contact stress	sigH	537.6	534.3
safety factor	SH	0.93	0.97
min safety fctr	SHmin	1.00	

BENDING STRESS (N/mm²)

allw stress num	sigFE	174.0	174.
permiss stress	sigFP	121.6	123.
"" (reference)	" ref	121.8	122.
root stress	sigF	144.2	104.
safety factor	SF	1.18	1.6
min safety fctr	SFmin	1.40	

```
**********************************
*      D E S I G N    U N I T    *
*      Gear Technology Centre    *
* User          Cranfield University*
* Organisation Cranfield University*
* Rating to ISO 6336    1 Apr 2005 *
* DU/GRF  ISO Rating  Version 3·5  *
**********************************
file not named
```

number of teeth	z	49	65
normal module	mn	3.000	
transvrs module	mt	3.000	
gear ratio	u	1.327	
centres	a	171.00	
facewidth	b	15.00	30.00
reference diam	d	147.00	195.00
base diameter	db	138.13	183.24
tip diameter	da	153.00	201.00
root diameter	df	139.50	187.50
tooth depth	h	6.750	6.750
internal diameter		0.0	0.0
norm pres angle	alphan	20.0000	
transv pres ang	alphat	20.0000	
wkng tr pr ang	alphawt	20.0000	
ref helix angle	beta	0.0000	
base helix ang	betab	0.0000	
prof shift coef	x	0.000	0.000
sum of "" coefs	Sigx	0.000	
bsc rack dedend	hfP/mn	1.250	1.250
bsc rk root rad	rofP/mn	0.250	0.250
residual protub	Spr/mn	0.000	0.000
root chord lgth	sFn/mn	2.177	2.227
bending mom arm	hFa/mn	0.958	0.980
root radius	roF/mn	0.424	0.399
tr contct ratio	epsalpha	1.774	

pinion material	St		
wheel material	St		
hardness	HV	137	137
material quality		MQ	MQ
roughns flnk/µm	Rz	18.0	18.0
roughns root/µm	Rz	18.0	18.0
viscosity @ 40C	nu	136	
pitting permitted?		yes	yes
reversing duty?		no	no
applicatn factr	KA	1.000	
required life/h		100	
load cycles	NL	4.47E6	3.37E
mesh power/kW	P	5.70	
torque/Nm	T	73.0	96.
tr tang force/N	Ft	993.2	
speed/RPM	n	745.0	561.
pitch line speed/m/s		5.73	
tip relief/µm	Ca	14	
helix modifictn	none		
fav contact pattn posn verifctn?		n	
wheel web thickness		0.00	
pinion offset	s	0.000	
hx dev elast/µm	fsh	0	
quality grade	q	10	10
hx dev manuf/µm	fma	36	
init'l misal/µm	Fbetax	36	
run-in misal/µm	Fbetay	1	
stiff/(N/mm/µm)	cgamma	20.45	
overlap ratio	epsbeta	0.000	

FACTORS

resonance ratio	N	0.183	
dynamic fct	Kv	1.495	

TOOTH FLANK

face load factr	KHbeta	1.078	
transv load fct	KHalpha	1.348	
zone factor	ZH	2.495	
elasticity fctr	ZE	189.812	
single pair fct	ZB/ZD	1.006	1.000
cont ratio fctr	Zepsilon	0.861	
helix ang factr	Zbeta	1.000	
life factor	ZN	1.380	1.409
lub inf fct	ZLZVZR	0.902	0.915
work-hardng fct	ZW	1.196	
size factor	ZX	1.000	

TOOTH ROOT

face load factr	KFbeta	1.054	1.0
transv load fct	KFalpha	1.486	
form factor	YF	1.221	1.1
stress conc fct	YS	2.286	2.3
notch parameter	qs	2.567	2.7
cont ratio fctr	Yepsilon	0.673	
helix ang factr	Ybeta	1.000	
life factor	YN	0.996	0.9
notch sensy fct	YdrelT	1.002	1.0
surface factor	YRrelT	0.977	0.9
size factor	YX	1.000	1.0

CONTACT STRESS (N/mm²)

allw stress num	sgHlm	327.0	327.0
permiss stress	sigHP	486.6	504.0
"" (reference)	" ref	286.7	286.7
contact stress	sigH	537.6	534.3
safety factor	SH	0.91	0.94
min safety fctr	SHmin	1.00	

BENDING STRESS (N/mm²)

allw stress num	sigFE	174.0	174.
permiss stress	sigFP	121.3	122.
"" (reference)	" ref	121.8	122.
root stress	sigF	144.2	104.
safety factor	SF	1.18	1.6
min safety fctr	SFmin	1.40	

```
**********************************
*      D E S I G N    U N I T    *
*      Gear Technology Centre    *
* User          Cranfield University*
* Organisation Cranfield University*
* Rating to ISO 6336    1 Apr 2005 *
* DU/GRF  ISO Rating  Version 3·5  *
**********************************
file not named
```

pinion material	St		
wheel material	St		
hardness	HV	137	137
material quality		MQ	MQ
roughns flnk/µm	Rz	18.0	18.0
roughns root/µm	Rz	18.0	18.0
viscosity @ 40C	nu	136	
pitting permitted?		yes	yes
reversing duty?		no	no

number of teeth	z	49	65
normal module	mn	3.000	
transvrs module	mt	3.000	
gear ratio	u	1.327	
centres	a	171.00	
facewidth	b	15.00	30.00
reference diam	d	147.00	195.00
base diameter	db	138.13	183.24
tip diameter	da	153.00	201.00
root diameter	df	139.50	187.50
tooth depth	h	6.750	6.750
internal diameter		0.0	0.0
norm pres angle	alphan	20.0000	
transv pres ang	alphat	20.0000	
wkng tr pr ang	alphawt	20.0000	
ref helix angle	beta	0.0000	
base helix ang	betab	0.0000	
prof shift coef	x	0.000	0.000
sum of "" coefs	Sigx	0.000	
bsc rack dedend	hfP/mn	1.250	1.250
bsc rk root rad	rofP/mn	0.250	0.250
residual protub	Spr/mn	0.000	0.000
root chord lgth	sFn/mn	2.177	2.227
bending mom arm	hFa/mn	0.958	0.980
root radius	roF/mn	0.424	0.399
tr contct ratio	epsalpha	1.774	

applicatn factr	KA	1.000	
required life/h		150	
load cycles	NL	6.71E6	5.05E
mesh power/kW	P	5.70	
torque/Nm	T	73.0	96.
tr tang force/N	Ft	993.2	
speed/RPM	n	745.0	561.
pitch line speed/m/s		5.73	
tip relief/µm	Ca	14	
helix modifictn	none		
fav contact pattn posn	verifctn?	n	
wheel web thickness		0.00	
pinion offset	s	0.000	
hx dev elast/µm	fsh	0	
quality grade	q	10	10
hx dev manuf/µm	fma	36	
init'l misal/µm	Fbetax	36	
run-in misal/µm	Fbetay	1	
stiff/(N/mm/µm)	cgamma	20.45	
overlap ratio	epsbeta	0.000	

FACTORS

resonance ratio	N	0.183	
dynamic fct	Kv	1.495	

TOOTH FLANK

face load factr	KHbeta	1.078	
transv load fct	KHalpha	1.348	
zone factor	ZH	2.495	
elasticity fctr	ZE	189.812	
single pair fct	ZB/ZD	1.006	1.000
cont ratio fctr	Zepsilon	0.861	
helix ang factr	Zbeta	1.000	
life factor	ZN	1.339	1.367
lub inf fct	ZLZVZR	0.884	0.896
work-hardng fct	ZW	1.196	
size factor	ZX	1.000	

TOOTH ROOT

face load factr	KFbeta	1.054	1.0
transv load fct	KFalpha	1.486	
form factor	YF	1.221	1.1
stress conc fct	YS	2.286	2.3
notch parameter	qs	2.567	2.7
cont ratio fctr	Yepsilon	0.673	
helix ang factr	Ybeta	1.000	
life factor	YN	0.992	0.9
notch sensy fct	YdrelT	1.002	1.0
surface factor	YRrelT	0.977	0.9
size factor	YX	1.000	1.0

CONTACT STRESS (N/mm²)

allw stress num	sgHlm	327.0	327.0
permiss stress	sigHP	462.8	479.2
"" (reference)	" ref	286.7	286.7
contact stress	sigH	537.6	534.3
safety factor	SH	0.86	0.90
min safety fctr	SHmin	1.00	

BENDING STRESS (N/mm²)

allw stress num	sigFE	174.0	174.
permiss stress	sigFP	120.8	122.
"" (reference)	" ref	121.8	122.
root stress	sigF	144.2	104.
safety factor	SF	1.17	1.6
min safety fctr	SFmin	1.40	

```
**********************************
*      D E S I G N    U N I T    *
*      Gear Technology Centre    *
* User          Cranfield University*
* Organisation Cranfield University*
* Rating to ISO 6336    1 Apr 2005 *
* DU/GRF  ISO Rating  Version 3·5  *
**********************************
file not named
```

pinion material	St						
wheel material	St						
hardness	HV	137	137				
material quality		MQ	MQ				
roughns flnk/µm	Rz	18.0	18.0				
roughns root/µm	Rz	18.0	18.0				
viscosity @ 40C	nu	136					
pitting permitted?		yes	yes				
reversing duty?		no	no				

number of teeth	z	49	65	applicatn factr	KA	1.000	
normal module	mn	3.000		required life/h		200	
transvrs module	mt	3.000		load cycles	NL	8.94E6	6.74E
gear ratio	u	1.327		mesh power/kW	P	5.70	
centres	a	171.00		torque/Nm	T	73.0	96.
facewidth	b	15.00	30.00	tr tang force/N	Ft	993.2	
reference diam	d	147.00	195.00	speed/RPM	n	745.0	561.
base diameter	db	138.13	183.24	pitch line speed/m/s		5.73	
tip diameter	da	153.00	201.00	tip relief/µm	Ca	14	
root diameter	df	139.50	187.50				
tooth depth	h	6.750	6.750	helix modifictn	none		
internal diameter		0.0	0.0	fav contact pattn posn	verifctn?		n
norm pres angle	alphan	20.0000		wheel web thickness		0.00	
transv pres ang	alphat	20.0000		pinion offset	s	0.000	
wkng tr pr ang	alphawt	20.0000					
ref helix angle	beta	0.0000					
base helix ang	betab	0.0000					
prof shift coef	x	0.000	0.000	hx dev elast/µm	fsh	0	
sum of "" coefs	Sigx	0.000		quality grade	q	10	10
bsc rack dedend	hfP/mn	1.250	1.250	hx dev manuf/µm	fma	36	
bsc rk root rad	rofP/mn	0.250	0.250	init'l misal/µm	Fbetax	36	
residual protub	Spr/mn	0.000	0.000	run-in misal/µm	Fbetay	1	
root chord lgth	sFn/mn	2.177	2.227	stiff/(N/mm/µm)	cgamma	20.45	
bending mom arm	hFa/mn	0.958	0.980				
root radius	roF/mn	0.424	0.399				
tr contct ratio	epsalpha	1.774		overlap ratio	epsbeta	0.000	

FACTORS

resonance ratio	N	0.183		dynamic fct	Kv	1.495	
TOOTH FLANK				TOOTH ROOT			
face load factr	KHbeta	1.078		face load factr	KFbeta	1.054	1.0
transv load fct	KHalpha	1.348		transv load fct	KFalpha	1.486	
zone factor	ZH	2.495		form factor	YF	1.221	1.1
elasticity fctr	ZE	189.812		stress conc fct	YS	2.286	2.3
single pair fct	ZB/ZD	1.006	1.000	notch parameter	qs	2.567	2.7
cont ratio fctr	Zepsilon	0.861		cont ratio fctr	Yepsilon	0.673	
helix ang factr	Zbeta	1.000		helix ang factr	Ybeta	1.000	
life factor	ZN	1.311	1.338	life factor	YN	0.989	0.9
lub inf fct	ZLZVZR	0.871	0.884	notch sensy fct	YdrelT	1.002	1.0
work-hardng fct	ZW	1.196		surface factor	YRrelT	0.977	0.9
size factor	ZX	1.000		size factor	YX	1.000	1.0
CONTACT STRESS (N/mm²)				BENDING STRESS (N/mm²)			
allw stress num	sgHlm	327.0	327.0	allw stress num	sigFE	174.0	174.
permiss stress	sigHP	446.6	462.5	permiss stress	sigFP	120.4	121.
"" (reference)	" ref	286.7	286.7	"" (reference)	" ref	121.8	122.
contact stress	sigH	537.6	534.3	root stress	sigF	144.2	104.
safety factor	SH	0.83	0.87	safety factor	SF	1.17	1.6
min safety fctr	SHmin	1.00		min safety fctr	SFmin	1.40	

```
**********************************
*      D E S I G N    U N I T    *
*      Gear Technology Centre    *
* User          Cranfield University*
* Organisation Cranfield University*
* Rating to ISO 6336    1 Apr 2005 *
* DU/GRF  ISO Rating  Version 3·5  *
**********************************
file not named
```

pinion material	St		
wheel material	St		
hardness	HV	137	137
material quality		MQ	MQ
roughns flnk/µm	Rz	18.0	18.0
roughns root/µm	Rz	18.0	18.0
viscosity @ 40C	nu	136	
pitting permitted?		yes	yes
reversing duty?		no	no

number of teeth	z	49	65
normal module	mn	3.000	
transvrs module	mt	3.000	
gear ratio	u	1.327	
centres	a	171.00	
facewidth	b	15.00	30.00
reference diam	d	147.00	195.00
base diameter	db	138.13	183.24
tip diameter	da	153.00	201.00
root diameter	df	139.50	187.50
tooth depth	h	6.750	6.750
internal diameter		0.0	0.0
norm pres angle	alphan	20.0000	
transv pres ang	alphat	20.0000	
wkng tr pr ang	alphawt	20.0000	
ref helix angle	beta	0.0000	
base helix ang	betab	0.0000	
prof shift coef	x	0.000	0.000
sum of "" coefs	Sigx	0.000	
bsc rack dedend	hfP/mn	1.250	1.250
bsc rk root rad	rofP/mn	0.250	0.250
residual protub	Spr/mn	0.000	0.000
root chord lgth	sFn/mn	2.177	2.227
bending mom arm	hFa/mn	0.958	0.980
root radius	roF/mn	0.424	0.399
tr contct ratio	epsalpha	1.774	

applicatn factr	KA	1.000	
required life/h		250	
load cycles	NL	1.12E7	8.42E
mesh power/kW	P	5.70	
torque/Nm	T	73.0	96.
tr tang force/N	Ft	993.2	
speed/RPM	n	745.0	561.
pitch line speed/m/s		5.73	
tip relief/µm	Ca	14	
helix modifictn	none		
fav contact pattn posn	verifctn?	n	
wheel web thickness		0.00	
pinion offset	s	0.000	
hx dev elast/µm	fsh	0	
quality grade	q	10	10
hx dev manuf/µm	fma	36	
init'l misal/µm	Fbetax	36	
run-in misal/µm	Fbetay	1	
stiff/(N/mm/µm)	cgamma	20.45	
overlap ratio	epsbeta	0.000	

FACTORS

resonance ratio	N	0.183	
dynamic fct	Kv	1.495	

TOOTH FLANK

face load factr	KHbeta	1.078	
transv load fct	KHalpha	1.348	
zone factor	ZH	2.495	
elasticity fctr	ZE	189.812	
single pair fct	ZB/ZD	1.006	1.000
cont ratio fctr	Zepsilon	0.861	
helix ang factr	Zbeta	1.000	
life factor	ZN	1.292	1.317
lub inf fct	ZLZVZR	0.863	0.874
work-hardng fct	ZW	1.196	
size factor	ZX	1.000	

TOOTH ROOT

face load factr	KFbeta	1.054	1.0
transv load fct	KFalpha	1.486	
form factor	YF	1.221	1.1
stress conc fct	YS	2.286	2.3
notch parameter	qs	2.567	2.7
cont ratio fctr	Yepsilon	0.673	
helix ang factr	Ybeta	1.000	
life factor	YN	0.987	0.9
notch sensy fct	YdrelT	1.002	1.0
surface factor	YRrelT	0.977	0.9
size factor	YX	1.000	1.0

CONTACT STRESS (N/mm²)

allw stress num	sgHlm	327.0	327.0
permiss stress	sigHP	435.9	449.9
"" (reference)	" ref	286.7	286.7
contact stress	sigH	537.6	534.3
safety factor	SH	0.81	0.84
min safety fctr	SHmin	1.00	

BENDING STRESS (N/mm²)

allw stress num	sigFE	174.0	174.
permiss stress	sigFP	120.1	121.
"" (reference)	" ref	121.8	122.
root stress	sigF	144.2	104.
safety factor	SF	1.17	1.6
min safety fctr	SFmin	1.40	

```
**********************************
*      D E S I G N    U N I T    *
*      Gear Technology Centre    *
* User          Cranfield University*
* Organisation Cranfield University*
* Rating to ISO 6336    1 Apr 2005 *
* DU/GRF  ISO Rating  Version 3·5  *
**********************************
file not named
```

pinion material	St		
wheel material	St		
hardness	HV	137	137
material quality		MQ	MQ
roughns flnk/µm	Rz	18.0	18.0
roughns root/µm	Rz	18.0	18.0
viscosity @ 40C	nu	136	
pitting permitted?		yes	yes
reversing duty?		no	no

applicatn factr	KA	1.000	
required life/h		300	
load cycles	NL	1.34E7	1.01E
mesh power/kW	P	5.70	
torque/Nm	T	73.0	96.
tr tang force/N	Ft	993.2	
speed/RPM	n	745.0	561.
pitch line speed/m/s		5.73	
tip relief/µm	Ca	14	
helix modifictn	none		
fav contact pattn posn	verifctn?	n	
wheel web thickness		0.00	
pinion offset	s	0.000	

number of teeth	z	49	65
normal module	mn	3.000	
transvrs module	mt	3.000	
gear ratio	u	1.327	
centres	a	171.00	
facewidth	b	15.00	30.00
reference diam	d	147.00	195.00
base diameter	db	138.13	183.24
tip diameter	da	153.00	201.00
root diameter	df	139.50	187.50
tooth depth	h	6.750	6.750
internal diameter		0.0	0.0
norm pres angle	alphan	20.0000	
transv pres ang	alphat	20.0000	
wkng tr pr ang	alphawt	20.0000	
ref helix angle	beta	0.0000	
base helix ang	betab	0.0000	
prof shift coef	x	0.000	0.000
sum of "" coefs	Sigx	0.000	
bsc rack dedend	hfP/mn	1.250	1.250
bsc rk root rad	rofP/mn	0.250	0.250
residual protub	Spr/mn	0.000	0.000
root chord lgth	sFn/mn	2.177	2.227
bending mom arm	hFa/mn	0.958	0.980
root radius	roF/mn	0.424	0.399
tr contct ratio	epsalpha	1.774	

hx dev elast/µm	fsh	0	
quality grade	q	10	10
hx dev manuf/µm	fma	36	
init'l misal/µm	Fbetax	36	
run-in misal/µm	Fbetay	1	
stiff/(N/mm/µm)	cgamma	20.45	
overlap ratio	epsbeta	0.000	

FACTORS

resonance ratio	N	0.183	
dynamic fct	Kv	1.495	

TOOTH FLANK

face load factr	KHbeta	1.078	
transv load fct	KHalpha	1.348	
zone factor	ZH	2.495	
elasticity fctr	ZE	189.812	
single pair fct	ZB/ZD	1.006	1.000
cont ratio fctr	Zepsilon	0.861	
helix ang factr	Zbeta	1.000	
life factor	ZN	1.278	1.299
lub inf fct	ZLZVZR	0.857	0.866
work-hardng fct	ZW	1.196	
size factor	ZX	1.000	

TOOTH ROOT

face load factr	KFbeta	1.054	1.0
transv load fct	KFalpha	1.486	
form factor	YF	1.221	1.1
stress conc fct	YS	2.286	2.3
notch parameter	qs	2.567	2.7
cont ratio fctr	Yepsilon	0.673	
helix ang factr	Ybeta	1.000	
life factor	YN	0.985	0.9
notch sensy fct	YdrelT	1.002	1.0
surface factor	YRrelT	0.977	0.9
size factor	YX	1.000	1.0

CONTACT STRESS (N/mm²)

allw stress num	sgHlm	327.0	327.0
permiss stress	sigHP	428.4	440.1
"" (reference)	" ref	286.7	286.7
contact stress	sigH	537.6	534.3
safety factor	SH	0.80	0.82
min safety fctr	SHmin	1.00	

BENDING STRESS (N/mm²)

allw stress num	sigFE	174.0	174.
permiss stress	sigFP	119.9	121.
"" (reference)	" ref	121.8	122.
root stress	sigF	144.2	104.
safety factor	SF	1.16	1.6
min safety fctr	SFmin	1.40	

```
**********************************
*      D E S I G N    U N I T    *
*      Gear Technology Centre    *
* User          Cranfield University*
* Organisation Cranfield University*
* Rating to ISO 6336    1 Apr 2005 *
* DU/GRF  ISO Rating  Version 3·5  *
**********************************
file not named
```

pinion material	St		
wheel material	St		
hardness	HV	137	137
material quality		MQ	MQ
roughns flnk/µm	Rz	18.0	18.0
roughns root/µm	Rz	18.0	18.0
viscosity @ 40C	nu	136	
pitting permitted?		yes	yes
reversing duty?		no	no

number of teeth	z	49	65
normal module	mn	3.000	
transvrs module	mt	3.000	
gear ratio	u	1.327	
centres	a	171.00	
facewidth	b	15.00	30.00
reference diam	d	147.00	195.00
base diameter	db	138.13	183.24
tip diameter	da	153.00	201.00
root diameter	df	139.50	187.50
tooth depth	h	6.750	6.750
internal diameter		0.0	0.0
norm pres angle	alphan	20.0000	
transv pres ang	alphat	20.0000	
wkng tr pr ang	alphawt	20.0000	
ref helix angle	beta	0.0000	
base helix ang	betab	0.0000	
prof shift coef	x	0.000	0.000
sum of "" coefs	Sigx	0.000	
bsc rack dedend	hfP/mn	1.250	1.250
bsc rk root rad	rofP/mn	0.250	0.250
residual protub	Spr/mn	0.000	0.000
root chord lgth	sFn/mn	2.177	2.227
bending mom arm	hFa/mn	0.958	0.980
root radius	roF/mn	0.424	0.399
tr contct ratio	epsalpha	1.774	

applicatn factr	KA	1.000	
required life/h		350	
load cycles	NL	1.56E7	1.18E
mesh power/kW	P	5.70	
torque/Nm	T	73.0	96.
tr tang force/N	Ft	993.2	
speed/RPM	n	745.0	561.
pitch line speed/m/s		5.73	
tip relief/µm	Ca	14	
helix modifictn	none		
fav contact pattn posn	verifctn?	n	
wheel web thickness		0.00	
pinion offset	s	0.000	
hx dev elast/µm	fsh	0	
quality grade	q	10	10
hx dev manuf/µm	fma	36	
init'l misal/µm	Fbetax	36	
run-in misal/µm	Fbetay	1	
stiff/(N/mm/µm)	cgamma	20.45	
overlap ratio	epsbeta	0.000	

FACTORS

resonance ratio	N	0.183	
dynamic fct	Kv	1.495	

TOOTH FLANK

face load factr	KHbeta	1.078	
transv load fct	KHalpha	1.348	
zone factor	ZH	2.495	
elasticity fctr	ZE	189.812	
single pair fct	ZB/ZD	1.006	1.000
cont ratio fctr	Zepsilon	0.861	
helix ang factr	Zbeta	1.000	
life factor	ZN	1.267	1.288
lub inf fct	ZLZVZR	0.852	0.861
work-hardng fct	ZW	1.196	
size factor	ZX	1.000	

TOOTH ROOT

face load factr	KFbeta	1.054	1.0
transv load fct	KFalpha	1.486	
form factor	YF	1.221	1.1
stress conc fct	YS	2.286	2.3
notch parameter	qs	2.567	2.7
cont ratio fctr	Yepsilon	0.673	
helix ang factr	Ybeta	1.000	
life factor	YN	0.983	0.9
notch sensy fct	YdrelT	1.002	1.0
surface factor	YRrelT	0.977	0.9
size factor	YX	1.000	1.0

CONTACT STRESS (N/mm²)

allw stress num	sgHlm	327.0	327.0
permiss stress	sigHP	422.2	433.7
"" (reference)	" ref	286.7	286.7
contact stress	sigH	537.6	534.3
safety factor	SH	0.79	0.81
min safety fctr	SHmin	1.00	

BENDING STRESS (N/mm²)

allw stress num	sigFE	174.0	174.
permiss stress	sigFP	119.7	121.
"" (reference)	" ref	121.8	122.
root stress	sigF	144.2	104.
safety factor	SF	1.16	1.6
min safety fctr	SFmin	1.40	

```
**********************************
*      D E S I G N    U N I T    *
*      Gear Technology Centre    *
* User          Cranfield University*
* Organisation Cranfield University*
* Rating to ISO 6336    1 Apr 2005 *
* DU/GRF  ISO Rating  Version 3·5  *
**********************************
file not named
```

pinion material	St		
wheel material	St		
hardness	HV	137	137
material quality		MQ	MQ
roughns flnk/µm	Rz	18.0	18.0
roughns root/µm	Rz	18.0	18.0
viscosity @ 40C	nu	136	
pitting permitted?		yes	yes
reversing duty?		no	no

number of teeth	z	49	65
normal module	mn	3.000	
transvrs module	mt	3.000	
gear ratio	u	1.327	
centres	a	171.00	
facewidth	b	15.00	30.00
reference diam	d	147.00	195.00
base diameter	db	138.13	183.24
tip diameter	da	153.00	201.00
root diameter	df	139.50	187.50
tooth depth	h	6.750	6.750
internal diameter		0.0	0.0
norm pres angle	alphan	20.0000	
transv pres ang	alphat	20.0000	
wkng tr pr ang	alphawt	20.0000	
ref helix angle	beta	0.0000	
base helix ang	betab	0.0000	
prof shift coef	x	0.000	0.000
sum of "" coefs	Sigx	0.000	
bsc rack dedend	hfP/mn	1.250	1.250
bsc rk root rad	rofP/mn	0.250	0.250
residual protub	Spr/mn	0.000	0.000
root chord lgth	sFn/mn	2.177	2.227
bending mom arm	hFa/mn	0.958	0.980
root radius	roF/mn	0.424	0.399
tr contct ratio	epsalpha	1.774	

applicatn factr	KA	1.000	
required life/h		400	
load cycles	NL	1.79E7	1.35E
mesh power/kW	P	5.70	
torque/Nm	T	73.0	96.
tr tang force/N	Ft	993.2	
speed/RPM	n	745.0	561.
pitch line speed/m/s		5.73	
tip relief/µm	Ca	14	
helix modifictn	none		
fav contact pattn posn	verifctn?	n	
wheel web thickness		0.00	
pinion offset	s	0.000	
hx dev elast/µm	fsh	0	
quality grade	q	10	10
hx dev manuf/µm	fma	36	
init'l misal/µm	Fbetax	36	
run-in misal/µm	Fbetay	1	
stiff/(N/mm/µm)	cgamma	20.45	
overlap ratio	epsbeta	0.000	

FACTORS

resonance ratio	N	0.183	
dynamic fct	Kv	1.495	

TOOTH FLANK

face load factr	KHbeta	1.078	
transv load fct	KHalpha	1.348	
zone factor	ZH	2.495	
elasticity fctr	ZE	189.812	
single pair fct	ZB/ZD	1.006	1.000
cont ratio fctr	Zepsilon	0.861	
helix ang factr	Zbeta	1.000	
life factor	ZN	1.258	1.278
lub inf fct	ZLZVZR	0.848	0.857
work-hardng fct	ZW	1.196	
size factor	ZX	1.000	

TOOTH ROOT

face load factr	KFbeta	1.054	1.0
transv load fct	KFalpha	1.486	
form factor	YF	1.221	1.1
stress conc fct	YS	2.286	2.3
notch parameter	qs	2.567	2.7
cont ratio fctr	Yepsilon	0.673	
helix ang factr	Ybeta	1.000	
life factor	YN	0.982	0.9
notch sensy fct	YdrelT	1.002	1.0
surface factor	YRrelT	0.977	0.9
size factor	YX	1.000	1.0

CONTACT STRESS (N/mm²)

allw stress num	sgHlm	327.0	327.0
permiss stress	sigHP	416.9	428.2
"" (reference)	" ref	286.7	286.7
contact stress	sigH	537.6	534.3
safety factor	SH	0.78	0.80
min safety fctr	SHmin	1.00	

BENDING STRESS (N/mm²)

allw stress num	sigFE	174.0	174.
permiss stress	sigFP	119.6	120.
"" (reference)	" ref	121.8	122.
root stress	sigF	144.2	104.
safety factor	SF	1.16	1.6
min safety fctr	SFmin	1.40	

```
**********************************
*      D E S I G N    U N I T    *
*      Gear Technology Centre    *
* User          Cranfield University*
* Organisation Cranfield University*
* Rating to ISO 6336    1 Apr 2005 *
* DU/GRF  ISO Rating  Version 3·5  *
**********************************
file not named
```

pinion material	St		
wheel material	St		
hardness	HV	137	137
material quality		MQ	MQ
roughns flnk/µm	Rz	18.0	18.0
roughns root/µm	Rz	18.0	18.0
viscosity @ 40C	nu	136	
pitting permitted?		yes	yes
reversing duty?		no	no

number of teeth	z	49	65
normal module	mn	3.000	
transvrs module	mt	3.000	
gear ratio	u	1.327	
centres	a	171.00	
facewidth	b	15.00	30.00
reference diam	d	147.00	195.00
base diameter	db	138.13	183.24
tip diameter	da	153.00	201.00
root diameter	df	139.50	187.50
tooth depth	h	6.750	6.750
internal diameter		0.0	0.0
norm pres angle	alphan	20.0000	
transv pres ang	alphat	20.0000	
wkng tr pr ang	alphawt	20.0000	
ref helix angle	beta	0.0000	
base helix ang	betab	0.0000	
prof shift coef	x	0.000	0.000
sum of "" coefs	Sigx	0.000	
bsc rack dedend	hfP/mn	1.250	1.250
bsc rk root rad	rofP/mn	0.250	0.250
residual protub	Spr/mn	0.000	0.000
root chord lgth	sFn/mn	2.177	2.227
bending mom arm	hFa/mn	0.958	0.980
root radius	roF/mn	0.424	0.399
tr contct ratio	epsalpha	1.774	

applicatn factr	KA	1.000	
required life/h		450	
load cycles	NL	2.01E7	1.52E
mesh power/kW	P	5.70	
torque/Nm	T	73.0	96.
tr tang force/N	Ft	993.2	
speed/RPM	n	745.0	561.
pitch line speed/m/s		5.73	
tip relief/µm	Ca	14	
helix modifictn	none		
fav contact pattn posn	verifctn?	n	
wheel web thickness		0.00	
pinion offset	s	0.000	
hx dev elast/µm	fsh	0	
quality grade	q	10	10
hx dev manuf/µm	fma	36	
init'l misal/µm	Fbetax	36	
run-in misal/µm	Fbetay	1	
stiff/(N/mm/µm)	cgamma	20.45	
overlap ratio	epsbeta	0.000	

FACTORS

resonance ratio	N	0.183	
dynamic fct	Kv	1.495	

TOOTH FLANK

face load factr	KHbeta	1.078	
transv load fct	KHalpha	1.348	
zone factor	ZH	2.495	
elasticity fctr	ZE	189.812	
single pair fct	ZB/ZD	1.006	1.000
cont ratio fctr	Zepsilon	0.861	
helix ang factr	Zbeta	1.000	
life factor	ZN	1.249	1.270
lub inf fct	ZLZVZR	0.844	0.853
work-hardng fct	ZW	1.196	
size factor	ZX	1.000	

TOOTH ROOT

face load factr	KFbeta	1.054	1.0
transv load fct	KFalpha	1.486	
form factor	YF	1.221	1.1
stress conc fct	YS	2.286	2.3
notch parameter	qs	2.567	2.7
cont ratio fctr	Yepsilon	0.673	
helix ang factr	Ybeta	1.000	
life factor	YN	0.981	0.9
notch sensy fct	YdrelT	1.002	1.0
surface factor	YRrelT	0.977	0.9
size factor	YX	1.000	1.0

CONTACT STRESS (N/mm²)

allw stress num	sgHlm	327.0	327.0
permiss stress	sigHP	412.3	423.5
"" (reference)	" ref	286.7	286.7
contact stress	sigH	537.6	534.3
safety factor	SH	0.77	0.79
min safety fctr	SHmin	1.00	

BENDING STRESS (N/mm²)

allw stress num	sigFE	174.0	174.
permiss stress	sigFP	119.4	120.
"" (reference)	" ref	121.8	122.
root stress	sigF	144.2	104.
safety factor	SF	1.16	1.6
min safety fctr	SFmin	1.40	

```
**********************************
*      D E S I G N    U N I T    *
*      Gear Technology Centre    *
* User          Cranfield University*
* Organisation Cranfield University*
* Rating to ISO 6336    1 Apr 2005 *
* DU/GRF  ISO Rating  Version 3·5  *
**********************************
file not named
```

pinion material	St		
wheel material	St		
hardness	HV	137	137
material quality		MQ	MQ
roughns flnk/µm	Rz	18.0	18.0
roughns root/µm	Rz	18.0	18.0
viscosity @ 40C	nu	136	
pitting permitted?		yes	yes
reversing duty?		no	no

number of teeth	z	49	65
normal module	mn	3.000	
transvrs module	mt	3.000	
gear ratio	u	1.327	
centres	a	171.00	
facewidth	b	15.00	30.00
reference diam	d	147.00	195.00
base diameter	db	138.13	183.24
tip diameter	da	153.00	201.00
root diameter	df	139.50	187.50
tooth depth	h	6.750	6.750
internal diameter		0.0	0.0
norm pres angle	alphan	20.0000	
transv pres ang	alphat	20.0000	
wkng tr pr ang	alphawt	20.0000	
ref helix angle	beta	0.0000	
base helix ang	betab	0.0000	
prof shift coef	x	0.000	0.000
sum of "" coefs	Sigx	0.000	
bsc rack dedend	hfP/mn	1.250	1.250
bsc rk root rad	rofP/mn	0.250	0.250
residual protub	Spr/mn	0.000	0.000
root chord lgth	sFn/mn	2.177	2.227
bending mom arm	hFa/mn	0.958	0.980
root radius	roF/mn	0.424	0.399
tr contct ratio	epsalpha	1.774	

applicatn factr	KA	1.000	
required life/h		500	
load cycles	NL	2.24E7	1.68E
mesh power/kW	P	5.70	
torque/Nm	T	73.1	96.
tr tang force/N	Ft	994.0	
speed/RPM	n	745.0	561.
pitch line speed/m/s		5.73	
tip relief/µm	Ca	14	
helix modifictn	none		
fav contact pattn posn	verifctn?	n	
wheel web thickness		0.00	
pinion offset	s	0.000	
hx dev elast/µm	fsh	0	
quality grade	q	10	10
hx dev manuf/µm	fma	36	
init'l misal/µm	Fbetax	36	
run-in misal/µm	Fbetay	1	
stiff/(N/mm/µm)	cgamma	20.46	
overlap ratio	epsbeta	0.000	

FACTORS

resonance ratio	N	0.183		dynamic fct	Kv	1.495	
TOOTH FLANK				TOOTH ROOT			
face load factr	KHbeta	1.078		face load factr	KFbeta	1.054	1.0
transv load fct	KHalpha	1.348		transv load fct	KFalpha	1.486	
zone factor	ZH	2.495		form factor	YF	1.221	1.1
elasticity fctr	ZE	189.812		stress conc fct	YS	2.286	2.3
single pair fct	ZB/ZD	1.006	1.000	notch parameter	qs	2.567	2.7
cont ratio fctr	Zepsilon	0.861		cont ratio fctr	Yepsilon	0.673	
helix ang factr	Zbeta	1.000		helix ang factr	Ybeta	1.000	
life factor	ZN	1.242	1.262	life factor	YN	0.980	0.9
lub inf fct	ZLZVZR	0.841	0.850	notch sensy fct	YdrelT	1.002	1.0
work-hardng fct	ZW	1.196		surface factor	YRrelT	0.977	0.9
size factor	ZX	1.000		size factor	YX	1.000	1.0
CONTACT STRESS (N/mm²)				BENDING STRESS (N/mm²)			
allw stress num	sgHlm	327.0	327.0	allw stress num	sigFE	174.0	174.
permiss stress	sigHP	408.2	419.3	permiss stress	sigFP	119.3	120.
"" (reference)	" ref	286.7	286.7	"" (reference)	" ref	121.8	122.
contact stress	sigH	537.8	534.5	root stress	sigF	144.2	104.
safety factor	SH	0.76	0.78	safety factor	SF	1.16	1.6
min safety fctr	SHmin	1.00		min safety fctr	SFmin	1.40	

```
**********************************
*      D E S I G N    U N I T    *
*      Gear Technology Centre    *
* User          Cranfield University*
* Organisation Cranfield University*
* Rating to ISO 6336    1 Apr 2005 *
* DU/GRF  ISO Rating  Version 3·5  *
**********************************
file not named
```

pinion material	St		
wheel material	St		
hardness	HV	137	137
material quality		MQ	MQ
roughns flnk/µm	Rz	18.0	18.0
roughns root/µm	Rz	18.0	18.0
viscosity @ 40C	nu	136	
pitting permitted?		yes	yes
reversing duty?		no	no

number of teeth	z	49	65
normal module	mn	3.000	
transvrs module	mt	3.000	
gear ratio	u	1.327	
centres	a	171.00	
facewidth	b	15.00	30.00
reference diam	d	147.00	195.00
base diameter	db	138.13	183.24
tip diameter	da	153.00	201.00
root diameter	df	139.50	187.50
tooth depth	h	6.750	6.750
internal diameter		0.0	0.0
norm pres angle	alphan	20.0000	
transv pres ang	alphat	20.0000	
wkng tr pr ang	alphawt	20.0000	
ref helix angle	beta	0.0000	
base helix ang	betab	0.0000	
prof shift coef	x	0.000	0.000
sum of "" coefs	Sigx	0.000	
bsc rack dedend	hfP/mn	1.250	1.250
bsc rk root rad	rofP/mn	0.250	0.250
residual protub	Spr/mn	0.000	0.000
root chord lgth	sFn/mn	2.177	2.227
bending mom arm	hFa/mn	0.958	0.980
root radius	roF/mn	0.424	0.399
tr contct ratio	epsalpha	1.774	

applicatn factr	KA	1.000	
required life/h		0	
load cycles	NL	0.00E0	0.00E
mesh power/kW	P	11.47	
torque/Nm	T	147.0	195.
tr tang force/N	Ft	2000.3	
speed/RPM	n	745.0	561.
pitch line speed/m/s		5.73	
tip relief/µm	Ca	14	
helix modifictn	none		
fav contact pattn posn	verifctn?	n	
wheel web thickness		0.00	
pinion offset	s	0.000	
hx dev elast/µm	fsh	0	
quality grade	q	10	10
hx dev manuf/µm	fma	36	
init'l misal/µm	Fbetax	36	
run-in misal/µm	Fbetay	1	
stiff/(N/mm/µm)	cgamma	22.67	
overlap ratio	epsbeta	0.000	

FACTORS

resonance ratio	N	0.174	
dynamic fct	Kv	1.277	

TOOTH FLANK

face load factr	KHbeta	1.051	
transv load fct	KHalpha	1.348	
zone factor	ZH	2.495	
elasticity fctr	ZE	189.812	
single pair fct	ZB/ZD	1.006	1.000
cont ratio fctr	Zepsilon	0.861	
helix ang factr	Zbeta	1.000	
life factor	ZN	1.600	1.600
lub inf fct	ZLZVZR	1.000	1.000
work-hardng fct	ZW	1.196	
size factor	ZX	1.000	

TOOTH ROOT

face load factr	KFbeta	1.035	1.0
transv load fct	KFalpha	1.486	
form factor	YF	1.221	1.1
stress conc fct	YS	2.286	2.3
notch parameter	qs	2.567	2.7
cont ratio fctr	Yepsilon	0.673	
helix ang factr	Ybeta	1.000	
life factor	YN	1.600	1.6
notch sensy fct	YdrelT	1.128	1.1
surface factor	YRrelT	1.000	1.0
size factor	YX	1.000	1.0

CONTACT STRESS (N/mm²)

allw stress num	sgHlm	327.0	327.0
permiss stress	sigHP	625.7	625.7
"" (reference)	" ref	286.7	286.7
contact stress	sigH	696.1	691.8
safety factor	SH	0.90	0.90
min safety fctr	SHmin	1.00	

BENDING STRESS (N/mm²)

allw stress num	sigFE	174.0	174.
permiss stress	sigFP	224.3	232.
"" (reference)	" ref	121.8	122.
root stress	sigF	243.6	176.
safety factor	SF	1.29	1.8
min safety fctr	SFmin	1.40	

```
**********************************
*      D E S I G N    U N I T    *
*      Gear Technology Centre    *
* User          Cranfield University*
* Organisation Cranfield University*
* Rating to ISO 6336    1 Apr 2005 *
* DU/GRF  ISO Rating  Version 3·5  *
**********************************
file not named
```

pinion material	St		
wheel material	St		
hardness	HV	137	137
material quality		MQ	MQ
roughns flnk/µm	Rz	18.0	18.0
roughns root/µm	Rz	18.0	18.0
viscosity @ 40C	nu	136	
pitting permitted?		yes	yes
reversing duty?		no	no

number of teeth	z	49	65
normal module	mn	3.000	
transvrs module	mt	3.000	
gear ratio	u	1.327	
centres	a	171.00	
facewidth	b	15.00	30.00
reference diam	d	147.00	195.00
base diameter	db	138.13	183.24
tip diameter	da	153.00	201.00
root diameter	df	139.50	187.50
tooth depth	h	6.750	6.750
internal diameter		0.0	0.0
norm pres angle	alphan	20.0000	
transv pres ang	alphat	20.0000	
wkng tr pr ang	alphawt	20.0000	
ref helix angle	beta	0.0000	
base helix ang	betab	0.0000	
prof shift coef	x	0.000	0.000
sum of "" coefs	Sigx	0.000	
bsc rack dedend	hfP/mn	1.250	1.250
bsc rk root rad	rofP/mn	0.250	0.250
residual protub	Spr/mn	0.000	0.000
root chord lgth	sFn/mn	2.177	2.227
bending mom arm	hFa/mn	0.958	0.980
root radius	roF/mn	0.424	0.399
tr contct ratio	epsalpha	1.774	

applicatn factr	KA	1.000	
required life/h		10	
load cycles	NL	4.47E5	3.37E
mesh power/kW	P	11.47	
torque/Nm	T	147.0	195.
tr tang force/N	Ft	2000.3	
speed/RPM	n	745.0	561.
pitch line speed/m/s		5.73	
tip relief/µm	Ca	14	
helix modifictn	none		
fav contact pattn posn	verifctn?	n	
wheel web thickness		0.00	
pinion offset	s	0.000	
hx dev elast/µm	fsh	0	
quality grade	q	10	10
hx dev manuf/µm	fma	36	
init'l misal/µm	Fbetax	36	
run-in misal/µm	Fbetay	1	
stiff/(N/mm/µm)	cgamma	22.67	
overlap ratio	epsbeta	0.000	

FACTORS

resonance ratio	N	0.174	
dynamic fct	Kv	1.277	

TOOTH FLANK

face load factr	KHbeta	1.051	
transv load fct	KHalpha	1.348	
zone factor	ZH	2.495	
elasticity fctr	ZE	189.812	
single pair fct	ZB/ZD	1.006	1.000
cont ratio fctr	Zepsilon	0.861	
helix ang factr	Zbeta	1.000	
life factor	ZN	1.600	1.600
lub inf fct	ZLZVZR	1.000	1.000
work-hardng fct	ZW	1.196	
size factor	ZX	1.000	

TOOTH ROOT

face load factr	KFbeta	1.035	1.0
transv load fct	KFalpha	1.486	
form factor	YF	1.221	1.1
stress conc fct	YS	2.286	2.3
notch parameter	qs	2.567	2.7
cont ratio fctr	Yepsilon	0.673	
helix ang factr	Ybeta	1.000	
life factor	YN	1.118	1.1
notch sensy fct	YdrelT	1.031	1.0
surface factor	YRrelT	0.983	0.9
size factor	YX	1.000	1.0

CONTACT STRESS (N/mm²)

allw stress num	sgHlm	327.0	327.0
permiss stress	sigHP	625.7	625.7
"" (reference)	" ref	286.7	286.7
contact stress	sigH	696.1	691.8
safety factor	SH	0.90	0.90
min safety fctr	SHmin	1.00	

BENDING STRESS (N/mm²)

allw stress num	sigFE	174.0	174.
permiss stress	sigFP	140.8	146.
"" (reference)	" ref	121.8	122.
root stress	sigF	243.6	176.
safety factor	SF	0.81	1.1
min safety fctr	SFmin	1.40	

```
**********************************
*      D E S I G N    U N I T    *
*      Gear Technology Centre    *
* User          Cranfield University*
* Organisation Cranfield University*
* Rating to ISO 6336    1 Apr 2005 *
* DU/GRF  ISO Rating  Version 3·5  *
**********************************
file not named
```

pinion material	St		
wheel material	St		
hardness	HV	137	137
material quality		MQ	MQ
roughns flnk/µm	Rz	18.0	18.0
roughns root/µm	Rz	18.0	18.0
viscosity @ 40C	nu	136	
pitting permitted?		yes	yes
reversing duty?		no	no

number of teeth	z	49	65
normal module	mn	3.000	
transvrs module	mt	3.000	
gear ratio	u	1.327	
centres	a	171.00	
facewidth	b	15.00	30.00
reference diam	d	147.00	195.00
base diameter	db	138.13	183.24
tip diameter	da	153.00	201.00
root diameter	df	139.50	187.50
tooth depth	h	6.750	6.750
internal diameter		0.0	0.0
norm pres angle	alphan	20.0000	
transv pres ang	alphat	20.0000	
wkng tr pr ang	alphawt	20.0000	
ref helix angle	beta	0.0000	
base helix ang	betab	0.0000	
prof shift coef	x	0.000	0.000
sum of "" coefs	Sigx	0.000	
bsc rack dedend	hfP/mn	1.250	1.250
bsc rk root rad	rofP/mn	0.250	0.250
residual protub	Spr/mn	0.000	0.000
root chord lgth	sFn/mn	2.177	2.227
bending mom arm	hFa/mn	0.958	0.980
root radius	roF/mn	0.424	0.399
tr contct ratio	epsalpha	1.774	

applicatn factr	KA	1.000	
required life/h		20	
load cycles	NL	8.94E5	6.74E
mesh power/kW	P	11.47	
torque/Nm	T	147.0	195.
tr tang force/N	Ft	2000.3	
speed/RPM	n	745.0	561.
pitch line speed/m/s		5.73	
tip relief/µm	Ca	14	
helix modifictn		none	
fav contact pattn posn verifctn?		n	
wheel web thickness		0.00	
pinion offset	s	0.000	
hx dev elast/µm	fsh	0	
quality grade	q	10	10
hx dev manuf/µm	fma	36	
init'l misal/µm	Fbetax	36	
run-in misal/µm	Fbetay	1	
stiff/(N/mm/µm)	cgamma	22.67	
overlap ratio	epsbeta	0.000	

FACTORS

resonance ratio	N	0.174	
dynamic fct	Kv	1.277	

TOOTH FLANK

face load factr	KHbeta	1.051	
transv load fct	KHalpha	1.348	
zone factor	ZH	2.495	
elasticity fctr	ZE	189.812	
single pair fct	ZB/ZD	1.006	1.000
cont ratio fctr	Zepsilon	0.861	
helix ang factr	Zbeta	1.000	
life factor	ZN	1.554	1.586
lub inf fct	ZLZVZR	0.979	0.994
work-hardng fct	ZW	1.196	
size factor	ZX	1.000	

TOOTH ROOT

face load factr	KFbeta	1.035	1.0
transv load fct	KFalpha	1.486	
form factor	YF	1.221	1.1
stress conc fct	YS	2.286	2.3
notch parameter	qs	2.567	2.7
cont ratio fctr	Yepsilon	0.673	
helix ang factr	Ybeta	1.000	
life factor	YN	1.074	1.0
notch sensy fct	YdrelT	1.020	1.0
surface factor	YRrelT	0.981	0.9
size factor	YX	1.000	1.0

CONTACT STRESS (N/mm²)

allw stress num	sgHlm	327.0	327.0
permiss stress	sigHP	595.0	616.6
"" (reference)	" ref	286.7	286.7
contact stress	sigH	696.1	691.8
safety factor	SH	0.85	0.89
min safety fctr	SHmin	1.00	

BENDING STRESS (N/mm²)

allw stress num	sigFE	174.0	174.
permiss stress	sigFP	133.6	138.
"" (reference)	" ref	121.8	122.
root stress	sigF	243.6	176.
safety factor	SF	0.77	1.1
min safety fctr	SFmin	1.40	

```
**********************************
*      D E S I G N    U N I T    *
*      Gear Technology Centre    *
* User          Cranfield University*
* Organisation Cranfield University*
* Rating to ISO 6336    1 Apr 2005 *
* DU/GRF  ISO Rating  Version 3·5  *
**********************************
file not named
```

pinion material	St		
wheel material	St		
hardness	HV	137	137
material quality		MQ	MQ
roughns flnk/µm	Rz	18.0	18.0
roughns root/µm	Rz	18.0	18.0
viscosity @ 40C	nu	136	
pitting permitted?		yes	yes
reversing duty?		no	no

number of teeth	z	49	65
normal module	mn	3.000	
transvrs module	mt	3.000	
gear ratio	u	1.327	
centres	a	171.00	
facewidth	b	15.00	30.00
reference diam	d	147.00	195.00
base diameter	db	138.13	183.24
tip diameter	da	153.00	201.00
root diameter	df	139.50	187.50
tooth depth	h	6.750	6.750
internal diameter		0.0	0.0
norm pres angle	alphan	20.0000	
transv pres ang	alphat	20.0000	
wkng tr pr ang	alphawt	20.0000	
ref helix angle	beta	0.0000	
base helix ang	betab	0.0000	
prof shift coef	x	0.000	0.000
sum of "" coefs	Sigx	0.000	
bsc rack dedend	hfP/mn	1.250	1.250
bsc rk root rad	rofP/mn	0.250	0.250
residual protub	Spr/mn	0.000	0.000
root chord lgth	sFn/mn	2.177	2.227
bending mom arm	hFa/mn	0.958	0.980
root radius	roF/mn	0.424	0.399
tr contct ratio	epsalpha	1.774	

applicatn factr	KA	1.000	
required life/h		50	
load cycles	NL	2.24E6	1.68E
mesh power/kW	P	11.47	
torque/Nm	T	147.0	195.
tr tang force/N	Ft	2000.3	
speed/RPM	n	745.0	561.
pitch line speed/m/s		5.73	
tip relief/µm	Ca	14	
helix modifictn	none		
fav contact pattn posn	verifctn?	n	
wheel web thickness		0.00	
pinion offset	s	0.000	
hx dev elast/µm	fsh	0	
quality grade	q	10	10
hx dev manuf/µm	fma	36	
init'l misal/µm	Fbetax	36	
run-in misal/µm	Fbetay	1	
stiff/(N/mm/µm)	cgamma	22.67	
overlap ratio	epsbeta	0.000	

FACTORS

resonance ratio	N	0.174	
dynamic fct	Kv	1.277	

TOOTH FLANK

face load factr	KHbeta	1.051	
transv load fct	KHalpha	1.348	
zone factor	ZH	2.495	
elasticity fctr	ZE	189.812	
single pair fct	ZB/ZD	1.006	1.000
cont ratio fctr	Zepsilon	0.861	
helix ang factr	Zbeta	1.000	
life factor	ZN	1.452	1.483
lub inf fct	ZLZVZR	0.934	0.948
work-hardng fct	ZW	1.196	
size factor	ZX	1.000	

TOOTH ROOT

face load factr	KFbeta	1.035	1.0
transv load fct	KFalpha	1.486	
form factor	YF	1.221	1.1
stress conc fct	YS	2.286	2.3
notch parameter	qs	2.567	2.7
cont ratio fctr	Yepsilon	0.673	
helix ang factr	Ybeta	1.000	
life factor	YN	1.017	1.0
notch sensy fct	YdrelT	1.007	1.0
surface factor	YRrelT	0.978	0.9
size factor	YX	1.000	1.0

CONTACT STRESS (N/mm²)

allw stress num	sgHlm	327.0	327.0
permiss stress	sigHP	530.4	549.5
"" (reference)	" ref	286.7	286.7
contact stress	sigH	696.1	691.8
safety factor	SH	0.76	0.79
min safety fctr	SHmin	1.00	

BENDING STRESS (N/mm²)

allw stress num	sigFE	174.0	174.
permiss stress	sigFP	124.5	128.
"" (reference)	" ref	121.8	122.
root stress	sigF	243.6	176.
safety factor	SF	0.72	1.0
min safety fctr	SFmin	1.40	

```
**********************************
*      D E S I G N    U N I T    *
*      Gear Technology Centre    *
* User          Cranfield University*
* Organisation Cranfield University*
* Rating to ISO 6336    1 Apr 2005 *
* DU/GRF  ISO Rating  Version 3·5  *
**********************************
file not named
```

pinion material	St		
wheel material	St		
hardness	HV	137	137
material quality		MQ	MQ
roughns flnk/µm	Rz	18.0	18.0
roughns root/µm	Rz	18.0	18.0
viscosity @ 40C	nu	136	
pitting permitted?		yes	yes
reversing duty?		no	no

number of teeth	z	49	65
normal module	mn	3.000	
transvrs module	mt	3.000	
gear ratio	u	1.327	
centres	a	171.00	
facewidth	b	15.00	30.00
reference diam	d	147.00	195.00
base diameter	db	138.13	183.24
tip diameter	da	153.00	201.00
root diameter	df	139.50	187.50
tooth depth	h	6.750	6.750
internal diameter		0.0	0.0
norm pres angle	alphan	20.0000	
transv pres ang	alphat	20.0000	
wkng tr pr ang	alphawt	20.0000	
ref helix angle	beta	0.0000	
base helix ang	betab	0.0000	
prof shift coef	x	0.000	0.000
sum of "" coefs	Sigx	0.000	
bsc rack dedend	hfP/mn	1.250	1.250
bsc rk root rad	rofP/mn	0.250	0.250
residual protub	Spr/mn	0.000	0.000
root chord lgth	sFn/mn	2.177	2.227
bending mom arm	hFa/mn	0.958	0.980
root radius	roF/mn	0.424	0.399
tr contct ratio	epsalpha	1.774	

applicatn factr	KA	1.000	
required life/h		80	
load cycles	NL	3.58E6	2.70E
mesh power/kW	P	11.47	
torque/Nm	T	147.0	195.
tr tang force/N	Ft	2000.3	
speed/RPM	n	745.0	561.
pitch line speed/m/s		5.73	
tip relief/µm	Ca	14	
helix modifictn	none		
fav contact pattn posn	verifctn?	n	
wheel web thickness		0.00	
pinion offset	s	0.000	
hx dev elast/µm	fsh	0	
quality grade	q	10	10
hx dev manuf/µm	fma	36	
init'l misal/µm	Fbetax	36	
run-in misal/µm	Fbetay	1	
stiff/(N/mm/µm)	cgamma	22.67	
overlap ratio	epsbeta	0.000	

FACTORS

resonance ratio	N	0.174	
dynamic fct	Kv	1.277	

TOOTH FLANK

face load factr	KHbeta	1.051	
transv load fct	KHalpha	1.348	
zone factor	ZH	2.495	
elasticity fctr	ZE	189.812	
single pair fct	ZB/ZD	1.006	1.000
cont ratio fctr	Zepsilon	0.861	
helix ang factr	Zbeta	1.000	
life factor	ZN	1.403	1.432
lub inf fct	ZLZVZR	0.912	0.925
work-hardng fct	ZW	1.196	
size factor	ZX	1.000	

TOOTH ROOT

face load factr	KFbeta	1.035	1.0
transv load fct	KFalpha	1.486	
form factor	YF	1.221	1.1
stress conc fct	YS	2.286	2.3
notch parameter	qs	2.567	2.7
cont ratio fctr	Yepsilon	0.673	
helix ang factr	Ybeta	1.000	
life factor	YN	0.998	1.0
notch sensy fct	YdrelT	1.002	1.0
surface factor	YRrelT	0.977	0.9
size factor	YX	1.000	1.0

CONTACT STRESS (N/mm²)

allw stress num	sgHlm	327.0	327.0
permiss stress	sigHP	500.3	518.2
"" (reference)	" ref	286.7	286.7
contact stress	sigH	696.1	691.8
safety factor	SH	0.72	0.75
min safety fctr	SHmin	1.00	

BENDING STRESS (N/mm²)

allw stress num	sigFE	174.0	174.
permiss stress	sigFP	121.6	123.
"" (reference)	" ref	121.8	122.
root stress	sigF	243.6	176.
safety factor	SF	0.70	0.9
min safety fctr	SFmin	1.40	

```
**********************************
*      D E S I G N    U N I T    *
*      Gear Technology Centre    *
* User          Cranfield University*
* Organisation Cranfield University*
* Rating to ISO 6336    1 Apr 2005 *
* DU/GRF  ISO Rating  Version 3·5  *
**********************************
file not named
```

pinion material	St							
wheel material	St							
hardness	HV	137	137					
material quality		MQ	MQ					
roughns flnk/µm	Rz	18.0	18.0					
roughns root/µm	Rz	18.0	18.0					
viscosity @ 40C	nu	136						
pitting permitted?		yes	yes					
reversing duty?		no	no					
applicatn factr	KA	1.000						
required life/h		100						
load cycles	NL	4.47E6	3.37E					
mesh power/kW	P	11.47						
torque/Nm	T	147.0	195.					
tr tang force/N	Ft	2000.0						
speed/RPM	n	745.0	561.					
pitch line speed/m/s		5.73						
tip relief/µm	Ca	14						
helix modifictn	none							
fav contact pattn posn		verifctn?	n					
wheel web thickness		0.00						
pinion offset	s	0.000						

number of teeth	z	49	65					
normal module	mn	3.000						
transvrs module	mt	3.000						
gear ratio	u	1.327						
centres	a	171.00						
facewidth	b	15.00	30.00					
reference diam	d	147.00	195.00					
base diameter	db	138.13	183.24					
tip diameter	da	153.00	201.00					
root diameter	df	139.50	187.50					
tooth depth	h	6.750	6.750					
internal diameter		0.0	0.0					
norm pres angle	alphan	20.0000						
transv pres ang	alphat	20.0000						
wkng tr pr ang	alphawt	20.0000						
ref helix angle	beta	0.0000						
base helix ang	betab	0.0000						
prof shift coef	x	0.000	0.000					
sum of "" coefs	Sigx	0.000						
bsc rack dedend	hfP/mn	1.250	1.250					
bsc rk root rad	rofP/mn	0.250	0.250					
residual protub	Spr/mn	0.000	0.000					
root chord lgth	sFn/mn	2.177	2.227					
bending mom arm	hFa/mn	0.958	0.980					
root radius	roF/mn	0.424	0.399					
tr contct ratio	epsalpha	1.774						

hx dev elast/µm	fsh	0						
quality grade	q	10	10					
hx dev manuf/µm	fma	36						
init'l misal/µm	Fbetax	36						
run-in misal/µm	Fbetay	1						
stiff/(N/mm/µm)	cgamma	22.67						
overlap ratio	epsbeta	0.000						

FACTORS

resonance ratio	N	0.174						
dynamic fct	Kv	1.277						

TOOTH FLANK

face load factr	KHbeta	1.051						
transv load fct	KHalpha	1.348						
zone factor	ZH	2.495						
elasticity fctr	ZE	189.812						
single pair fct	ZB/ZD	1.006	1.000					
cont ratio fctr	Zepsilon	0.861						
helix ang factr	Zbeta	1.000						
life factor	ZN	1.380	1.409					
lub inf fct	ZLZVZR	0.902	0.915					
work-hardng fct	ZW	1.196						
size factor	ZX	1.000						

TOOTH ROOT

face load factr	KFbeta	1.035	1.0					
transv load fct	KFalpha	1.486						
form factor	YF	1.221	1.1					
stress conc fct	YS	2.286	2.3					
notch parameter	qs	2.567	2.7					
cont ratio fctr	Yepsilon	0.673						
helix ang factr	Ybeta	1.000						
life factor	YN	0.996	0.9					
notch sensy fct	YdrelT	1.002	1.0					
surface factor	YRrelT	0.977	0.9					
size factor	YX	1.000	1.0					

CONTACT STRESS (N/mm²)

allw stress num	sgHlm	327.0	327.0					
permiss stress	sigHP	486.6	504.0					
"" (reference)	" ref	286.7	286.7					
contact stress	sigH	696.1	691.8					
safety factor	SH	0.70	0.73					
min safety fctr	SHmin	1.00						

BENDING STRESS (N/mm²)

allw stress num	sigFE	174.0	174.					
permiss stress	sigFP	121.3	122.					
"" (reference)	" ref	121.8	122.					
root stress	sigF	243.6	176.					
safety factor	SF	0.70	0.9					
min safety fctr	SFmin	1.40						

```
**********************************
*      D E S I G N   U N I T     *
*      Gear Technology Centre    *
* User          Cranfield University*
* Organisation Cranfield University*
* Rating to ISO 6336    1 Apr 2005 *
* DU/GRF  ISO Rating  Version 3·5  *
**********************************
file not named
```

pinion material	St		
wheel material	St		
hardness	HV	137	137
material quality		MQ	MQ
roughns flnk/µm	Rz	18.0	18.0
roughns root/µm	Rz	18.0	18.0
viscosity @ 40C	nu	136	
pitting permitted?		yes	yes
reversing duty?		no	no

number of teeth	z	49	65
normal module	mn	3.000	
transvrs module	mt	3.000	
gear ratio	u	1.327	
centres	a	171.00	
facewidth	b	15.00	30.00
reference diam	d	147.00	195.00
base diameter	db	138.13	183.24
tip diameter	da	153.00	201.00
root diameter	df	139.50	187.50
tooth depth	h	6.750	6.750
internal diameter		0.0	0.0
norm pres angle	alphan	20.0000	
transv pres ang	alphat	20.0000	
wkng tr pr ang	alphawt	20.0000	
ref helix angle	beta	0.0000	
base helix ang	betab	0.0000	
prof shift coef	x	0.000	0.000
sum of "" coefs	Sigx	0.000	
bsc rack dedend	hfP/mn	1.250	1.250
bsc rk root rad	rofP/mn	0.250	0.250
residual protub	Spr/mn	0.000	0.000
root chord lgth	sFn/mn	2.177	2.227
bending mom arm	hFa/mn	0.958	0.980
root radius	roF/mn	0.424	0.399
tr contct ratio	epsalpha	1.774	

applicatn factr	KA	1.000	
required life/h		150	
load cycles	NL	6.71E6	5.05E
mesh power/kW	P	11.47	
torque/Nm	T	147.0	195.
tr tang force/N	Ft	2000.0	
speed/RPM	n	745.0	561.
pitch line speed/m/s		5.73	
tip relief/µm	Ca	14	
helix modifictn	none		
fav contact pattn posn	verifctn?	n	
wheel web thickness		0.00	
pinion offset	s	0.000	
hx dev elast/µm	fsh	0	
quality grade	q	10	10
hx dev manuf/µm	fma	36	
init'l misal/µm	Fbetax	36	
run-in misal/µm	Fbetay	1	
stiff/(N/mm/µm)	cgamma	22.67	
overlap ratio	epsbeta	0.000	

FACTORS

resonance ratio	N	0.174		dynamic fct	Kv	1.277	
TOOTH FLANK				TOOTH ROOT			
face load factr	KHbeta	1.051		face load factr	KFbeta	1.035	1.0
transv load fct	KHalpha	1.348		transv load fct	KFalpha	1.486	
zone factor	ZH	2.495		form factor	YF	1.221	1.1
elasticity fctr	ZE	189.812		stress conc fct	YS	2.286	2.3
single pair fct	ZB/ZD	1.006	1.000	notch parameter	qs	2.567	2.7
cont ratio fctr	Zepsilon	0.861		cont ratio fctr	Yepsilon	0.673	
helix ang factr	Zbeta	1.000		helix ang factr	Ybeta	1.000	
life factor	ZN	1.339	1.367	life factor	YN	0.992	0.9
lub inf fct	ZLZVZR	0.884	0.896	notch sensy fct	YdrelT	1.002	1.0
work-hardng fct	ZW	1.196		surface factor	YRrelT	0.977	0.9
size factor	ZX	1.000		size factor	YX	1.000	1.0
CONTACT STRESS (N/mm²)				BENDING STRESS (N/mm²)			
allw stress num	sgHlm	327.0	327.0	allw stress num	sigFE	174.0	174.
permiss stress	sigHP	462.8	479.2	permiss stress	sigFP	120.8	122.
"" (reference)	" ref	286.7	286.7	"" (reference)	" ref	121.8	122.
contact stress	sigH	696.1	691.8	root stress	sigF	243.6	176.
safety factor	SH	0.66	0.69	safety factor	SF	0.69	0.9
min safety fctr	SHmin	1.00		min safety fctr	SFmin	1.40	

```
**********************************
*      D E S I G N    U N I T    *
*      Gear Technology Centre    *
* User          Cranfield University*
* Organisation Cranfield University*
* Rating to ISO 6336    1 Apr 2005 *
* DU/GRF  ISO Rating  Version 3·5  *
**********************************
file not named
```

pinion material	St							
wheel material	St							
hardness	HV	137	137					
material quality		MQ	MQ					
roughns flnk/µm	Rz	18.0	18.0					
roughns root/µm	Rz	18.0	18.0					
viscosity @ 40C	nu	136						
pitting permitted?		yes	yes					
reversing duty?		no	no					
applicatn factr	KA	1.000						
required life/h		200						
load cycles	NL	8.94E6	6.74E					
mesh power/kW	P	11.47						
torque/Nm	T	147.0	195.					
tr tang force/N	Ft	2000.0						
speed/RPM	n	745.0	561.					
pitch line speed/m/s		5.73						
tip relief/µm	Ca	14						
helix modifictn	none							
fav contact pattn posn		verifctn?	n					
wheel web thickness		0.00						
pinion offset	s	0.000						

number of teeth	z	49	65
normal module	mn	3.000	
transvrs module	mt	3.000	
gear ratio	u	1.327	
centres	a	171.00	
facewidth	b	15.00	30.00
reference diam	d	147.00	195.00
base diameter	db	138.13	183.24
tip diameter	da	153.00	201.00
root diameter	df	139.50	187.50
tooth depth	h	6.750	6.750
internal diameter		0.0	0.0
norm pres angle	alphan	20.0000	
transv pres ang	alphat	20.0000	
wkng tr pr ang	alphawt	20.0000	
ref helix angle	beta	0.0000	
base helix ang	betab	0.0000	
prof shift coef	x	0.000	0.000
sum of "" coefs	Sigx	0.000	
bsc rack dedend	hfP/mn	1.250	1.250
bsc rk root rad	rofP/mn	0.250	0.250
residual protub	Spr/mn	0.000	0.000
root chord lgth	sFn/mn	2.177	2.227
bending mom arm	hFa/mn	0.958	0.980
root radius	roF/mn	0.424	0.399
tr contct ratio	epsalpha	1.774	

hx dev elast/µm	fsh	0					
quality grade	q	10	10				
hx dev manuf/µm	fma	36					
init'l misal/µm	Fbetax	36					
run-in misal/µm	Fbetay	1					
stiff/(N/mm/µm)	cgamma	22.67					
overlap ratio	epsbeta	0.000					

FACTORS

resonance ratio	N	0.174		dynamic fct	Kv	1.277	
TOOTH FLANK				TOOTH ROOT			
face load factr	KHbeta	1.051		face load factr	KFbeta	1.035	1.0
transv load fct	KHalpha	1.348		transv load fct	KFalpha	1.486	
zone factor	ZH	2.495		form factor	YF	1.221	1.1
elasticity fctr	ZE	189.812		stress conc fct	YS	2.286	2.3
single pair fct	ZB/ZD	1.006	1.000	notch parameter	qs	2.567	2.7
cont ratio fctr	Zepsilon	0.861		cont ratio fctr	Yepsilon	0.673	
helix ang factr	Zbeta	1.000		helix ang factr	Ybeta	1.000	
life factor	ZN	1.311	1.338	life factor	YN	0.989	0.9
lub inf fct	ZLZVZR	0.871	0.884	notch sensy fct	YdrelT	1.002	1.0
work-hardng fct	ZW	1.196		surface factor	YRrelT	0.977	0.9
size factor	ZX	1.000		size factor	YX	1.000	1.0
CONTACT STRESS (N/mm²)				BENDING STRESS (N/mm²)			
allw stress num	sgHlm	327.0	327.0	allw stress num	sigFE	174.0	174.
permiss stress	sigHP	446.6	462.5	permiss stress	sigFP	120.4	121.
"" (reference)	" ref	286.7	286.7	"" (reference)	" ref	121.8	122.
contact stress	sigH	696.1	691.8	root stress	sigF	243.6	176.
safety factor	SH	0.64	0.67	safety factor	SF	0.69	0.9
min safety fctr	SHmin	1.00		min safety fctr	SFmin	1.40	

```
**********************************
*      D E S I G N    U N I T    *
*      Gear Technology Centre    *
* User          Cranfield University*
* Organisation Cranfield University*
* Rating to ISO 6336    1 Apr 2005 *
* DU/GRF  ISO Rating  Version 3·5  *
**********************************
file not named
```

pinion material	St		
wheel material	St		
hardness	HV	137	137
material quality		MQ	MQ
roughns flnk/µm	Rz	18.0	18.0
roughns root/µm	Rz	18.0	18.0
viscosity @ 40C	nu	136	
pitting permitted?		yes	yes
reversing duty?		no	no

applicatn factr	KA	1.000	
required life/h		250	
load cycles	NL	1.12E7	8.42E
mesh power/kW	P	11.47	
torque/Nm	T	147.0	195.
tr tang force/N	Ft	2000.0	
speed/RPM	n	745.0	561.
pitch line speed/m/s		5.73	
tip relief/µm	Ca	14	
helix modifictn	none		
fav contact pattn posn	verifctn?	n	
wheel web thickness		0.00	
pinion offset	s	0.000	
hx dev elast/µm	fsh	0	
quality grade	q	10	10
hx dev manuf/µm	fma	36	
init'l misal/µm	Fbetax	36	
run-in misal/µm	Fbetay	1	
stiff/(N/mm/µm)	cgamma	22.67	

number of teeth	z	49	65
normal module	mn	3.000	
transvrs module	mt	3.000	
gear ratio	u	1.327	
centres	a	171.00	
facewidth	b	15.00	30.00
reference diam	d	147.00	195.00
base diameter	db	138.13	183.24
tip diameter	da	153.00	201.00
root diameter	df	139.50	187.50
tooth depth	h	6.750	6.750
internal diameter		0.0	0.0
norm pres angle	alphan	20.0000	
transv pres ang	alphat	20.0000	
wkng tr pr ang	alphawt	20.0000	
ref helix angle	beta	0.0000	
base helix ang	betab	0.0000	
prof shift coef	x	0.000	0.000
sum of "" coefs	Sigx	0.000	
bsc rack dedend	hfP/mn	1.250	1.250
bsc rk root rad	rofP/mn	0.250	0.250
residual protub	Spr/mn	0.000	0.000
root chord lgth	sFn/mn	2.177	2.227
bending mom arm	hFa/mn	0.958	0.980
root radius	roF/mn	0.424	0.399
tr contct ratio	epsalpha	1.774	
overlap ratio	epsbeta	0.000	

FACTORS

resonance ratio	N	0.174	
dynamic fct	Kv	1.277	

TOOTH FLANK

face load factr	KHbeta	1.051	
transv load fct	KHalpha	1.348	
zone factor	ZH	2.495	
elasticity fctr	ZE	189.812	
single pair fct	ZB/ZD	1.006	1.000
cont ratio fctr	Zepsilon	0.861	
helix ang factr	Zbeta	1.000	
life factor	ZN	1.292	1.317
lub inf fct	ZLZVZR	0.863	0.874
work-hardng fct	ZW	1.196	
size factor	ZX	1.000	

TOOTH ROOT

face load factr	KFbeta	1.035	1.0
transv load fct	KFalpha	1.486	
form factor	YF	1.221	1.1
stress conc fct	YS	2.286	2.3
notch parameter	qs	2.567	2.7
cont ratio fctr	Yepsilon	0.673	
helix ang factr	Ybeta	1.000	
life factor	YN	0.987	0.9
notch sensy fct	YdrelT	1.002	1.0
surface factor	YRrelT	0.977	0.9
size factor	YX	1.000	1.0

CONTACT STRESS (N/mm²)

allw stress num	sgHlm	327.0	327.0
permiss stress	sigHP	435.9	449.9
"" (reference)	" ref	286.7	286.7
contact stress	sigH	696.1	691.8
safety factor	SH	0.63	0.65
min safety fctr	SHmin	1.00	

BENDING STRESS (N/mm²)

allw stress num	sigFE	174.0	174.
permiss stress	sigFP	120.1	121.
"" (reference)	" ref	121.8	122.
root stress	sigF	243.6	176.
safety factor	SF	0.69	0.9
min safety fctr	SFmin	1.40	

```
**********************************
*      D E S I G N    U N I T    *
*      Gear Technology Centre    *
* User          Cranfield University*
* Organisation Cranfield University*
* Rating to ISO 6336    1 Apr 2005 *
* DU/GRF  ISO Rating  Version 3·5  *
**********************************
file not named
```

pinion material	St		
wheel material	St		
hardness	HV	137	137
material quality		MQ	MQ
roughns flnk/µm	Rz	18.0	18.0
roughns root/µm	Rz	18.0	18.0
viscosity @ 40C	nu	136	
pitting permitted?		yes	yes
reversing duty?		no	no

applicatn factr	KA	1.000	
required life/h		300	
load cycles	NL	1.34E7	1.01E
mesh power/kW	P	11.47	
torque/Nm	T	147.0	195.
tr tang force/N	Ft	2000.0	
speed/RPM	n	745.0	561.
pitch line speed/m/s		5.73	
tip relief/µm	Ca	14	
helix modifictn	none		
fav contact pattn posn	verifctn?	n	
wheel web thickness		0.00	
pinion offset	s	0.000	

number of teeth	z	49	65
normal module	mn	3.000	
transvrs module	mt	3.000	
gear ratio	u	1.327	
centres	a	171.00	
facewidth	b	15.00	30.00
reference diam	d	147.00	195.00
base diameter	db	138.13	183.24
tip diameter	da	153.00	201.00
root diameter	df	139.50	187.50
tooth depth	h	6.750	6.750
internal diameter		0.0	0.0
norm pres angle	alphan	20.0000	
transv pres ang	alphat	20.0000	
wkng tr pr ang	alphawt	20.0000	
ref helix angle	beta	0.0000	
base helix ang	betab	0.0000	
prof shift coef	x	0.000	0.000
sum of "" coefs	Sigx	0.000	
bsc rack dedend	hfP/mn	1.250	1.250
bsc rk root rad	rofP/mn	0.250	0.250
residual protub	Spr/mn	0.000	0.000
root chord lgth	sFn/mn	2.177	2.227
bending mom arm	hFa/mn	0.958	0.980
root radius	roF/mn	0.424	0.399
tr contct ratio	epsalpha	1.774	

hx dev elast/µm	fsh	0	
quality grade	q	10	10
hx dev manuf/µm	fma	36	
init'l misal/µm	Fbetax	36	
run-in misal/µm	Fbetay	1	
stiff/(N/mm/µm)	cgamma	22.67	
overlap ratio	epsbeta	0.000	

FACTORS

resonance ratio	N	0.174	
dynamic fct	Kv	1.277	

TOOTH FLANK

face load factr	KHbeta	1.051	
transv load fct	KHalpha	1.348	
zone factor	ZH	2.495	
elasticity fctr	ZE	189.812	
single pair fct	ZB/ZD	1.006	1.000
cont ratio fctr	Zepsilon	0.861	
helix ang factr	Zbeta	1.000	
life factor	ZN	1.278	1.299
lub inf fct	ZLZVZR	0.857	0.866
work-hardng fct	ZW	1.196	
size factor	ZX	1.000	

TOOTH ROOT

face load factr	KFbeta	1.035	1.0
transv load fct	KFalpha	1.486	
form factor	YF	1.221	1.1
stress conc fct	YS	2.286	2.3
notch parameter	qs	2.567	2.7
cont ratio fctr	Yepsilon	0.673	
helix ang factr	Ybeta	1.000	
life factor	YN	0.985	0.9
notch sensy fct	YdrelT	1.002	1.0
surface factor	YRrelT	0.977	0.9
size factor	YX	1.000	1.0

CONTACT STRESS (N/mm²)

allw stress num	sgHlm	327.0	327.0
permiss stress	sigHP	428.4	440.1
"" (reference)	" ref	286.7	286.7
contact stress	sigH	696.1	691.8
safety factor	SH	0.62	0.64
min safety fctr	SHmin	1.00	

BENDING STRESS (N/mm²)

allw stress num	sigFE	174.0	174.
permiss stress	sigFP	119.9	121.
"" (reference)	" ref	121.8	122.
root stress	sigF	243.6	176.
safety factor	SF	0.69	0.9
min safety fctr	SFmin	1.40	

```
**********************************
*      D E S I G N    U N I T    *
*      Gear Technology Centre    *
* User          Cranfield University*
* Organisation Cranfield University*
* Rating to ISO 6336    1 Apr 2005 *
* DU/GRF  ISO Rating  Version 3·5  *
**********************************
file not named
```

pinion material	St		
wheel material	St		
hardness	HV	137	137
material quality		MQ	MQ
roughns flnk/µm	Rz	18.0	18.0
roughns root/µm	Rz	18.0	18.0
viscosity @ 40C	nu	136	
pitting permitted?		yes	yes
reversing duty?		no	no

number of teeth	z	49	65
normal module	mn	3.000	
transvrs module	mt	3.000	
gear ratio	u	1.327	
centres	a	171.00	
facewidth	b	15.00	30.00
reference diam	d	147.00	195.00
base diameter	db	138.13	183.24
tip diameter	da	153.00	201.00
root diameter	df	139.50	187.50
tooth depth	h	6.750	6.750
internal diameter		0.0	0.0
norm pres angle	alphan	20.0000	
transv pres ang	alphat	20.0000	
wkng tr pr ang	alphawt	20.0000	
ref helix angle	beta	0.0000	
base helix ang	betab	0.0000	
prof shift coef	x	0.000	0.000
sum of "" coefs	Sigx	0.000	
bsc rack dedend	hfP/mn	1.250	1.250
bsc rk root rad	rofP/mn	0.250	0.250
residual protub	Spr/mn	0.000	0.000
root chord lgth	sFn/mn	2.177	2.227
bending mom arm	hFa/mn	0.958	0.980
root radius	roF/mn	0.424	0.399
tr contct ratio	epsalpha	1.774	

applicatn factr	KA	1.000	
required life/h		350	
load cycles	NL	1.56E7	1.18E
mesh power/kW	P	11.47	
torque/Nm	T	147.0	195.
tr tang force/N	Ft	2000.0	
speed/RPM	n	745.0	561.
pitch line speed/m/s		5.73	
tip relief/µm	Ca	14	
helix modifictn	none		
fav contact pattn posn verifctn?		n	
wheel web thickness		0.00	
pinion offset	s	0.000	
hx dev elast/µm	fsh	0	
quality grade	q	10	10
hx dev manuf/µm	fma	36	
init'l misal/µm	Fbetax	36	
run-in misal/µm	Fbetay	1	
stiff/(N/mm/µm)	cgamma	22.67	
overlap ratio	epsbeta	0.000	

FACTORS

resonance ratio	N	0.174		dynamic fct	Kv	1.277	
TOOTH FLANK				**TOOTH ROOT**			
face load factr	KHbeta	1.051		face load factr	KFbeta	1.035	1.0
transv load fct	KHalpha	1.348		transv load fct	KFalpha	1.486	
zone factor	ZH	2.495		form factor	YF	1.221	1.1
elasticity fctr	ZE	189.812		stress conc fct	YS	2.286	2.3
single pair fct	ZB/ZD	1.006	1.000	notch parameter	qs	2.567	2.7
cont ratio fctr	Zepsilon	0.861		cont ratio fctr	Yepsilon	0.673	
helix ang factr	Zbeta	1.000		helix ang factr	Ybeta	1.000	
life factor	ZN	1.267	1.288	life factor	YN	0.983	0.9
lub inf fct	ZLZVZR	0.852	0.861	notch sensy fct	YdrelT	1.002	1.0
work-hardng fct	ZW	1.196		surface factor	YRrelT	0.977	0.9
size factor	ZX	1.000		size factor	YX	1.000	1.0
CONTACT STRESS (N/mm²)				**BENDING STRESS (N/mm²)**			
allw stress num	sgHlm	327.0	327.0	allw stress num	sigFE	174.0	174.
permiss stress	sigHP	422.2	433.7	permiss stress	sigFP	119.7	121.
"" (reference)	" ref	286.7	286.7	"" (reference)	" ref	121.8	122.
contact stress	sigH	696.1	691.8	root stress	sigF	243.6	176.
safety factor	SH	0.61	0.63	safety factor	SF	0.69	0.9
min safety fctr	SHmin	1.00		min safety fctr	SFmin	1.40	

```
**********************************
*      D E S I G N    U N I T    *
*      Gear Technology Centre    *
* User          Cranfield University*
* Organisation Cranfield University*
* Rating to ISO 6336    1 Apr 2005 *
* DU/GRF  ISO Rating  Version 3·5  *
**********************************
file not named
```

pinion material	St		
wheel material	St		
hardness	HV	137	137
material quality		MQ	MQ
roughns flnk/µm	Rz	18.0	18.0
roughns root/µm	Rz	18.0	18.0
viscosity @ 40C	nu	136	
pitting permitted?		yes	yes
reversing duty?		no	no

number of teeth	z	49	65
normal module	mn	3.000	
transvrs module	mt	3.000	
gear ratio	u	1.327	
centres	a	171.00	
facewidth	b	15.00	30.00
reference diam	d	147.00	195.00
base diameter	db	138.13	183.24
tip diameter	da	153.00	201.00
root diameter	df	139.50	187.50
tooth depth	h	6.750	6.750
internal diameter		0.0	0.0
norm pres angle	alphan	20.0000	
transv pres ang	alphat	20.0000	
wkng tr pr ang	alphawt	20.0000	
ref helix angle	beta	0.0000	
base helix ang	betab	0.0000	
prof shift coef	x	0.000	0.000
sum of "" coefs	Sigx	0.000	
bsc rack dedend	hfP/mn	1.250	1.250
bsc rk root rad	rofP/mn	0.250	0.250
residual protub	Spr/mn	0.000	0.000
root chord lgth	sFn/mn	2.177	2.227
bending mom arm	hFa/mn	0.958	0.980
root radius	roF/mn	0.424	0.399
tr contct ratio	epsalpha	1.774	

applicatn factr	KA	1.000	
required life/h		400	
load cycles	NL	1.79E7	1.35E
mesh power/kW	P	11.47	
torque/Nm	T	147.0	195.
tr tang force/N	Ft	2000.0	
speed/RPM	n	745.0	561.
pitch line speed/m/s		5.73	
tip relief/µm	Ca	14	
helix modifictn	none		
fav contact pattn posn	verifctn?	n	
wheel web thickness		0.00	
pinion offset	s	0.000	
hx dev elast/µm	fsh	0	
quality grade	q	10	10
hx dev manuf/µm	fma	36	
init'l misal/µm	Fbetax	36	
run-in misal/µm	Fbetay	1	
stiff/(N/mm/µm)	cgamma	22.67	
overlap ratio	epsbeta	0.000	

FACTORS

resonance ratio	N	0.174	
dynamic fct	Kv	1.277	

TOOTH FLANK

face load factr	KHbeta	1.051	
transv load fct	KHalpha	1.348	
zone factor	ZH	2.495	
elasticity fctr	ZE	189.812	
single pair fct	ZB/ZD	1.006	1.000
cont ratio fctr	Zepsilon	0.861	
helix ang factr	Zbeta	1.000	
life factor	ZN	1.258	1.278
lub inf fct	ZLZVZR	0.848	0.857
work-hardng fct	ZW	1.196	
size factor	ZX	1.000	

TOOTH ROOT

face load factr	KFbeta	1.035	1.0
transv load fct	KFalpha	1.486	
form factor	YF	1.221	1.1
stress conc fct	YS	2.286	2.3
notch parameter	qs	2.567	2.7
cont ratio fctr	Yepsilon	0.673	
helix ang factr	Ybeta	1.000	
life factor	YN	0.982	0.9
notch sensy fct	YdrelT	1.002	1.0
surface factor	YRrelT	0.977	0.9
size factor	YX	1.000	1.0

CONTACT STRESS (N/mm²)

allw stress num	sgHlm	327.0	327.0
permiss stress	sigHP	416.9	428.2
"" (reference)	" ref	286.7	286.7
contact stress	sigH	696.1	691.8
safety factor	SH	0.60	0.62
min safety fctr	SHmin	1.00	

BENDING STRESS (N/mm²)

allw stress num	sigFE	174.0	174.
permiss stress	sigFP	119.6	120.
"" (reference)	" ref	121.8	122.
root stress	sigF	243.6	176.
safety factor	SF	0.69	0.9
min safety fctr	SFmin	1.40	

```
**********************************
*      D E S I G N    U N I T    *
*      Gear Technology Centre    *
* User          Cranfield University*
* Organisation Cranfield University*
* Rating to ISO 6336    1 Apr 2005 *
* DU/GRF  ISO Rating  Version 3·5  *
**********************************
file not named
```

pinion material	St						
wheel material	St						
hardness	HV	137	137				
material quality		MQ	MQ				
roughns flnk/µm	Rz	18.0	18.0				
roughns root/µm	Rz	18.0	18.0				
viscosity @ 40C	nu	136					
pitting permitted?		yes	yes				
reversing duty?		no	no				

number of teeth	z	49	65	applicatn factr	KA	1.000	
normal module	mn	3.000		required life/h		450	
transvrs module	mt	3.000		load cycles	NL	2.01E7	1.52E
gear ratio	u	1.327		mesh power/kW	P	11.47	
centres	a	171.00		torque/Nm	T	147.0	195.
facewidth	b	15.00	30.00	tr tang force/N	Ft	2000.0	
reference diam	d	147.00	195.00	speed/RPM	n	745.0	561.
base diameter	db	138.13	183.24	pitch line speed/m/s		5.73	
tip diameter	da	153.00	201.00	tip relief/µm	Ca	14	
root diameter	df	139.50	187.50	helix modifictn	none		
tooth depth	h	6.750	6.750	fav contact pattn posn	verifctn?	n	
internal diameter		0.0	0.0	wheel web thickness		0.00	
norm pres angle	alphan	20.0000		pinion offset	s	0.000	
transv pres ang	alphat	20.0000					
wkng tr pr ang	alphawt	20.0000					
ref helix angle	beta	0.0000					
base helix ang	betab	0.0000					
prof shift coef	x	0.000	0.000	hx dev elast/µm	fsh	0	
sum of "" coefs	Sigx	0.000		quality grade	q	10	10
bsc rack dedend	hfP/mn	1.250	1.250	hx dev manuf/µm	fma	36	
bsc rk root rad	rofP/mn	0.250	0.250	init'l misal/µm	Fbetax	36	
residual protub	Spr/mn	0.000	0.000	run-in misal/µm	Fbetay	1	
root chord lgth	sFn/mn	2.177	2.227	stiff/(N/mm/µm)	cgamma	22.67	
bending mom arm	hFa/mn	0.958	0.980				
root radius	roF/mn	0.424	0.399				
tr contct ratio	epsalpha	1.774		overlap ratio	epsbeta	0.000	
FACTORS							
resonance ratio	N	0.174		dynamic fct	Kv	1.277	
TOOTH FLANK				TOOTH ROOT			
face load factr	KHbeta	1.051		face load factr	KFbeta	1.035	1.0
transv load fct	KHalpha	1.348		transv load fct	KFalpha	1.486	
zone factor	ZH	2.495		form factor	YF	1.221	1.1
elasticity fctr	ZE	189.812		stress conc fct	YS	2.286	2.3
single pair fct	ZB/ZD	1.006	1.000	notch parameter	qs	2.567	2.7
cont ratio fctr	Zepsilon	0.861		cont ratio fctr	Yepsilon	0.673	
helix ang factr	Zbeta	1.000		helix ang factr	Ybeta	1.000	
life factor	ZN	1.249	1.270	life factor	YN	0.981	0.9
lub inf fct	ZLZVZR	0.844	0.853	notch sensy fct	YdrelT	1.002	1.0
work-hardng fct	ZW	1.196		surface factor	YRrelT	0.977	0.9
size factor	ZX	1.000		size factor	YX	1.000	1.0
CONTACT STRESS (N/mm²)				BENDING STRESS (N/mm²)			
allw stress num	sgHlm	327.0	327.0	allw stress num	sigFE	174.0	174.
permiss stress	sigHP	412.3	423.5	permiss stress	sigFP	119.4	120.
"" (reference)	" ref	286.7	286.7	"" (reference)	" ref	121.8	122.
contact stress	sigH	696.1	691.8	root stress	sigF	243.6	176.
safety factor	SH	0.59	0.61	safety factor	SF	0.69	0.9
min safety fctr	SHmin	1.00		min safety fctr	SFmin	1.40	

```
**********************************
*      D E S I G N    U N I T    *
*      Gear Technology Centre    *
* User          Cranfield University*
* Organisation Cranfield University*
* Rating to ISO 6336    1 Apr 2005 *
* DU/GRF  ISO Rating  Version 3·5  *
**********************************
file not named
```

pinion material	St		
wheel material	St		
hardness	HV	137	137
material quality		MQ	MQ
roughns flnk/µm	Rz	18.0	18.0
roughns root/µm	Rz	18.0	18.0
viscosity @ 40C	nu	136	
pitting permitted?		yes	yes
reversing duty?		no	no

number of teeth	z	49	65
normal module	mn	3.000	
transvrs module	mt	3.000	
gear ratio	u	1.327	
centres	a	171.00	
facewidth	b	15.00	30.00
reference diam	d	147.00	195.00
base diameter	db	138.13	183.24
tip diameter	da	153.00	201.00
root diameter	df	139.50	187.50
tooth depth	h	6.750	6.750
internal diameter		0.0	0.0
norm pres angle	alphan	20.0000	
transv pres ang	alphat	20.0000	
wkng tr pr ang	alphawt	20.0000	
ref helix angle	beta	0.0000	
base helix ang	betab	0.0000	
prof shift coef	x	0.000	0.000
sum of "" coefs	Sigx	0.000	
bsc rack dedend	hfP/mn	1.250	1.250
bsc rk root rad	rofP/mn	0.250	0.250
residual protub	Spr/mn	0.000	0.000
root chord lgth	sFn/mn	2.177	2.227
bending mom arm	hFa/mn	0.958	0.980
root radius	roF/mn	0.424	0.399
tr contct ratio	epsalpha	1.774	

applicatn factr	KA	1.000	
required life/h		500	
load cycles	NL	2.24E7	1.68E
mesh power/kW	P	11.47	
torque/Nm	T	147.0	195.
tr tang force/N	Ft	2000.0	
speed/RPM	n	745.0	561.
pitch line speed/m/s		5.73	
tip relief/µm	Ca	14	
helix modifictn	none		
fav contact pattn posn	verifctn?	n	
wheel web thickness		0.00	
pinion offset	s	0.000	
hx dev elast/µm	fsh	0	
quality grade	q	10	10
hx dev manuf/µm	fma	36	
init'l misal/µm	Fbetax	36	
run-in misal/µm	Fbetay	1	
stiff/(N/mm/µm)	cgamma	22.67	
overlap ratio	epsbeta	0.000	

FACTORS

resonance ratio	N	0.174	
dynamic fct	Kv	1.277	

TOOTH FLANK

face load factr	KHbeta	1.051	
transv load fct	KHalpha	1.348	
zone factor	ZH	2.495	
elasticity fctr	ZE	189.812	
single pair fct	ZB/ZD	1.006	1.000
cont ratio fctr	Zepsilon	0.861	
helix ang factr	Zbeta	1.000	
life factor	ZN	1.242	1.262
lub inf fct	ZLZVZR	0.841	0.850
work-hardng fct	ZW	1.196	
size factor	ZX	1.000	

TOOTH ROOT

face load factr	KFbeta	1.035	1.0
transv load fct	KFalpha	1.486	
form factor	YF	1.221	1.1
stress conc fct	YS	2.286	2.3
notch parameter	qs	2.567	2.7
cont ratio fctr	Yepsilon	0.673	
helix ang factr	Ybeta	1.000	
life factor	YN	0.980	0.9
notch sensy fct	YdrelT	1.002	1.0
surface factor	YRrelT	0.977	0.9
size factor	YX	1.000	1.0

CONTACT STRESS (N/mm²)

allw stress num	sgHlm	327.0	327.0
permiss stress	sigHP	408.2	419.3
"" (reference)	" ref	286.7	286.7
contact stress	sigH	696.1	691.8
safety factor	SH	0.59	0.61
min safety fctr	SHmin	1.00	

BENDING STRESS (N/mm²)

allw stress num	sigFE	174.0	174.
permiss stress	sigFP	119.3	120.
"" (reference)	" ref	121.8	122.
root stress	sigF	243.6	176.
safety factor	SF	0.69	0.9
min safety fctr	SFmin	1.40	

```
**********************************
*      D E S I G N    U N I T    *
*      Gear Technology Centre    *
* User          Cranfield University*
* Organisation Cranfield University*
* Rating to ISO 6336    1 Apr 2005 *
* DU/GRF  ISO Rating  Version 3·5  *
**********************************
file not named
```

pinion material	St							
wheel material	St							
hardness	HV	137	137					
material quality		MQ	MQ					
roughns flnk/µm	Rz	18.0	18.0					
roughns root/µm	Rz	18.0	18.0					
viscosity @ 40C	nu	136						
pitting permitted?		yes	yes					
reversing duty?		no	no					
applicatn factr	KA	1.000						
required life/h		0						
load cycles	NL	0.00E0	0.00E					
mesh power/kW	P	17.16						
torque/Nm	T	220.0	291.					
tr tang force/N	Ft	2993.2						
speed/RPM	n	745.0	561.					
pitch line speed/m/s		5.73						
tip relief/µm	Ca	14						
helix modifictn	none							
fav contact pattn posn	verifctn?	n						
wheel web thickness		0.00						
pinion offset	s	0.000						

number of teeth	z	49	65
normal module	mn	3.000	
transvrs module	mt	3.000	
gear ratio	u	1.327	
centres	a	171.00	
facewidth	b	15.00	30.00
reference diam	d	147.00	195.00
base diameter	db	138.13	183.24
tip diameter	da	153.00	201.00
root diameter	df	139.50	187.50
tooth depth	h	6.750	6.750
internal diameter		0.0	0.0
norm pres angle	alphan	20.0000	
transv pres ang	alphat	20.0000	
wkng tr pr ang	alphawt	20.0000	
ref helix angle	beta	0.0000	
base helix ang	betab	0.0000	
prof shift coef	x	0.000	0.000
sum of "" coefs	Sigx	0.000	
bsc rack dedend	hfP/mn	1.250	1.250
bsc rk root rad	rofP/mn	0.250	0.250
residual protub	Spr/mn	0.000	0.000
root chord lgth	sFn/mn	2.177	2.227
bending mom arm	hFa/mn	0.958	0.980
root radius	roF/mn	0.424	0.399
tr contct ratio	epsalpha	1.774	

hx dev elast/µm	fsh	0					
quality grade	q	10	10				
hx dev manuf/µm	fma	36					
init'l misal/µm	Fbetax	36					
run-in misal/µm	Fbetay	1					
stiff/(N/mm/µm)	cgamma	22.67					
overlap ratio	epsbeta	0.000					

FACTORS

resonance ratio	N	0.174		dynamic fct	Kv	1.198	

TOOTH FLANK

face load factr	KHbeta	1.036	
transv load fct	KHalpha	1.348	
zone factor	ZH	2.495	
elasticity fctr	ZE	189.812	
single pair fct	ZB/ZD	1.006	1.000
cont ratio fctr	Zepsilon	0.861	
helix ang factr	Zbeta	1.000	
life factor	ZN	1.600	1.600
lub inf fct	ZLZVZR	1.000	1.000
work-hardng fct	ZW	1.196	
size factor	ZX	1.000	

TOOTH ROOT

face load factr	KFbeta	1.025	1.0
transv load fct	KFalpha	1.486	
form factor	YF	1.221	1.1
stress conc fct	YS	2.286	2.3
notch parameter	qs	2.567	2.7
cont ratio fctr	Yepsilon	0.673	
helix ang factr	Ybeta	1.000	
life factor	YN	1.600	1.6
notch sensy fct	YdrelT	1.128	1.1
surface factor	YRrelT	1.000	1.0
size factor	YX	1.000	1.0

CONTACT STRESS (N/mm²)

allw stress num	sgHlm	327.0	327.0
permiss stress	sigHP	625.7	625.7
"" (reference)	" ref	286.7	286.7
contact stress	sigH	819.2	814.1
safety factor	SH	0.76	0.77
min safety fctr	SHmin	1.00	

BENDING STRESS (N/mm²)

allw stress num	sigFE	174.0	174.
permiss stress	sigFP	224.3	232.
"" (reference)	" ref	121.8	122.
root stress	sigF	338.8	245.
safety factor	SF	0.93	1.3
min safety fctr	SFmin	1.40	

```
**********************************
*      D E S I G N    U N I T    *
*      Gear Technology Centre    *
* User          Cranfield University*
* Organisation Cranfield University*
* Rating to ISO 6336    1 Apr 2005 *
* DU/GRF  ISO Rating  Version 3·5  *
**********************************
file not named
```

pinion material	St							
wheel material	St							
hardness	HV	137	137					
material quality		MQ	MQ					
roughns flnk/µm	Rz	18.0	18.0					
roughns root/µm	Rz	18.0	18.0					
viscosity @ 40C	nu	136						
pitting permitted?		yes	yes					
reversing duty?		no	no					
applicatn factr	KA	1.000						
required life/h		10						
load cycles	NL	4.47E5	3.37E					
mesh power/kW	P	17.16						
torque/Nm	T	220.0	291.					
tr tang force/N	Ft	2993.2						
speed/RPM	n	745.0	561.					
pitch line speed/m/s		5.73						
tip relief/µm	Ca	14						
helix modifictn	none							
fav contact pattn posn		verifctn?	n					
wheel web thickness		0.00						
pinion offset	s	0.000						

number of teeth	z	49	65					
normal module	mn	3.000						
transvrs module	mt	3.000						
gear ratio	u	1.327						
centres	a	171.00						
facewidth	b	15.00	30.00					
reference diam	d	147.00	195.00					
base diameter	db	138.13	183.24					
tip diameter	da	153.00	201.00					
root diameter	df	139.50	187.50					
tooth depth	h	6.750	6.750					
internal diameter		0.0	0.0					
norm pres angle	alphan	20.0000						
transv pres ang	alphat	20.0000						
wkng tr pr ang	alphawt	20.0000						
ref helix angle	beta	0.0000						
base helix ang	betab	0.0000						
prof shift coef	x	0.000	0.000					
sum of "" coefs	Sigx	0.000						
bsc rack dedend	hfP/mn	1.250	1.250					
bsc rk root rad	rofP/mn	0.250	0.250					
residual protub	Spr/mn	0.000	0.000					
root chord lgth	sFn/mn	2.177	2.227					
bending mom arm	hFa/mn	0.958	0.980					
root radius	roF/mn	0.424	0.399					
tr contct ratio	epsalpha	1.774						

hx dev elast/µm	fsh	0						
quality grade	q	10	10					
hx dev manuf/µm	fma	36						
init'l misal/µm	Fbetax	36						
run-in misal/µm	Fbetay	1						
stiff/(N/mm/µm)	cgamma	22.67						
overlap ratio	epsbeta	0.000						

FACTORS

resonance ratio	N	0.174						
dynamic fct	Kv	1.198						

TOOTH FLANK

face load factr	KHbeta	1.036						
transv load fct	KHalpha	1.348						
zone factor	ZH	2.495						
elasticity fctr	ZE	189.812						
single pair fct	ZB/ZD	1.006	1.000					
cont ratio fctr	Zepsilon	0.861						
helix ang factr	Zbeta	1.000						
life factor	ZN	1.600	1.600					
lub inf fct	ZLZVZR	1.000	1.000					
work-hardng fct	ZW	1.196						
size factor	ZX	1.000						

TOOTH ROOT

face load factr	KFbeta	1.025	1.0					
transv load fct	KFalpha	1.486						
form factor	YF	1.221	1.1					
stress conc fct	YS	2.286	2.3					
notch parameter	qs	2.567	2.7					
cont ratio fctr	Yepsilon	0.673						
helix ang factr	Ybeta	1.000						
life factor	YN	1.118	1.1					
notch sensy fct	YdrelT	1.031	1.0					
surface factor	YRrelT	0.983	0.9					
size factor	YX	1.000	1.0					

CONTACT STRESS (N/mm²)

allw stress num	sgHlm	327.0	327.0					
permiss stress	sigHP	625.7	625.7					
"" (reference)	" ref	286.7	286.7					
contact stress	sigH	819.2	814.1					
safety factor	SH	0.76	0.77					
min safety fctr	SHmin	1.00						

BENDING STRESS (N/mm²)

allw stress num	sigFE	174.0	174.					
permiss stress	sigFP	140.8	146.					
"" (reference)	" ref	121.8	122.					
root stress	sigF	338.8	245.					
safety factor	SF	0.58	0.8					
min safety fctr	SFmin	1.40						

```
**********************************
*      D E S I G N    U N I T    *
*      Gear Technology Centre    *
* User          Cranfield University*
* Organisation Cranfield University*
* Rating to ISO 6336    1 Apr 2005 *
* DU/GRF  ISO Rating  Version 3·5  *
**********************************
file not named
```

pinion material	St		
wheel material	St		
hardness	HV	137	137
material quality		MQ	MQ
roughns flnk/µm	Rz	18.0	18.0
roughns root/µm	Rz	18.0	18.0
viscosity @ 40C	nu	136	
pitting permitted?		yes	yes
reversing duty?		no	no

number of teeth	z	49	65
normal module	mn	3.000	
transvrs module	mt	3.000	
gear ratio	u	1.327	
centres	a	171.00	
facewidth	b	15.00	30.00
reference diam	d	147.00	195.00
base diameter	db	138.13	183.24
tip diameter	da	153.00	201.00
root diameter	df	139.50	187.50
tooth depth	h	6.750	6.750
internal diameter		0.0	0.0
norm pres angle	alphan	20.0000	
transv pres ang	alphat	20.0000	
wkng tr pr ang	alphawt	20.0000	
ref helix angle	beta	0.0000	
base helix ang	betab	0.0000	
prof shift coef	x	0.000	0.000
sum of "" coefs	Sigx	0.000	
bsc rack dedend	hfP/mn	1.250	1.250
bsc rk root rad	rofP/mn	0.250	0.250
residual protub	Spr/mn	0.000	0.000
root chord lgth	sFn/mn	2.177	2.227
bending mom arm	hFa/mn	0.958	0.980
root radius	roF/mn	0.424	0.399
tr contct ratio	epsalpha	1.774	

applicatn factr	KA	1.000	
required life/h		20	
load cycles	NL	8.94E5	6.74E
mesh power/kW	P	17.16	
torque/Nm	T	220.0	291.
tr tang force/N	Ft	2992.5	
speed/RPM	n	745.0	561.
pitch line speed/m/s		5.73	
tip relief/µm	Ca	14	
helix modifictn	none		
fav contact pattn posn verifctn?		n	
wheel web thickness		0.00	
pinion offset	s	0.000	
hx dev elast/µm	fsh	0	
quality grade	q	10	10
hx dev manuf/µm	fma	36	
init'l misal/µm	Fbetax	36	
run-in misal/µm	Fbetay	1	
stiff/(N/mm/µm)	cgamma	22.67	
overlap ratio	epsbeta	0.000	

FACTORS

resonance ratio	N	0.174	
dynamic fct	Kv	1.198	

TOOTH FLANK

face load factr	KHbeta	1.036	
transv load fct	KHalpha	1.348	
zone factor	ZH	2.495	
elasticity fctr	ZE	189.812	
single pair fct	ZB/ZD	1.006	1.000
cont ratio fctr	Zepsilon	0.861	
helix ang factr	Zbeta	1.000	
life factor	ZN	1.554	1.586
lub inf fct	ZLZVZR	0.979	0.994
work-hardng fct	ZW	1.196	
size factor	ZX	1.000	

TOOTH ROOT

face load factr	KFbeta	1.025	1.0
transv load fct	KFalpha	1.486	
form factor	YF	1.221	1.1
stress conc fct	YS	2.286	2.3
notch parameter	qs	2.567	2.7
cont ratio fctr	Yepsilon	0.673	
helix ang factr	Ybeta	1.000	
life factor	YN	1.074	1.0
notch sensy fct	YdrelT	1.020	1.0
surface factor	YRrelT	0.981	0.9
size factor	YX	1.000	1.0

CONTACT STRESS (N/mm²)

allw stress num	sgHlm	327.0	327.0
permiss stress	sigHP	595.0	616.6
"" (reference)	" ref	286.7	286.7
contact stress	sigH	819.1	814.1
safety factor	SH	0.73	0.76
min safety fctr	SHmin	1.00	

BENDING STRESS (N/mm²)

allw stress num	sigFE	174.0	174.
permiss stress	sigFP	133.6	138.
"" (reference)	" ref	121.8	122.
root stress	sigF	338.7	245.
safety factor	SF	0.55	0.7
min safety fctr	SFmin	1.40	

```
**********************************
*      D E S I G N    U N I T    *
*      Gear Technology Centre    *
* User          Cranfield University*
* Organisation Cranfield University*
* Rating to ISO 6336    1 Apr 2005 *
* DU/GRF  ISO Rating  Version 3·5  *
**********************************
file not named
```

pinion material	St						
wheel material	St						
hardness	HV	137	137				
material quality		MQ	MQ				
roughns flnk/µm	Rz	18.0	18.0				
roughns root/µm	Rz	18.0	18.0				
viscosity @ 40C	nu	136					
pitting permitted?		yes	yes				
reversing duty?		no	no				

number of teeth	z	49	65	applicatn factr	KA	1.000	
normal module	mn	3.000		required life/h		50	
transvrs module	mt	3.000		load cycles	NL	2.24E6	1.68E
gear ratio	u	1.327		mesh power/kW	P	17.16	
centres	a	171.00		torque/Nm	T	220.0	291.
facewidth	b	15.00	30.00	tr tang force/N	Ft	2992.5	
reference diam	d	147.00	195.00	speed/RPM	n	745.0	561.
base diameter	db	138.13	183.24	pitch line speed/m/s		5.73	
tip diameter	da	153.00	201.00	tip relief/µm	Ca	14	
root diameter	df	139.50	187.50	helix modifictn	none		
tooth depth	h	6.750	6.750	fav contact pattn posn	verifctn?	n	
internal diameter		0.0	0.0	wheel web thickness		0.00	
norm pres angle	alphan	20.0000		pinion offset	s	0.000	
transv pres ang	alphat	20.0000					
wkng tr pr ang	alphawt	20.0000					
ref helix angle	beta	0.0000					
base helix ang	betab	0.0000					
prof shift coef	x	0.000	0.000	hx dev elast/µm	fsh	0	
sum of "" coefs	Sigx	0.000		quality grade	q	10	10
bsc rack dedend	hfP/mn	1.250	1.250	hx dev manuf/µm	fma	36	
bsc rk root rad	rofP/mn	0.250	0.250	init'l misal/µm	Fbetax	36	
residual protub	Spr/mn	0.000	0.000	run-in misal/µm	Fbetay	1	
root chord lgth	sFn/mn	2.177	2.227	stiff/(N/mm/µm)	cgamma	22.67	
bending mom arm	hFa/mn	0.958	0.980				
root radius	roF/mn	0.424	0.399				
tr contct ratio	epsalpha	1.774		overlap ratio	epsbeta	0.000	
FACTORS							
resonance ratio	N	0.174		dynamic fct	Kv	1.198	
TOOTH FLANK				TOOTH ROOT			
face load factr	KHbeta	1.036		face load factr	KFbeta	1.025	1.0
transv load fct	KHalpha	1.348		transv load fct	KFalpha	1.486	
zone factor	ZH	2.495		form factor	YF	1.221	1.1
elasticity fctr	ZE	189.812		stress conc fct	YS	2.286	2.3
single pair fct	ZB/ZD	1.006	1.000	notch parameter	qs	2.567	2.7
cont ratio fctr	Zepsilon	0.861		cont ratio fctr	Yepsilon	0.673	
helix ang factr	Zbeta	1.000		helix ang factr	Ybeta	1.000	
life factor	ZN	1.452	1.483	life factor	YN	1.017	1.0
lub inf fct	ZLZVZR	0.934	0.948	notch sensy fct	YdrelT	1.007	1.0
work-hardng fct	ZW	1.196		surface factor	YRrelT	0.978	0.9
size factor	ZX	1.000		size factor	YX	1.000	1.0
CONTACT STRESS (N/mm²)				BENDING STRESS (N/mm²)			
allw stress num	sgHlm	327.0	327.0	allw stress num	sigFE	174.0	174.
permiss stress	sigHP	530.4	549.5	permiss stress	sigFP	124.5	128.
"" (reference)	" ref	286.7	286.7	"" (reference)	" ref	121.8	122.
contact stress	sigH	819.1	814.1	root stress	sigF	338.7	245.
safety factor	SH	0.65	0.68	safety factor	SF	0.51	0.7
min safety fctr	SHmin	1.00		min safety fctr	SFmin	1.40	

```
**********************************
*      D E S I G N    U N I T    *
*      Gear Technology Centre    *
* User          Cranfield University*
* Organisation Cranfield University*
* Rating to ISO 6336    1 Apr 2005 *
* DU/GRF  ISO Rating  Version 3·5  *
**********************************
file not named
```

pinion material	St		
wheel material	St		
hardness	HV	137	137
material quality		MQ	MQ
roughns flnk/µm	Rz	18.0	18.0
roughns root/µm	Rz	18.0	18.0
viscosity @ 40C	nu	136	
pitting permitted?		yes	yes
reversing duty?		no	no

number of teeth	z	49	65
normal module	mn	3.000	
transvrs module	mt	3.000	
gear ratio	u	1.327	
centres	a	171.00	
facewidth	b	15.00	30.00
reference diam	d	147.00	195.00
base diameter	db	138.13	183.24
tip diameter	da	153.00	201.00
root diameter	df	139.50	187.50
tooth depth	h	6.750	6.750
internal diameter		0.0	0.0
norm pres angle	alphan	20.0000	
transv pres ang	alphat	20.0000	
wkng tr pr ang	alphawt	20.0000	
ref helix angle	beta	0.0000	
base helix ang	betab	0.0000	
prof shift coef	x	0.000	0.000
sum of "" coefs	Sigx	0.000	
bsc rack dedend	hfP/mn	1.250	1.250
bsc rk root rad	rofP/mn	0.250	0.250
residual protub	Spr/mn	0.000	0.000
root chord lgth	sFn/mn	2.177	2.227
bending mom arm	hFa/mn	0.958	0.980
root radius	roF/mn	0.424	0.399
tr contct ratio	epsalpha	1.774	

applicatn factr	KA	1.000	
required life/h		80	
load cycles	NL	3.58E6	2.70E
mesh power/kW	P	17.16	
torque/Nm	T	220.0	291.
tr tang force/N	Ft	2992.5	
speed/RPM	n	745.0	561.
pitch line speed/m/s		5.73	
tip relief/µm	Ca	14	
helix modifictn	none		
fav contact pattn posn	verifctn?	n	
wheel web thickness		0.00	
pinion offset	s	0.000	
hx dev elast/µm	fsh	0	
quality grade	q	10	10
hx dev manuf/µm	fma	36	
init'l misal/µm	Fbetax	36	
run-in misal/µm	Fbetay	1	
stiff/(N/mm/µm)	cgamma	22.67	
overlap ratio	epsbeta	0.000	

FACTORS

resonance ratio	N	0.174	
dynamic fct	Kv	1.198	

TOOTH FLANK

face load factr	KHbeta	1.036	
transv load fct	KHalpha	1.348	
zone factor	ZH	2.495	
elasticity fctr	ZE	189.812	
single pair fct	ZB/ZD	1.006	1.000
cont ratio fctr	Zepsilon	0.861	
helix ang factr	Zbeta	1.000	
life factor	ZN	1.403	1.432
lub inf fct	ZLZVZR	0.912	0.925
work-hardng fct	ZW	1.196	
size factor	ZX	1.000	

CONTACT STRESS (N/mm²)

allw stress num	sgHlm	327.0	327.0
permiss stress	sigHP	500.3	518.2
"" (reference)	" ref	286.7	286.7
contact stress	sigH	819.1	814.1
safety factor	SH	0.61	0.64
min safety fctr	SHmin	1.00	

TOOTH ROOT

face load factr	KFbeta	1.025	1.0
transv load fct	KFalpha	1.486	
form factor	YF	1.221	1.1
stress conc fct	YS	2.286	2.3
notch parameter	qs	2.567	2.7
cont ratio fctr	Yepsilon	0.673	
helix ang factr	Ybeta	1.000	
life factor	YN	0.998	1.0
notch sensy fct	YdrelT	1.002	1.0
surface factor	YRrelT	0.977	0.9
size factor	YX	1.000	1.0

BENDING STRESS (N/mm²)

allw stress num	sigFE	174.0	174.
permiss stress	sigFP	121.6	123.
"" (reference)	" ref	121.8	122.
root stress	sigF	338.7	245.
safety factor	SF	0.50	0.7
min safety fctr	SFmin	1.40	

```
**********************************
*      D E S I G N    U N I T    *
*      Gear Technology Centre    *
* User          Cranfield University*
* Organisation Cranfield University*
* Rating to ISO 6336    1 Apr 2005 *
* DU/GRF  ISO Rating  Version 3·5  *
**********************************
file not named
```

pinion material	St		
wheel material	St		
hardness	HV	137	137
material quality		MQ	MQ
roughns flnk/µm	Rz	18.0	18.0
roughns root/µm	Rz	18.0	18.0
viscosity @ 40C	nu	136	
pitting permitted?		yes	yes
reversing duty?		no	no

number of teeth	z	49	65
normal module	mn	3.000	
transvrs module	mt	3.000	
gear ratio	u	1.327	
centres	a	171.00	
facewidth	b	15.00	30.00
reference diam	d	147.00	195.00
base diameter	db	138.13	183.24
tip diameter	da	153.00	201.00
root diameter	df	139.50	187.50
tooth depth	h	6.750	6.750
internal diameter		0.0	0.0
norm pres angle	alphan	20.0000	
transv pres ang	alphat	20.0000	
wkng tr pr ang	alphawt	20.0000	
ref helix angle	beta	0.0000	
base helix ang	betab	0.0000	
prof shift coef	x	0.000	0.000
sum of "" coefs	Sigx	0.000	
bsc rack dedend	hfP/mn	1.250	1.250
bsc rk root rad	rofP/mn	0.250	0.250
residual protub	Spr/mn	0.000	0.000
root chord lgth	sFn/mn	2.177	2.227
bending mom arm	hFa/mn	0.958	0.980
root radius	roF/mn	0.424	0.399
tr contct ratio	epsalpha	1.774	

applicatn factr	KA	1.000	
required life/h		100	
load cycles	NL	4.47E6	3.37E
mesh power/kW	P	17.16	
torque/Nm	T	220.0	291.
tr tang force/N	Ft	2992.5	
speed/RPM	n	745.0	561.
pitch line speed/m/s		5.73	
tip relief/µm	Ca	14	
helix modifictn	none		
fav contact pattn posn verifctn?		n	
wheel web thickness		0.00	
pinion offset	s	0.000	
hx dev elast/µm	fsh	0	
quality grade	q	10	10
hx dev manuf/µm	fma	36	
init'l misal/µm	Fbetax	36	
run-in misal/µm	Fbetay	1	
stiff/(N/mm/µm)	cgamma	22.67	
overlap ratio	epsbeta	0.000	

FACTORS

resonance ratio	N	0.174	
dynamic fct	Kv	1.198	

TOOTH FLANK

face load factr	KHbeta	1.036	
transv load fct	KHalpha	1.348	
zone factor	ZH	2.495	
elasticity fctr	ZE	189.812	
single pair fct	ZB/ZD	1.006	1.000
cont ratio fctr	Zepsilon	0.861	
helix ang factr	Zbeta	1.000	
life factor	ZN	1.380	1.409
lub inf fct	ZLZVZR	0.902	0.915
work-hardng fct	ZW	1.196	
size factor	ZX	1.000	

CONTACT STRESS (N/mm²)

allw stress num	sgHlm	327.0	327.0
permiss stress	sigHP	486.6	504.0
"" (reference)	" ref	286.7	286.7
contact stress	sigH	819.1	814.1
safety factor	SH	0.59	0.62
min safety fctr	SHmin	1.00	

TOOTH ROOT

face load factr	KFbeta	1.025	1.0
transv load fct	KFalpha	1.486	
form factor	YF	1.221	1.1
stress conc fct	YS	2.286	2.3
notch parameter	qs	2.567	2.7
cont ratio fctr	Yepsilon	0.673	
helix ang factr	Ybeta	1.000	
life factor	YN	0.996	0.9
notch sensy fct	YdrelT	1.002	1.0
surface factor	YRrelT	0.977	0.9
size factor	YX	1.000	1.0

BENDING STRESS (N/mm²)

allw stress num	sigFE	174.0	174.
permiss stress	sigFP	121.3	122.
"" (reference)	" ref	121.8	122.
root stress	sigF	338.7	245.
safety factor	SF	0.50	0.7
min safety fctr	SFmin	1.40	

```
**********************************
*      D E S I G N    U N I T    *
*      Gear Technology Centre    *
* User          Cranfield University*
* Organisation Cranfield University*
* Rating to ISO 6336    1 Apr 2005 *
* DU/GRF  ISO Rating  Version 3·5  *
**********************************
file not named
```

pinion material	St		
wheel material	St		
hardness	HV	137	137
material quality		MQ	MQ
roughns flnk/µm	Rz	18.0	18.0
roughns root/µm	Rz	18.0	18.0
viscosity @ 40C	nu	136	
pitting permitted?		yes	yes
reversing duty?		no	no

number of teeth	z	49	65
normal module	mn	3.000	
transvrs module	mt	3.000	
gear ratio	u	1.327	
centres	a	171.00	
facewidth	b	15.00	30.00
reference diam	d	147.00	195.00
base diameter	db	138.13	183.24
tip diameter	da	153.00	201.00
root diameter	df	139.50	187.50
tooth depth	h	6.750	6.750
internal diameter		0.0	0.0
norm pres angle	alphan	20.0000	
transv pres ang	alphat	20.0000	
wkng tr pr ang	alphawt	20.0000	
ref helix angle	beta	0.0000	
base helix ang	betab	0.0000	
prof shift coef	x	0.000	0.000
sum of "" coefs	Sigx	0.000	
bsc rack dedend	hfP/mn	1.250	1.250
bsc rk root rad	rofP/mn	0.250	0.250
residual protub	Spr/mn	0.000	0.000
root chord lgth	sFn/mn	2.177	2.227
bending mom arm	hFa/mn	0.958	0.980
root radius	roF/mn	0.424	0.399
tr contct ratio	epsalpha	1.774	

applicatn factr	KA	1.000	
required life/h		150	
load cycles	NL	6.71E6	5.05E
mesh power/kW	P	17.16	
torque/Nm	T	220.0	291.
tr tang force/N	Ft	2992.5	
speed/RPM	n	745.0	561.
pitch line speed/m/s		5.73	
tip relief/µm	Ca	14	
helix modifictn	none		
fav contact pattn posn	verifctn?	n	
wheel web thickness		0.00	
pinion offset	s	0.000	
hx dev elast/µm	fsh	0	
quality grade	q	10	10
hx dev manuf/µm	fma	36	
init'l misal/µm	Fbetax	36	
run-in misal/µm	Fbetay	1	
stiff/(N/mm/µm)	cgamma	22.67	
overlap ratio	epsbeta	0.000	

FACTORS

resonance ratio	N	0.174	
dynamic fct	Kv	1.198	

TOOTH FLANK

face load factr	KHbeta	1.036	
transv load fct	KHalpha	1.348	
zone factor	ZH	2.495	
elasticity fctr	ZE	189.812	
single pair fct	ZB/ZD	1.006	1.000
cont ratio fctr	Zepsilon	0.861	
helix ang factr	Zbeta	1.000	
life factor	ZN	1.339	1.367
lub inf fct	ZLZVZR	0.884	0.896
work-hardng fct	ZW	1.196	
size factor	ZX	1.000	

TOOTH ROOT

face load factr	KFbeta	1.025	1.0
transv load fct	KFalpha	1.486	
form factor	YF	1.221	1.1
stress conc fct	YS	2.286	2.3
notch parameter	qs	2.567	2.7
cont ratio fctr	Yepsilon	0.673	
helix ang factr	Ybeta	1.000	
life factor	YN	0.992	0.9
notch sensy fct	YdrelT	1.002	1.0
surface factor	YRrelT	0.977	0.9
size factor	YX	1.000	1.0

CONTACT STRESS (N/mm²)

allw stress num	sgHlm	327.0	327.0
permiss stress	sigHP	462.8	479.2
"" (reference)	" ref	286.7	286.7
contact stress	sigH	819.1	814.1
safety factor	SH	0.56	0.59
min safety fctr	SHmin	1.00	

BENDING STRESS (N/mm²)

allw stress num	sigFE	174.0	174.
permiss stress	sigFP	120.8	122.
"" (reference)	" ref	121.8	122.
root stress	sigF	338.7	245.
safety factor	SF	0.50	0.7
min safety fctr	SFmin	1.40	

```
**********************************
*      D E S I G N    U N I T    *
*      Gear Technology Centre    *
* User          Cranfield University*
* Organisation Cranfield University*
* Rating to ISO 6336    1 Apr 2005 *
* DU/GRF  ISO Rating  Version 3·5  *
**********************************
file not named
```

pinion material	St		
wheel material	St		
hardness	HV	137	137
material quality		MQ	MQ
roughns flnk/µm	Rz	18.0	18.0
roughns root/µm	Rz	18.0	18.0
viscosity @ 40C	nu	136	
pitting permitted?		yes	yes
reversing duty?		no	no

number of teeth	z	49	65
normal module	mn	3.000	
transvrs module	mt	3.000	
gear ratio	u	1.327	
centres	a	171.00	
facewidth	b	15.00	30.00
reference diam	d	147.00	195.00
base diameter	db	138.13	183.24
tip diameter	da	153.00	201.00
root diameter	df	139.50	187.50
tooth depth	h	6.750	6.750
internal diameter		0.0	0.0
norm pres angle	alphan	20.0000	
transv pres ang	alphat	20.0000	
wkng tr pr ang	alphawt	20.0000	
ref helix angle	beta	0.0000	
base helix ang	betab	0.0000	
prof shift coef	x	0.000	0.000
sum of "" coefs	Sigx	0.000	
bsc rack dedend	hfP/mn	1.250	1.250
bsc rk root rad	rofP/mn	0.250	0.250
residual protub	Spr/mn	0.000	0.000
root chord lgth	sFn/mn	2.177	2.227
bending mom arm	hFa/mn	0.958	0.980
root radius	roF/mn	0.424	0.399
tr contct ratio	epsalpha	1.774	

applicatn factr	KA	1.000	
required life/h		200	
load cycles	NL	8.94E6	6.74E
mesh power/kW	P	17.16	
torque/Nm	T	220.0	291.
tr tang force/N	Ft	2992.5	
speed/RPM	n	745.0	561.
pitch line speed/m/s		5.73	
tip relief/µm	Ca	14	
helix modifictn	none		
fav contact pattn posn verifctn?		n	
wheel web thickness		0.00	
pinion offset	s	0.000	
hx dev elast/µm	fsh	0	
quality grade	q	10	10
hx dev manuf/µm	fma	36	
init'l misal/µm	Fbetax	36	
run-in misal/µm	Fbetay	1	
stiff/(N/mm/µm)	cgamma	22.67	
overlap ratio	epsbeta	0.000	

FACTORS

resonance ratio	N	0.174	
dynamic fct	Kv	1.198	

TOOTH FLANK				TOOTH ROOT			
face load factr	KHbeta	1.036		face load factr	KFbeta	1.025	1.0
transv load fct	KHalpha	1.348		transv load fct	KFalpha	1.486	
zone factor	ZH	2.495		form factor	YF	1.221	1.1
elasticity fctr	ZE	189.812		stress conc fct	YS	2.286	2.3
single pair fct	ZB/ZD	1.006	1.000	notch parameter	qs	2.567	2.7
cont ratio fctr	Zepsilon	0.861		cont ratio fctr	Yepsilon	0.673	
helix ang factr	Zbeta	1.000		helix ang factr	Ybeta	1.000	
life factor	ZN	1.311	1.338	life factor	YN	0.989	0.9
lub inf fct	ZLZVZR	0.871	0.884	notch sensy fct	YdrelT	1.002	1.0
work-hardng fct	ZW	1.196		surface factor	YRrelT	0.977	0.9
size factor	ZX	1.000		size factor	YX	1.000	1.0

CONTACT STRESS (N/mm²)				BENDING STRESS (N/mm²)			
allw stress num	sgHlm	327.0	327.0	allw stress num	sigFE	174.0	174.
permiss stress	sigHP	446.6	462.5	permiss stress	sigFP	120.4	121.
"" (reference)	" ref	286.7	286.7	"" (reference)	" ref	121.8	122.
contact stress	sigH	819.1	814.1	root stress	sigF	338.7	245.
safety factor	SH	0.55	0.57	safety factor	SF	0.50	0.7
min safety fctr	SHmin	1.00		min safety fctr	SFmin	1.40	

```
**********************************
*      D E S I G N    U N I T    *
*      Gear Technology Centre    *
* User          Cranfield University*
* Organisation Cranfield University*
* Rating to ISO 6336    1 Apr 2005 *
* DU/GRF  ISO Rating  Version 3·5  *
**********************************
file not named
```

pinion material	St		
wheel material	St		
hardness	HV	137	137
material quality		MQ	MQ
roughns flnk/µm	Rz	18.0	18.0
roughns root/µm	Rz	18.0	18.0
viscosity @ 40C	nu	136	
pitting permitted?		yes	yes
reversing duty?		no	no

number of teeth	z	49	65
normal module	mn	3.000	
transvrs module	mt	3.000	
gear ratio	u	1.327	
centres	a	171.00	
facewidth	b	15.00	30.00
reference diam	d	147.00	195.00
base diameter	db	138.13	183.24
tip diameter	da	153.00	201.00
root diameter	df	139.50	187.50
tooth depth	h	6.750	6.750
internal diameter		0.0	0.0
norm pres angle	alphan	20.0000	
transv pres ang	alphat	20.0000	
wkng tr pr ang	alphawt	20.0000	
ref helix angle	beta	0.0000	
base helix ang	betab	0.0000	
prof shift coef	x	0.000	0.000
sum of "" coefs	Sigx	0.000	
bsc rack dedend	hfP/mn	1.250	1.250
bsc rk root rad	rofP/mn	0.250	0.250
residual protub	Spr/mn	0.000	0.000
root chord lgth	sFn/mn	2.177	2.227
bending mom arm	hFa/mn	0.958	0.980
root radius	roF/mn	0.424	0.399
tr contct ratio	epsalpha	1.774	

applicatn factr	KA	1.000	
required life/h		250	
load cycles	NL	1.12E7	8.42E
mesh power/kW	P	17.16	
torque/Nm	T	220.0	291.
tr tang force/N	Ft	2992.5	
speed/RPM	n	745.0	561.
pitch line speed/m/s		5.73	
tip relief/µm	Ca	14	
helix modifictn	none		
fav contact pattn posn	verifctn?	n	
wheel web thickness		0.00	
pinion offset	s	0.000	
hx dev elast/µm	fsh	0	
quality grade	q	10	10
hx dev manuf/µm	fma	36	
init'l misal/µm	Fbetax	36	
run-in misal/µm	Fbetay	1	
stiff/(N/mm/µm)	cgamma	22.67	
overlap ratio	epsbeta	0.000	

FACTORS

resonance ratio	N	0.174	
dynamic fct	Kv	1.198	

TOOTH FLANK

face load factr	KHbeta	1.036	
transv load fct	KHalpha	1.348	
zone factor	ZH	2.495	
elasticity fctr	ZE	189.812	
single pair fct	ZB/ZD	1.006	1.000
cont ratio fctr	Zepsilon	0.861	
helix ang factr	Zbeta	1.000	
life factor	ZN	1.292	1.317
lub inf fct	ZLZVZR	0.863	0.874
work-hardng fct	ZW	1.196	
size factor	ZX	1.000	

CONTACT STRESS (N/mm²)

allw stress num	sgHlm	327.0	327.0
permiss stress	sigHP	435.9	449.9
"" (reference)	" ref	286.7	286.7
contact stress	sigH	819.1	814.1
safety factor	SH	0.53	0.55
min safety fctr	SHmin	1.00	

TOOTH ROOT

face load factr	KFbeta	1.025	1.0
transv load fct	KFalpha	1.486	
form factor	YF	1.221	1.1
stress conc fct	YS	2.286	2.3
notch parameter	qs	2.567	2.7
cont ratio fctr	Yepsilon	0.673	
helix ang factr	Ybeta	1.000	
life factor	YN	0.987	0.9
notch sensy fct	YdrelT	1.002	1.0
surface factor	YRrelT	0.977	0.9
size factor	YX	1.000	1.0

BENDING STRESS (N/mm²)

allw stress num	sigFE	174.0	174.
permiss stress	sigFP	120.1	121.
"" (reference)	" ref	121.8	122.
root stress	sigF	338.7	245.
safety factor	SF	0.50	0.6
min safety fctr	SFmin	1.40	

```
**********************************
*      D E S I G N    U N I T    *
*      Gear Technology Centre    *
* User          Cranfield University*
* Organisation Cranfield University*
* Rating to ISO 6336    1 Apr 2005 *
* DU/GRF  ISO Rating  Version 3·5  *
**********************************
file not named
```

pinion material	St		
wheel material	St		
hardness	HV	137	137
material quality		MQ	MQ
roughns flnk/µm	Rz	18.0	18.0
roughns root/µm	Rz	18.0	18.0
viscosity @ 40C	nu	136	
pitting permitted?		yes	yes
reversing duty?		no	no

number of teeth	z	49	65
normal module	mn	3.000	
transvrs module	mt	3.000	
gear ratio	u	1.327	
centres	a	171.00	
facewidth	b	15.00	30.00
reference diam	d	147.00	195.00
base diameter	db	138.13	183.24
tip diameter	da	153.00	201.00
root diameter	df	139.50	187.50
tooth depth	h	6.750	6.750
internal diameter		0.0	0.0
norm pres angle	alphan	20.0000	
transv pres ang	alphat	20.0000	
wkng tr pr ang	alphawt	20.0000	
ref helix angle	beta	0.0000	
base helix ang	betab	0.0000	
prof shift coef	x	0.000	0.000
sum of "" coefs	Sigx	0.000	
bsc rack dedend	hfP/mn	1.250	1.250
bsc rk root rad	rofP/mn	0.250	0.250
residual protub	Spr/mn	0.000	0.000
root chord lgth	sFn/mn	2.177	2.227
bending mom arm	hFa/mn	0.958	0.980
root radius	roF/mn	0.424	0.399
tr contct ratio	epsalpha	1.774	

applicatn factr	KA	1.000	
required life/h		300	
load cycles	NL	1.34E7	1.01E
mesh power/kW	P	17.16	
torque/Nm	T	220.0	291.
tr tang force/N	Ft	2992.5	
speed/RPM	n	745.0	561.
pitch line speed/m/s		5.73	
tip relief/µm	Ca	14	
helix modifictn	none		
fav contact pattn posn verifctn?		n	
wheel web thickness		0.00	
pinion offset	s	0.000	
hx dev elast/µm	fsh	0	
quality grade	q	10	10
hx dev manuf/µm	fma	36	
init'l misal/µm	Fbetax	36	
run-in misal/µm	Fbetay	1	
stiff/(N/mm/µm)	cgamma	22.67	
overlap ratio	epsbeta	0.000	

FACTORS

resonance ratio	N	0.174		dynamic fct	Kv	1.198	
TOOTH FLANK				TOOTH ROOT			
face load factr	KHbeta	1.036		face load factr	KFbeta	1.025	1.0
transv load fct	KHalpha	1.348		transv load fct	KFalpha	1.486	
zone factor	ZH	2.495		form factor	YF	1.221	1.1
elasticity fctr	ZE	189.812		stress conc fct	YS	2.286	2.3
single pair fct	ZB/ZD	1.006	1.000	notch parameter	qs	2.567	2.7
cont ratio fctr	Zepsilon	0.861		cont ratio fctr	Yepsilon	0.673	
helix ang factr	Zbeta	1.000		helix ang factr	Ybeta	1.000	
life factor	ZN	1.278	1.299	life factor	YN	0.985	0.9
lub inf fct	ZLZVZR	0.857	0.866	notch sensy fct	YdrelT	1.002	1.0
work-hardng fct	ZW	1.196		surface factor	YRrelT	0.977	0.9
size factor	ZX	1.000		size factor	YX	1.000	1.0
CONTACT STRESS (N/mm²)				BENDING STRESS (N/mm²)			
allw stress num	sgHlm	327.0	327.0	allw stress num	sigFE	174.0	174.
permiss stress	sigHP	428.4	440.1	permiss stress	sigFP	119.9	121.
"" (reference)	" ref	286.7	286.7	"" (reference)	" ref	121.8	122.
contact stress	sigH	819.1	814.1	root stress	sigF	338.7	245.
safety factor	SH	0.52	0.54	safety factor	SF	0.50	0.6
min safety fctr	SHmin	1.00		min safety fctr	SFmin	1.40	

```
**********************************
*      D E S I G N   U N I T     *
*      Gear Technology Centre    *
* User          Cranfield University*
* Organisation Cranfield University*
* Rating to ISO 6336    1 Apr 2005 *
* DU/GRF  ISO Rating  Version 3·5  *
**********************************
file not named
```

pinion material	St		
wheel material	St		
hardness	HV	137	137
material quality		MQ	MQ
roughns flnk/µm	Rz	18.0	18.0
roughns root/µm	Rz	18.0	18.0
viscosity @ 40C	nu	136	
pitting permitted?		yes	yes
reversing duty?		no	no

number of teeth	z	49	65
normal module	mn	3.000	
transvrs module	mt	3.000	
gear ratio	u	1.327	
centres	a	171.00	
facewidth	b	15.00	30.00
reference diam	d	147.00	195.00
base diameter	db	138.13	183.24
tip diameter	da	153.00	201.00
root diameter	df	139.50	187.50
tooth depth	h	6.750	6.750
internal diameter		0.0	0.0
norm pres angle	alphan	20.0000	
transv pres ang	alphat	20.0000	
wkng tr pr ang	alphawt	20.0000	
ref helix angle	beta	0.0000	
base helix ang	betab	0.0000	
prof shift coef	x	0.000	0.000
sum of "" coefs	Sigx	0.000	
bsc rack dedend	hfP/mn	1.250	1.250
bsc rk root rad	rofP/mn	0.250	0.250
residual protub	Spr/mn	0.000	0.000
root chord lgth	sFn/mn	2.177	2.227
bending mom arm	hFa/mn	0.958	0.980
root radius	roF/mn	0.424	0.399
tr contct ratio	epsalpha	1.774	

applicatn factr	KA	1.000	
required life/h		350	
load cycles	NL	1.56E7	1.18E
mesh power/kW	P	17.16	
torque/Nm	T	220.0	291.
tr tang force/N	Ft	2992.5	
speed/RPM	n	745.0	561.
pitch line speed/m/s		5.73	
tip relief/µm	Ca	14	
helix modifictn	none		
fav contact pattn posn	verifctn?	n	
wheel web thickness		0.00	
pinion offset	s	0.000	
hx dev elast/µm	fsh	0	
quality grade	q	10	10
hx dev manuf/µm	fma	36	
init'l misal/µm	Fbetax	36	
run-in misal/µm	Fbetay	1	
stiff/(N/mm/µm)	cgamma	22.67	
overlap ratio	epsbeta	0.000	

FACTORS

resonance ratio	N	0.174	
dynamic fct	Kv	1.198	

TOOTH FLANK

face load factr	KHbeta	1.036	
transv load fct	KHalpha	1.348	
zone factor	ZH	2.495	
elasticity fctr	ZE	189.812	
single pair fct	ZB/ZD	1.006	1.000
cont ratio fctr	Zepsilon	0.861	
helix ang factr	Zbeta	1.000	
life factor	ZN	1.267	1.288
lub inf fct	ZLZVZR	0.852	0.861
work-hardng fct	ZW	1.196	
size factor	ZX	1.000	

TOOTH ROOT

face load factr	KFbeta	1.025	1.0
transv load fct	KFalpha	1.486	
form factor	YF	1.221	1.1
stress conc fct	YS	2.286	2.3
notch parameter	qs	2.567	2.7
cont ratio fctr	Yepsilon	0.673	
helix ang factr	Ybeta	1.000	
life factor	YN	0.983	0.9
notch sensy fct	YdrelT	1.002	1.0
surface factor	YRrelT	0.977	0.9
size factor	YX	1.000	1.0

CONTACT STRESS (N/mm²)

allw stress num	sgHlm	327.0	327.0
permiss stress	sigHP	422.2	433.7
"" (reference)	" ref	286.7	286.7
contact stress	sigH	819.1	814.1
safety factor	SH	0.52	0.53
min safety fctr	SHmin	1.00	

BENDING STRESS (N/mm²)

allw stress num	sigFE	174.0	174.
permiss stress	sigFP	119.7	121.
"" (reference)	" ref	121.8	122.
root stress	sigF	338.7	245.
safety factor	SF	0.49	0.6
min safety fctr	SFmin	1.40	

```
**********************************
*      D E S I G N   U N I T     *
*      Gear Technology Centre    *
* User          Cranfield University*
* Organisation Cranfield University*
* Rating to ISO 6336    1 Apr 2005 *
* DU/GRF  ISO Rating  Version 3·5  *
**********************************
file not named
```

pinion material	St		
wheel material	St		
hardness	HV	137	137
material quality		MQ	MQ
roughns flnk/µm	Rz	18.0	18.0
roughns root/µm	Rz	18.0	18.0
viscosity @ 40C	nu	136	
pitting permitted?		yes	yes
reversing duty?		no	no

number of teeth	z	49	65
normal module	mn	3.000	
transvrs module	mt	3.000	
gear ratio	u	1.327	
centres	a	171.00	
facewidth	b	15.00	30.00
reference diam	d	147.00	195.00
base diameter	db	138.13	183.24
tip diameter	da	153.00	201.00
root diameter	df	139.50	187.50
tooth depth	h	6.750	6.750
internal diameter		0.0	0.0
norm pres angle	alphan	20.0000	
transv pres ang	alphat	20.0000	
wkng tr pr ang	alphawt	20.0000	
ref helix angle	beta	0.0000	
base helix ang	betab	0.0000	
prof shift coef	x	0.000	0.000
sum of "" coefs	Sigx	0.000	
bsc rack dedend	hfP/mn	1.250	1.250
bsc rk root rad	rofP/mn	0.250	0.250
residual protub	Spr/mn	0.000	0.000
root chord lgth	sFn/mn	2.177	2.227
bending mom arm	hFa/mn	0.958	0.980
root radius	roF/mn	0.424	0.399
tr contct ratio	epsalpha	1.774	

applicatn factr	KA	1.000	
required life/h		400	
load cycles	NL	1.79E7	1.35E
mesh power/kW	P	17.16	
torque/Nm	T	220.0	291.
tr tang force/N	Ft	2992.5	
speed/RPM	n	745.0	561.
pitch line speed/m/s		5.73	
tip relief/µm	Ca	14	
helix modifictn	none		
fav contact pattn posn verifctn?		n	
wheel web thickness		0.00	
pinion offset	s	0.000	
hx dev elast/µm	fsh	0	
quality grade	q	10	10
hx dev manuf/µm	fma	36	
init'l misal/µm	Fbetax	36	
run-in misal/µm	Fbetay	1	
stiff/(N/mm/µm)	cgamma	22.67	
overlap ratio	epsbeta	0.000	

FACTORS

resonance ratio	N	0.174	
dynamic fct	Kv	1.198	

TOOTH FLANK

face load factr	KHbeta	1.036	
transv load fct	KHalpha	1.348	
zone factor	ZH	2.495	
elasticity fctr	ZE	189.812	
single pair fct	ZB/ZD	1.006	1.000
cont ratio fctr	Zepsilon	0.861	
helix ang factr	Zbeta	1.000	
life factor	ZN	1.258	1.278
lub inf fct	ZLZVZR	0.848	0.857
work-hardng fct	ZW	1.196	
size factor	ZX	1.000	

CONTACT STRESS (N/mm²)

allw stress num	sgHlm	327.0	327.0
permiss stress	sigHP	416.9	428.2
"" (reference)	" ref	286.7	286.7
contact stress	sigH	819.1	814.1
safety factor	SH	0.51	0.53
min safety fctr	SHmin	1.00	

TOOTH ROOT

face load factr	KFbeta	1.025	1.0
transv load fct	KFalpha	1.486	
form factor	YF	1.221	1.1
stress conc fct	YS	2.286	2.3
notch parameter	qs	2.567	2.7
cont ratio fctr	Yepsilon	0.673	
helix ang factr	Ybeta	1.000	
life factor	YN	0.982	0.9
notch sensy fct	YdrelT	1.002	1.0
surface factor	YRrelT	0.977	0.9
size factor	YX	1.000	1.0

BENDING STRESS (N/mm²)

allw stress num	sigFE	174.0	174.
permiss stress	sigFP	119.6	120.
"" (reference)	" ref	121.8	122.
root stress	sigF	338.7	245.
safety factor	SF	0.49	0.6
min safety fctr	SFmin	1.40	

```
**********************************
*      D E S I G N    U N I T    *
*      Gear Technology Centre    *
* User          Cranfield University*
* Organisation Cranfield University*
* Rating to ISO 6336    1 Apr 2005 *
* DU/GRF  ISO Rating  Version 3·5  *
**********************************
file not named
```

				pinion material	St		
				wheel material	St		
				hardness	HV	137	137
				material quality		MQ	MQ
				roughns flnk/µm	Rz	18.0	18.0
				roughns root/µm	Rz	18.0	18.0
				viscosity @ 40C	nu	136	
				pitting permitted?		yes	yes
				reversing duty?		no	no
number of teeth	z	49	65	applicatn factr	KA	1.000	
normal module	mn	3.000		required life/h		450	
transvrs module	mt	3.000		load cycles	NL	2.01E7	1.52E
gear ratio	u	1.327		mesh power/kW	P	17.16	
centres	a	171.00		torque/Nm	T	220.0	291.
facewidth	b	15.00	30.00	tr tang force/N	Ft	2992.5	
reference diam	d	147.00	195.00	speed/RPM	n	745.0	561.
base diameter	db	138.13	183.24	pitch line speed/m/s		5.73	
tip diameter	da	153.00	201.00	tip relief/µm	Ca	14	
root diameter	df	139.50	187.50	helix modifictn	none		
tooth depth	h	6.750	6.750	fav contact pattn posn	verifctn?	n	
internal diameter		0.0	0.0	wheel web thickness		0.00	
norm pres angle	alphan	20.0000		pinion offset	s	0.000	
transv pres ang	alphat	20.0000					
wkng tr pr ang	alphawt	20.0000					
ref helix angle	beta	0.0000					
base helix ang	betab	0.0000					
prof shift coef	x	0.000	0.000	hx dev elast/µm	fsh	0	
sum of "" coefs	Sigx	0.000		quality grade	q	10	10
bsc rack dedend	hfP/mn	1.250	1.250	hx dev manuf/µm	fma	36	
bsc rk root rad	rofP/mn	0.250	0.250	init'l misal/µm	Fbetax	36	
residual protub	Spr/mn	0.000	0.000	run-in misal/µm	Fbetay	1	
root chord lgth	sFn/mn	2.177	2.227	stiff/(N/mm/µm)	cgamma	22.67	
bending mom arm	hFa/mn	0.958	0.980				
root radius	roF/mn	0.424	0.399				
tr contct ratio	epsalpha	1.774		overlap ratio	epsbeta	0.000	
FACTORS							
resonance ratio	N	0.174		dynamic fct	Kv	1.198	
TOOTH FLANK				TOOTH ROOT			
face load factr	KHbeta	1.036		face load factr	KFbeta	1.025	1.0
transv load fct	KHalpha	1.348		transv load fct	KFalpha	1.486	
zone factor	ZH	2.495		form factor	YF	1.221	1.1
elasticity fctr	ZE	189.812		stress conc fct	YS	2.286	2.3
single pair fct	ZB/ZD	1.006	1.000	notch parameter	qs	2.567	2.7
cont ratio fctr	Zepsilon	0.861		cont ratio fctr	Yepsilon	0.673	
helix ang factr	Zbeta	1.000		helix ang factr	Ybeta	1.000	
life factor	ZN	1.249	1.270	life factor	YN	0.981	0.9
lub inf fct	ZLZVZR	0.844	0.853	notch sensy fct	YdrelT	1.002	1.0
work-hardng fct	ZW	1.196		surface factor	YRrelT	0.977	0.9
size factor	ZX	1.000		size factor	YX	1.000	1.0
CONTACT STRESS (N/mm²)				BENDING STRESS (N/mm²)			
allw stress num	sgHlm	327.0	327.0	allw stress num	sigFE	174.0	174.
permiss stress	sigHP	412.3	423.5	permiss stress	sigFP	119.4	120.
"" (reference)	" ref	286.7	286.7	"" (reference)	" ref	121.8	122.
contact stress	sigH	819.1	814.1	root stress	sigF	338.7	245.
safety factor	SH	0.50	0.52	safety factor	SF	0.49	0.6
min safety fctr	SHmin	1.00		min safety fctr	SFmin	1.40	

```
**********************************
*      D E S I G N    U N I T    *
*      Gear Technology Centre    *
* User          Cranfield University*
* Organisation Cranfield University*
* Rating to ISO 6336    1 Apr 2005 *
* DU/GRF  ISO Rating  Version 3·5  *
**********************************
file not named
```

pinion material	St		
wheel material	St		
hardness	HV	137	137
material quality		MQ	MQ
roughns flnk/µm	Rz	18.0	18.0
roughns root/µm	Rz	18.0	18.0
viscosity @ 40C	nu	136	
pitting permitted?		yes	yes
reversing duty?		no	no

number of teeth	z	49	65
normal module	mn	3.000	
transvrs module	mt	3.000	
gear ratio	u	1.327	
centres	a	171.00	
facewidth	b	15.00	30.00
reference diam	d	147.00	195.00
base diameter	db	138.13	183.24
tip diameter	da	153.00	201.00
root diameter	df	139.50	187.50
tooth depth	h	6.750	6.750
internal diameter		0.0	0.0
norm pres angle	alphan	20.0000	
transv pres ang	alphat	20.0000	
wkng tr pr ang	alphawt	20.0000	
ref helix angle	beta	0.0000	
base helix ang	betab	0.0000	
prof shift coef	x	0.000	0.000
sum of "" coefs	Sigx	0.000	
bsc rack dedend	hfP/mn	1.250	1.250
bsc rk root rad	rofP/mn	0.250	0.250
residual protub	Spr/mn	0.000	0.000
root chord lgth	sFn/mn	2.177	2.227
bending mom arm	hFa/mn	0.958	0.980
root radius	roF/mn	0.424	0.399
tr contct ratio	epsalpha	1.774	

applicatn factr	KA	1.000	
required life/h		500	
load cycles	NL	2.24E7	1.68E
mesh power/kW	P	17.16	
torque/Nm	T	220.0	291.
tr tang force/N	Ft	2992.5	
speed/RPM	n	745.0	561.
pitch line speed/m/s		5.73	
tip relief/µm	Ca	14	
helix modifictn	none		
fav contact pattn posn	verifctn?	n	
wheel web thickness		0.00	
pinion offset	s	0.000	
hx dev elast/µm	fsh	0	
quality grade	q	10	10
hx dev manuf/µm	fma	36	
init'l misal/µm	Fbetax	36	
run-in misal/µm	Fbetay	1	
stiff/(N/mm/µm)	cgamma	22.67	
overlap ratio	epsbeta	0.000	

FACTORS

resonance ratio	N	0.174	
dynamic fct	Kv	1.198	

TOOTH FLANK

face load factr	KHbeta	1.036	
transv load fct	KHalpha	1.348	
zone factor	ZH	2.495	
elasticity fctr	ZE	189.812	
single pair fct	ZB/ZD	1.006	1.000
cont ratio fctr	Zepsilon	0.861	
helix ang factr	Zbeta	1.000	
life factor	ZN	1.242	1.262
lub inf fct	ZLZVZR	0.841	0.850
work-hardng fct	ZW	1.196	
size factor	ZX	1.000	

TOOTH ROOT

face load factr	KFbeta	1.025	1.0
transv load fct	KFalpha	1.486	
form factor	YF	1.221	1.1
stress conc fct	YS	2.286	2.3
notch parameter	qs	2.567	2.7
cont ratio fctr	Yepsilon	0.673	
helix ang factr	Ybeta	1.000	
life factor	YN	0.980	0.9
notch sensy fct	YdrelT	1.002	1.0
surface factor	YRrelT	0.977	0.9
size factor	YX	1.000	1.0

CONTACT STRESS (N/mm²)

allw stress num	sgHlm	327.0	327.0
permiss stress	sigHP	408.2	419.3
"" (reference)	" ref	286.7	286.7
contact stress	sigH	819.1	814.1
safety factor	SH	0.50	0.52
min safety fctr	SHmin	1.00	

BENDING STRESS (N/mm²)

allw stress num	sigFE	174.0	174.
permiss stress	sigFP	119.3	120.
"" (reference)	" ref	121.8	122.
root stress	sigF	338.7	245.
safety factor	SF	0.49	0.6
min safety fctr	SFmin	1.40	

Appendix C

Gear Teeth Surface Pitting Visual Inspection Results

For 220 Nm test 1

Operating Time (hours)	% of gear pitted area recorded by inspector A	% of gear pitted area recorded by inspector B	% of gear pitted area (average)
9	4.4	4.6	4.5
20	7.5	9.1	8.3
31	12.5	12.5	12.5
41	17.6	20.0	18.8
54	21.0	23.4	22.2
70	31.3	35.3	33.3
91	36.0	37.0	36.5
116	50.0	50.0	50.0

For 220 Nm test 2

Operating Time (hours)	% of gear pitted area recorded by inspector A	% of gear pitted area recorded by inspector B	% of gear pitted area (average)
17	7.4	9.2	8.3
28	13.1	11.9	12.5
40	18.2	15.2	16.7
52	26.1	23.9	25.0
70	35.2	34.2	34.7
86	46.4	43.6	45.0

For 147 Nm test 1

Operating Time (hours)	% of gear pitted area recorded by inspector A	% of gear pitted area recorded by inspector B	% of gear pitted area (average)
24	4.0	4.4	4.2
46	16.0	17.4	16.7
70	23.7	26.3	25.0
94	31.6	35.0	33.3
118	40.2	43.2	41.7
143	50.0	50.0	50.0

For 147 Nm test 2

Operating Time (hours)	% of gear pitted area recorded by inspector A	% of gear pitted area recorded by inspector B	% of gear pitted area (average)
24	4.3	4.1	4.2
48	14.8	14.4	14.6
72	25.3	24.7	25.0
96	34.2	31.4	33.3
121	42.5	40.9	41.7
145	50.0	50.0	50.0

For 73 Nm test 1

Operating Time (hours)	% of gear pitted area recorded by inspector A	% of gear pitted area recorded by inspector B	% of gear pitted area (average)
45	4.2	4.2	4.2
95	8.2	8.4	8.3
145	11.2	11.0	11.1
196	13.6	14.2	13.9
268	29.9	31.3	30.6
353	33.8	32.8	33.3
425	33.8	32.8	33.3
485	33.8	32.8	33.3

For 73 Nm test 2

Operating Time (hours)	% of gear pitted area recorded by inspector A	% of gear pitted area recorded by inspector B	% of gear pitted area (average)
49	6.1	6.5	6.3
96	12.3	12.7	12.5
144	16.4	17.0	16.7
193	24.2	25.8	25.0
241	26.8	28.8	27.8
290	35.1	36.3	35.7
341	40.7	42.7	41.7
403	40.7	42.7	41.7
472	50.0	50.0	50.0

Appendix D

Derivation of Oil Film Thickness Formula

The viscosity of all fluid, including lubricants, is affected by two important factors: temperature and pressure. The viscosity of a lubricant increases as pressure increases. For highly loaded contacts such as gears and rolling element bearings, the viscosity and pressure relationship are important. This relationship depends on the relative concentration of paraffinic, naphthenic and aromatic components in the lubricant, and it cannot be generalised as accurately as the viscosity temperature relationship. On the contrary, viscosity of a lubricant increases with decreased temperature. The viscosity properties of a lubricant are typically given at two temperatures: 40 ^{0}C and 100 ^{0}C (104 ^{0}F and 212 ^{0}F). The variation of viscosity with temperature can be determined using MacCoull equation [103]:

$$\ln\ln(V_k + 0.7) = A + B\ln T \qquad (D.1)$$

Where V_k = Kinematics viscosity

T = Absolute temperature in Kelvin

A, B = Lubricant property constants

In order to find the kinematics viscosity of a particular lubricant, equation D.1 can be rearranged:

$$V_k = (e^{e^{(A-B\ln T)}}) - 0.7 \qquad (D.2)$$

Using the information given by the lubricant manufacturer, viscosities for the lubricant, Castrol EP 80W-90, used in these experiments at 40 ^{0}C and 100 ^{0}C were 132.03 cSt and 13.88 cSt respectively (see table D1).

Lubricant properties	**Castrol EP 80W-90**	**TMC 20W-50**
Kinematics viscosity (mm^2/s)		
@ 40°C	132.0	136.0
@ 100°C	13.9	17.0
Viscosity index (VI)	101	136
Density @ 15°C (g/cm^3)	0.893	0.888

Table D1 Properties of the lubricants employed in the tests.

By substituting the viscosities at 40 ^{0}C and 100 ^{0}C into equation D.2 and solving for A and B simultaneously, the kinematics viscosity of the lubricant is given by:

$$V_k = (e^{e^{(21.28-3.43\ln T)}}) - 0.7 \qquad \text{(D.3)}$$

Dowson and Higginson [32] simplified the oil film thickness calculation using the various researchers' experimental work and results (see equation D.4). Two important assumptions were employed during this derivation:

- The load factor was neglected as its effect is small compared to the speed factor. This assumption just served as an initial estimate.
- Since common lubricant data available does not reflect the absolute viscosity and density of the lubricant, the computation of minimum oil film thickness using kinematics viscosity with reasonable assumption of constant density within small temperature variation will be sufficient.

$$h = 16(\eta_0 uR)^{0.5} \qquad \text{(D.4)}$$

h = Oil film thickness in μm

η_0 = Dynamics viscosity in Pas

u = Entraining velocity in m/s

R = Equivalent radius in m

R can be obtained by:

$$\text{Equivalent radius, } R = \frac{(R_1 \sin\phi + s)(R_2 \sin\phi - s)}{(R_1 + R_2)\sin\phi} \qquad \text{(D.5)}$$

and μ by:

$$\text{Entraining velocity, } u = \frac{\pi N_1}{30}(R_1 \sin\phi - \frac{s}{2}(r-1)) \qquad \text{(D.6)}$$

Where gear ratio, $r = \frac{R_2}{R_1}$ and always expressed as a number larger than 1.

s = the distance between pitch line and contact point

R_1 = pitch radius of the pinion

R_2 = pitch radius of the wheel

ϕ = pressure angle

N_1 = rotational speed of pinion

To simplify this derivation, the contact between the meshing teeth will be assumed to be on the pitch line, which implies s= 0. Substituting s= 0, equations D.5 and D.6 are simplified to:

$$R = R_1(\frac{r}{r+1})\sin\phi \qquad \text{(D.7)}$$

$$u = V_1 \sin\phi \qquad \text{(D.8)}$$

where V_1 is the pitch line velocity of pinion

Alexander [103] defined the dynamic viscosity:

$$Dynamic Viscosity(cP) = Kinematics Viscosity(cSt) X density(g/ml) \quad \text{(D.9)}$$

Converting equation (D.9) to metric units:

$$Dynamic Viscosity(Pas) = Kinematics Viscosity(cSt) X (\frac{density(g/ml)}{1000}) \quad \text{(D.10)}$$

Using an average density of 0.893 g/ml (refers to table D1) and combining equations D.7, D.8 and D.10. The final form of equation D.4 is as follows:

$$h_{\min} = 0.350 \sin\phi (V_k V_1 d_1 (\frac{r}{r+1})^{0.5} \quad \text{(D.11)}$$

Where V_k = Kinematics viscosity of the lubricant (cSt)

ϕ = Normal pressure angle of contact (Degree)

d_1 = Pinion pitch circle diameter (m)

Appendix E

Derivation of Tooth Resonance

In the derivation of tooth resonance frequency, the tooth deflection during gear mesh has to be determined. In general, the total deflections of the gear tooth during meshing of the gears can be attributed by [104, 105]: (1) deflection due to flattening of asperities on gear teeth surfaces (2) deflection due to compression at the gear teeth contact surfaces, (3) deflection due to shear and the gear rim and (4) deflection as a cantilever beam. In order to simplify the computation for the total deflection and resonance frequency of the gear tooth, the gear tooth shape was transformed into a simple cantilever beam structure, see figure E1. The deflections due to flattening of asperities, compression of gear teeth surfaces, shear and gear rim were neglected in this instance. In addition, the deflection will be computed based on the applied load that is transmitted through the pitch-line rather than the gear tooth tip, as the latter will give a lower resonance frequency.

$$I = \frac{bh^3}{12} \tag{E.1}$$

$$\mathrm{E}\left(\frac{d^2y}{dx^2}\right) = \frac{Mx}{I} = \frac{FLx}{I} \tag{E.2}$$

Where E= Young modules of the tooth

b= Face width of the tooth

F= Loading on the tooth

L= Height of the tooth

h= Thickness of the tooth

x= Length of tooth at pitch-line

y= Deflection of tooth at pitch-line

After double integrating equation E.2,

$$y = -\frac{FL}{2EI}x^2 + C_1x + C_2 \tag{E.3}$$

Using boundary conditions of: $x = 0$, $y = 0$ and $x = 0$, $\frac{dy}{dx} = 0$. The tooth deflection is given by:

$$y = -\frac{FL}{2EI}x^2 \tag{E.4}$$

The cantilever beam can be further modelled as a standard spring-mass system. The spring constant K can then be calculated from this equation.

$$K = \frac{F}{y} = \frac{2EI}{L^3} \tag{E.5}$$

Using the concept of spring-mass systems, the natural frequency of the single tooth can be easily obtained by:

$$f_n = \frac{w_n}{2\pi} = \frac{1}{2\pi}\sqrt{\frac{K}{m}} \tag{E.6}$$

Where m is the weight of the tooth, which is the product of density and volume of the tooth.

Using the equations E.5 and E.6 together with the geometrical and material information of the gear tooth or cantilever beam showed in table E1, the calculated tooth natural frequency is determined to be 75 kHz for all test conditions. This results is deemed significantly higher compared to the methodology entailed in [104] where the resonance

frequency of the gear tooth was computed based on deflection due to depression at gear tooth surface and as a cantilever beam. The gear tooth resonance frequency is determined to 36 kHz which is significantly out of the AE ranges. With the inclusion of the deflections due to the gear rim, shear load and flattening of asperities on gear teeth surfaces, the resonance frequency will be further reduced until within the vibration detectable ranges. This is one of the reasons for employing vibration technique as condition monitoring tool.

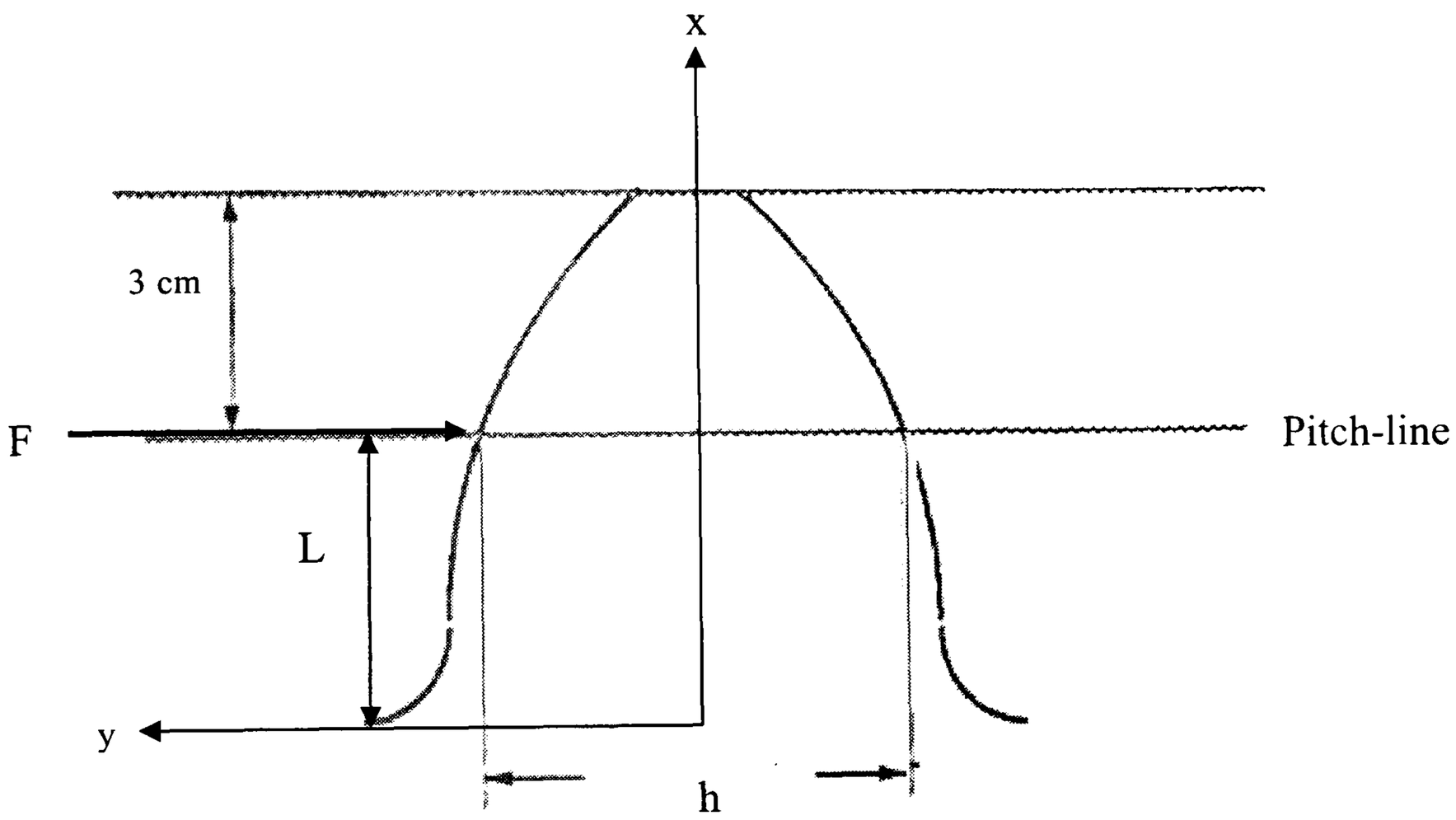

Transformed into

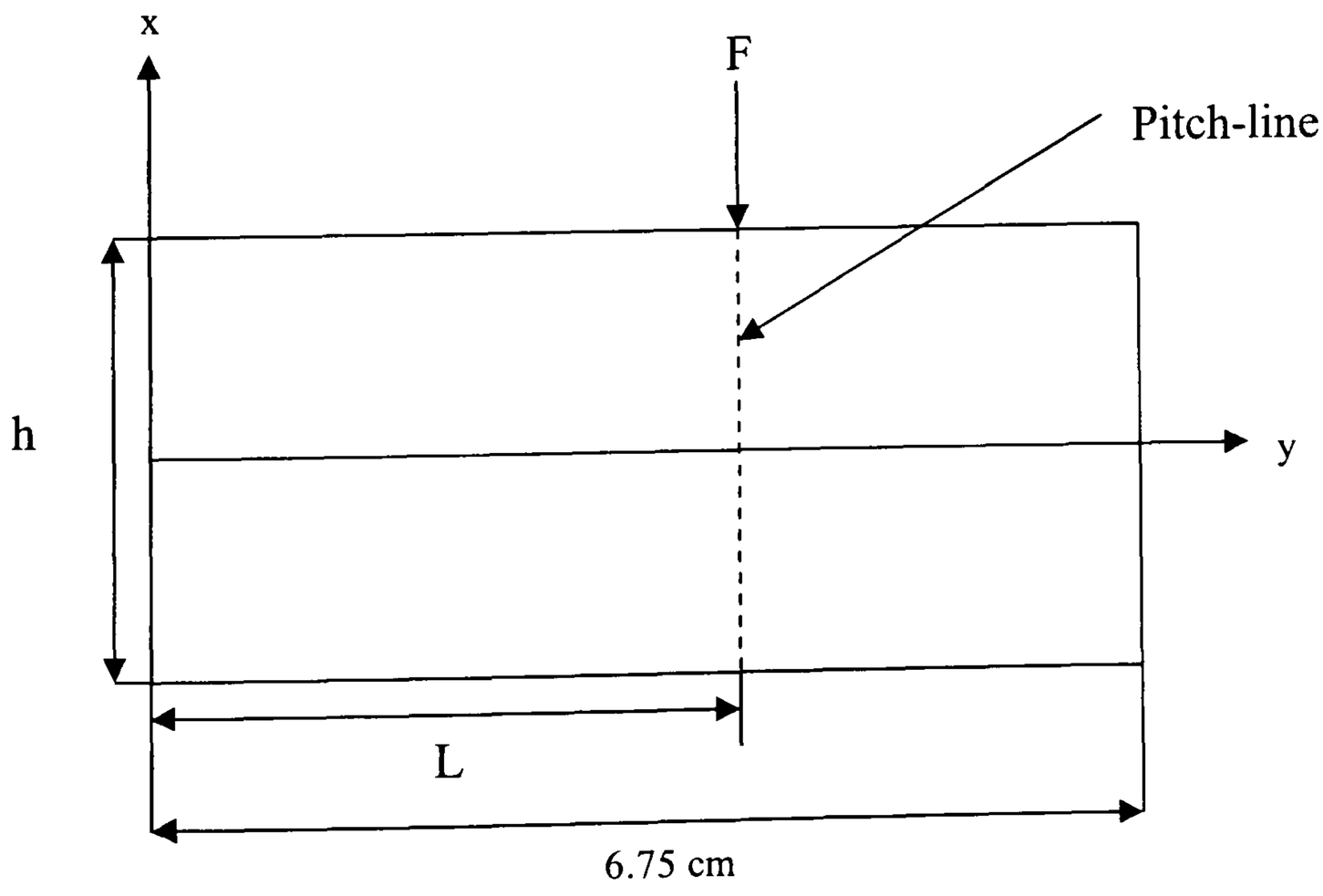

Figure E1 Transformation of the gear tooth to a cantilever beam

b (m)	0.03
h (m)	0.00425
L (m)	0.00375
E (GN/m^2)	205
Density (kg/m^3)	7930
Volume (m^3)	$8.6x10^{-7}$

Table E1 Geometrical and material data of the gear tooth.

Appendix F

Pitting Progressions

Pitting Progression for applied torque of 220 Nm

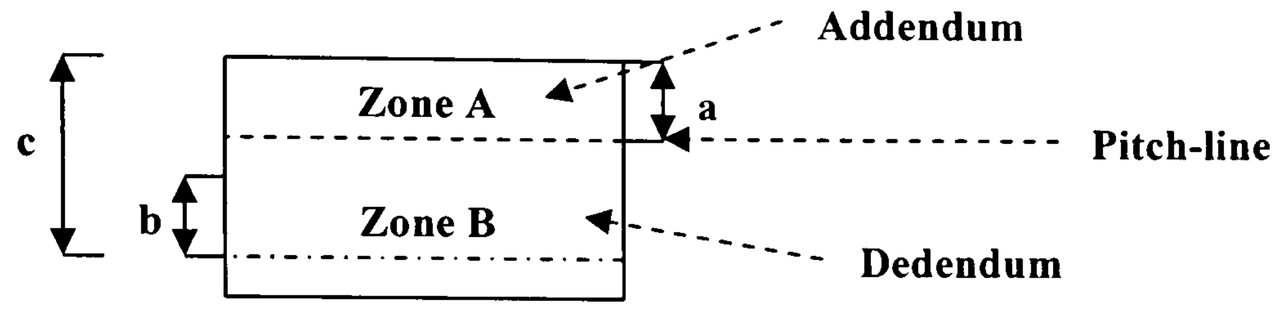

* All dimensions in mm.

Time Interval (hours)	220-Test 1		Time Interval (hours)	220-Test 2	
	Zone A	Zone B		Zone A	Zone B
9	Wear-in marks a = 3	Light pitting across face width b < 0.5 c = 5	0		
20	Scoring marks a = 2	Pitting moving towards pitch-line. Similar no. of pits but deeper in depth 0.5 < b < 1 8.3% pitting area c = 5	17	Scoring marks a = 2.5	Light pitting across face width b = 0.5 8.3% pitting area c = 5
31	Scoring marks a = 2.5	Pitting moving towards pitch-line. Pits are deeper and bigger b = 1 (cover about ¾ of this range) 12.5% pitting area c = 5	28	Scoring marks a = 2.5	Pitting moving towards pitch-line. Pits are deeper and bigger b = 1 (cover about ¾ of this range) 12.5% pitting area c = 5
41	Scoring marks a = 2.5	Pitting moving towards pitch-line. Pits are bigger and deeper b = 1.5 (cover about ¾ of this range) 18.8% pitting area c = 5	40	Scoring marks a = 2.5	Pitting moving towards pitch-line. Pits are bigger and deeper b = 1.5 (cover about 2/3 of this range) 16.7% pitting area c = 5
54	Scoring marks a = 2.5	More pitting and pits touched the pitch-line b = 2 (cover about 2/3 of this range) 22.2% pitting area c = 5	52	Scoring marks a = 2.5	More pitting and pits touch the pitch-line b = 2 (cover about 3/4 of this range) 25.0% pitting area c = 5
70	Scoring marks a = 2.5	Pitting moving downward to the dedendum. More pits b = 2 33.3% pitting area c = 6	70	Scoring marks a = 2.5	Pitting moving downward to the dedendum. More pits b = 2.5 (cover about 5/6 of this range) 34.7% pitting area c = 5.5

91	Scoring marks a = 3	Pits touched the pitch-line and spread across the face width b = 2.5 (cover about 7/8 of this range) 36.5% pitting area c = 6	86	Scoring marks a = 2.5	Pits reached the pitch-line and spread across the face width b = 3 (cover about 9 10 of this range) 45.0% pitting area c = 5.5
116	Scoring marks a = 3	Almost every tooth has large pits across face width and reached the pitch-line b = 3, 50.0% pitting area c = 6			

Pitting Progression for applied torque of 147 Nm

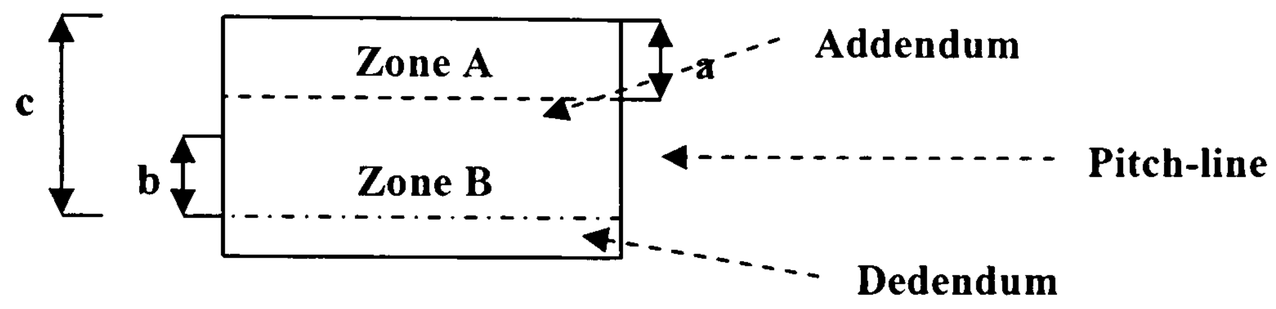

* All dimensions in mm.

Time Interval (hours)	147-Test 1		Time Interval (hours)	147-Test 2	
	Zone A	Zone B		Zone A	Zone B
24	Wear-in marks a = 3	Light pitting across half the face width b < 0.5 4.2% pitting area c = 4.5	24	Wear-in marks a = 3.5	Light pitting across one quarter the face width b = 1 (cover about 1/4 of this range) 4.2% pitting area c = 5
46	Wear-in marks a = 3	Pitting moving towards pitch-line. Some teeth have pitting at addendum b= 1 16.7% pitting area c = 5	48	Wear-in marks a = 3..5	Pitting moving towards pitch-line. Very deep pits along the bottom. b = 1.5 (cover about 7/12 of this range) 14.6% pitting area c = 5.5
70	Wear-in marks a = 3	Pitting moving towards pitch-line. b = 1.5 25.0% pitting area c = 5	72	Wear-in marks a = 3.5	Pitting moving across face width, deeper pits at lower regions. b = 1.5 25.0% pitting area c = 5.5
94	Wear-in marks a = 3	Pitting moving towards pitch-line. b = 2 33.3% pitting area c = 5	96	Wear-in marks a = 3.5	Pitting moving towards pitch-line. More teeth with increased no. and deeper pits at the addendum. b = 2 33.3% pitting area c = 5.5

118	Wear-in marks a = 3	Pitting moving towards pitch-line. b = 2.5 41.7% pitting area c = 5	121	Wear-in marks a = 2.5	Pitting moving towards pitch-line. More teeth with deeper pits at the addendum. b = 2.5 41.7% pitting area c = 5.5
143	Wear-in marks a = 2.5	Pitting reached pitch-line b = 3 50.0% pitting area c = 5.5	145	Scoring marks a = 2.5	Pitting moving reached pitch-line. Some teeth with very deep pitting at the addendum. b = 3 50.0% pitting area c = 5.5

Pitting Progression for applied torque of 73 Nm

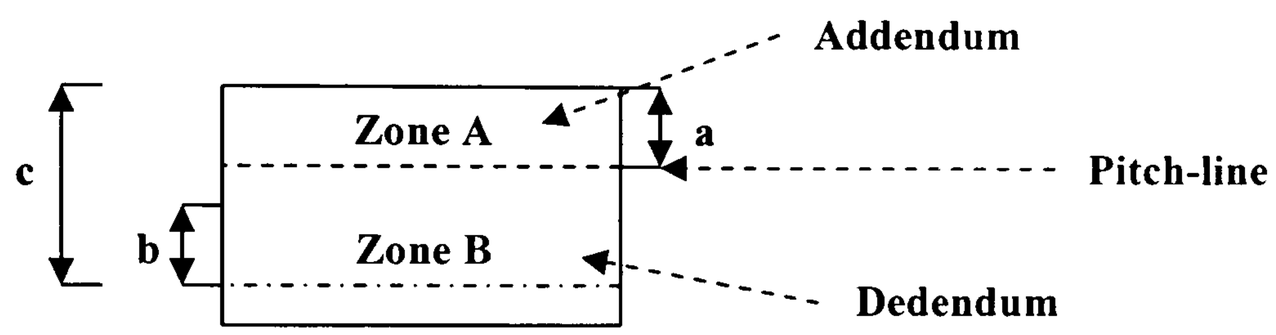

* All dimensions in mm.

Time Interval (hours)	73-Test 1		Time Interval (hours)	73-Test 2	
	Zone A	Zone B		Zone A	Zone B
45	Wear-in marks a = 3	Light pitting across half the face width b < 0.5 c = 5	49	Wear-in marks a = 2.5	Light pitting across one quarter of the face width. Some teeth have pitting at addendum. b= 1.5 (cover about 1/4of this range) 6.3% pitting area c = 5
95	Wear-in marks a = 3	Pitting moving towards pitch-line and occupied half of the face width. b= 1 (cover about ½ of this range) 8.3% pitting area c = 5	96	Wear-in marks a = 2.5	Pitting moving across pitch-line and occupied half of the face width. b= 1.5 (cover about ½ of this range) 12.5% pitting area c = 5.5
145	Wear-in marks a = 3	Pitting moving towards pitch-line and concentrated pitted on the right 1/3 of face width. b = 2 (cover about 1/3 of this range) 11.1% pitting area c = 5	144	Wear-in marks a = 2.5	Pitting moving across pitch-line and occupied 2 3 of the face width. Pits got deeper. b= 1.5 (cover about 2 3 of this range) 16.7% pitting area c = 5.5

196	Wear-in marks a = 3	Pitting moving towards pitch-line and concentrated pitted on the right 1/3 of face width. b = 2.5 (cover about 1/3 of this range) 13.9% pitting area c = 5.5	193	Wear-in marks a = 2.5	Pitting moving across pitch-line and occupied the whole of face width. b = 1.5 (cover about 1 3 of this range) 25.0% pitting area c = 5.5
268	Wear-in marks a = 3	Pitting moving towards pitch-line. b = 1.5 full face width & b = 1 (cover about 1/3 of this range) 30.6% pitting area c = 5.5	241	Wear-in marks a = 2.5	Pitting moving towards pitch-line. Almost all teeth has 25% pitting area, the rest has 27.8%. Some pitting over pitch-line b = 2.5 (cover about 2 3 of this range) 27.8% pitting area c = 5.5
353	Wear-in marks a = 3	Pitting moving towards pitch-line. Only 3 to 4 teeth have this pitting area. b = 1.5 half face width & b = 2.5 half face width 33.3% pitting area c = 5.5	290	Wear-in marks a =2.5	Pitting moving towards pitch-line. Pitch-line covered with pits b = 2.5 (cover about 6 7 of this range) 35.7% pitting area c = 5.5
425	Wear-in marks a = 3	Pitting moving towards pitch-line. 6 to 8 teeth have this pitting area. b = 1.5 half face width & b = 2.5 half face width 33.3% pitting area c = 5.5	341	Wear-in marks a = 2.5	Pitting reached pitch-line. Almost all teeth have 33.3% pitting area, only a few teeth have 41.7%. b = 2.5 41.7% pitting area c = 5.5
485	Wear-in marks a = 3	Pitting moving towards pitch-line. 11 to 15 teeth have this pitting area. b = 1.5 half face width & b = 2.5 half face width 33.3% pitting area c = 5.5	403	Wear-in marks a = 2.5	The no. of teeth with 41.7% pitted area has increased from a few to 50% of the total no. of gear teeth. b = 2.5 41.7% pitting area c = 5.5
			472	Wear-in marks a = 2.5	Most teeth have 41.7% of gear pitted area, others reached 50%. b = 3 50.0% pitting area c = 5.5

* The test was terminated since the pitting area did not increase, but this percentage of pitted area was spreading across all the rest of gear teeth. This implied localised pitting has been developed into distributed pitting.

Appendix G

Gear Teeth Surface Roughness Measurements

Surface textures of the two new gear teeth were measured in both the radial and axial directions of the gears and used as a reference for pitted gear teeth comparison. After the end of each gear fatigue test, the pinion gear tooth with the greatest pitted area was removed for texture measurements. These measurements were subsequently compared with the reference measurement of the undamaged pinion gear teeth.

Tables G1 provides a summary of the surface texture measurements for both the undamaged and damaged gear teeth surfaces under all test conditions.

	Radial Direction				Axial Direction			
	1st Ra (μm)	2nd Ra (μm)	Average Ra (μm)	Composite Ra (μm)	1st Ra (μm)	2nd Ra (μm)	Average Ra (μm)	Composite Ra (μm)
Undamaged Gear surface (reference)	1.5234	1,2211	1.3723	1.9524	0.6110	0.7210	0.6660	0.9451
50% gear pitted area for 220 Nm	2.5485	2.4999	2.5242	3.5699	2.3898	2.6682	2.5290	3.5820
50% gear pitted area for 147 Nm	3.6705	1.8836	2.7771	4.1256	2.1569	1.2570	1.7070	2.4965
50% gear pitted area for 73 Nm	1.7012	1.9538	1.8275	2.5906	2.1086	1.4834	1.7960	2.5781

Tables G1 Surface texture measurements for both the undamaged and damaged gear teeth surfaces under all test conditions

Taylor Hobson

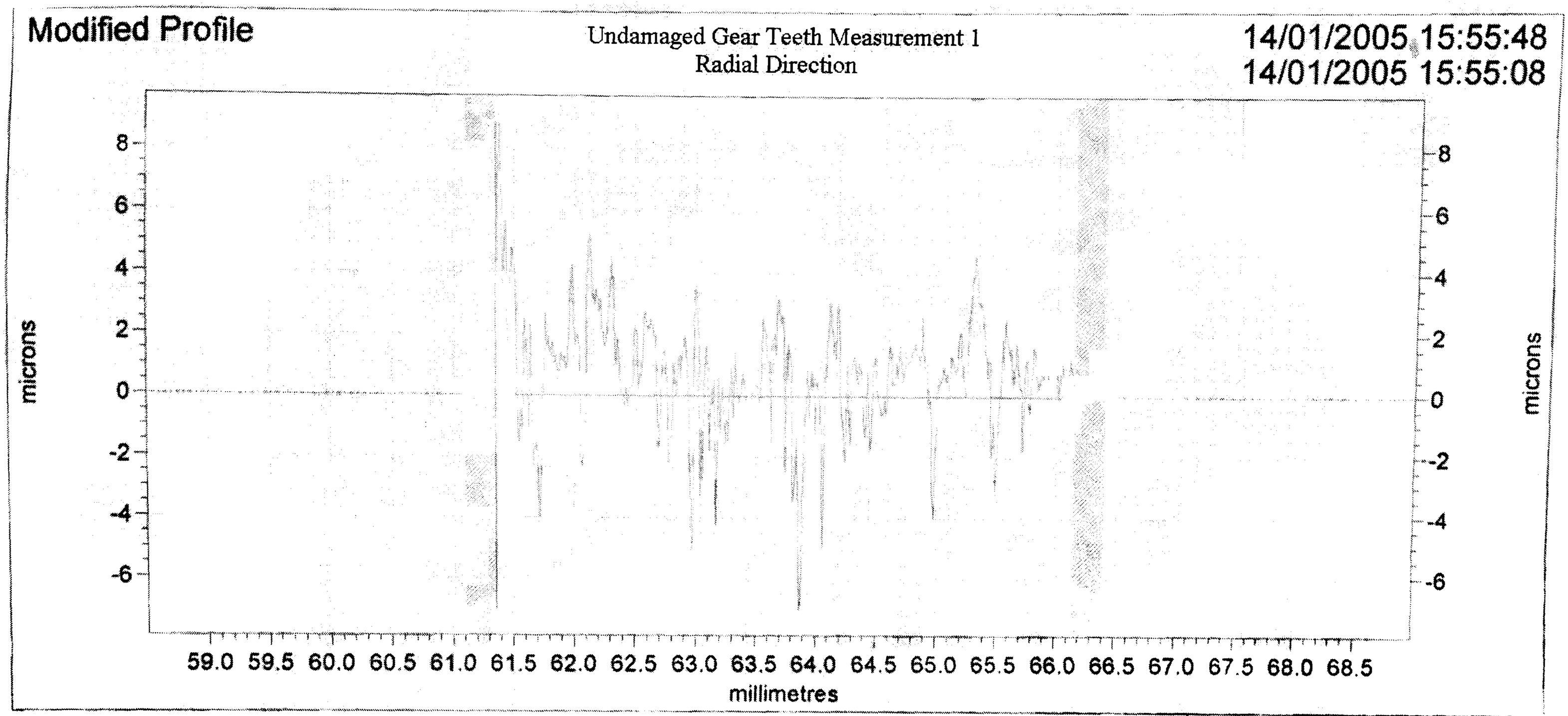

			Slope	-7.853	°
Ra	1.5234	µm	Rq	2.0106	µm
			Rt	15.9242	µm
			Rz	8.6886	µm

Taylor Hobson

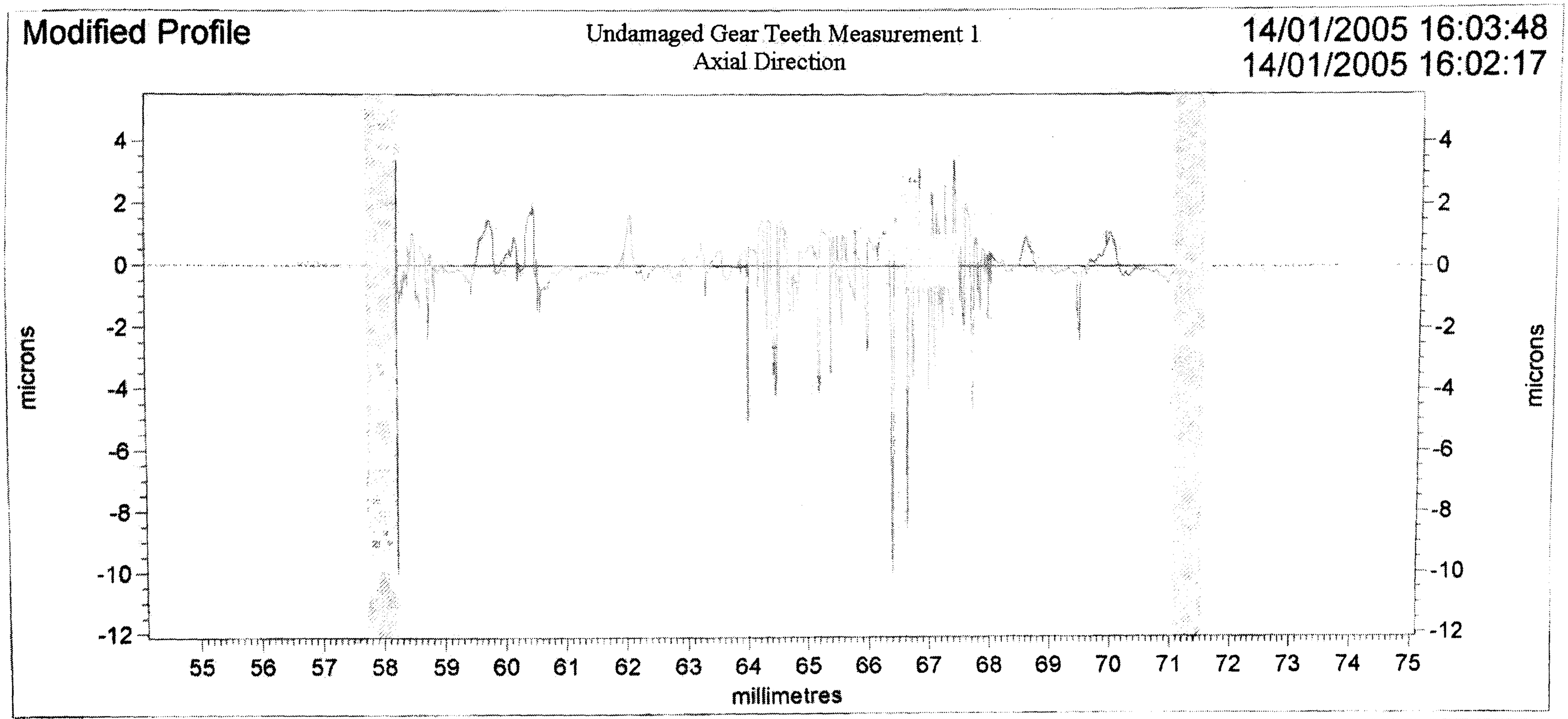

		Slope	-0.225	°	
Ra	0.6110	µm	Rq	1.0348	µm
			Rt	13.4128	µm
			Rz	3.7742	µm

Taylor Hobson

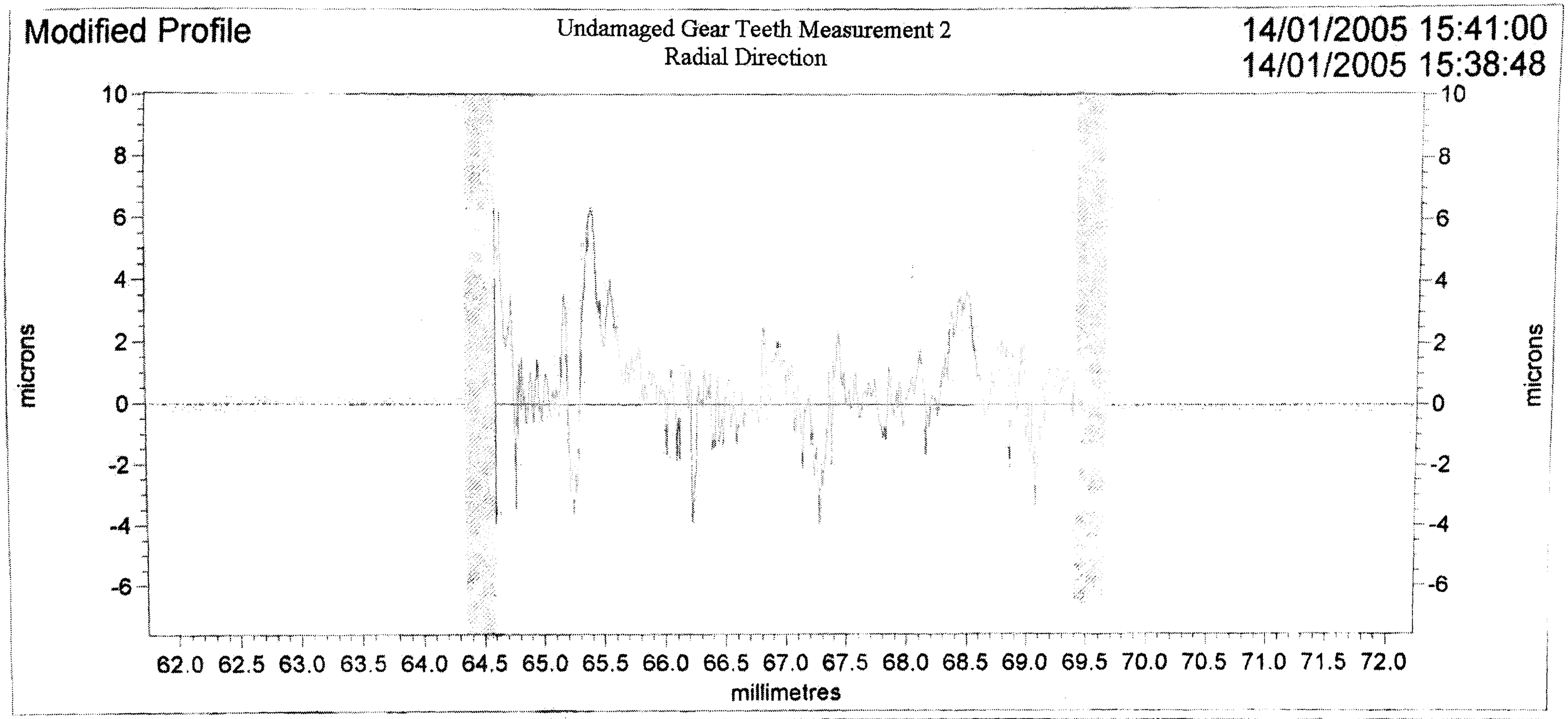

		Slope	-4.593	°
Ra	1.2211 µm	Rq	1.6980	µm
		Rt	10.2927	µm
		Rz	7.0122	µm

Taylor Hobson

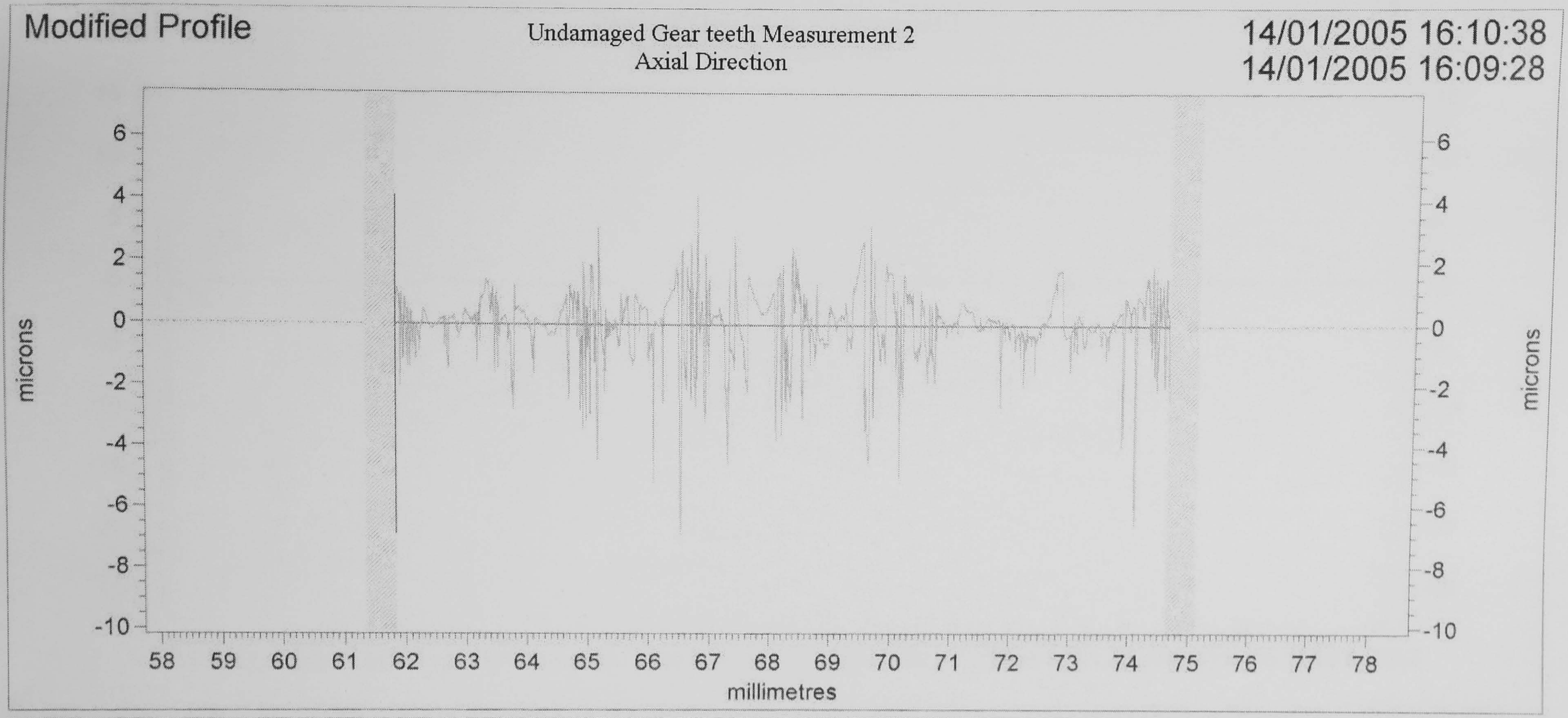

		Slope	-0.053	°			
Ra	0.7210	µm	Rq	1.0690	µm		
			Rt	11.0366	µm		
			Rz	5.3928	µm		

Taylor Hobson

Modified Profile

Damaged Gear Teeth Measurement 1
Radial Direction (220 Nm)

17/02/2005 15:21:39
17/02/2005 15:21:18

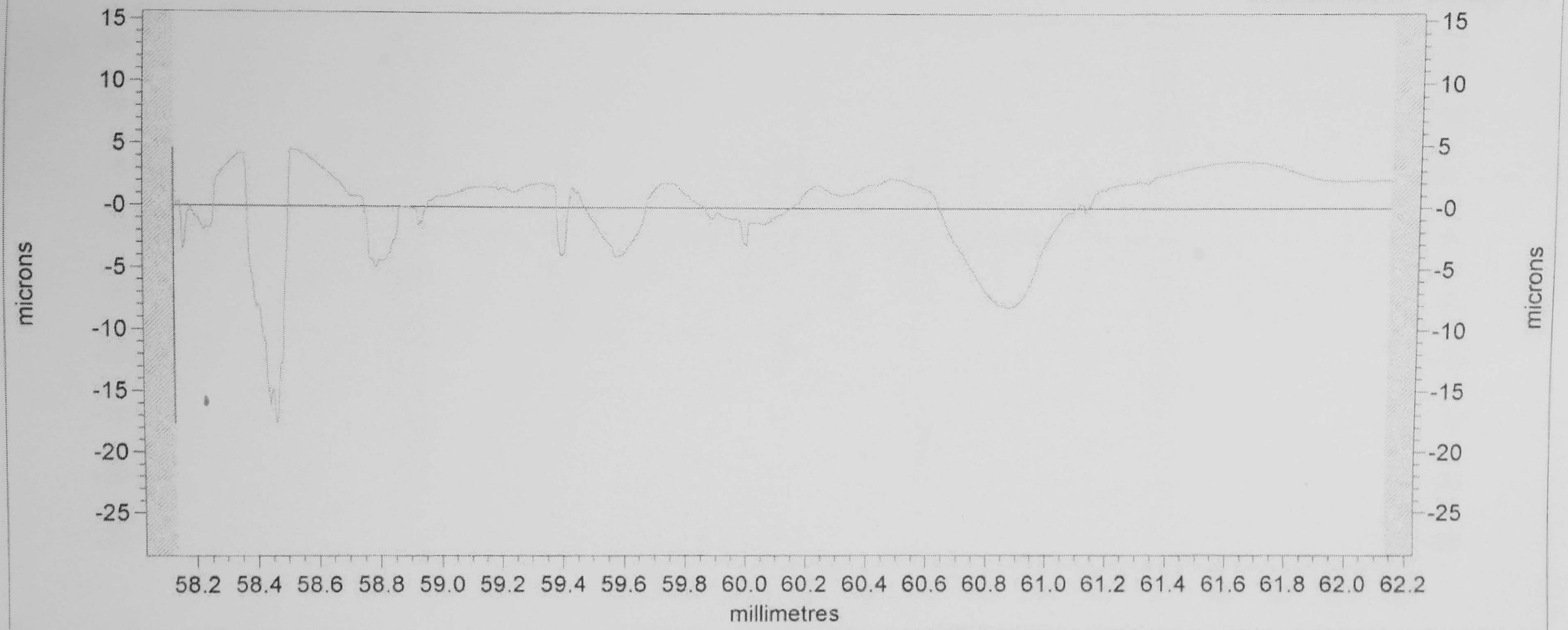

		Slope	-1.890	°			
Ra	2.5485	µm	Rq	3.4443	µm		
			Rt	22.2946	µm		
			Rz	9.1500	µm		

Taylor Hobson

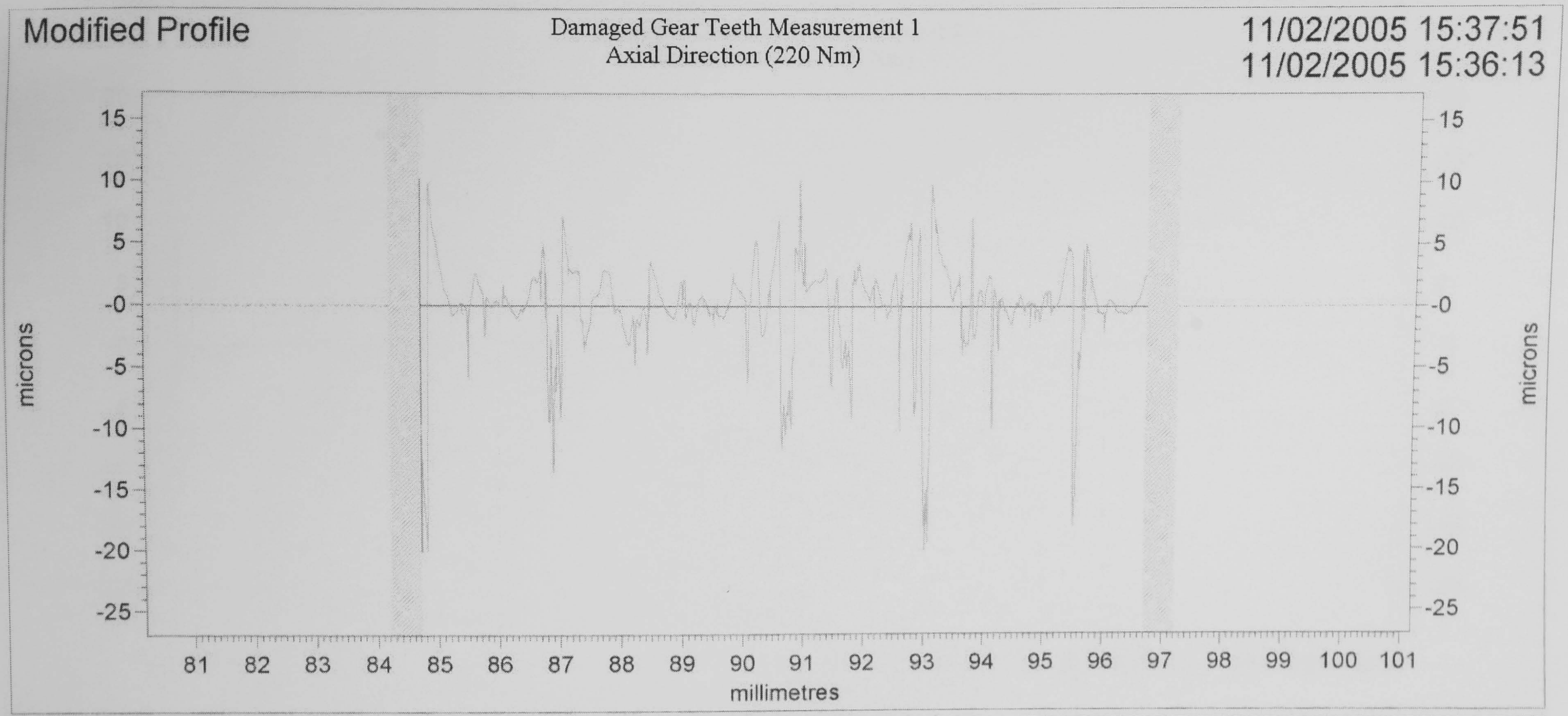

		Slope	-0.064	°			
Ra	2.3898	µm	Rq	3.8437	µm		
			Rt	30.3323	µm		
			Rz	14.2980	µm		

Taylor Hobson

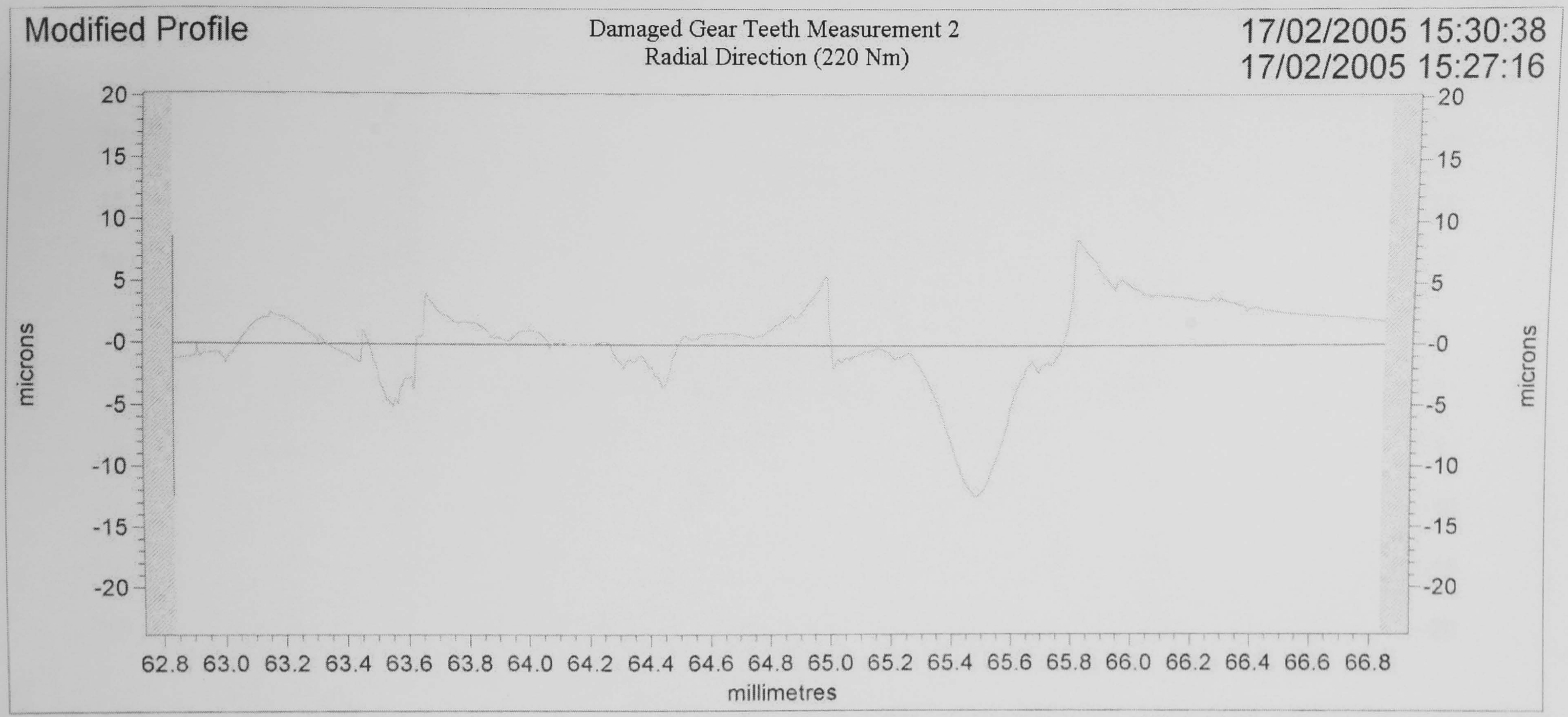

		Slope	-2.570	°			
Ra	2.4999	µm	Rq	3.4841	µm		
			Rt	21.0740	µm		
			Rz	9.4729	µm		

Taylor Hobson

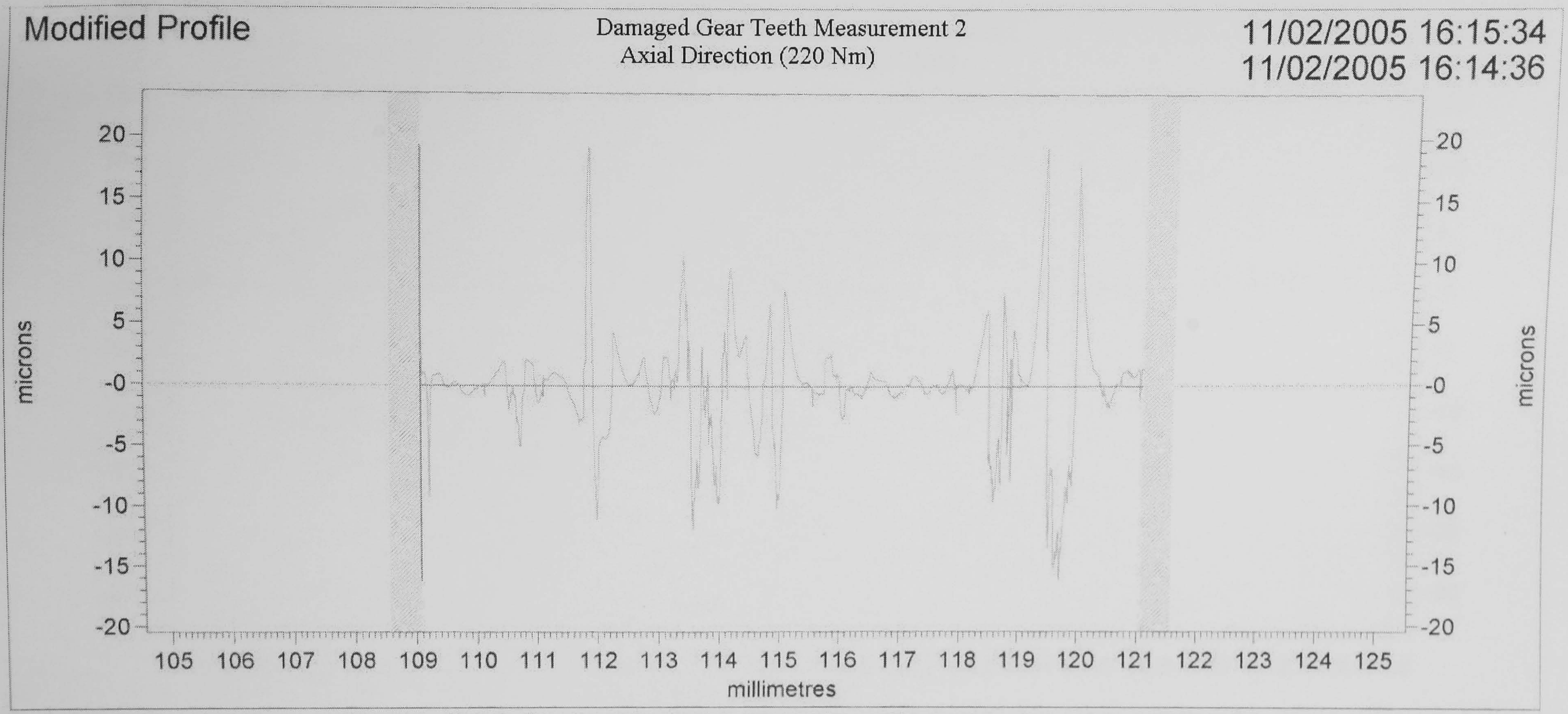

			Slope	-0.266	°			
Ra	2.6682	µm	Rq	4.3853	µm			
			Rt	35.5931	µm			
			Rz	14.0662	µm			

Taylor Hobson

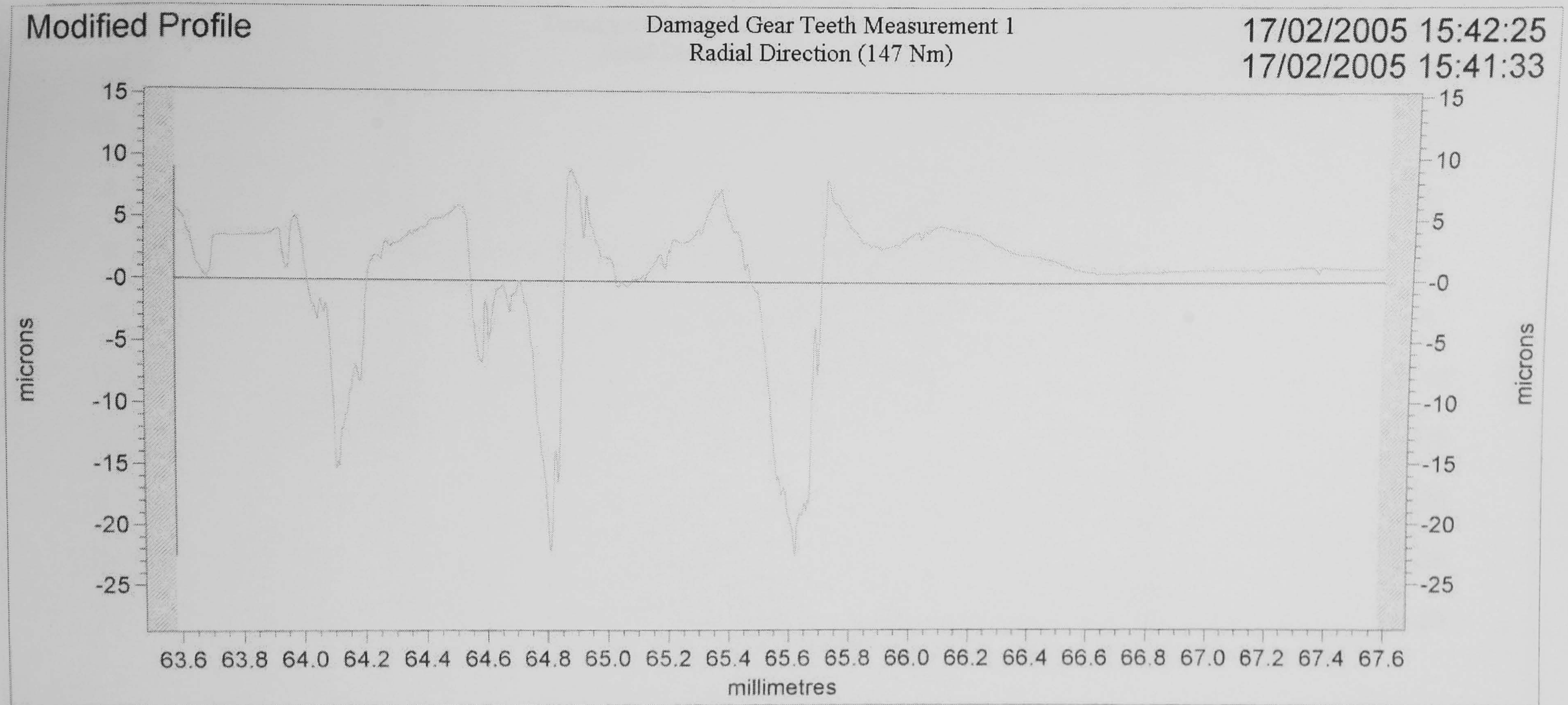

			Slope	-3.320	°			
Ra	3.6705	µm	Rq	5.3987	µm			
			Rt	31.5444	µm			
			Rz	17.4935	µm			

Taylor Hobson

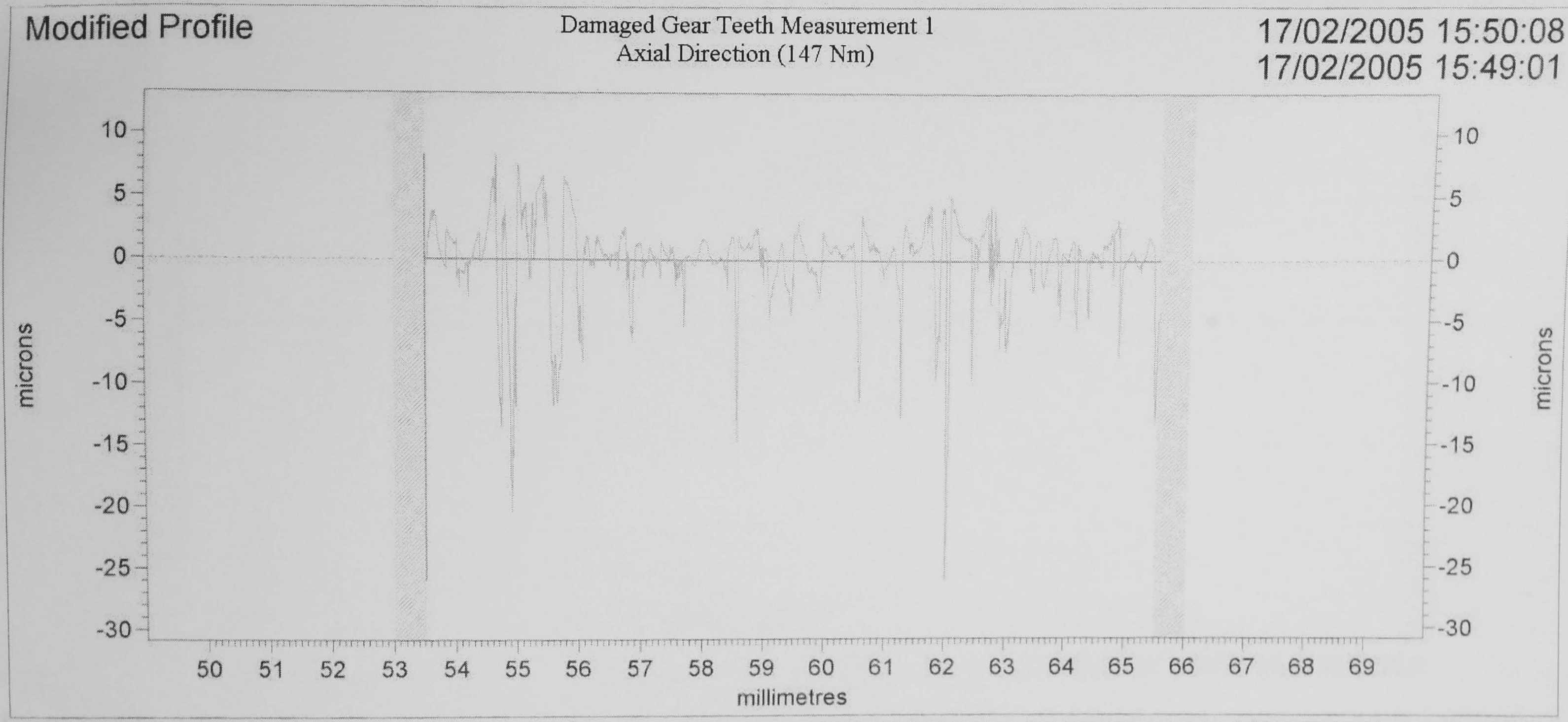

			Slope	0.251	°		
Ra	2.1569	µm	Rq	3.4259	µm		
			Rt	34.3869	µm		
			Rz	14.3025	µm		

Taylor Hobson

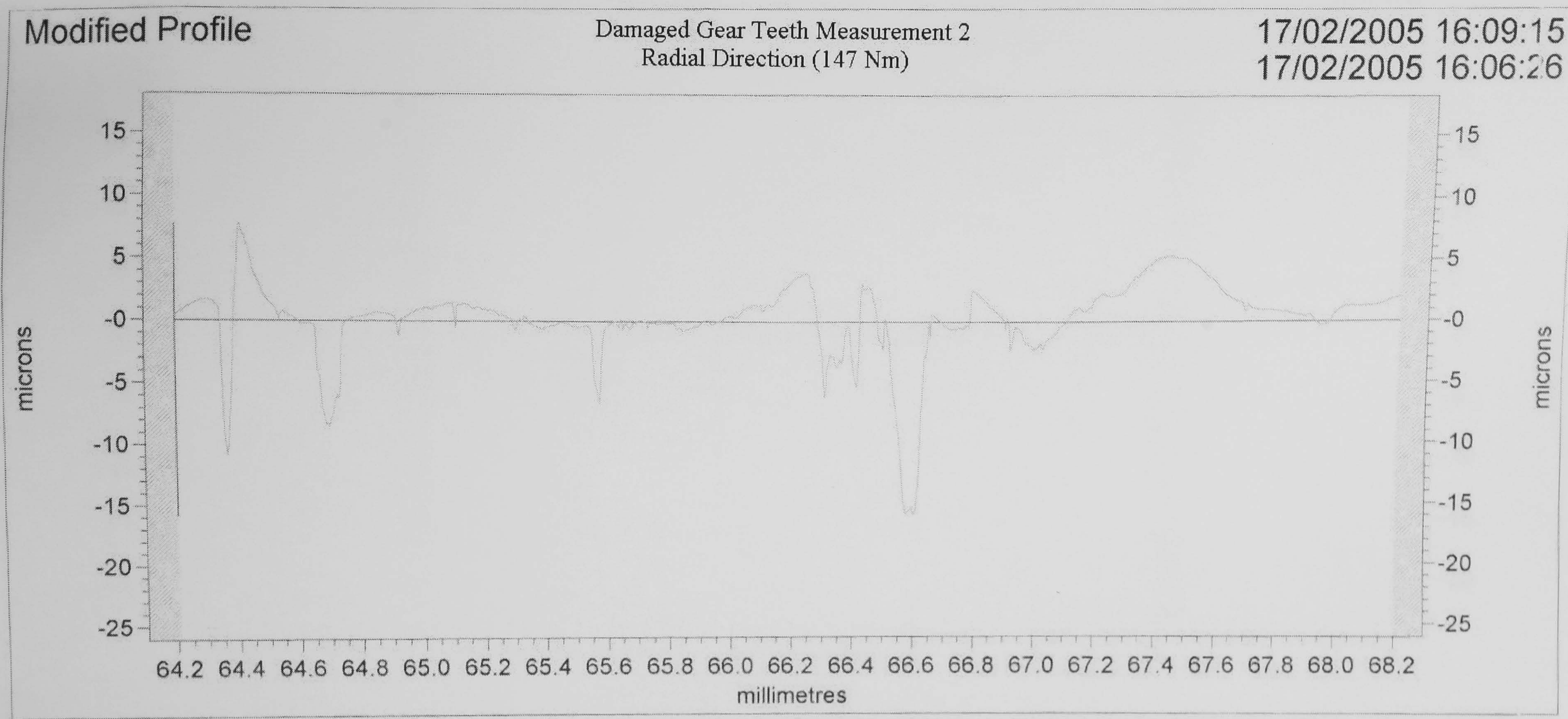

		Slope	-0.832	°			
Ra	1.8836	µm	Rq	3.0783	µm		
			Rt	23.5311	µm		
			Rz	14.5620	µm		

Taylor Hobson

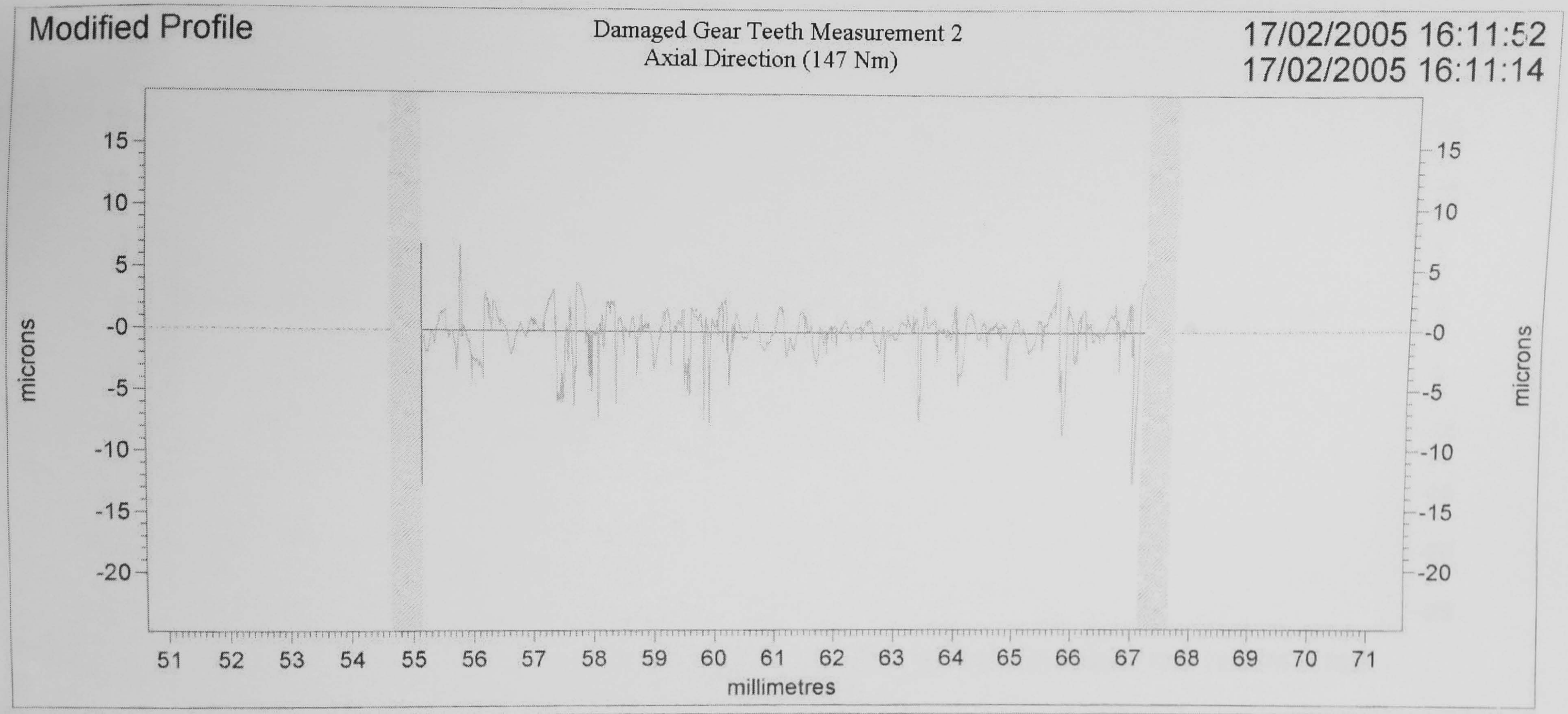

		Slope	-0.463	°			
Ra	1.2570	µm	Rq	1.9062	µm		
			Rt	19.6579	µm		
			Rz	8.4172	µm		

Taylor Hobson

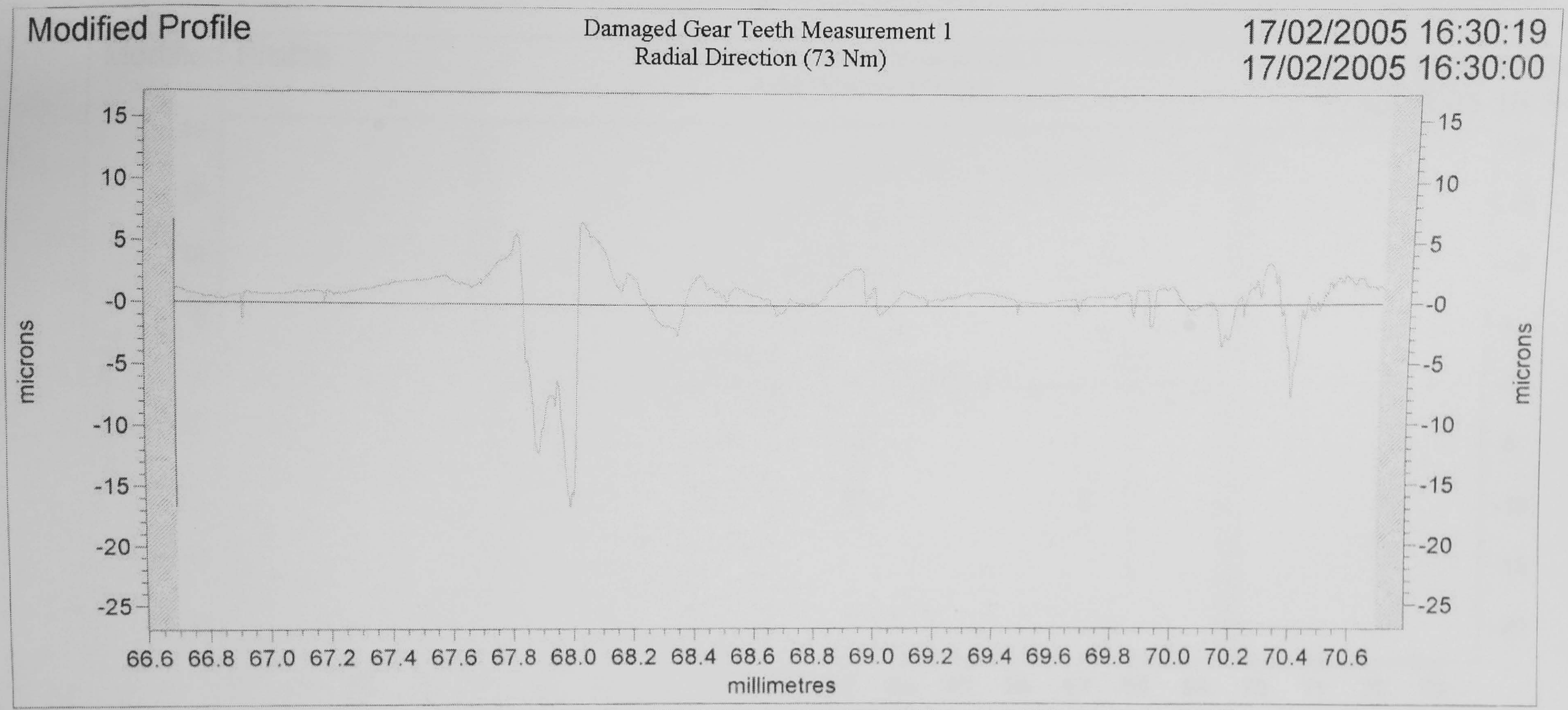

			Slope	-6.541	°			
Ra	1.7012	µm	Rq	2.7701	µm			
			Rt	23.3764	µm			
			Rz	9.0979	µm			

Taylor Hobson

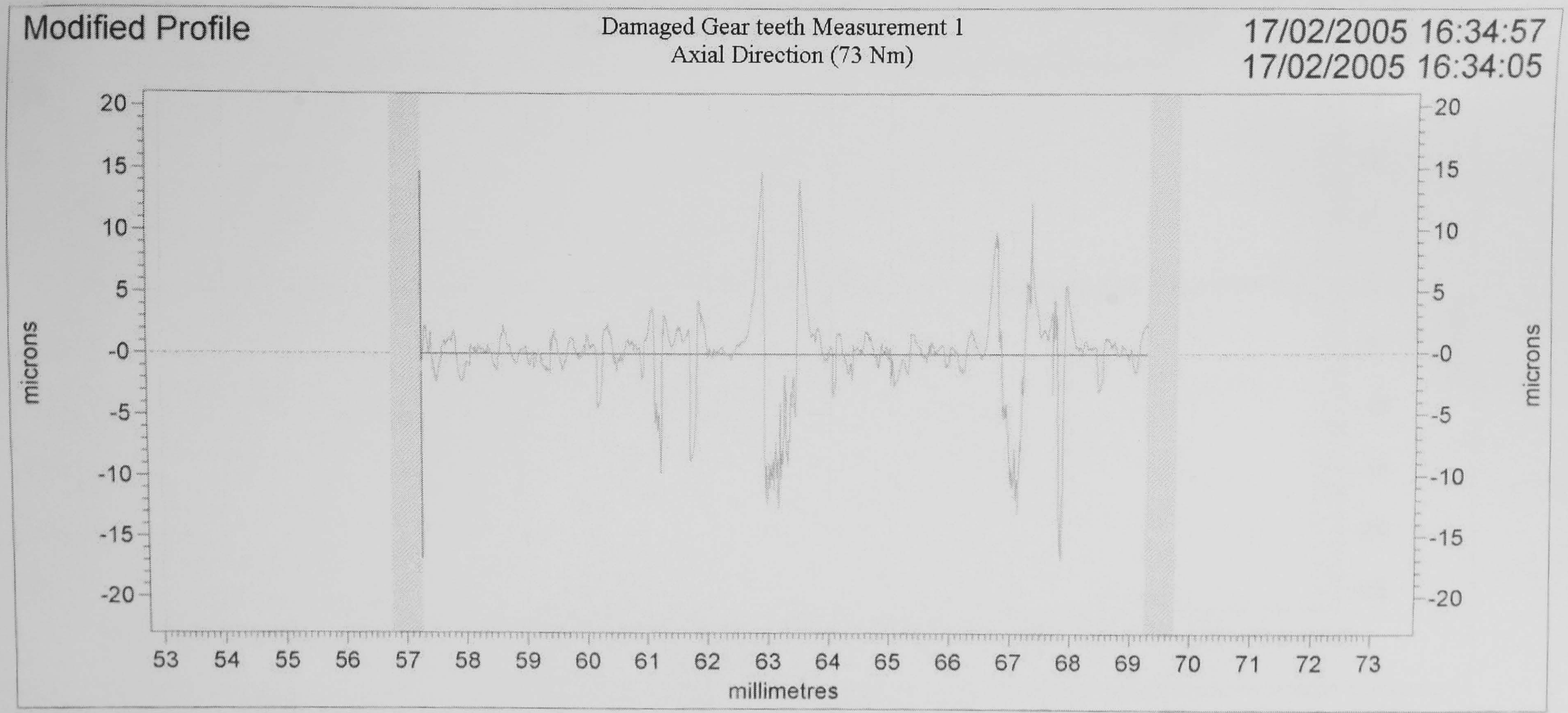

			Slope	0.327	°			
Ra	2.1086	µm	Rq	3.5322	µm			
			Rt	31.6744	µm			
			Rz	11.1909	µm			

Taylor Hobson

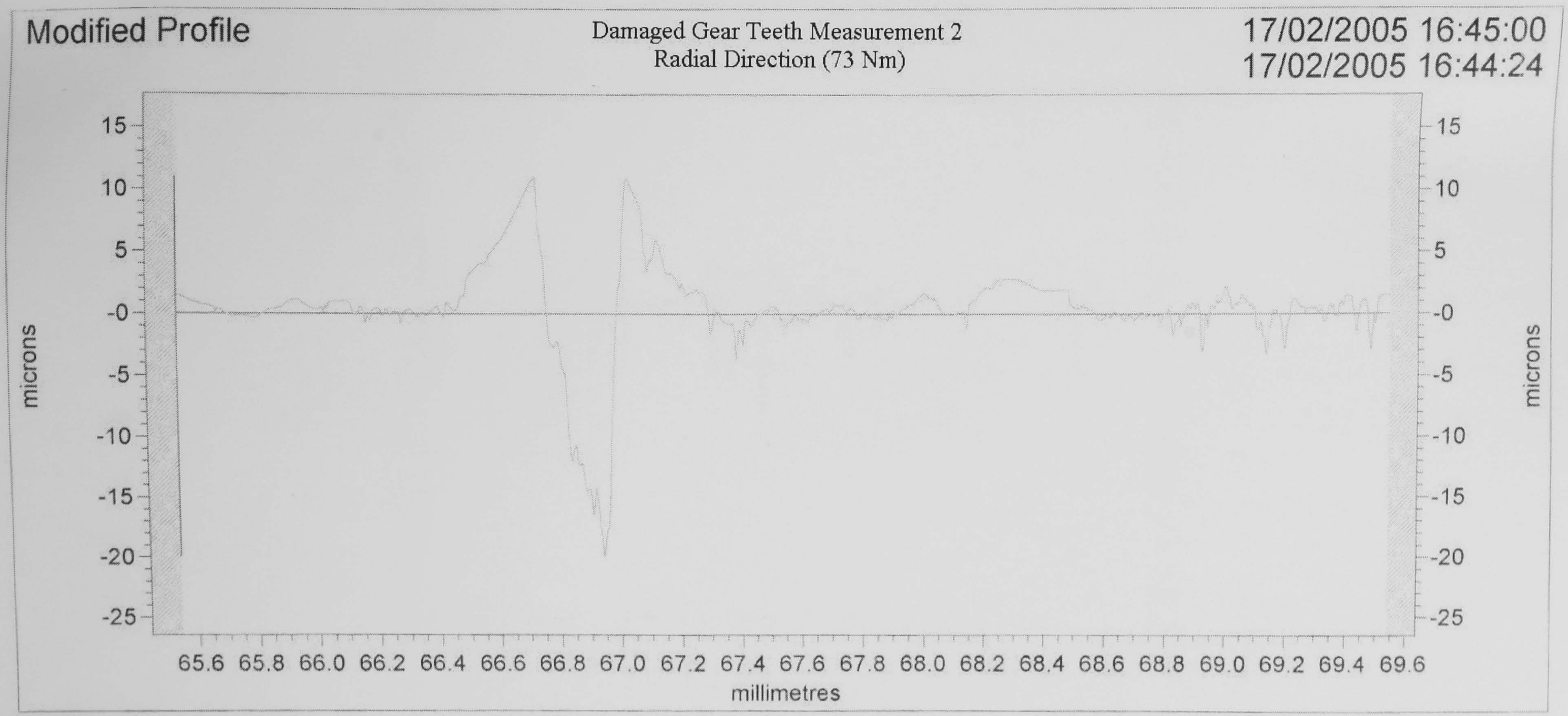

			Slope	0.948	°			
Ra	1.9538	µm	Rq	3.7538	µm			
			Rt	30.8984	µm			
			Rz	10.0376	µm			

Taylor Hobson

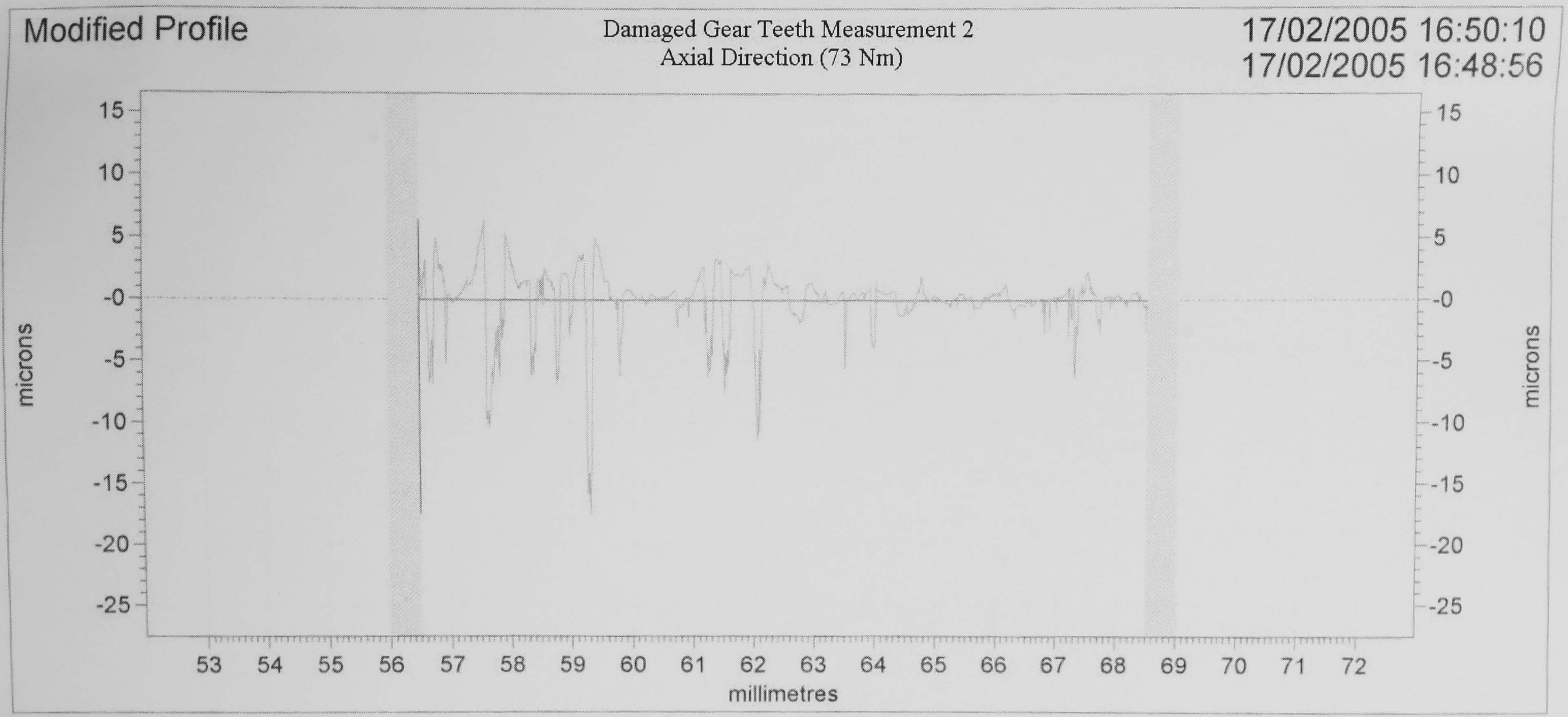

			Slope	-0.037	°			
Ra	1.4834	µm	Rq	2.4983	µm			
			Rt	23.8806	µm			
			Rz	9.1979	µm			